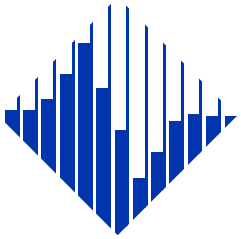

PACIFIC EARTHQUAKE ENGINEERING
RESEARCH CENTER

Selection and Scaling of Ground Motions for Nonlinear Response History Analysis of Buildings in Performance-Based Earthquake Engineering

N. Simon Kwong

Anil K. Chopra

Department of Civil and Environmental Engineering
University of California, Berkeley

PEER Report No. 2015/11
Pacific Earthquake Engineering Research Center
Headquarters at the University of California, Berkeley

December 2015

PEER 2015/11
December 2015

Disclaimer

The opinions, findings, and conclusions or recommendations expressed in this publication are those of the author(s) and do not necessarily reflect the views of the study sponsor(s) or the Pacific Earthquake Engineering Research Center.

Selection and Scaling of Ground Motions for Nonlinear Response History Analysis of Buildings in Performance-Based Earthquake Engineering

N. Simon Kwong

Anil K. Chopra

Department of Civil and Environmental Engineering
University of California, Berkeley

PEER Report 2015/11
Pacific Earthquake Engineering Research Center
Headquarters at the University of California, Berkeley

December 2015

Abstract

This report investigates the issue of selecting and scaling ground motions as input excitations for response history analyses of buildings in performance-based earthquake engineering. Many ground motion selection and modification (GMSM) procedures have been developed to select ground motions for a wide variety of objectives. This report focuses on the selection and scaling of single, horizontal components of ground motion for estimating seismic demand hazard curves (SDHCs) of multistory frames at a given site.

Chapter 2 develops a framework for evaluating GMSM procedures in their ability to provide accurate estimates of SDHCs. The notion of a benchmark SDHC is introduced, enabling biases caused by GMSM procedures to be isolated from other sources of bias. More importantly, the ability to quantify bias facilitates the identification of intensity measures (IMs) that are sufficient; an IM, which may be scalar or vector-valued, is defined to be *sufficient for a response quantity*, or engineering demand parameter (EDP), when the EDP is sensitive to only this IM and no other features of the ground motion [1]. However, the application of the framework in this chapter is limited by the availability of recorded ground motions and prediction models for EDP of structures.

The framework developed in Chapter 2 is applied to synthetic ground motions in Chapter 3, where biases in estimates of SDHCs caused by GMSM procedures can be estimated for any structural system and any EDP. However, the use of synthetic ground motions gives rise to the issue of developing *benchmark-consistent* ground-motion prediction models. Based on the results from Chapters 2-3, it is hypothesised that the potential bias in any SDHC estimate is caused directly by two important properties of the particular selection of ground motions: (i) hazard consistency and (ii) IM sufficiency.

A novel ground-motion selection procedure, rooted in the theory of Importance Sampling, is developed in Chapter 4 that allows: (i) hazard consistency of the selected motions to be directly enforced for a user-specified collection of IMs, and (ii) SDHCs of a structure to be estimated from a single ensemble of ground motions, with the option of avoiding record scaling altogether. This procedure, together with two other contemporary GMSM procedures – (i) "exact" Conditional Spectrum and (ii) Generalized Conditional Intensity Measure – are evaluated in Chapters 5-6 for several structural systems and EDPs at a specified site. In these chapters, the amount of effort involved in implementing these procedures for estimating SDHCs is summarized in a step-by-step form, and the magnitude of biases caused by these procedures are documented.

[1] Strictly speaking, only IMs that are *insufficient* may be identified.

Acknowledgments

The research in this report was supported primarily by the National Science Foundation Graduate Research Fellowship Program under Grant No. DGE 1106400. This support is gratefully acknowledged. Any opinions, findings, and conclusions or recommendations expressed in this work are those of the authors and do not necessarily reflect the views of the National Science Foundation.

We are indebted to Dr. Robin K. McGuire for his active participation in the research that led to Chapters 2-4, and for his advice on the overall direction of the project. We are also grateful to Professor Jack W. Baker for his careful review of Chapters 2-4, leading to significant improvements.

We would like to acknowledge Professors Brendon A. Bradley, Norman A. Abrahamson, Yousef Bozorgnia, and Ting Lin for fruitful discussions related to various parts of this work. We thank Dr. Mayssa N. Dabaghi for providing the MATLAB routines to implement Rezaeian's stochastic model, and Dr. Yoshifumi Yamamoto for providing the synthetic ground motions and clarifying various parts of his dissertation. Finally, we are grateful to Professor Curt B. Haselton for providing us with computer models of the multistory buildings that were studied in this report, and to Dr. Frank McKenna for his advice on effective ways of implementing more than 40,000 response history analyses of multistory buildings in OpenSEES and on processing the results.

Table of Contents

List of Tables

List of Figures

List of Abbreviations

AS08 Abrahamson & Silva 2008

ASI Acceleration spectrum intensity

BA08 Boore & Atkinson 2008

BJ08 Baker & Jayaram 2008

CAV Cumulative absolute velocity

CB08 Campbell & Bozorgnia 2008

CCDF Complementary cumulative distribution function

CI Confidence interval

CS The Conditional Spectrum approach

CY08 Chiou & Youngs 2008

DBE Design basis earthquake

DSI Displacement spectrum intensity

EDP Engineering demand parameter

GCIM The Generalized Conditional Intensity Measure approach

GM Ground motion

GMPM Ground-motion-prediction model

GMSM Ground motion selection and modification

IDA Incremental Dynamic Analysis

IF Importance Function

IM Intensity measure

IMHC Intensity measure hazard curve

IMK Ibarra-Medina-Krawinkler

IS Importance Sampling

MCE Maximum considered earthquake

MFA Maximum (over all stories) peak floor accelerations

MSDR Maximum (over all stories) peak story drift ratios

MVLN Multivariate lognormal

OLS Ordinary least squares

PDF Probability density function

PEER Pacific Earthquake Engineering Research

PFA Peak floor accelerations

PFD Peak (over time) floor displacements

PGA Peak ground acceleration

PGD Peak ground displacement

PGV Peak ground velocity

PSDA Probabilistic seismic demand analysis

PSDR Peak story drift ratios

PSHA Probabilistic seismic hazard analysis

RHA Response history analysis

SDF Single-Degree-of-Freedom

SDHC Seismic demand hazard curve

TC06 Tothong & Cornell 2006

Chapter 1

Introduction

Nonlinear response history analyses (RHAs) play a major role in performance-based earthquake engineering (PBEE) of buildings. By performing RHAs of a computer model of the building subjected to an input ground motion [1], seismic demands can be computed to determine seismic demand hazard curves (SDHCs). In PBEE of buildings, the computed seismic demands are used as inputs to fragility functions for predicting (both structural and non-structural) damage [Porter et al., 2007]; e.g., SDHCs can be integrated with fragility functions to provide annual rates of damage exceedance. By predicting damage as a function of the seismic demand instead of the ground-motion intensity (e.g., peak ground acceleration, etc.), the resulting estimate of damage is more informative because the variability in the estimate is reduced. Similarly, losses due to earthquakes (e.g., repair costs, business downtime, casualties, etc.) may be better predicted (through consequence functions) with knowledge about the damage in buildings (see e.g., Section 3.9 in [Applied Technology Council, 2012]). Thus, nonlinear RHAs of building models are an important step in the estimation of losses due to earthquakes.

However, one of the key challenges in this approach is the selection and scaling of ground motions to serve as input excitations for nonlinear RHAs. Researchers have proposed many different ways to select ground motions. Some have proposed to select on the basis of matching seismological parameters for a given earthquake scenario [Chapman, 1995, Stewart et al., 2001, American Society of Civil Engineers, 2010] whereas others have suggested to select on the basis of spectral shape [Malhotra, 2003, Kottke and Rathje, 2008, Baker and Cornell, 2006b]. In fact, many different intensity measures (IMs) have been investigated and/or developed for selection purposes [Akkar and Özen, 2005, Riddell, 2007, Luco and Cornell, 2007, Yang et al., 2009, Kalkan and Chopra, 2011]. With such a wide variety of parameters to choose from, how does one identify those that are most desirable?

Regardless of the selection approach, ground motions are often scaled by factors of varying degrees before RHAs are performed. Although scaling offers the advantage of reducing the variability in the resulting demands [Shome et al., 1998], such modification of data raises

[1] In this report, the phrase "ground motion" refers to ground acceleration as a function of time, or ground motion time series.

many questions. For example, some researchers have argued that there is no need to limit the scale factors [Bommer and Acevedo, 2004, Watson-Lamprey and Abrahamson, 2006] and that scaling does not cause bias in the demands [Iervolino and Cornell, 2005]. On the other hand, some have found that scaling may induce bias, depending on how ground motions were selected [Luco and Bazzurro, 2007, Baker, 2007a]. Moreover, other researchers have suggested that the value of the results from scaling is questionable, providing limited if any information [Grigoriu, 2010].

The objectives of this report are as follows:

1. To develop a rigorous approach for evaluating SDHCs of a structure from any ground-motion selection and modification (GMSM) procedure.
2. To understand the underlying reasons why bias in the demands is observed in some cases but not in others, leading to conflicting conclusions in the literature.
3. To develop a rigorous procedure for selecting ground motions with the option of avoiding record scaling altogether.
4. To comprehensively evaluate contemporary GMSM procedures in their ability to provide accurate estimates of the SDHCs of a structure at a given site.

In Chapter 2, various objectives for performing RHAs are organized, leading to the objective of estimating SDHCs as the appropriate choice for rigorously evaluating GMSM procedures. The notion of a *benchmark* is introduced, and its importance in the context of evaluating GMSM procedures is discussed. It is found that the potential bias in any SDHC estimate is directly caused by hazard inconsistencies in the specific selection of ground motions with respect to IMs that are influential to the response. As long as ground motions are selected to be hazard-consistent with respect to a vector-valued IM that is sufficient, then the resulting SDHC estimates are unbiased, irrespective of the level of record scaling.

The framework developed in Chapter 2 is applied to synthetic ground motions in Chapter 3 in order to evaluate GMSM procedures for any structure and any response quantity of interest. Equipped with a rigorous benchmark, the relationship between SDHC bias, hazard consistency, and IM sufficiency is confirmed. Most importantly, the benchmark SDHC enables researchers to distinguish IMs (e.g., spectral shape, etc.) that are *insufficient* from those that are *approximately sufficient* for the response quantity of interest. Additionally, the issue of benchmark consistency arises for the first time as a consequence of evaluating GMSM procedures with synthetic ground motions; this issue is thoroughly addressed in this chapter.

In Chapter 4, an Importance Sampling-based ground-motion selection procedure is developed to take advantage of unscaled yet intense ground motions for estimating SDHCs. This procedure permits hazard consistency of the selected motions to be *directly* enforced

for a wide range of IMs and exceedance rates, through different choices of the Importance Function. Furthermore, the procedure enables SDHCs of a structure to be estimated from a *single* ensemble of ground motions. The chapter concludes with recommendations for inputs to this procedure: (i) vector of IMs for ground motion selection **IM**, (ii) number of ground motions to be selected for RHAs n, (iii) maximum acceptable scale factor SF_{max}, and (iv) target fraction of scaled ground motions γ.

Using the concept of a benchmark, as developed in Chapters 2-3, two state-of-the-art GMSM procedures – (i) "exact" Conditional Spectrum, and (ii) Generalized Conditional Intensity Measure (GCIM) – are comprehensively evaluated in Chapter 5. First, the implementation of each procedure for estimating SDHCs is summarized in a step-by-step form; these implementations can be quite involved, requiring several ensembles of ground motions to be iteratively selected until they are consistent with the target over a wide range of IMs. Second, the procedures are evaluated in their ability to accurately estimate SDHCs for several structural systems and response quantities at a given site. Typically, these state-of-the-art procedures provide excellent estimates of the SDHC; however, it is found that spectral shape can be *insufficient* for estimating the annual rate of collapse and for estimating floor accelerations. Furthermore, even a large vector of IMs that includes spectral accelerations, peak ground measures, spectrum intensities, and cumulative effects can be insufficient for estimating floor accelerations. Finally, the limitations of the bias-checking procedure in GCIM are identified, where it is shown that misleading conclusions may be obtained from the bias-checking procedure.

The Importance Sampling-based procedure from Chapter 4 is evaluated in Chapter 6. For the cases considered, the SDHCs from the Importance Sampling procedure are demonstrated to be unbiased for all systems and all response quantities when ground motions are not scaled. When the procedure is implemented with scaled ground motions, the resulting SDHCs are biased for a few of the cases considered. The epistemic uncertainty in the SDHC estimates from the Importance Sampling procedure is controlled primarily by the Importance Function and secondarily by the number of ground motions. Given a judiciously chosen Importance Function, the procedure greatly simplifies the problem of selecting ground motions for estimating SDHCs; the selection of the Importance Function is discussed in this chapter. Finally, the Importance Sampling procedure's ability to accurately estimate SDHCs for several structural systems from a *single* ensemble of ground motions is discussed.

Chapter 2

A framework for the evaluation of ground motion selection and modification procedures

2.1 Preview

This chapter develops a framework to evaluate ground motion selection and modification (GMSM) procedures. The context is probabilistic seismic demand analysis (PSDA), where response history analyses (RHAs) of a given structure, using ground motions determined by a GMSM procedure, are performed in order to estimate the seismic demand hazard curve (SDHC) for the structure at a given site. Currently, a GMSM procedure is evaluated in this context by comparing several resulting estimates of the SDHC, each derived from a different definition of the conditioning intensity measure (IM). Using a simple case study, we demonstrate that conclusions from such an approach are not always definitive; therefore, an alternative approach is desirable. In the alternative proposed herein, all estimates of the SDHC from GMSM procedures are compared against a benchmark SDHC under a common set of ground-motion information. This benchmark SDHC is determined by incorporating a prediction model for the seismic demand into the probabilistic seismic hazard analysis (PSHA) calculations. To develop an understanding of why one GMSM procedure may provide more accurate estimates of the SDHC than another procedure, we identify the role of "IM sufficiency" in the relationship between (1) bias in the SDHC estimate and (2) "hazard consistency" of the corresponding ground motions obtained from a GMSM procedure. Finally, we provide examples of how misleading conclusions may potentially be obtained from erroneous implementations of the proposed framework.

2.2 Introduction

Ground-motion selection and modification (GMSM) procedures determine the necessary input ground motions for response history analyses (RHAs) of structures. Response history analyses of a structure are often performed in order to estimate the seismic demands, for

one or more engineering demand parameters [1] (EDPs), resulting from a given ensemble of ground motions. The modification of ground motions can be classified into two approaches: (1) amplitude scaling and (2) spectrum matching in the time or frequency domains. The framework developed herein applies primarily to the former and secondarily to the latter.

Many different GMSM procedures are available in the literature. Some select and scale on the basis of scalar intensity measures (IMs). For instance, the spectral acceleration [2] at the fundamental period of the structure, $A(T_1)$, is a popular choice as an IM for record scaling (e.g., [Watson-Lamprey and Abrahamson, 2006, Shome et al., 1998]). Alternative choices for such scalar IMs include the peak deformation of inelastic single-degree-of-freedom (SDF) systems (e.g., [Tothong and Luco, 2007, Luco and Cornell, 2007, Kalkan and Chopra, 2011]). Several procedures select and scale ground motions on the basis of vector-valued IMs. For example, selecting records whose response spectra most closely matches a target spectrum is a common approach (e.g., [Kottke and Rathje, 2008, Baker, 2011]). A review of various GMSM procedures is provided in Appendix A of [PEER GMSM Working Group, 2009] and in [Katsanos et al., 2010].

There has been much interest in evaluating GMSM procedures. For example, the Pacific Earthquake Engineering Research (PEER) GMSM working group [PEER GMSM Working Group, 2009], Heo et al. [Heo et al., 2010], and Hancock et al. [Hancock et al., 2008] all compared estimates of the median demand of a structure, from RHAs for ground motions determined by GMSM methods, against a 'benchmark' that is defined differently in each of these studies. In the first study, the benchmark is derived from a regression model of the EDP as a function of IMs and the regression is applied to both scaled and unscaled ground motions; this benchmark is referred to as the Point-Of-Comparison [Watson-Lamprey, 2007, PEER GMSM Working Group, 2009]. In the study by Heo et al., the benchmark is also derived from a regression model of the EDP as a function of IMs; however, the regression is applied to only unscaled ground motions. Hancock et al. derive the benchmark from a regression model of the EDP as a function of seismological parameters (i.e., earthquake magnitude, distance, etc.), and the regression is applied to only unscaled ground motions.

In order to meaningfully evaluate GMSM procedures, the objective of the associated RHAs of the structure must be clearly stated. For example, researchers have been interested in probability distributions of the demand for a given:

1. earthquake scenario;
2. ground-motion scenario;
3. intensity level; and
4. time frame.

[1] 'Engineering demand parameter' is a synonym for 'response quantity'.

[2] In this document, "spectral acceleration" refers to the pseudo-acceleration [Chopra, 2011] for 5% damping corresponding to the arbitrary horizontal component of ground motion [Baker and Cornell, 2006c].

The PEER GMSM working group considered the estimation of the median and the complete distribution of 1 and 2 as four separate objectives of GMSM methods [PEER GMSM Working Group, 2009]. They define an *earthquake scenario* as an earthquake with a specific magnitude, M, distance, R, and rupture information (e.g., style of faulting, dip angle, shear wave velocity of the site, etc.) and a *ground motion scenario* as an earthquake scenario with a specified value of $A(T_1)$. Herein we use *rupture scenario* as a synonym for earthquake scenario.

The estimation of distributions 1 and 3 above are referred to as a scenario-based assessment and an intensity-based assessment, respectively [Applied Technology Council, 2012, NEHRP Consultants Joint Venture, 2011]. In an intensity-based assessment, the IM may be defined as a scalar or a vector; for example, it may be defined as the spectral acceleration at one vibration period or at several periods (i.e., a response spectrum). The estimation of distribution 4 is known as a time-based assessment, where the specified time frame depends on the needs of decision makers (e.g., one year, 50 years, etc.) [Applied Technology Council, 2012], and the probabilities are converted from annual rates of exceedance based on an assumption of earthquake occurrence in time [3] [McGuire, 2004]. The process of determining these exceedance rates, or seismic demand hazard curves (SDHCs), is known as a risk-based assessment [NEHRP Consultants Joint Venture, 2011], or a probabilistic seismic demand analysis (PSDA) [Shome, 1999].

This study develops a framework for evaluating GMSM procedures in the context of PSDA. This choice is motivated by the fact that for a given structure at a given site, distributions 1-3 above are not "unique"; for example, different versions of distribution 3 exist for different definitions of the IM and for different intensity levels under consideration [Bradley, 2013a]. In contrast, the SDHC from PSDA is unique for a given structure at a given site [Bradley, 2012c].

In the proposed framework, all estimates of the SDHC from GMSM procedures are compared against a benchmark SDHC under a common set of ground motion information. The benchmark SDHC is determined by incorporating an EDP prediction model that is developed from unmodified ground motions into the probabilistic seismic hazard analysis (PSHA) calculations. Currently, a GMSM procedure is evaluated in the context of PSDA by comparing several resulting estimates of the SDHC, each derived from a different definition of the conditioning IM. To illustrate an important but subtle limitation of this approach, PSDA is critically examined next and a simple structural model at a realistic site is chosen as the case study.

2.3 Probabilistic Seismic Demand Analysis

The objective of performing RHAs in PSDA is to develop a SDHC for a given structure at a given site. Denoted by the symbol $\lambda_{EDP}(z)$, a SDHC is a plot of the annual rate of exceedance, λ, against the seismic demand; it is similar to a traditional hazard curve in PSHA

[3] In this study, all conversions are made with the Poisson assumption.

except that the IM on the horizontal axis has been replaced by the EDP. Once developed, SDHCs are used to: (1) determine the annual rate of seismic demand exceeding a particular structural capacity, or (2) determine the seismic demand associated with a specified annual rate of exceedance.

The SDHC is governed by (see e.g., [Shome et al., 1998, Baker and Cornell, 2005, Bradley, 2012c]):

$$\lambda_{EDP}(z) = \int \Pr(EDP > z \mid IM = x) \cdot |\mathrm{d}\lambda_{IM}(x)| \tag{2.1}$$

where $\Pr(EDP > z \mid IM = x)$ is the probability of EDP exceeding demand level z given intensity level x, and $\lambda_{IM}(x)$ is the intensity measure hazard curve (IMHC). In Equation 2.1, the IM is often defined as the spectral acceleration at a conditioning period of vibration, T^*, while the EDP is commonly defined as the maximum story drift ratio over all stories of a multistory building [Lin et al., 2013b]. However, the IM may be defined in many different ways. For example, it may be defined as peak ground acceleration (PGA), peak ground velocity (PGV), or significant duration [Bradley, 2012c]. Alternatively, it may be defined as a vector of IMs (e.g., $\{A(T_1), M\}$, or $\{A(T_1), \epsilon(T_1)\}$, where $\epsilon(T_1)$ is the number of standard deviations between the observed and the predicted value of $A(T_1)$); if it is defined as a vector, then Equation 2.1 needs to be modified appropriately [Baker and Cornell, 2005]. Note that Equation 2.1 has been extended to consider a vector of EDPs (e.g., drift ratios for individual stories, etc.) [Bradley, 2012c] and to account for the possibility of structural collapses (see e.g., [Shome, 1999, Baker and Cornell, 2005, Lin et al., 2013b]); however, these extensions are beyond the scope of this study.

The SDHC is typically computed from the following equation:

$$\widehat{\lambda}_{EDP}(z) = \sum_{i=1}^{N_{IM}} \widehat{\Pr}(EDP > z \mid IM = x_i) \cdot |\Delta\widetilde{\lambda}_{IM}(x_i)| \tag{2.2}$$

where N_{IM} is the number of intensity levels considered, and x_i is the i^{th} intensity level; $\Delta\widetilde{\lambda}_{IM}(x_i)$ is the discrete form of $|\mathrm{d}\lambda_{IM}(x)|$, which is obtained from PSHA, while $\widehat{\Pr}(EDP > z \mid IM = x_i)$ is the discrete form of $\Pr(EDP > z \mid IM = x)$, which is computed from RHAs of the structure. The 'hat' symbols in Equation 2.2 serve to emphasize that the quantities computed are *estimates* (of the corresponding exact quantities in Equation 2.1) that depend primarily on the particular choice of ground motions selected for RHAs of the structure. This implies that different GMSM procedures lead to different estimates of the SDHC. The meaning of the tilde symbol in $\widetilde{\lambda}_{IM}(x_i)$ will become evident in Section 2.4.

The steps to compute a SDHC in PSDA, when $IM \equiv A(T^*)$ are schematically illustrated in Figure 2.1. The IMHC for $A(T^*)$ is shown in Figure 2.1a. The number of intensity levels, N_{IM}, is chosen to satisfactorily approximate the integral and $|\mathrm{d}\lambda_{IM}(x)|$ in Equation 2.1. For illustration only, Figure 2.1a shows three intensity levels and the discrete form of $|\mathrm{d}\lambda_{IM}(x)|$ at intensity level x_o.

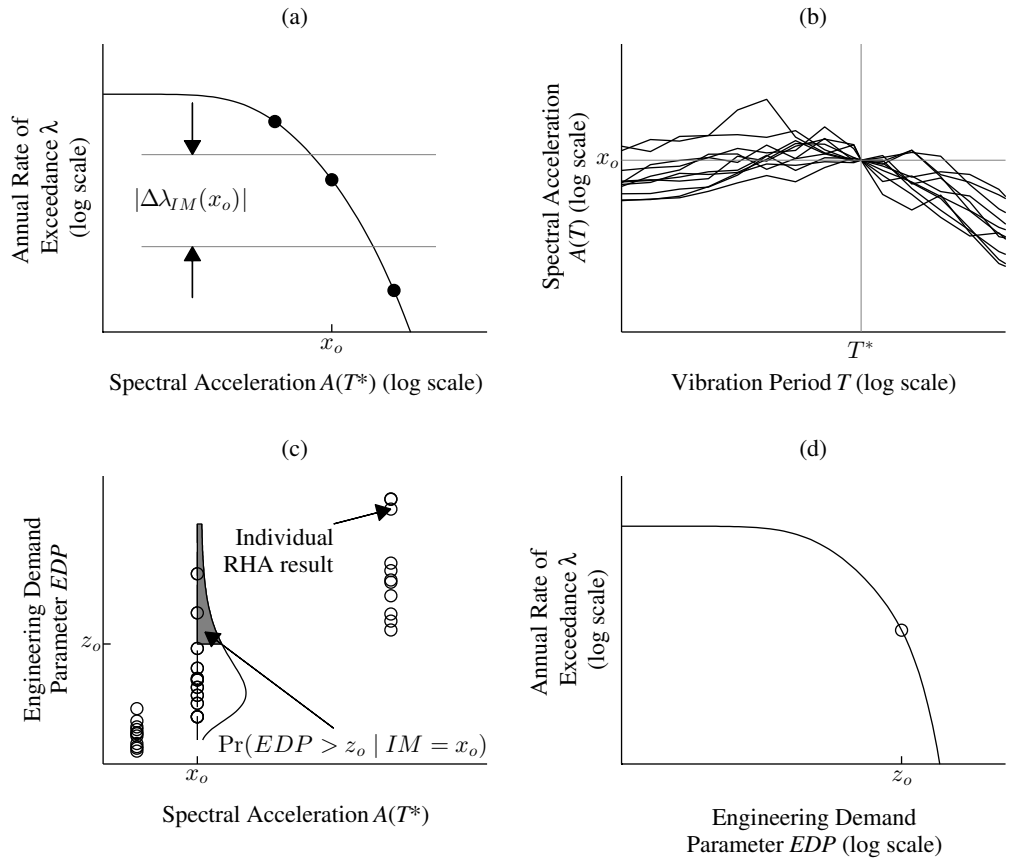

Figure 2.1: The elements of PSDA when $IM \equiv A(T^*)$: (a) discretization of the IMHC, $\lambda_{IM}(x)$; (b) ground motions selected and scaled such that $IM = x_o$; (c) estimation of $\Pr(EDP > z \mid IM = x)$ from RHAs of the structure; and (d) resulting SDHC, $\lambda_{EDP}(z)$.

For each i^{th} intensity level, an intensity-based assessment of seismic demand is conducted to determine $\widehat{\Pr}(EDP > z \mid IM = x_i)$. First, an ensemble of scaled ground motions is selected as excitations for RHAs of the system. Recorded ground motions are often scaled because the record-to-record variability of interest is conditioned so that the IM is exactly equal to x_i. Consequently, all candidate ground motions are first scaled, so that $IM = x_i$, before a subset of them are selected as excitations for RHAs of the structure. For example, the response spectra of one such ensemble, with each ground motion scaled to satisfy $A(T^*) = x_o$, are shown in Figure 2.1b.

Next, RHAs of the structure are performed for the selected ensemble, and the computed values of EDPs are processed by statistical inference methods. The list of EDPs corresponding to the ensemble in Figure 2.1b is depicted as circles above $A(T^*) = x_o$ in Figure 2.1c. A lognormal distribution is used to model $\Pr(EDP > z \mid IM = x_i)$, and the two parameters of this distribution are estimated by the mean, $\widehat{\mu}_{\ln EDP}$, and standard deviation, $\widehat{\sigma}_{\ln EDP}$, of

the list of logarithmic EDPs [Baker, 2007b, Wasserman, 2004]:

$$\widehat{\Pr}(EDP > z \mid IM = x_i) = 1 - \Phi\left(\frac{\ln z - \widehat{\mu}_{\ln EDP}}{\widehat{\sigma}_{\ln EDP}}\right) \tag{2.3}$$

where $\Phi(\cdot)$ denotes the cumulative distribution function of the standard normal distribution. For illustration, the probability of EDP exceeding z_o given intensity x_o is shown as the shaded area in Figure 2.1c. Although a lognormal distribution is commonly employed, an alternative is to apply nonparametric inference to the results from RHAs [Vamvatsikos and Cornell, 2004, Baker, 2007b]:

$$\widehat{\Pr}(EDP > z \mid IM = x_i) = \frac{1}{n}\sum_{l=1}^{n} I(z_l > z) \tag{2.4}$$

where n is the number of records selected for intensity level x_i, z_l is the value of EDP for the l^{th} record, and $I(\cdot)$ denotes the indicator function (i.e., $I(z_l > z) = 1$ only if $z_l > z$; otherwise, it is equal to zero); we will revisit Equation 2.4 in Section 2.7.

To illustrate how a GMSM procedure is utilized to estimate a SDHC in PSDA, first consider how to estimate the annual rate of the EDP exceeding some demand level, say z_o. Substituting $\widehat{\Pr}(EDP > z_o \mid IM = x_i)$, computed from either Eqs 2.3 or 2.4, in Equation 2.2 leads to $\widehat{\lambda}_{EDP}(z_o)$, which is identified by the circle in Figure 2.1d. Repeating such calculations for all demand levels leads to the SDHC shown in Figure 2.1d.

How can we evaluate a GMSM procedure in its ability to provide 'unbiased' estimates of the SDHC? We define a SDHC estimate to be *unbiased* or *accurate* if it is practically equal to the SDHC from Equation 2.1 (i.e., $\widehat{\lambda}_{EDP}(z) \approx \lambda_{EDP}(z)$); otherwise, it is *biased* or *inaccurate* (i.e., $\widehat{\lambda}_{EDP}(z) \neq \lambda_{EDP}(z)$). Two approaches have been proposed to assess whether the resulting SDHC estimates from a given GMSM procedure are biased or not:

1. Compare the SDHC estimate from Equation 2.2, which is based on a scalar IM, against another estimate from a version of Equation 2.2 where the IM is vector-valued. If the two estimates are appreciably different, then they are biased; if they are practically equal to each other, then they are unbiased [Baker and Cornell, 2006b].

2. Compare the SDHC estimate from Equation 2.2, based on one definition of the scalar IM, against another estimate from Equation 2.2, based on a different definition of the scalar IM. If the two estimates are practically equal to each other, then they are unbiased [Bradley, 2012c, Lin et al., 2013b].

As will be demonstrated later, the two approaches above are not always adequate for definitively evaluating a GMSM procedure in its ability to provide unbiased estimates of the SDHC. Since Equation 2.1 is valid for any definition of the IM, $\lambda_{EDP}(z)$ determined from Equation 2.1 for one definition must be identical to $\lambda_{EDP}(z)$ determined from Equation 2.1

for another definition. Therefore, if SDHC estimates from a GMSM procedure are unbiased, then $\widehat{\lambda}_{EDP}(z)$ computed from Equation 2.2 for one definition of the IM must be practically equal to another estimate from Equation 2.2 for a different definition of the IM. However, the converse of this statement is not true: the fact that the two SDHC estimates (corresponding to two different IMs) are practically equal to each other does not *necessarily* imply that SDHC estimates from the GMSM procedure are unbiased. This subtle but important limitation is illustrated next with a simple case study.

2.4 Case Study

Site, Structural Model, and Engineering Demand Parameter

The University of California, Berkeley is selected as the example site. Its latitude and longitude coordinates are 37.876 °N and 122.251 °W, respectively. The shear wave velocity, V_{s30}, is specified as 600 m/sec, and the basin depths, $Z_{1.0}$ and $Z_{2.5}$, are specified as 0.1 and 1 km respectively. OpenSHA [Field et al., 2005] is used to perform PSHA; the "USGS/CGS 2002 Adj. Cal. ERF" model is chosen for the earthquake rupture forecast, 5 km is specified for the rupture offset, and background seismicity is excluded.

The selected system is a 5% damped bilinear SDF model with 5% post-yield hardening. Its natural period of small-amplitude vibration, T_1, is 1 sec and its yield displacement, u_y, is $0.2g \times (T_1/2\pi)^2$. The EDP of interest is its peak deformation, u_m. We estimate the SDHC for this particular response quantity using RHAs of the system due to ground motions determined by a GMSM procedure as follows.

Intensity Measure Hazard Curve

The IMHC shown schematically in Figure 2.1a is obtained from PSHA for a given site. It is governed by the standard equation (see e.g., [McGuire, 2004]):

$$\lambda_{IM}(x) = \sum_{i=1}^{N_{src}} \nu_i \cdot \left\{ \int\int \Pr(IM > x \mid M = m, R = r) f_{R|M}(r \mid m) f_M(m)\, \mathrm{d}r\, \mathrm{d}m \right\}_i \qquad (2.5)$$

where N_{src} is the number of earthquake sources, ν_i is the activity rate for the i^{th} earthquake source, $\Pr(IM > x \mid M = m, R = r)$ is the probability of IM exceeding level x for a given earthquake scenario, $f_{R|M}(r \mid m)$ is the probability density function (PDF) of distance for a given magnitude, and $f_M(m)$ is the PDF of magnitude. The activity rate, magnitude PDF, and distance PDF for each of the N_{src} earthquake sources are supplied by an *earthquake rupture forecast*, whereas the probability distribution of IM for a given earthquake scenario is obtained from a ground-motion-prediction model (GMPM) [4].

[4] GMPMs are also known as "ground-motion-prediction equations" (GMPEs) and were formerly referred to as "attenuation relationships". In the context of GMPMs, the phrase "ground motion" refers to an IM whereas in the rest of this study, the phrase refers to ground acceleration as a function of time; the two different uses of "ground motion" should be clear from the context.

In practice, $\lambda_{IM}(x)$ in Equation 2.5 is computed from the following equation:

$$\widetilde{\lambda}_{IM}(x) = \sum_{i=1}^{N_{src}} \nu_i \cdot \left\{ \sum_m \sum_r \widetilde{\Pr}(IM > x \mid M = m, R = r) \Pr(M = m, R = r) \right\}_i \qquad (2.6)$$

Comparing Equation 2.5 against Equation 2.6, we see that the integrals have been replaced with summations, the PDFs have been replaced with a joint probability mass function, and two expressions have been annotated with tilde symbols. Similar to Equation 2.2, the tilde symbols in Equation 2.6 serve to emphasize the fact that the quantities computed are *estimates* (of the corresponding exact quantities in Equation 2.5) that depend primarily on the particular set of ground motions selected in developing the GMPM. Consequently, different GMPMs lead to different estimates of the IMHC, $\widetilde{\lambda}_{IM}(x)$.

Four estimates of an IMHC at the selected site – for two definitions of the conditioning IM – are presented in Figure 2.2. They correspond to four GMPMs: (1) Campbell & Bozorgnia 2008 (CB08) [Campbell and Bozorgnia, 2008], (2) Boore & Atkinson 2008 (BA08) [Boore and Atkinson, 2008], (3) Abrahamson & Silva 2008 (AS08) [Abrahamson and Silva, 2008], and (4) Chiou & Youngs 2008 (CY08) [Chiou and Youngs, 2008]; the differences among the four IMHC estimates are apparent. Which IMHC should one choose to proceed? This question is answered in Section 2.6 but for now, the CB08 model is chosen, and the resulting IMHC is discretized to compute $\Delta\widetilde{\lambda}_{IM}(x_i)$ in Equation 2.2. For each conditioning IM, the IMHC is discretized with $N_{IM} = 11$ intensity levels corresponding to 11 hazard levels: 99%, 80%, 50%, 20%, 10%, 5%, 2%, 1%, 0.5%, 0.2%, and 0.1% probability of exceedance in 50 years, which are identical to those in [Bradley, 2012c]. For each intensity level, $\widehat{\Pr}(EDP > z \mid A(T^*) = x_i)$ is obtained from an intensity-based assessment (Figure 2.1c).

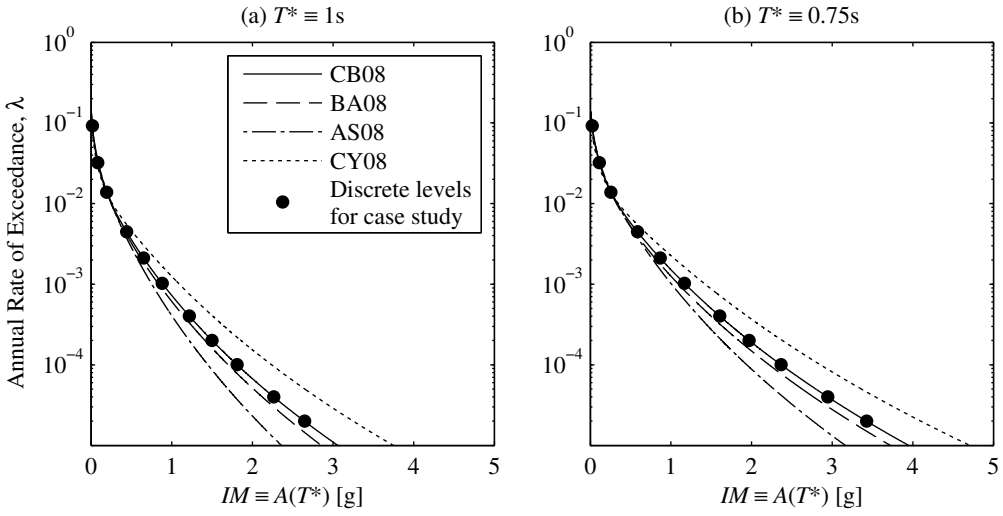

Figure 2.2: Four estimates of the IMHC for the conditioning IM in Equation 2.2: (a) $IM \equiv A(1sec)$; and (b) $IM \equiv A(0.75sec)$.

Intensity-Based Assessment

As shown in Figure 2.1, a single intensity-based assessment involves (1) ground-motion selection (Figure 2.1b), (2) RHAs of the structural system due to the selected ensemble (Figure 2.1c), and (3) statistical inference (Figure 2.1c), at a specified intensity level. In this case study, each intensity-based assessment computes $\widehat{\Pr}(EDP > z \mid A(T^*) = x_i)$ from Equation 2.3, using the results from RHAs of the structure for $n = 44$ ground motions. To illustrate the limitation of the two approaches for evaluating GMSM procedures (mentioned at the end of Section 2.3), we select two GMSM procedures: (1) Incremental Dynamic Analysis (IDA) [Vamvatsikos and Cornell, 2002], and (2) a special case of the Generalized Conditional Intensity Measure approach (GCIM) [Bradley, 2010a, Bradley, 2012a, Bradley, 2012c]. In IDA, a single 'seed' ensemble of ground motions is scaled to multiple intensity levels; here, the Far-Field record set from FEMA P695 [Applied Technology Council, 2009], which contains $n = 44$ records from the PEER Next-Generation Attenuation database [Power et al., 2008], is selected as the seed ensemble. Since some readers may not be familiar with GCIM, which is a generalization of the Conditional Spectrum approach (CS) [Jayaram et al., 2011], we will first briefly review CS and then identify the generalizations that led to GCIM.

Figure 2.3 schematically illustrates the steps involved in CS-based ground-motion selection at some particular intensity level, say x_o from Figure 2.1. First, the seismic hazard at $A(T^*) \approx x_o$ is deaggregated [McGuire, 1995] to obtain the percent contribution to the hazard from an earthquake with magnitude M at distance R; it is summarized by a mean M and a mean R (Figure 2.3a). The US Geological Survey online hazard tool provides deaggregation for $A(T^*) > x_o$ [Bazzurro and Cornell, 1999], thus requiring an additional step to convert the results to obtain deaggregation for $A(T^*) \approx x_o$ [Baker and Cornell, 2005].

Next, the probability distribution of response spectrum, for a given earthquake scenario with mean M at mean R, is determined (Figure 2.3b). For a given vibration period, T, the probability distribution is modeled with a lognormal distribution and its two parameters are obtained from a selected GMPM. The mean values of M and R from deaggregation (Figure 2.3a) are used as inputs to this GMPM; other inputs (e.g., style of faulting, dip, etc.) are inferred [Baker, 2011]. For example, a GMPM provides the median and one-sigma response spectra, which are shown in Figure 2.3b as solid and chain lines, respectively. In practice, the distribution of response spectrum is determined for a specific range of vibration periods, which are denoted as $\mathbf{T}_{IM}$ in Figure 2.3b; typically, T^* is equal to T_1, and $\mathbf{T}_{IM}$ consists of 50 logarithmically spaced periods between $0.2T_1$ to $2T_1$ [Baker, 2011].

For a given rupture scenario, the collection of spectral acceleration values at vibration periods $\mathbf{T}_{IM}$ is viewed as a random vector. Due to lognormality, the logarithm of the response spectrum follows a multivariate normal distribution [Jayaram and Baker, 2008]. In order to specify the covariance matrix for this distribution, the correlations between spectral ordinates at different vibration periods are needed and are available in the literature [Baker and Cornell, 2006a, Baker and Jayaram, 2008]. An example of this multivariate normal distribution is schematically shown in Figure 2.3b. When $A(T^*)$ is conditioned to be equal to x_o, the logarithm of the response spectrum still follows a multivariate normal distribution

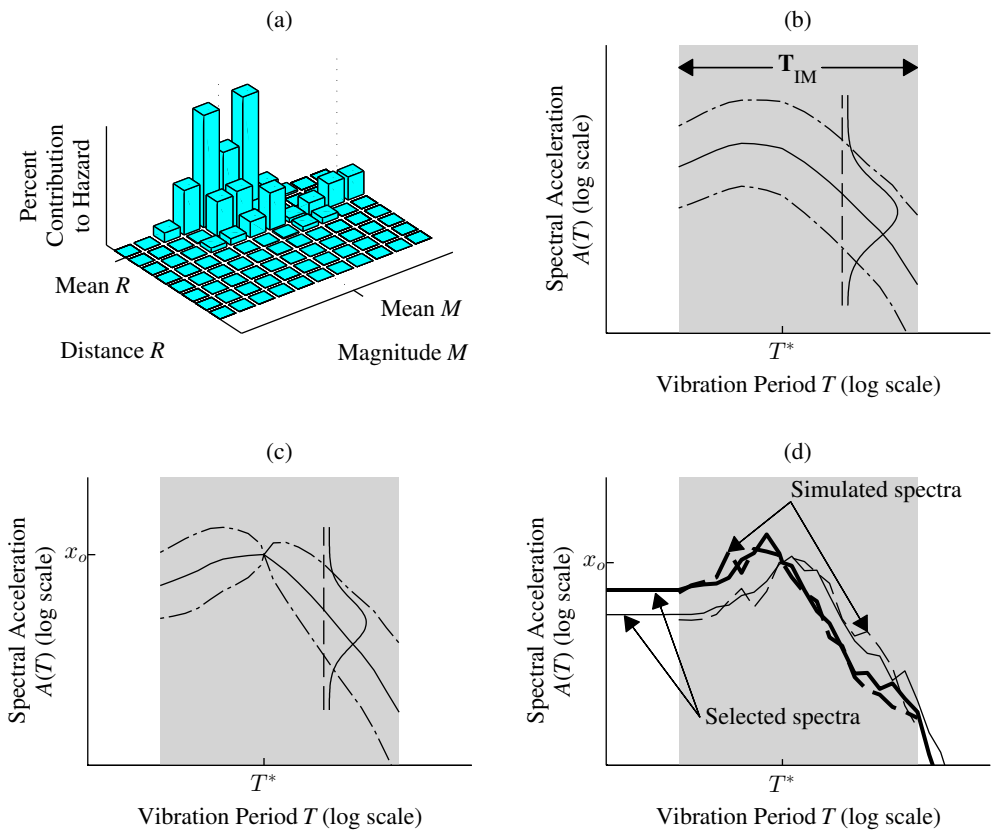

Figure 2.3: Schematic illustration of the Conditional Spectra approach [Jayaram et al., 2011] to ground motion selection at some particular intensity level, say x_o, of $IM \equiv A(T^*)$: (a) deaggregation to determine mean M and mean R; (b) definition of $\mathbf{T}_{IM}$ and marginal distributions of $A(T)$ from a single GMPM for a given earthquake scenario with mean M at mean R; (c) Conditional Spectrum; and (d) ground motion selection based on comparing recorded against simulated response spectra.

but with different parameters [Jayaram et al., 2011]; this is illustrated in Figure 2.3c.

Suppose n records are desired to estimate $\Pr(EDP > z \mid A(T^*) = x_o)$. To select these records, all candidate motions are first scaled so that $A(T^*) = x_o$. Then, n response spectra are randomly generated (Figure 2.3d) from the multivariate normal distribution in Figure 2.3c. For each simulated spectrum, a record whose scaled response spectrum most closely matches the simulated one is selected (Figure 2.3d). Such matching is quantified by the sum-of-squared-errors metric in CS [Jayaram et al., 2011]. Because ground motions are matched to randomly generated response spectra, the ensemble obtained from a single implementation of CS is *not* unique.

GCIM generalizes CS in four main aspects. First, GCIM considers IMs in addition to spectral accelerations for record selection. Consistent with the notation employed in [Bradley,

2010a], the complete vector of IMs for selection is denoted as **IM**, the conditioning scalar IM used for record scaling is denoted as IM_j, and all IMs that are not used for record scaling but are used for selection are denoted as $\mathbf{IM}_i$; that is, $\mathbf{IM} = \{IM_j, \mathbf{IM}_i\}$. Thus, PGA, PGV, or significant duration are all valid options for specifying IM_j or any element of $\mathbf{IM}_i$. Second, GCIM offers the option of weighting IMs. Third, a more sophisticated version of the target spectrum than that shown in Figure 2.3c is derived in GCIM. Instead of the mean M-R, the conditional distribution in Figure 2.3c is computed for *each and every* scenario in Figure 2.3a, and the percent contributions are used to combine all such distributions [Bradley, 2010a]; this feature avoids the need to inflate standard deviations in CS [Lin et al., 2013b]. Fourth, the variability of IM_i, for a given value of IM_j, is incorporated into the sum-of-squared-errors metric for the selection of records.

In the special case of GCIM chosen herein, denoted by GCIM-SA, **IM** comprises spectral accelerations with all periods equally weighted (i.e., $\mathbf{IM} \equiv \{A(T^*), A(\mathbf{T}_{IM_i})\}$). As a result, GCIM-SA differs from CS only in (1) the construction of the target spectrum and (2) the metric utilized for record selection. For each intensity level, the GCIM-SA target spectrum and the n corresponding simulated response spectra (Figure 2.3d) are obtained from Bradley's GCIM application in OpenSHA [Bradley, 2012a]; the model by Baker & Jayaram 2008 (BJ08) [Baker and Jayaram, 2008] is used to determine the correlations between spectral ordinates at different vibration periods. For each of the n simulated spectra, the record whose response spectrum most closely matches the simulated one, which is quantified by the generalized metric in GCIM (Eq 10 in [Bradley, 2012a]), is selected from the PEER Next-Generation Attenuation database (Figure 2.3d) [5]. As in CS, the selected ensemble obtained from a single implementation of GCIM-SA is not unique.

As an example of the GCIM-SA target spectrum, the one for $IM_j \equiv A(1s)$ at 2% probability of exceedance in 50 years, computed with the CB08 model, is shown in Figure 2.4 as dark solid lines. As illustrated in the figure, it is computed at 11 vibration periods: $\mathbf{T}_{IM} = \{0.05, 0.1, 0.2, 0.3, 0.5, 0.75, 1, 2, 3, 5, 10\}$. Unlike the target spectrum from CS, the one from GCIM-SA does not follow a multivariate normal distribution. Hence, the median (Figure 2.4a) and the interquartile range (Figure 2.4b) are employed to summarize the probability distribution of response spectrum; the median $A(T)$ corresponds to a probability of 0.50, whereas the interquartile range of $A(T)$ refers to the difference between the values of $A(T)$ at two probabilities: (1) 0.75 and (2) 0.25.

Figure 2.4 also depicts the GCIM-SA target spectrum computed from three other GMPMs: (1) BA08, (2) AS08, and (3) CY08. Although each of the four targets corresponds to the same probability of exceedance, the conditioning value of $A(1s)$ is different, as seen in Figure 2.4a and in Figure 2.2a. Furthermore, the differences among the four interquartile ranges are apparent, which is especially noticeable at short vibration periods in Figure 2.4b. Since the CB08 model was already chosen for determining $|\Delta\widetilde{\lambda}_{IM}(x_i)|$ in Equation 2.2 (Figure 2.2a) and conducting deaggregation (Figure 2.3a), it is also chosen for the construction

[5] Instead of selecting scaled ground motions, note that ground motions from the PEER database may be spectrum matched to each of these simulated spectra [Seifried, 2013].

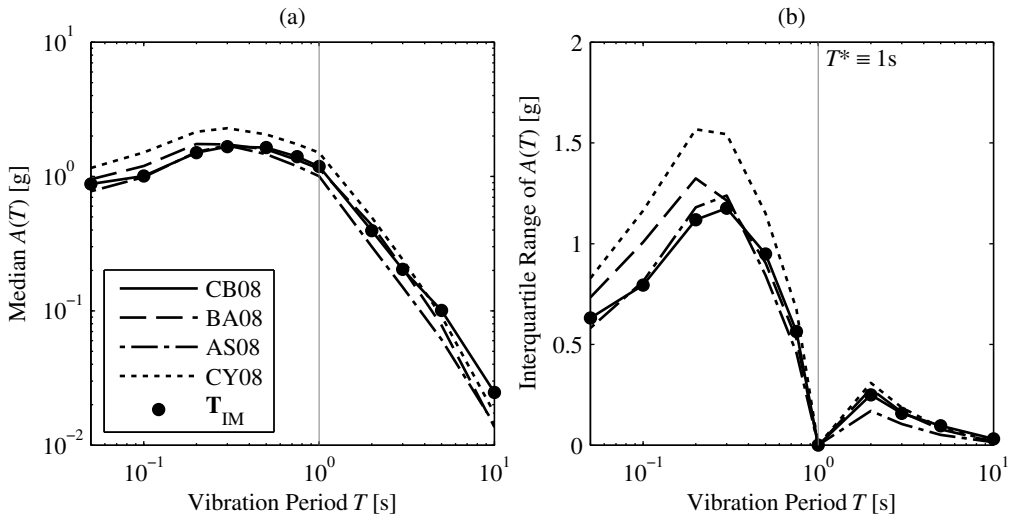

Figure 2.4: Target conditional response spectra from GCIM-SA for $IM_j \equiv A(1s)$ at 2% probability of exceedance in 50 years: (a) median $A(T)$; and (b) interquartile range of $A(T)$.

of the target spectrum in this case study; hence, GCIM-SA also differs from the "exact CS", where the target spectra is determined from multiple GMPMs [Lin et al., 2013a, Carlton and Abrahamson, 2014].

Seismic Demand Hazard Curve

Figure 2.5 presents estimates of the SDHC from IDA and from GCIM-SA for three different definitions of the conditioning IM. For each scalar IM and each GMSM procedure, the SDHC estimate was computed from Equation 2.2 (Figure 2.1); in total, $N_{IM_j} \times 2 = 22$ deaggegrations were conducted and $N_{IM_j} \times n \times 2 \times 2 = 1936$ RHAs were performed. For the vector-valued IM, the SDHC estimates are obtained by the approach outlined in [Baker and Cornell, 2005]. Note that the results correspond to highly inelastic behavior and are meaningful only at exceedance rates above around 2×10^{-5} because the lowest probability of exceedance considered in the discretization is 0.1% in 50 years. To facilitate interpretation of these curves, the guidelines corresponding to the design basis earthquake (DBE) and maximum considered earthquake (MCE) levels are also provided [6].

According to approach 2 at the end of Section 2.3, Figure 2.5 suggests that the IDA estimates are more accurate [7] than the GCIM-SA estimates. For both GMSM procedures, the SDHC estimate from $A(1s)$ is noticeably different than that from $A(0.75s)$ at exceedance rates below the MCE level. However, the difference between these two SDHC estimates, which corresponds to two different definitions of T^*, is smaller for IDA than for GCIM-SA.

[6] The DBE level corresponds to a rate of 2×10^{-3} and a return period of 475 years; the MCE level corresponds to a rate of 4×10^{-4} and a return period of 2475 years.

[7] Recall that the concepts of 'accuracy' and 'bias' were defined at the end of Section 2.3.

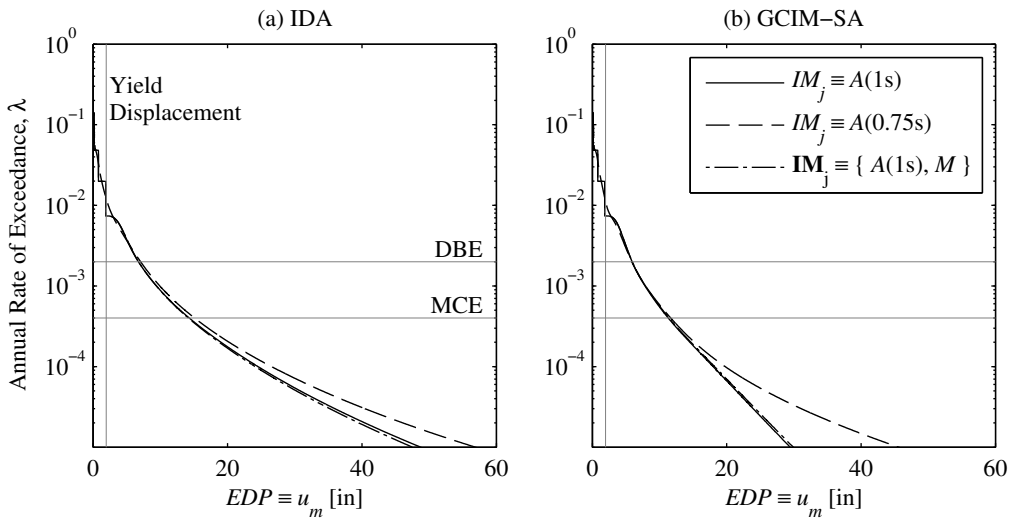

Figure 2.5: Estimates of the SDHC from PSDA, for three different conditioning IMs: (a) IDA; and (b) GCIM-SA.

Based on this observation alone, the IDA estimates appear to be more accurate than those from GCIM-SA.

Approach 1 at the end of Section 2.3 leads to a different conclusion. For each GMSM procedure, the SDHC estimate from $A(1s)$ is practically equal to that from $\{A(1s), M\}$. Based on this observation alone, *both* GMSM procedures seem to produce unbiased estimates of the SDHC. However, the IDA estimate for $A(1s)$ is significantly different than the GCIM-SA estimate for $A(1s)$, contradicting the claim that both SDHC estimates are unbiased.

Since the ground motions from GCIM-SA are scaled much more severely than those from IDA in Figure 2.5, it is not immediately obvious as to which of the two GMSM procedures provides more accurate estimates of the SDHC. For example, consider the scale factors that were employed to compute the SDHCs in Figure 2.5 corresponding to $IM_j \equiv A(1s)$. These scale factors are shown in Figure 2.6; observe that at each intensity level, the median scale factor from GCIM-SA is larger than that from IDA. If one started with the preconceived notion that small scale factors are desirable, then one would conclude that IDA is the more preferable procedure. As will be demonstrated later in Section 2.7 however, the results from GCIM-SA are more accurate than those from IDA, despite the fact that larger scale factors were employed.

The preceding discussion considered only two definitions of the conditioning IM when implementing each of the two approaches at the end of Section 2.3. This was done solely to emphasize a subtle point: the practical equality between two SDHCs from different conditioning IMs does not *necessarily* indicate that an unbiased SDHC has been obtained. In practical implementation of these two approaches, many more definitions of the conditioning

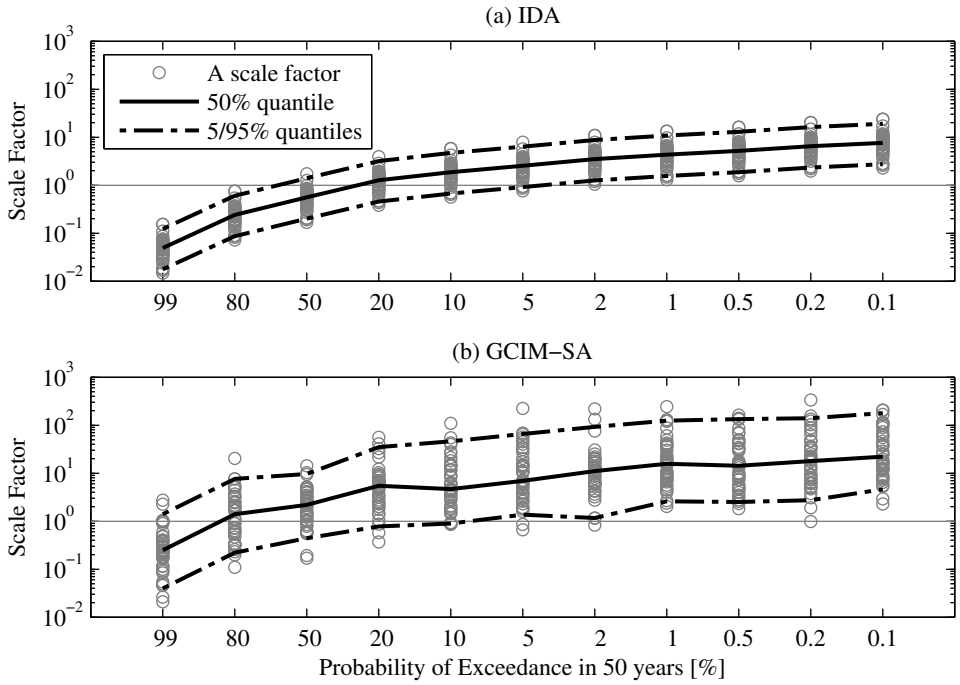

Figure 2.6: Scale factors employed in PSDA when $IM_j \equiv A(1s)$; in each panel, $n = 44$ scale factors are shown for each of the $N_{IM_j} = 11$ intensity levels: (a) IDA and (b) GCIM-SA.

IM than those shown in Figure 2.5 are considered before conclusions are drawn. For example, several significantly different scalar IMs were considered when implementing approach 2 in [Bradley, 2012c] and in [Lin et al., 2013b]. It is important to note however, that as more definitions of IM_j are considered, more RHAs are necessary in the evaluation because for one definition of IM_j and one GMSM procedure, a total of $N_{IM_j} \times n$ RHAs are required to compute the SDHC. To supplement the two approaches at the end of Section 2.3 when evaluating GMSM procedures and to quantify bias in any estimate of the SDHC, we propose an alternative approach that involves the notion of a benchmark SDHC.

2.5 The Benchmark Seismic Demand Hazard Curve

Instead of choosing definitions for the conditioning IM in order to evaluate the accuracy of SDHC estimates from GMSM procedures (Figure 2.5), we propose to compare such estimates against a benchmark SDHC that is developed from unmodified ground motions. The benchmark SDHC is determined by accounting for all plausible rupture scenarios near the site, as is done in PSHA. Comparing the SDHCs in Figure 2.5 against the IMHCs in Figure 2.2, we see that EDP in PSDA plays the same role as IM in PSHA. Thus, if we replace the IM in Equation 2.6 by the EDP, then the benchmark SDHC may be computed from the following

equation:

$$\widetilde{\lambda}_{EDP}(z) = \sum_{i=1}^{N_{src}} \nu_i \cdot \left\{ \sum_m \sum_r \widetilde{\Pr}(EDP > z \mid M = m, R = r) \Pr(M = m, R = r) \right\}_i \quad (2.7)$$

where $\widetilde{\Pr}(EDP > z \mid M = m, R = r)$ is determined from unmodified ground motions by a process similar to the development of a GMPM in PSHA.

The elements of computing a benchmark SDHC for a given structure at a given site are schematically illustrated in Figure 2.7. The specification of an activity rate, a PDF for magnitude (Figure 2.7b), and a PDF for distance (Figure 2.7c) for each of the N_{src} earthquake sources (Figure 2.7a) is identical to that in the PSHA for the site. For the case study described earlier, the benchmark SDHC is computed with the same earthquake rupture forecast introduced in Section 2.4.

Like PSHA, a prediction model is needed to estimate the probability of EDP exceeding level z for a given rupture scenario (Figure 2.7d). For example, Heo et al. developed such a prediction model for the maximum inter-story drift of a 4- and 12-story building by (1) performing 200 nonlinear RHAs of each building, (2) exploring many different models to predict each EDP as a function of IMs, and (3) choosing the optimal model on the basis of regression diagnostics; to predict an EDP for a given rupture scenario, the optimal model is combined with a GMPM [Heo et al., 2010]. As another example, Hancock et al. developed a prediction model for several EDPs of an 8-story building by (1) performing 1656 nonlinear RHAs of the building, (2) exploring many different functional forms to predict each EDP directly as a function of the rupture scenario, and (3) again choosing the final model on the basis of regression diagnostics [Hancock et al., 2008]. Such an onerous undertaking is generally difficult to justify since the resulting prediction model is limited only to the structure considered. However, we note that a prediction model is readily available for two special cases: (1) EDP is the normalized base shear, $A(T)/g$ of 5% damped linear elastic SDF systems [Baker and Cornell, 2006c], and (2) EDP is the peak deformation, u_m, of 5% damped bilinear SDF systems with 5% post-yield hardening [Tothong and Cornell, 2006].

The distribution of u_m for a given rupture scenario is obtained herein from the Tothong & Cornell 2006 (TC06) model [Tothong and Cornell, 2006]. However, the TC06 model requires the peak deformation of the corresponding linear system, u_o, as an input. Because u_o is not known a priori for a given rupture scenario [Tothong and Cornell, 2006], the TC06 model must be combined with a GMPM to determine the desired distribution of u_m. Consequently, different GMPMs lead to different benchmark SDHCs, which is schematically shown in Figure 2.7e. Which benchmark SDHC should one choose? This question is answered in the next section.

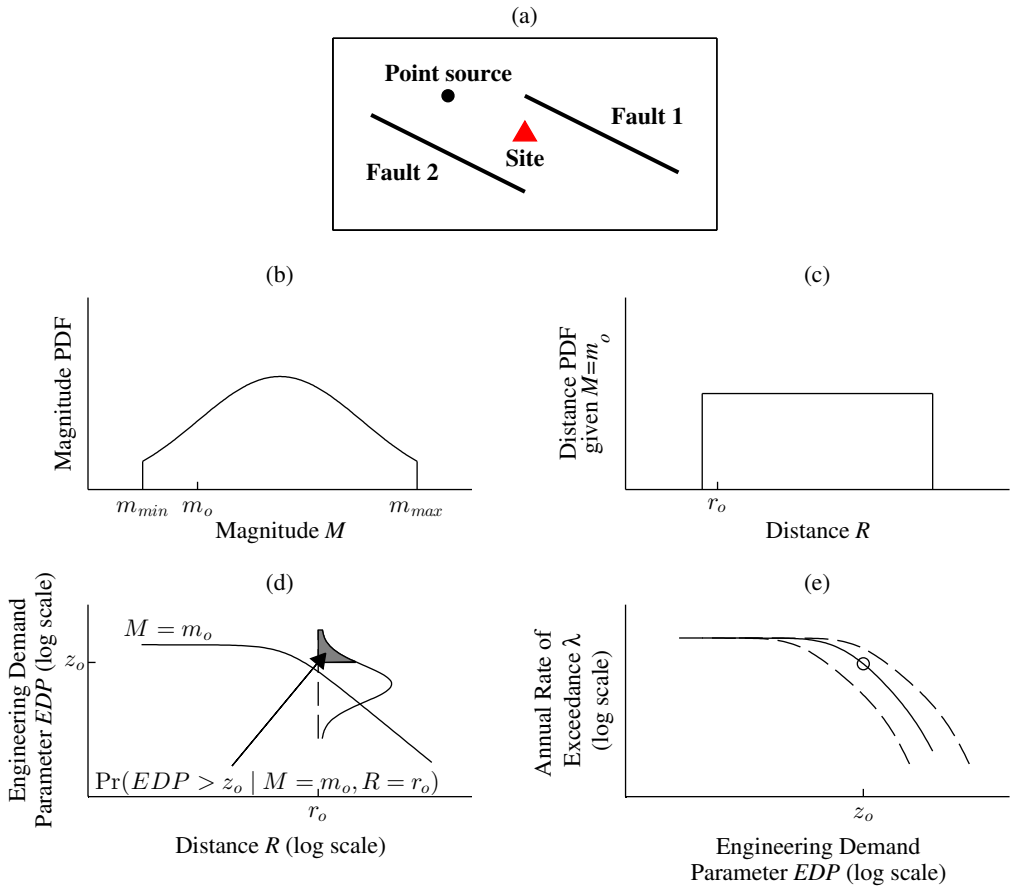

Figure 2.7: The elements of computing a benchmark SDHC: (a) specification of N_{src} earthquake sources and corresponding activity rates, ν_i; for the i^{th} source, a (b) PDF for magnitude, $f_M(m)$; (c) PDF for distance given magnitude, $f_{R|M}(r \mid m_o)$; and (d) probability distribution of demand for a given earthquake scenario, $\Pr(EDP > z \mid M = m_o, R = r_o)$, are shown; and (e) benchmark SDHCs from various prediction models.

2.6 Proposed Framework to Evaluate GMSM Procedures in PSDA

The proposed framework is schematically presented in Figure 2.8. We propose to compare estimates of the SDHC from GMSM procedures, $\widehat{\lambda}_{EDP}(z)$ from Equation 2.2, against a benchmark SDHC, $\widetilde{\lambda}_{EDP}(z)$ from Equation 2.7, under a *single set* of ground motion information for the site. This single set includes an earthquake rupture forecast, a database of many plausible records, and prediction models derived from these records (i.e., a single GMPM for one IM, a single GMPM for another IM, a single model for the correlation among two IMs, etc.). It is important that the same ground motion information be chosen when computing $\widetilde{\lambda}_{IM}(x)$ and $\widetilde{\lambda}_{EDP}(z)$ because the purpose of the comparison between $\widehat{\lambda}_{EDP}(z)$ from Equation 2.2 and $\widetilde{\lambda}_{EDP}(z)$ from Equation 2.7 is to isolate the effects of a particular

GMSM procedure on the resulting SDHC estimate, which is emphasized by the hat symbols in Equation 2.2.

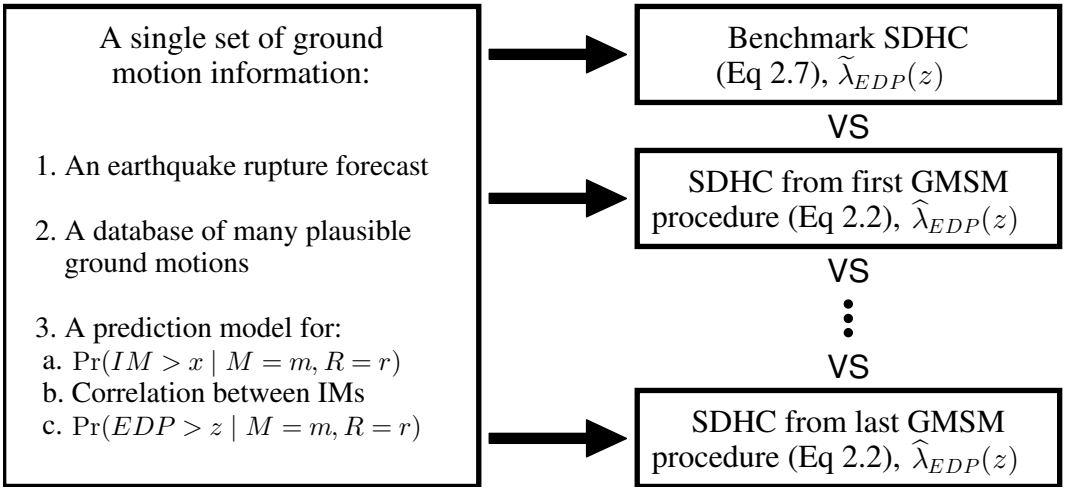

Figure 2.8: Schematic illustration of the proposed framework for evaluating GMSM procedures in their ability to accurately estimate the SDHC.

As shown in Figure 2.8, the proposed framework does *not* compare $\widehat{\lambda}_{EDP}(z)$ against the SDHC from Equation 2.1, $\lambda_{EDP}(z)$, because the latter cannot be calculated for realistic problems, which is why the PEER GMSM working group refers to their benchmark as a "Point-Of-Comparison", or a "High-End-Prediction" [PEER GMSM Working Group, 2009]. However, we note that this inability to calculate $\lambda_{EDP}(z)$ is an example of *epistemic uncertainty*; it arises from the fact that our data and knowledge are always incomplete. For example, $\Pr(IM > x \mid M = m, R = r)$ in Equation 2.5 is not known with absolute certainty since it is estimated with a *limited* collection of ground motions and an *assumed* functional form. Consequently, several GMPMs have been developed to estimate this term, leading to multiple IMHCs in Figure 2.2 and multiple target spectra in Figure 2.4. Another example of epistemic uncertainty is portrayed in Figure 2.7e, where different EDP prediction models lead to different SDHCs. With these variety of models, it might seem difficult to claim a single model as the benchmark.

We overcome this apparent difficulty by recognizing that the purpose of comparing $\widehat{\lambda}_{EDP}(z)$ against a benchmark is to establish the causal relationship between a particular GMSM procedure and the potential bias in its resulting estimate of the SDHC. Therefore, we propose that any EDP prediction model may be chosen, as long as all variables other than the GMSM procedure are controlled as much as possible. For example, any GMPM may be chosen to obtain the final EDP prediction model (see e.g., [Tothong and Cornell, 2006, Heo et al., 2010]) when computing the benchmark SDHC (Equation 2.7), as long as $\widetilde{\lambda}_{IM}(x)$ in Equation 2.2 is given by the IMHC resulting from the *same* GMPM. As another example, if a particular functional form was chosen to develop the prediction model for an EDP, then the *same* functional form should be employed to predict the IM as a function of

a rupture scenario (e.g., [Hancock et al., 2008]). Unlike the Point-Of-Comparison in [PEER GMSM Working Group, 2009], we recommend that the EDP prediction model be developed from *unmodified* ground motions because otherwise, it is impossible to establish the causal relationship between the modification of ground motions and the potential bias in its resulting SDHC; however, this recommendation will result in a small number of inelastic responses for some structures (see end of Section 2.8).

2.7 Bias, Hazard Consistency, and IM Sufficiency

The results from implementing the proposed framework (Figure 2.8), using the CB08 model, are presented in Figure 2.9. The benchmark SDHC is obtained from Equation 2.7 with $\widetilde{\Pr}(EDP > z \mid M = m, R = r)$ given by the TC06-CB08 model and the PSDA-based estimates of the SDHC are repeated from Figure 2.5. Comparing the PSDA-based estimates against the benchmark, we see that both GMSM procedures, IDA and GCIM-SA, lead to essentially unbiased results at exceedance rates above the DBE level and biased results at rates below the MCE level. Furthermore, the curves from GCIM-SA are more accurate than those from IDA, and those corresponding to $T^* \equiv 1$ sec are more accurate than those corresponding to $T^* \equiv 0.75$ sec. The latter observation suggests that the choice of the conditioning period is important in PSDA, which confirms the conclusion by Lin et al. [Lin et al., 2013b]. We also observe that the bias increases with decreasing exceedance rates; using the GCIM-SA curve corresponding to $T^* \equiv 1$ sec as an example, the estimated demand differs from the benchmark by 1% at the DBE level, and by 12% at the MCE level. Without a benchmark, it would be impossible to make such statements with regard to the accuracy of any SDHC estimate from a GMSM procedure.

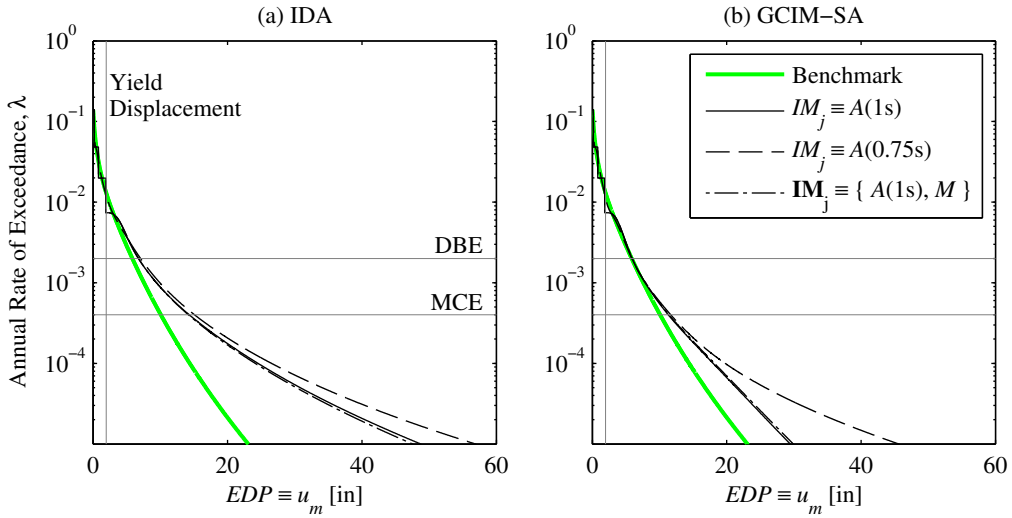

Figure 2.9: Comparison of various estimates of the SDHC from PSDA against the benchmark SDHC: (a) IDA and (b) GCIM-SA.

The IDA and GCIM-SA estimates of the SDHC, corresponding to $A(1s)$ in Figure 2.9, are compared directly against each other and against the benchmark SDHC in Figure 2.10a. This direct comparison confirms that the results from both procedures are unbiased above the DBE level; at rates below this level, the GCIM-SA estimate is more accurate than that from IDA. Such a comparison between the two GMSM procedures does not require that the CB08 model be chosen as the GMPM for spectral acceleration at various vibration periods. As previously mentioned in Section 2.6, any single GMPM may be chosen as long as it is utilized in *all* estimates of the SDHC. The comparison in Figure 2.10a is repeated for three other GMPMs in Figure 2.10b-d, implying that a total of $N_{IM_j} \times n \times 2 \times 4 = 3872$ RHAs were performed. As expected from earlier discussion, the benchmark SDHC changes for each GMPM and the SDHC estimate from each GMSM procedure also changes with GMPMs. However, the SDHC estimate from GCIM-SA remains consistently more accurate than that from IDA below the DBE level. Figure 2.10 also shows that the GCIM-SA estimate is essentially unbiased for AS08 and CY08 but is somewhat biased for the other two GMPMs. The discrepancy between the benchmark SDHC and the GCIM-SA estimate varies for each GMPM because the GCIM-SA estimate – for each of the four separate implementations – is not unique (Section 2.4). For example, when another estimate of the SDHC from GCIM-SA is computed using the AS08 model, a different selection of ground motions (Figure 2.3d) and hence a different SDHC estimate would be obtained; this new SDHC would not be equal to the benchmark SDHC determined by the AS08 model, unlike the GCIM-SA curve shown in Figure 2.10c.

Why are the estimates from GCIM-SA more accurate than those from IDA even though larger scale factors were employed in GCIM-SA (Figure 2.6)? This question is answered by introducing the concept of "hazard consistency". Originally defined by Lin et al. [Lin et al., 2013b], an ensemble [8] of ground motions is *hazard consistent for some IM*, if the estimated IMHC from the ensemble, $\widehat{\lambda}_{IM}(y)$, is practically equal to the IMHC determined by PSHA, $\widetilde{\lambda}_{IM}(x)$ from Equation 2.6. Once $N_{IM_j} \times n$ records have been selected to determine a SDHC, estimating an IMHC from such an ensemble is just a matter of (1) replacing EDP with IM in Eqs 2.2 and 2.4, and (2) applying these equations to the selected ground motions. Specifically, the estimated IMHC from the ensemble is computed from:

$$\widehat{\lambda}_{IM}(y) = \sum_{k=1}^{N_{IM_j}} \widehat{\Pr}(IM > y \mid IM_j = x_k) \cdot |\Delta\widetilde{\lambda}_{IM_j}(x_k)| \tag{2.8}$$

where IM_j was previously defined near the end of Section 2.4 and $\widehat{\Pr}(IM > y \mid IM_j = x_k)$ is determined from:

$$\widehat{\Pr}(IM > y \mid IM_j = x_k) = \frac{1}{n}\sum_{l=1}^{n} I(y_l > y) \tag{2.9}$$

where y_l is the value of IM for record l that has been scaled to intensity x_k.

[8] In the context of hazard consistency, the word 'ensemble' refers to all $N_{IM_j} \times n$ ground motions utilized for a single estimate of the SDHC.

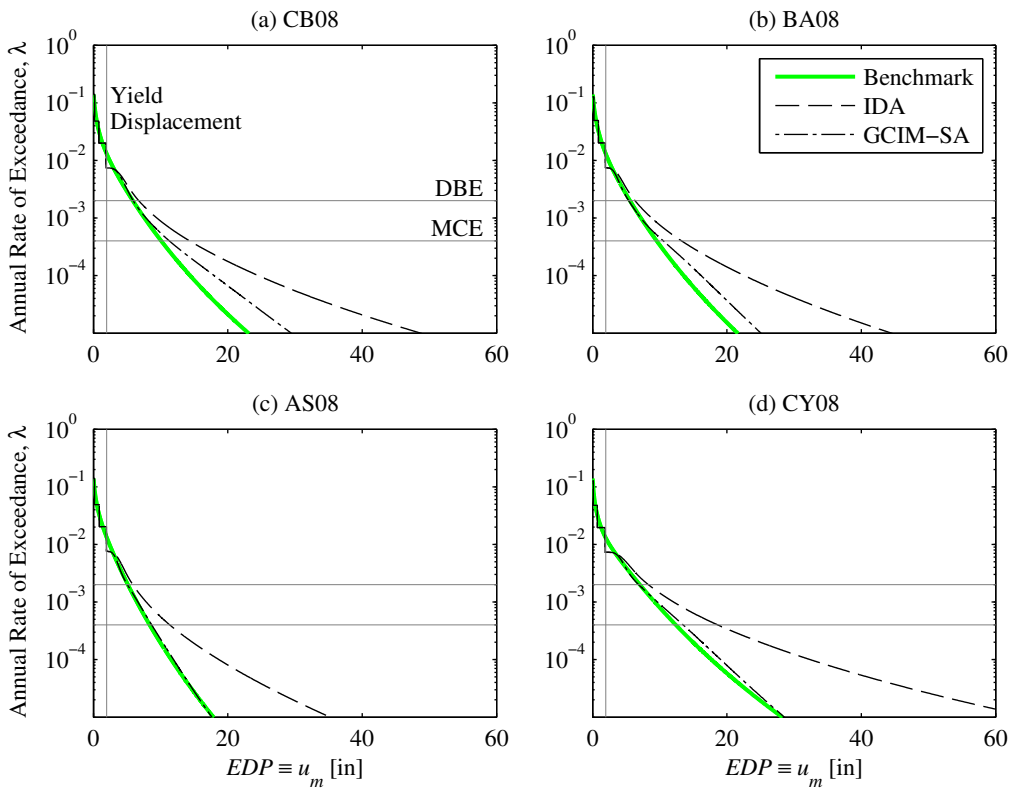

Figure 2.10: Comparison of SDHC estimates from IDA and from GCIM-SA, when $IM_j \equiv A(1s)$, against the benchmark SDHC, for four different GMPMs: (a) CB08; (b) BA08; (c) AS08; and (d) CY08.

For the choice of GMPM $\equiv$ CB08 and $IM_j \equiv A(1s)$, Figure 2.11 examines the hazard consistency of the ground motions selected from IDA and GCIM-SA for IM defined as spectral acceleration at various vibration periods. The PSHA curves are obtained from Equation 2.6 with $\widetilde{\Pr}(IM > x \mid M = m, R = r)$ given by the CB08 model. For each GMSM procedure, the estimated IMHCs are obtained by applying Eqs 2.8 and 2.9 to the 484 motions that were used to construct the corresponding SDHC estimate in Figure 2.10a.

In Figure 2.10a, the SDHC estimate from GCIM-SA is more accurate than that from IDA because the ground motions selected from GCIM-SA are hazard consistent for *more* IMs than those selected from IDA. Figure 2.11 demonstrates that the ground motions from GCIM-SA are hazard consistent for spectral acceleration at nearly all the vibration periods shown (except for 0.1 sec and 10 sec). This is so because records were selected for a given value of $A(T^*)$ to deliberately match the distribution of $A(T)$ at these periods (see Figure 2.4 and Figure 2.3d in Section 2.4). In contrast, one does not have control over the hazard consistency of the ground motions from IDA for such IMs. Although (1) the ground motions from GCIM-SA are hazard consistent for $A(T)$ between T_1 to $3T_1$ (Figure 2.11c-e), and (2) the GCIM-SA estimate is more accurate than that from IDA (Figure 2.10a), it is nevertheless

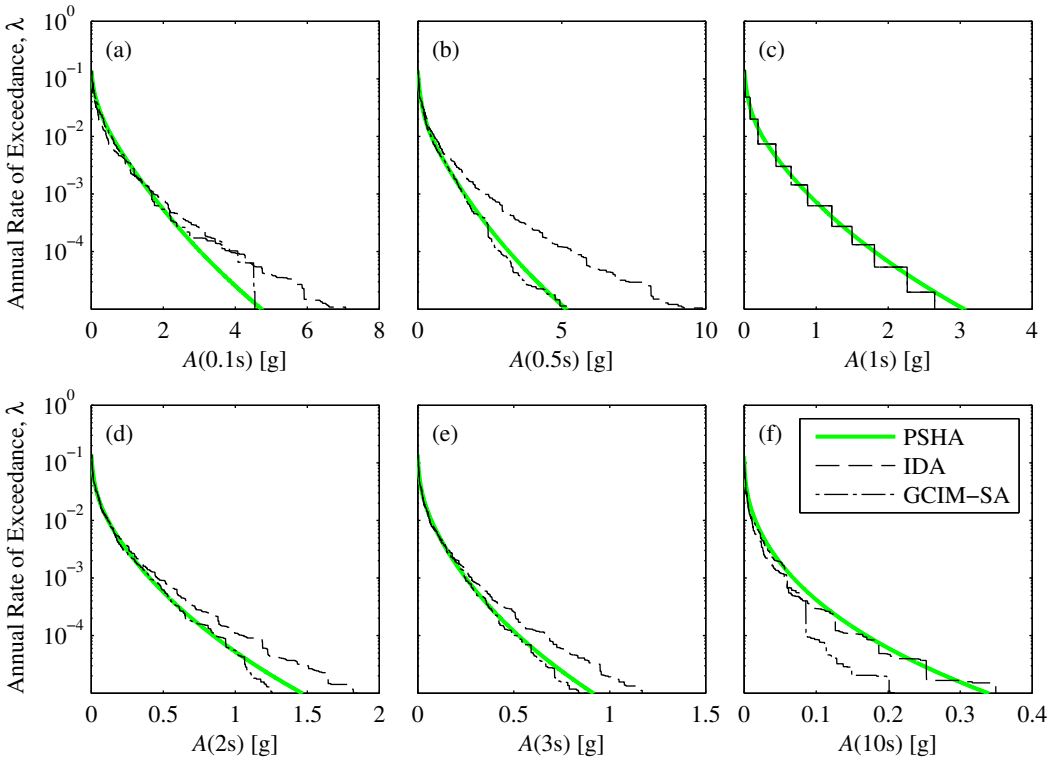

Figure 2.11: Hazard consistency of the ground motions selected from $IM_j \equiv A(1s)$ for spectral acceleration at: (a) 0.1s; (b) 0.5s; (c) 1s; (d) 2s; (e) 3s; and (f) 10s.

biased at rates below the MCE level.

This bias below the MCE level is due to the fact that the vector-valued IM, defined as $A(T)$ at T_1, $2T_1$, and $3T_1$, is *not* a 'sufficient' IM for $EDP \equiv u_m$. An IM, which may be scalar or vector-valued, is defined to be *sufficient* for an EDP when, given a fixed value of this IM, the record-to-record variability of the EDP does not depend on any other aspects of the record [Shome et al., 1998, Luco and Cornell, 2007]. If a vector-valued IM (e.g., $A(T)$ at T between T_1 and $3T_1$) is indeed sufficient for u_m, then the fact that ground motions are hazard consistent for this IM must imply that the corresponding SDHC estimate is unbiased; as a corollary, if the ground motions are hazard consistent for a vector-valued IM, then the fact that the corresponding estimate of the SDHC is biased must imply that the vector-valued IM is insufficient for the EDP of interest. To motivate this assertion, we next consider two definitions of a scalar IM.

First, let us define IM as EDP [Luco and Cornell, 2007]. This implies that IM is sufficient for EDP because once a fixed value of EDP is given, the variability of EDP does not depend on any other aspects of the ground motion. If ground motions were selected to be hazard consistent *for this particular definition* of the IM, then by definition of hazard consistency, $\widehat{\lambda}_{IM}(y)$ from Equation 2.8 will be practically equal to $\widetilde{\lambda}_{IM}(x)$ from Equation 2.6.

This is equivalent to stating that the SDHC estimate is unbiased, since $IM \equiv EDP$.

Second, let us define IM as IM_j. Since ground motions are scaled to IM_j in PSDA (Figure 2.1b), they are *always* hazard consistent *for this particular definition* of the IM. For example, Figure 2.11c shows that the selected motions from both GMSM procedures are hazard consistent for $IM_j \equiv A(1s)$; in fact, the estimated IMHCs from both procedures are identical because the term $\widehat{\Pr}(IM > y \mid IM_j = x_k)$ in Equation 2.8 becomes a step function when $IM \equiv IM_j$. The fact that the ground motions from both procedures are hazard consistent for $A(1s)$ implies that the corresponding SDHC estimates are unbiased at exceedance rates above the DBE level (Figure 2.10a), because (1) $A(1s)$ is a sufficient IM for the peak deformation of the corresponding linear system, u_o, and (2) $EDP \equiv u_m$ is approximately equal to u_o at rates above the DBE level. On the other hand, the SDHC estimates are biased at rates below the MCE level, even though the selected motions from both procedures are hazard consistent for $A(1s)$, because $A(1s)$ alone is not a sufficient IM for $EDP \equiv u_m$.

Since $A(1s)$ is not a sufficient IM for u_m, then u_m must depend on other aspects of the ground motion. Figure 2.12 examines the hazard consistency of the same records from Figure 2.11, for six miscellaneous IMs. Specifically, these IMs include PGA, PGV, acceleration spectrum intensity (ASI), cumulative absolute velocity (CAV), and two measures of significant duration: (1) D_{5-75}, and (2) D_{5-95}. The CB08 model was used to develop the PSHA curves for PGA and PGV, the Bradley 2010 model [Bradley, 2010b] for ASI, the Campbell & Bozorgnia 2010 model [Campbell and Bozorgnia, 2010] for CAV, and the Bommer et al. 2009 model [Bommer et al., 2009] for duration. As in Figure 2.11, the estimated IMHCs were obtained from Eqs 2.8 and 2.9.

Figure 2.12a-c and Figure 2.12e-f demonstrate that the ground motions from GCIM-SA are hazard consistent for PGA, PGV, ASI, D_{5-75}, and D_{5-95}. Since the corresponding SDHC estimate is biased at exceedance rates below the MCE level (Figure 2.10a), we conclude that the vector-valued IM, defined as a collection of PGA, PGV, ASI, D_{5-75}, and D_{5-95}, *must not be sufficient* for u_m. In other words, the bias in the SDHC estimate is influenced by the hazard consistency of the ground motions for *other* IMs. However, such a vector-valued IM appears to be less insufficient than $A(1s)$ alone, since the GCIM-SA estimate of the SDHC is more accurate than that from IDA (Figure 2.10a). In summary, we conclude that severely scaled ground motions (Figure 2.6) may still lead to an accurate estimate of the SDHC as long as they are hazard consistent *for an IM that is sufficient*.

In general, an IM – scalar or vector-valued – will almost never be truly sufficient for an EDP that is related to the inelastic response of realistic models of structures. As a result, even if ground motions are deliberately forced to be hazard consistent for a vector-valued IM (as in procedures like CS or GCIM), the modification of ground motions in PSDA (e.g., Figure 2.1b) will likely lead to some degree of bias in the subsequent SDHC estimates. Without a benchmark to compare against, such bias cannot be quantified. Fortunately, the framework and benchmark proposed in this study enable a direct determination of the bias.

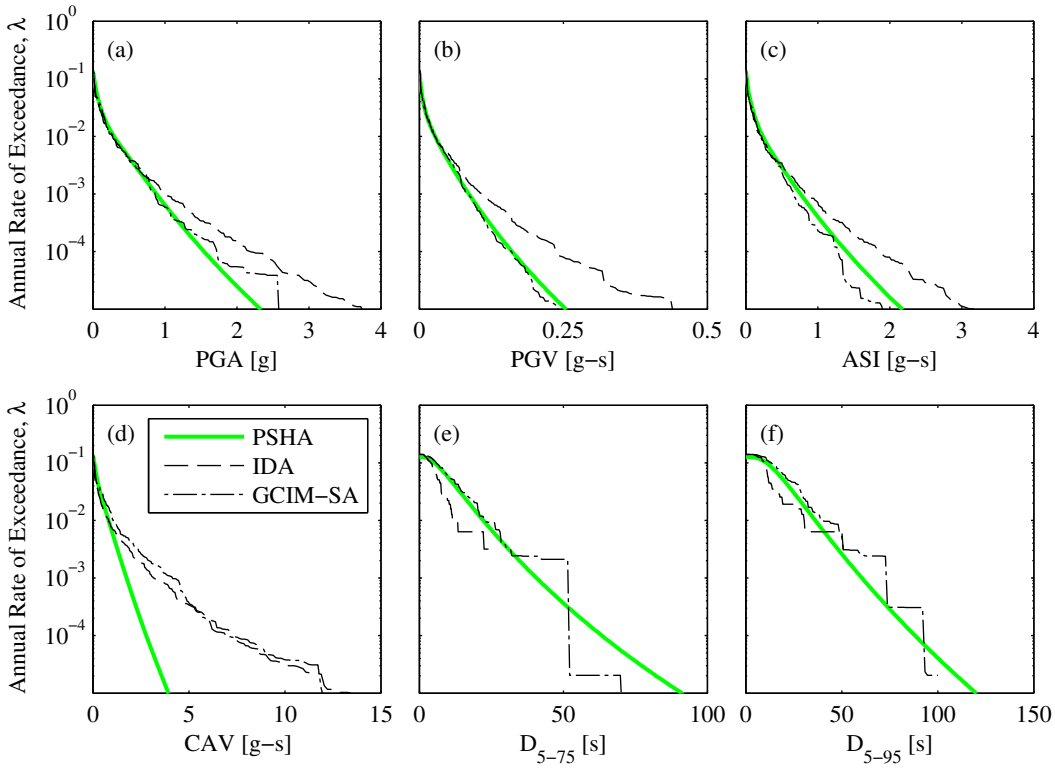

Figure 2.12: Hazard consistency of the ground motions selected from $IM_j \equiv A(1s)$ for several miscellaneous IMs: (a) PGA; (b) PGV; (c) ASI; (d) CAV; (e) D_{5-75}; and (f) D_{5-95}.

2.8 Avoiding a Potential Pitfall

If we want to establish the causal relationship between a particular GMSM procedure and the potential bias in its resulting estimate of the SDHC, then we must specify the *same* GMPM in both the benchmark SDHC and the estimate from the GMSM procedure, as illustrated in Figure 2.8. This was done for the results shown in Figure 2.10 since for each of the four cases, the same GMPM was chosen for both the benchmark SDHC and the GMSM-based estimates. By controlling the GMPM in this manner, the discrepancies between a PSDA-based estimate of the SDHC and the benchmark SDHC are due primarily to the GMSM procedure.

If we do not specify a common GMPM for both the benchmark and the GMSM-based estimate, then the resulting observations are misleading. For example, consider Figure 2.13a, where the GCIM-SA curve in Figure 2.11c is compared against two different PSHA-based IMHCs: (1) that from Figure 2.11c, and (2) that from a weighted average of the four IMHCs in Figure 2.2a. The weighted IMHC might be considered as a 'best estimate' of the target IMHC for comparison (see e.g., the US Geological Survey online hazard tool); however, it is erroneous to use this curve for examining hazard consistency of the ground motions from the GCIM-SA procedure that employs the CB08 model (Figure 2.4). Another example is

illustrated in Figure 2.13b, where the GCIM-SA curve in Figure 2.10a is compared against two benchmark SDHCs: (1) that in Figure 2.10a, and (2) that from a weighted average of the four benchmark SDHCs in Figure 2.10. It is erroneous to use the weighted benchmark SDHC for evaluating the accuracy of the SDHC that is determined from the CB08 model. If one insists on specifying the weighted SDHC as the benchmark, then (1) the *same* weights should be employed in determining $\widetilde{\lambda}_{IM}(x_i)$ in Equation 2.2, and (2) ground motions should be selected via the "exact CS" [Lin et al., 2013a] for a fair comparison.

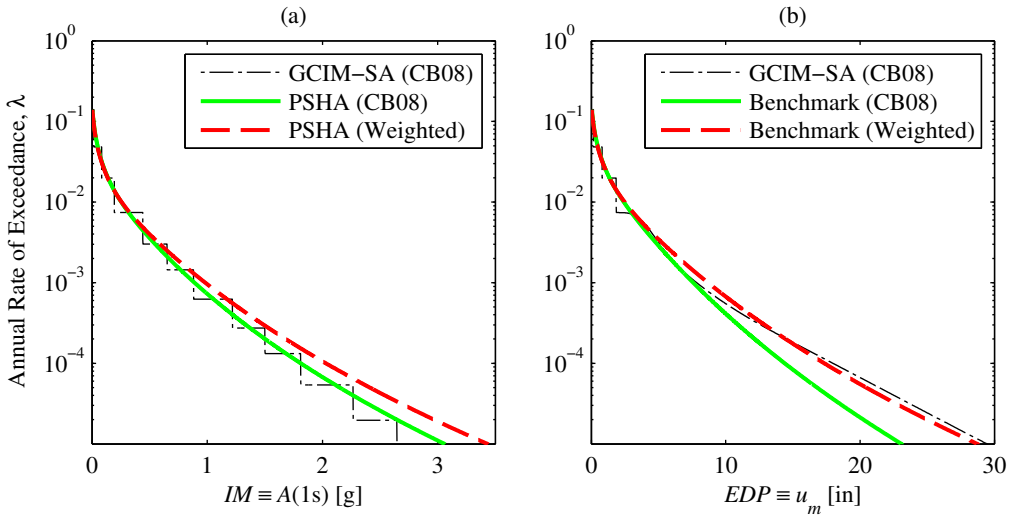

Figure 2.13: Two examples for illustrating the importance of specifying a common GMPM when implementing the proposed framework: (a) 'hazard consistency' of the ground motions from GCIM-SA when $IM \equiv A(1s)$; and (b) GCIM-SA estimate of the SDHC versus 'the benchmark'.

There are two limitations of the proposed framework in this study (Figure 2.8). First, the framework can only be applied when an EDP prediction model is readily available for the structure (e.g., bilinear SDF systems in [Tothong and Cornell, 2006], the 4-story building in [Heo et al., 2010], the 8-story building in [Hancock et al., 2008], etc.). In general, it is a major computational task to develop an EDP prediction model for a realistic structure because the number of necessary RHAs is typically large (e.g., 200 RHAs of a 12-story building were performed in [Heo et al., 2010]) and the selection of an optimal functional form requires an iterative approach. Second, the range of applicability of the proposed framework is limited by the availability of recorded ground motions. As shown in Figure 2.8, the prediction model for EDP is to be developed from a database of *unmodified* ground motions because the purpose of the comparison between the resulting benchmark SDHC and an estimate from a GMSM procedure is to reveal potential biases from the modification of ground motions. However, such a recommendation will result in a small number of inelastic responses when the number of intense (relative to the strength of the structure) ground motions in the database is small.

2.9 Conclusions

This investigation of developing a framework for the evaluation of GMSM procedures has led to the following conclusions:

1. Meaningful evaluation of GMSM procedures requires clearly stating the objective of the RHAs of the structure. In this study, four objectives are identified, and the evaluation of GMSM procedures is investigated when the objective of the RHAs is to estimate a SDHC for a given structure at a given site.

2. Using a simple case study, we highlight an important but subtle limitation of the existing approaches for evaluating GMSM procedures in PSDA: the practical equality between two SDHCs from different conditioning IMs does not *necessarily* indicate that an unbiased SDHC has been obtained. Consequently, an alternative approach for evaluating GMSM procedures in PSDA is desirable.

3. To quantify bias in any estimate of the SDHC, we introduce the notion of a benchmark SDHC, which is determined by incorporating an EDP prediction model that is developed from unmodified ground motions into the PSHA calculations. Consequently, this study is limited by the availability of EDP prediction models and the availability of recorded ground motions.

4. With the variety of benchmarks in past studies, it might seem difficult to claim a single choice as the benchmark. We overcome this apparent difficulty by recognizing that (1) different choices correspond to different instances of epistemic uncertainty, (2) the purpose of a benchmark is to isolate the effects of GMSM procedures on the resulting SDHC estimates, and (3) the same ground-motion information should be utilized in obtaining the benchmark SDHC and all estimates of the SDHC from GMSM procedures.

5. To develop an understanding of why one GMSM procedure may provide more accurate estimates of the SDHC than another, we identify the role of IM sufficiency in the relationship between (1) bias in the SDHC and (2) hazard consistency of the corresponding selected ground motions. If the IM, scalar or vector-valued, used for record selection is sufficient, then ensuring hazard consistency of the selected ground motions for this IM implies that the corresponding estimate of the SDHC is unbiased, even when the ground motions are scaled by large scale factors; as a corollary, if the ground motions are hazard consistent for a vector-valued IM, then the fact that the corresponding estimate of the SDHC is observed to be biased implies that the IM is *not* sufficient for the EDP of interest. Therefore, accurate estimates of the SDHC may be obtained from severely scaled ground motions, as long as the selected motions are hazard consistent *for an IM that is sufficient*.

6. We do not know, *a priori*, which IM is sufficient for an arbitrary EDP associated with the inelastic response of a realistic structure; in fact, rarely will an IM that is sufficient exist. Consequently, the modification of ground motions in PSDA will likely cause

some amount of bias in the SDHC estimate, despite the fact that ground motions may be hazard consistent for some vector-valued IM. Without a benchmark to compare against, such bias cannot be quantified.

7. When implementing the proposed framework for the evaluation of GMSM procedures, one may draw misleading conclusions if the benchmark SDHC and a PSDA-based estimate are not derived from a common set of ground-motion information.

Chapter 3

Evaluation of GMSM Procedures using Synthetic Ground Motions

3.1 Preview

This study presents a novel approach for evaluating ground motion selection and modification (GMSM) procedures in the context of probabilistic seismic demand analysis (PSDA). In essence, synthetic ground motions are employed to derive the benchmark seismic demand hazard curve (SDHC), for any structure and response quantity of interest, and to establish the causal relationship between a GMSM procedure and the bias in its resulting estimate of the SDHC. An example is presented to illustrate how GMSM procedures may be evaluated using synthetic motions. To demonstrate the robustness of the proposed approach, two significantly different stochastic models for simulating ground motions are considered. By quantifying the bias in any estimate of the SDHC, the proposed approach enables the analyst to rank GMSM procedures in their ability to accurately estimate the SDHC, examine the sufficiency of intensity measures (IMs) employed in ground motion selection, and assess the significance of the conditioning IM in PSDA.

3.2 Introduction

Ground motions [1] required to conduct nonlinear response history analysis (RHA) of structures may either be recorded or synthetic; recorded ground motions are obtained from strong-motion instruments whereas synthetic ground motions are simulated from models [Douglas and Aochi, 2008]. Such models may be purely physics-based, purely stochastic, or a combination of the two. Recorded ground motions are usually modified because *intense* records, typically of interest in earthquake engineering, are scarce.

Many ground-motion selection and modification (GMSM) procedures have been devel-

[1] In this report, "ground motion" refers to ground acceleration as a function of time (i.e., an accelerogram). Although the same term also refers occasionally to an intensity measure (as in "ground-motion-prediction models"), its meaning should be clear from the context.

oped. For example, several records may be selected on the basis of magnitude and distance [Shome et al., 1998, Stewart et al., 2001], or spectral shape [Baker and Cornell, 2006b, Baker, 2011]. Selected records are sometimes amplitude scaled [Shome et al., 1998, Baker and Cornell, 2005] and other times adjusted with wavelets such that the response spectrum of the modified record is compatible with a target spectrum (see e.g., [Hancock et al., 2008]). A review of many GMSM procedures may be found in Appendix A of [PEER GMSM Working Group, 2009] and in [Katsanos et al., 2010]. How should one choose among the variety of GMSM procedures available? This question will be answered in this chapter.

Among the variety of contexts where RHAs are conducted [Kwong et al., 2014], we choose probabilistic seismic demand analysis (PSDA) [Shome et al., 1998], which is also known as a risk-based assessment [NEHRP Consultants Joint Venture, 2011]. For a given structure at a given site, a PSDA couples probabilistic seismic hazard analysis (PSHA) of the site with RHA of the structure in order to determine the seismic demand hazard curve (SDHC) of an engineering demand parameter (EDP). The exact SDHC, $\lambda_{EDP}(z)$, is governed by

$$\lambda_{EDP}(z) = \int \Pr(EDP > z \mid IM^* = x) \cdot |\mathrm{d}\lambda_{IM^*}(x)| \tag{3.1}$$

where IM^* denotes the conditioning intensity measure (IM), $\lambda_{IM^*}(x)$ denotes its corresponding exact hazard curve, and $\Pr(EDP > z \mid IM^* = x)$ denotes the exact complementary cumulative distribution function (CCDF) of EDP when the intensity level is equal to x [2]. In practical application, $\lambda_{EDP}(z)$ is estimated from

$$\widehat{\lambda}_{EDP}(z) = \sum_{i=1}^{N_{IM^*}} \widehat{\Pr}(EDP > z \mid IM^* = x_i) \cdot |\Delta\widetilde{\lambda}_{IM^*}(x_i)| \tag{3.2}$$

where $\widetilde{\lambda}_{IM^*}(x_i)$ denotes the intensity measure hazard curve (IMHC) that is computed from a particular ground-motion-prediction model (GMPM) in PSHA, N_{IM^*} denotes the number of intensity levels chosen to approximate the integral in Equation 3.1, and $\widehat{\Pr}(EDP > z \mid IM^* = x_i)$ denotes the CCDF of EDP that is determined by performing RHAs of the structure for an ensemble of ground motions from a GMSM procedure. To include the possibility of structural collapse, $\widehat{\Pr}(EDP > z \mid IM^* = x_i)$ in Equation 3.2 may be expanded to obtain

$$\widehat{\Pr}(EDP > z \mid IM^* = x_i) = \widehat{\Pr}(EDP > z \mid \mathrm{NC}, IM^* = x_i)\,[1 - \widehat{p}_C(x_i)] + \widehat{p}_C(x_i) \tag{3.3}$$

where NC denotes the event corresponding to "No Collapse", and $\widehat{p}_C(\cdot)$ refers to the fragility function that is determined from multiple ensembles of ground motions that have been scaled to different intensity levels [Baker, 2015]. At each intensity level x_i, an ensemble of ground motions is obtained from a GMSM procedure (e.g., Incremental Dynamic Analysis (IDA) [Vamvatsikos and Cornell, 2004], Conditional Spectrum [Jayaram et al., 2011], etc.). A SDHC estimate from Equation 3.2, corresponding to a particular GMSM procedure, is defined to be *unbiased* when it is essentially equal to $\lambda_{EDP}(z)$; it is defined to be *biased* when it differs significantly from $\lambda_{EDP}(z)$.

[2] In this study, an asterisk is included to the symbol IM when denoting a conditioning intensity measure.

It is currently difficult to definitively evaluate the accuracy of any estimate of the SDHC because the exact SDHC, $\lambda_{EDP}(z)$, is unknown. To circumvent this limitation, the accuracy of a SDHC estimate is often judged by comparing it against several other estimates of the SDHC, each determined from the same GMSM procedure but selecting different definitions of the conditioning IM in Equation 3.2 [Bradley, 2012c, Lin et al., 2013b]. With enough definitions of the conditioning IM, close agreement between the corresponding SDHCs suggests that the associated GMSM procedure provides unbiased estimates of the SDHC. However, the SDHCs from different definitions of the conditioning IM are almost always different from each other and without a "benchmark" for comparison, it is difficult to judge the accuracy of any SDHC estimate. Alternatively, the potential bias may be approximated using the Generalized Conditional Intensity Measure approach [Bradley, 2010a]; however, the quality of such approximations is also difficult to ascertain for lack of a benchmark. To supplement the conclusions from the previous approaches, SDHC estimates were compared against a benchmark SDHC that was computed from a prediction model for the EDP [Kwong et al., 2014]. With this approach, the bias of any SDHC estimate may be quantified; however, it is limited by the availability of prediction models for the EDP and structure of interest, and such prediction models are in turn limited by the availability of recorded ground motions.

This chapter establishes *the causal relationship* between a GMSM procedure and the bias in its resulting SDHC estimate by using a large database of synthetic ground motions to determine the "benchmark" SDHC and to control as many variables as possible. By comparing Equation 3.2 against Equation 3.1, three major sources of bias may be identified: (1) approximation of the integral in Equation 3.1 with a summation in Equation 3.2, (2) approximation of $\lambda_{IM^*}(x)$ with $\widetilde{\lambda}_{IM^*}(x)$, and (3) approximation of $\Pr(EDP > z \mid IM^* = x)$ with $\widehat{\Pr}(EDP > z \mid IM^* = x)$, which is obtained from RHAs of the structure for an ensemble of ground motions determined by a GMSM procedure. The first source can be essentially eliminated if N_{IM^*} is adequately large. The second source can be essentially eliminated with the aid of synthetic ground motions (Section 3.6). With these two contributions eliminated, potential biases from a particular GMSM procedure can be identified (third source). This approach with synthetic ground motions is developed in the next section.

3.3 Proposed Approach to Evaluate GMSM Procedures

The proposed approach is schematically illustrated in Figure 3.1 [3]. The SDHC estimate from each GMSM procedure, $\widehat{\lambda}_{EDP}(z)$, is compared against the benchmark SDHC, $\lambda_{EDP}(z)$, under a controlled setting; the benchmark SDHC is computed from a large database of synthetic ground motions and each GMSM-based SDHC is computed from a subset of this database. It is important to derive all SDHCs from a common set of ground motion information (i.e., earthquake rupture forecast, GMPMs, etc.) because the purpose of each comparison in Figure 3.1 is to isolate the effect of the GMSM procedure on its resulting SDHC estimate.

[3] Unlike the approach in [Kwong et al., 2014], the approach herein employs synthetic ground motions and as a result, the corresponding benchmark SDHC and prediction models are significantly different.

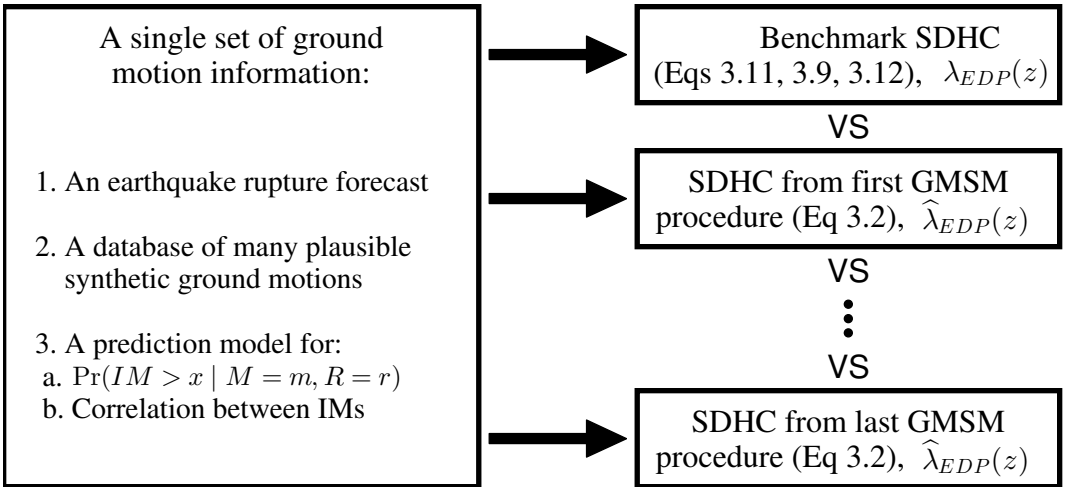

Figure 3.1: Schematic illustration of the framework for evaluating GMSM procedures using synthetic ground motions.

To develop this common set of ground-motion information for a given site, an earthquake rupture forecast and a database of ground motions are needed. Each of the N_{src} earthquake sources is characterized by an activity rate, ν, and a probability density function (PDF) for earthquake magnitude and distance, $f_{M,R}(m,r)$. Next, a model for simulating synthetic ground motions is chosen for the given site; although only two stochastic models are illustrated herein – Rezaeian-Der Kiureghian [Rezaeian and Der Kiureghian, 2010] and Yamamoto-Baker [Yamamoto, 2011] – other well-vetted models (e.g., physics-based, hybrid, etc.) may be considered. A large number of intense synthetic ground motions is then simulated from the chosen model, for the specified earthquake rupture forecast (Section 3.4).

This large database of intense ground motions enables computation of the exact hazard curves, $\lambda_{IM^*}(x)$ and $\lambda_{EDP}(z)$ in Equation 3.1, which are unique for a given ground motion simulation model (Section 3.5); however, the number of synthetic ground motions in such databases is nevertheless finite. Furthermore, different ground motion simulation models lead to different $\lambda_{IM^*}(x)$ and $\lambda_{EDP}(z)$. For this reason, the hazard curves that correspond to a particular database of synthetic ground motions are referred to as the *benchmark* (as opposed to "exact") hazard curves. Note that such a benchmark could not have been determined from recorded ground motions for lack of an adequate number of intense records.

Several contemporary GMSM procedures (e.g., [Baker and Cornell, 2006b], [Jayaram et al., 2011], [Bradley, 2010a], etc.) require GMPMs to select ground motions. Therefore, new GMPMs from the previously simulated database of ground motions was developed, as shown in the left part of Figure 3.1. These GMPMs may then be used to construct IMHCs, $\widetilde{\lambda}_{IM}(x)$, or perform deaggregation [McGuire, 2004]. Since our objective is to isolate the effect of a GMSM procedure on the resulting SDHC estimate, it is mandatory that the GMPM-based IMHC, $\widetilde{\lambda}_{IM^*}(x)$ in Equation 3.2, be essentially equal to the benchmark IMHC,

$\lambda_{IM^*}(x)$ in Equation 3.1. For this reason, the GMPMs developed in this study are referred to as *benchmark-consistent* GMPMs (Section 3.6).

For each GMSM procedure of interest, a corresponding SDHC estimate is determined from the ground-motion information depicted in the left part of Figure 3.1 (Section 3.7). Specifically, all GMSM procedures select and modify a subset of the previously simulated database of ground motions. If prediction models are needed as input to the GMSM procedure, then the benchmark-consistent prediction models that are developed in Section 3.6 are employed. For each GMSM procedure, the corresponding estimate of the SDHC is obtained from Equation 3.2 and compared against the benchmark SDHC, $\lambda_{EDP}(z)$. Since (1) $\lambda_{EDP}(z)$ may now be determined from synthetic ground motions (Section 3.5), and (2) $\widetilde{\lambda}_{IM^*}(x)$ is essentially equal to $\lambda_{IM^*}(x)$ (Section 3.6), a comparison of $\widehat{\lambda}_{EDP}(z)$ against $\lambda_{EDP}(z)$ indicates the bias caused by the corresponding GMSM procedure (Section 3.7). To illustrate this approach for evaluating GMSM procedures, an example is presented below; the details of this example are described next.

3.4 Case Study

Site, Stochastic Models, and Databases of Synthetic Ground Motions

The simple site illustrated in Figure 3.2a is selected for this study [4]. The site is situated on soil with a shear-wave velocity, V_{s30}, of 400 m/s and a basin depth, $Z_{2.5}$, of 1 km. A single strike-slip fault with an activity rate of $\nu = 0.02$ earthquakes per year is located 10 km away from the site. All earthquakes are assumed to occur at a fixed distance, $R = 10$ km; in contrast, the magnitude of each earthquake, M, is random and follows the PDF that is given by the Youngs & Coppersmith model [Youngs and Coppersmith, 1985] (Figure 3.2b). This completes the specification of an earthquake rupture forecast in Figure 3.1.

There are several advantages to selecting a simple site. For the selected site, the general equation governing any IMHC in PSHA (see e.g., [McGuire, 2004]) is greatly simplified:

$$\begin{aligned}\lambda_{IM}(x) &= \sum_{i=1}^{N_{src}} \nu_i \cdot \left\{ \int\int \Pr(IM > x \mid M = m, R = r) f_{R|M}(r \mid m) f_M(m)\, \mathrm{d}r\, \mathrm{d}m \right\}_i \\ &= \nu \cdot \left\{ \int \Pr(IM > x \mid M = m) f_M(m)\, \mathrm{d}m \right\} \end{aligned} \tag{3.4}$$

where $\Pr(IM > x \mid M = m)$ refers to the CCDF of the IM for a given earthquake magnitude. This simplification facilitates the computation of benchmark hazard curves (Section 3.5) and the development of benchmark-consistent GMPMs (Section 3.6). Furthermore, such a simple site is sufficient to illustrate the approach described in Section 3.3.

[4] Except for the activity rate, this site is identical to that considered in Section 5.4 of Yamamoto's Ph.D. dissertation [Yamamoto, 2011].

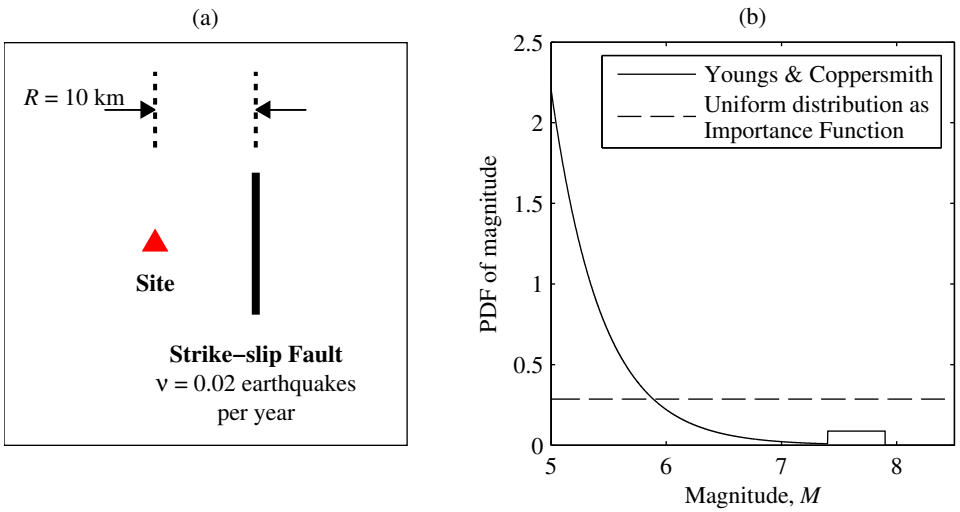

Figure 3.2: Source characterization for case study site: (a) specification of earthquake source; and (b) PDF of magnitude for the strike-slip fault.

Two stochastic models, referred to as Rezaeian [Rezaeian and Der Kiureghian, 2008, Rezaeian and Der Kiureghian, 2010] and Yamamoto [Yamamoto, 2011, Yamamoto and Baker, 2013], are employed to simulate synthetic ground motions. Two models are chosen in order to test the robustness of the proposed approach for evaluating GMSM procedures. Given magnitude, distance, style-of-faulting, and V_{s30} as inputs, Rezaeian's model simulates a ground motion by time-modulating a filtered white-noise stochastic process. The resulting ground motion is fully nonstationary because the parameters of both (1) the time-modulating function and (2) the filter vary with time. In contrast, Yamamoto's model simulates a fully nonstationary ground motion via the Wavelet Packet Transform. Example waveforms from Rezaeian's model can be seen in Figs 7-8 of [Rezaeian and Der Kiureghian, 2010]; example waveforms from Yamamoto's model can be seen in Figs 4-5 of [Yamamoto and Baker, 2013].

For each stochastic model, a database of 10^4 synthetic ground motions is randomly simulated. The Youngs & Coppersmith PDF of magnitude in Figure 3.2b, $f_M(m)$, indicates that a wide range of magnitudes is possible for the given site. Therefore, a natural approach to simulate a database that adequately covers the range of possible magnitudes is to first generate 10^4 random values of magnitude from $f_M(m)$, and then simulate a ground motion for each of the 10^4 magnitudes. However, the number of *intense* ground motions in such a database would be small, as suggested by $f_M(m)$ in Figure 3.2b. To overcome this limitation, Yamamoto and Baker proposed to employ the concept of Importance Sampling [Yamamoto, 2011], a standard procedure in statistics (see e.g., Section 24.3 of [Wasserman, 2004]). Using the uniform distribution in Figure 3.2b as the Importance Function, $g_M(m)$, 10^4 values of magnitude are randomly generated and the corresponding value of Importance Sampling weights, $w(m) = f_M(m) \div g_M(m)$, are saved. Corresponding to each of the 10^4 values of magnitude, a synthetic ground motion is randomly simulated from the two stochastic models.

Structural Models and Engineering Demand Parameters

To highlight the generality of the proposed approach, two nonlinear SDF systems and two EDPs are considered. Although SDF systems are chosen to facilitate reproducibility of the results in this study, any structural model and EDP may be chosen (see end of Section 3.8). The first SDF structure is a 5%-damped bilinear system with a linear vibration period, T_1, of 1 sec, a yield displacement of $0.2\text{g} \times (T_1/2\pi)^2$, and a post-yield hardening ratio of 5%. The second SDF structure is a 3.4%-damped degrading system with a linear vibration period, T_1, of 1.1 sec, a yield displacement of $0.18\text{g} \times (T_1/2\pi)^2$, and a post-yield softening ratio of 2%; it is the first-mode inelastic SDF system of the 4-story building considered in [Bobadilla and Chopra, 2007]. For each SDF structure, the SDHCs corresponding to two EDPs are of interest: (1) peak deformation, u_m, and (2) peak total acceleration, $\ddot{u}_o^t$.

The force-deformation relationships for the two selected SDF structures are presented in Figure 3.3. The relationship for the degrading system is represented by the Modified Ibarra-Medina-Krawinkler (IMK) model [Ibarra et al., 2005] with peak-oriented hysteretic response; the specific parameters for this model may be found in Tables 4.2 and 4.3 of [Bobadilla and Chopra, 2007]. The post-yield hardening portrayed in Figure 3.3a indicates that collapse is impossible for the bilinear system. In contrast, collapse is possible for the degrading system because the Modified IMK model captures both stiffness and strength deterioration (Figure 3.3b). Strictly speaking, collapse occurs when the deformation of the system increases without bounds. Practically however, collapse is defined herein as the event where the peak deformation exceeds 29 inches (see e.g., Section 3.2.2 of [PEER GMSM Working Group, 2009]), which corresponds to the ultimate rotation capacity that is specified in the Modified IMK model.

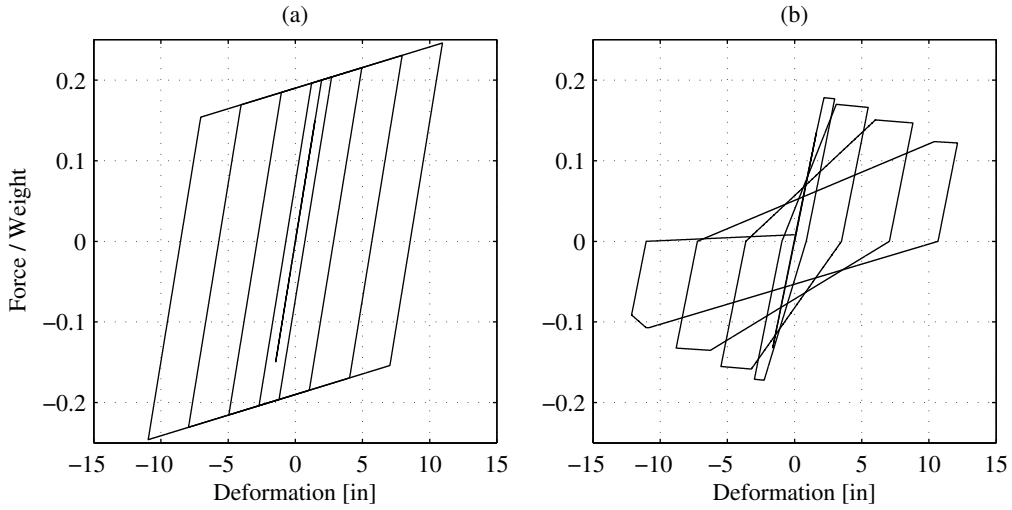

Figure 3.3: Force-deformation relationships from cyclic pushover analysis: (a) bilinear; (b) Modified IMK model with peak-oriented response.

GMSM Procedures

To emphasize the flexibility of the proposed approach, two significantly different GMSM procedures are considered in this study: (1) IDA [Vamvatsikos and Cornell, 2004], and (2) a special case of the Generalized Conditional Intensity Measure approach (GCIM) [Bradley, 2010a, Bradley, 2012a, Bradley, 2012c], where only spectral accelerations, $A(T)$, are considered as IMs for ground motion selection; this special case is denoted by GCIM-SA. The IDA represents a simple and well known technique for estimating SDHCs in PSDA (see e.g., [Applied Technology Council, 2009]), whereas GCIM-SA is a more sophisticated GMSM procedure. The latter permits examination of the premise that spectral shape is a sufficient IM [Luco and Cornell, 2007] for EDPs of nonlinear SDF systems.

3.5 Benchmark Hazard Curves

For a specified ground motion simulation model, a unique set of hazard curves, $\lambda_{IM}(x)$ and $\lambda_{EDP}(z)$ in Equation 3.1, exist. These hazard curves may be approximated from a database of synthetic ground motions; the theory for such calculations is presented next.

Intensity Measure Hazard Curve

The exact hazard curve for any IM at the site described in Section 3.4 is governed by Equation 3.4. In this equation, $f_M(m)$ is given by the PDF shown in Figure 3.2b and $\Pr(IM > x \mid M = m)$ is given by the stochastic model for randomly simulating ground motions. If magnitudes were randomly generated from $f_M(m)$ and used as input to the selected stochastic model, then $\lambda_{IM}(x)$ may be computed from the usual Monte Carlo estimator (see e.g., Section 4.5 of [Ross, 2013]):

$$\lambda_{IM}^{(\mathrm{MC})}(x) = \frac{\nu}{N} \sum_{i=1}^{N} I(x_i > x) \tag{3.5}$$

where the superscript MC refers to "Monte Carlo", N is the total number of synthetic ground motions in a database, x_i is the value of IM for the i^{th} ground motion, and $I(\cdot)$ denotes the indicator function, which is equal to unity when the event inside the parenthesis occurs and zero otherwise. When N is very large, $\lambda_{IM}^{(\mathrm{MC})}(x)$ is essentially equal to $\lambda_{IM}(x)$.

As mentioned earlier in Section 3.4, each database of synthetic ground motions was obtained using magnitudes that are randomly generated from the uniform distribution in Figure 3.2b, $g_M(m)$, instead of $f_M(m)$. Replacing $f_M(m)$ in Equation 3.4 with $f_M(m) \times g_M(m) \div g_M(m)$ leads to

$$\lambda_{IM}(x) = \nu \cdot \left\{ \int \left[\Pr(IM > x \mid M = m) \frac{f_M(m)}{g_M(m)} \right] g_M(m)\, \mathrm{d}m \right\} \tag{3.6}$$

Defining the ratio of $f_M(m)$ over $g_M(m)$ as the Importance Sampling weight, $w(m)$, the benchmark IMHC may therefore be computed from

$$\lambda_{IM}(x) \simeq \frac{\nu}{N} \sum_{i=1}^{N} [I(x_i > x) \cdot w(m_i)] \tag{3.7}$$

where m_i is randomly generated from $g_M(m)$ instead of $f_M(m)$, and x_i now refers to the value of IM for the corresponding i^{th} ground motion. For example, application of Equation 3.7 to the database of $N = 10^4$ synthetic ground motions from Rezaeian's model leads to the results shown by thick solid curves in Figure 3.4. As demonstrated in this figure, Equation 3.7 may be used to compute benchmark IMHCs for a wide variety of IMs.

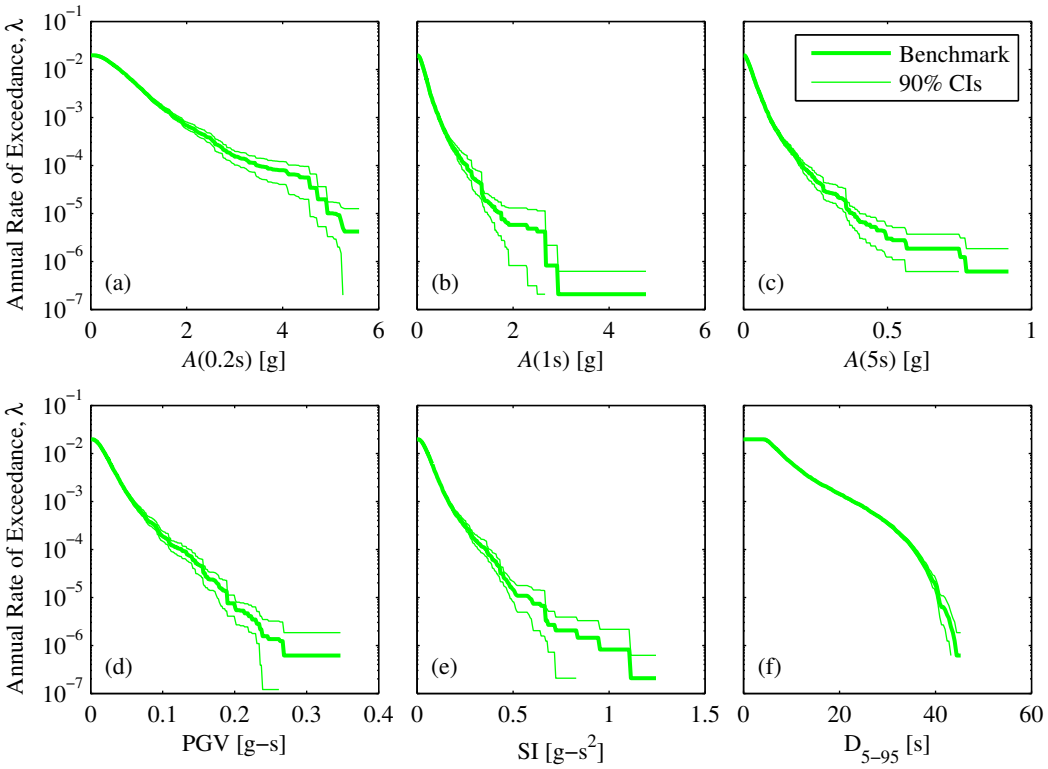

Figure 3.4: Benchmark IMHCs determined from 10^4 ground motions simulated by Rezaeian's stochastic model, for several IMs: (a) $A(0.2s)$; (b) $A(1s)$; (c) $A(5s)$; (d) peak ground velocity (PGV); (e) spectrum intensity (SI); (f) 5-95% significant duration, D_{5-95}.

There is epistemic uncertainty in the benchmark IMHCs because they are developed from a finite number of ground motions. For example, the value of the benchmark hazard curve in Figure 3.4b is zero at intensity levels greater than 4.77g because the largest value of $A(1s)$ observed in the database is 4.77g. For another database of 10^4 ground motions simulated by Rezaeian's model, the largest observed value of $A(1s)$ will be different and hence the corresponding value of the benchmark IMHC will be different. To assess the quality of results achieved by using $N = 10^4$, a 90% confidence interval was determined for

each IMHC by the bootstrap procedure [Efron and Tibshirani, 1993] with 100 bootstrap samples. With these confidence intervals, we see in Figure 3.4 that at high exceedance rates (i.e., rates above 10^{-3} or return periods less than 1000 years), the approximation expressed in Equation 3.7 is nearly perfect. As the exceedance rate decreases, the quality of the approximation deteriorates, which should be recognized when interpreting subsequent results.

Seismic Demand Hazard Curve when Collapse is Impossible

For structural models where collapse is impossible, the steps to develop a benchmark SDHC for any EDP are nearly identical to that just presented for the benchmark IMHC. By replacing IM in Equation 3.4 with EDP, the equation that governs the exact SDHC at this site becomes

$$\lambda_{EDP}(z) = \nu \cdot \left\{ \int \Pr(EDP > z \mid M = m) f_M(m) \, \mathrm{d}m \right\} \tag{3.8}$$

By replacing $f_M(m)$ in Equation 3.8 with $f_M(m) \times g_M(m) \div g_M(m)$ and applying the concept of Importance Sampling as before, the benchmark SDHC for structures where collapse is impossible may be computed from

$$\lambda_{EDP}(z \mid \mathrm{NC}) \simeq \frac{\nu}{N'} \sum_{i=1}^{N'} [I(z_i > z) \cdot w(m_i)] \tag{3.9}$$

where NC stands for "No Collapse", N' is the total number of ground motions where collapse did not occur, and z_i is the value of the EDP corresponding to the i^{th} ground motion. Observe that the benchmark SDHC can be computed from Equation 3.9, without a prediction model for the EDP [Kwong et al., 2014]. However, depending on the exceedance rates of interest, a large number of RHAs may be necessary to implement the calculations in Equation 3.9.

With ground motions simulated by Rezaian's stochastic model, the benchmark SDHCs for the bilinear system are presented in the top row of Figure 3.5. For each EDP, the thick solid curve is computed by Equation 3.9 from the $N' = N = 10^4$ values of the EDP corresponding to the database of synthetic motions. As in Section 3.5, the 90% confidence intervals for these benchmark SDHCs are again obtained from the bootstrap procedure with 100 bootstrap samples.

To facilitate interpretation of these curves, exceedance rates of 2×10^{-3} (return period of 500 years) and 4×10^{-4} (return period of 2500 years), that correspond roughly to the design basis earthquake (DBE) and maximum considered earthquake (MCE) levels specified in [American Society of Civil Engineers, 2010], are noted in Figure 3.5. At exceedance rates above the MCE level, the 90% confidence intervals indicate that the approximation in Equation 3.9 is nearly perfect. Although the quality of this approximation deteriorates for decreasing exceedance rates, the thick solid curves are still referred to as "benchmark" for the purpose of revealing potential biases in SDHC estimates from a GMSM procedure. In passing, note that the system responds nonlinearly at exceedance rates below around

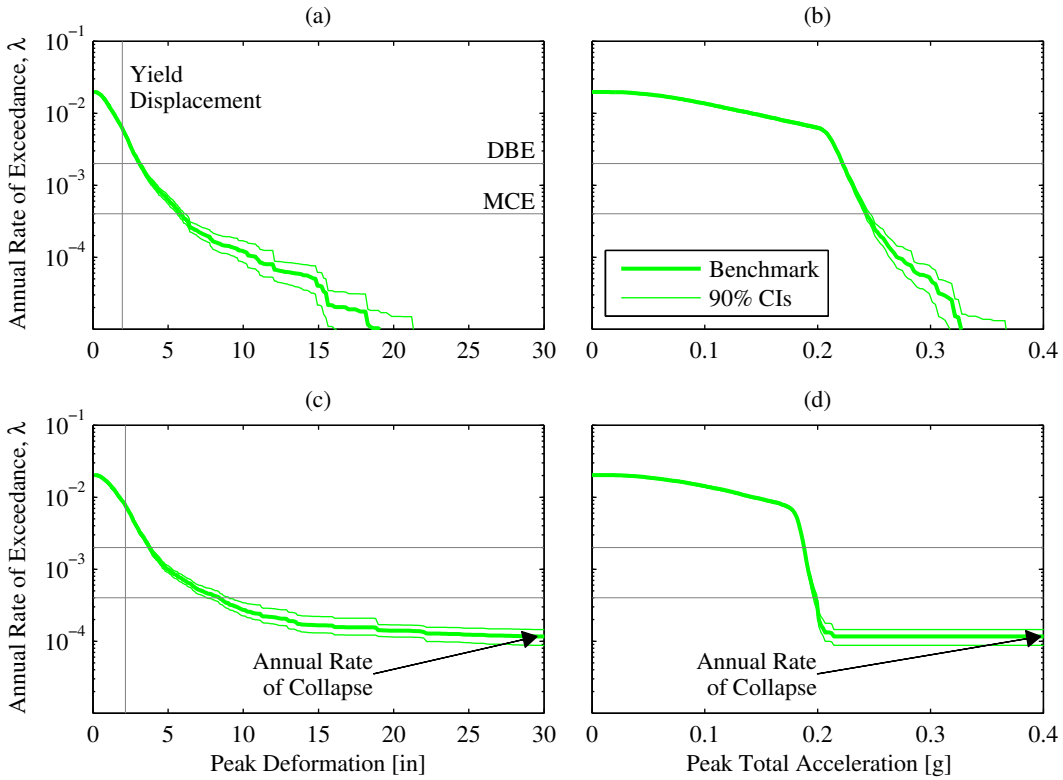

Figure 3.5: Benchmark SDHCs determined from 10^4 ground motions simulated by Rezaeian's stochastic model: (a-b) u_m and $\ddot{u}_o^t$ of bilinear system, respectively; (c-d) u_m and $\ddot{u}_o^t$ of degrading system, respectively.

6×10^{-3}, as indicated by the yield displacement identified in Figure 3.5a and the sudden change in slope in Figure 3.5b.

Seismic Demand Hazard Curve when Collapse Is Possible

Using the total probability theorem and assuming that the probability of EDP exceeding z is equal to unity when the structure collapses [Baker and Cornell, 2005] [5], the term $\Pr(EDP > z \mid M = m)$ in Equation 3.8 is expanded:

$$\Pr(EDP > z \mid M = m) = \Pr(EDP > z, \text{NC} \mid M = m) + \Pr(\text{C} \mid M = m) \tag{3.10}$$

where NC and C denote events corresponding to "No Collapse" and "Collapse", respectively. Substituting Equation 3.10 into Equation 3.8 and rearranging terms leads to

$$\lambda_{EDP}(z) = \lambda_{EDP}(z \mid \text{NC}) \left[1 - \frac{\lambda_C}{\nu}\right] + \lambda_C \tag{3.11}$$

[5] If a different assumption is desired (e.g., assuming $\Pr(PFA > z \mid \text{C}, M = m) = \Pr(PGA > z \mid \text{C}, M = m)$ instead of $\Pr(PFA > z \mid \text{C}, M = m) = 1$, where PFA and PGA denote, respectively, peak floor acceleration of a multistory building and peak ground acceleration [Lin et al., 2013b]), then Equations 3.10-3.11 should be modified appropriately.

where $\lambda_{EDP}(z \mid \text{NC})$ is the benchmark SDHC given that collapse is impossible, and λ_C is the annual rate of collapse.

Computation of the benchmark SDHC for any structural model, with the possibility of collapse, can be organized in five steps. First, RHA of the structure is performed for all N ground motions in the database. Second, the N results from RHA are subdivided into EDP values for the N' non-collapsed cases and $N - N'$ collapsed cases. Third, $\lambda_{EDP}(z \mid \text{NC})$ is determined by applying Equation 3.9 to only the N' values of EDP. Fourth, all N RHA results are employed to compute the annual rate of collapse, λ_C, from

$$\lambda_C \simeq \frac{\nu}{N} \sum_{i=1}^{N} [I(\text{C}_i) \cdot w(m_i)] \tag{3.12}$$

where $I(\text{C}_i)$ is equal to 1 if collapse is observed for the i^{th} ground motion and equal to zero otherwise. Fifth, $\lambda_{EDP}(z \mid \text{NC})$ and λ_C from the latter two steps are substituted in Equation 3.11 to obtain the final benchmark SDHC, $\lambda_{EDP}(z)$. With ground motions simulated by Rezaeian's stochastic model, the benchmark SDHCs of the degrading system are presented in the bottom row of Figure 3.5. As the value of the EDP increases, the benchmark SDHC approaches the annual rate of collapse (Figure 3.5c-d), and the quality of the approximations in Equations 3.9 and 3.12 decreases, as indicated by wider confidence intervals.

3.6 Benchmark-Consistent Prediction Models

Prediction models, which provide the probability distribution of an IM for a given rupture scenario, are needed to select ground motions in contemporary GMSM procedures (e.g., [Jayaram et al., 2011, Bradley, 2010a]). In order to isolate the effect of a GMSM procedure on its resulting SDHC estimate, prediction models must be consistent with the particular database of synthetic ground motions (Figure 3.1); otherwise, an additional source of bias would be introduced. For example, if the GMPM-based IMHC in Equation 3.2, $\widetilde{\lambda}_{IM^*}(x)$, is significantly different than the benchmark IMHC in Equation 3.1, $\lambda_{IM^*}(x)$, then any difference between $\widehat{\lambda}_{EDP}(z)$ in Equation 3.2 and $\lambda_{EDP}(z)$ in Equation 3.1 cannot be solely attributed to the GMSM procedure under consideration. This section describes how such benchmark-consistent prediction models are developed.

Ground-Motion-Prediction Model

Figure 3.6 illustrates how the median value of $IM \equiv A(1s)$ is estimated for a given magnitude. For each database of 10^4 ground motions (Section 3.4), the logarithmic values of $A(1s)$ are plotted against magnitude. Ordinary least squares (OLS) regression is then performed to determine the predicted median as a polynomial function of magnitude, which is shown in solid black. The degree of the polynomial function is chosen such that its corresponding regression results do not differ appreciably from those corresponding to the next higher degree. Based on this criterion, the functional forms for Rezaeian's and Yamamoto's stochastic

models were determined as:

$$\ln IM = b_0 + b_1 M + \epsilon \qquad \ln IM = c_0 + c_1 M + c_2 M^2 + \epsilon \tag{3.13}$$

respectively, where for a given value of magnitude, ϵ is a zero mean normally distributed random variable with standard deviation σ; the b's and c's are coefficients to be estimated from regression analysis.

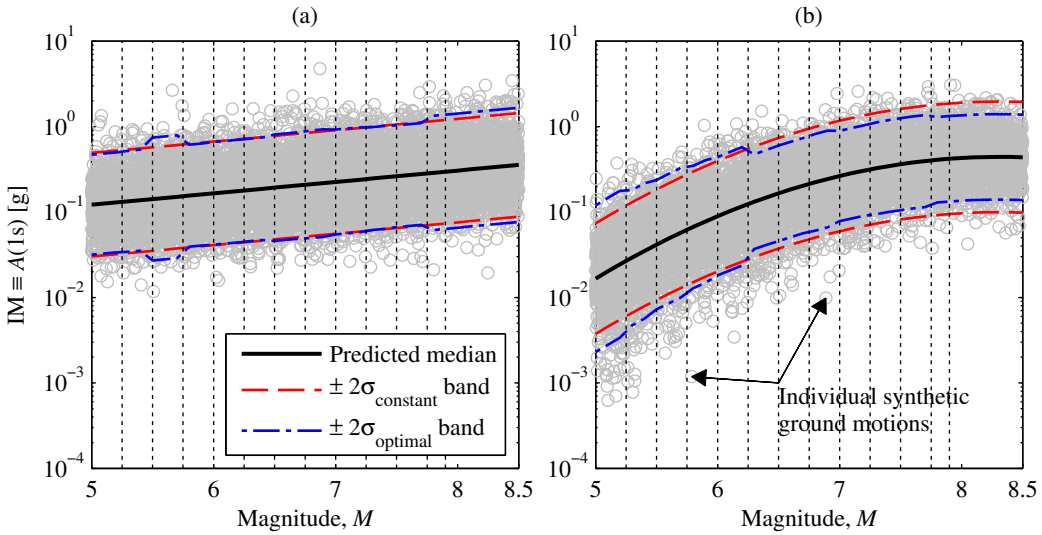

Figure 3.6: Example of GMPM development using synthetic ground motions: (a) Rezaeian's stochastic model; (b) Yamamoto's stochastic model.

Synthetic ground motions for the simple site (Figure 3.2) makes the development of GMPMs herein more manageable than that performed in practice with recorded ground motions. For example, there is no need to apply the random effects model or the two-stage regression technique, since each synthetic ground motion corresponds to an earthquake with a unique magnitude. Therefore, the terms associated with seismological parameters other than magnitude (e.g., distance, style-of-faulting, etc.) that appear in practical GMPMs [Abrahamson et al., 2008] are not relevant for this particular site (see Section 3.4). Consequently, the development of GMPMs reduces to estimating the CCDF of IM for a given magnitude, $\Pr(IM > x \mid M = m)$ in Equation 3.4, assumed to be lognormal.

Figure 3.6 permits three additional observations about the development of GMPMs from synthetic ground motions. First, the estimate of the median IM at large magnitudes is robust because the magnitudes in the ground motion database were randomly generated from the uniform PDF instead of the Youngs & Coppersmith PDF (Figure 3.2b). Second, the relationship between IM and M is unaffected by Importance Sampling since it is specified by the ground motion simulation model. Third, the standard deviation of the IM, σ, depends on magnitude for Yamamoto's model because the $\pm 2\sigma_{constant}$ band in Figure 3.6b covers fewer ground motions at large M than at small M; in contrast, σ is essentially independent of

magnitude in Rezaeian's model because the $\pm 2\sigma_{constant}$ band in Figure 3.6a covers a similar amount of data at all M. For generality, σ is modeled as a function of magnitude in both stochastic models.

A natural way to model σ as a function of magnitude is to divide the magnitude domain into discrete bins and determine a value of σ at each bin. We chose the 12 bins shown in Figure 3.6. For each magnitude interval, the value of σ may be obtained by applying OLS to the binned ground motions; such values are denoted by σ_{binned}. At magnitudes beyond the domain of $f_M(m)$ in Figure 3.2b, σ is given by that from the closest magnitude bin.

Once a GMPM is finalized, $\widetilde{\Pr}(IM > x \mid M = m)$ is known and the corresponding IMHC may be computed from a discrete form of Equation 3.4:

$$\widetilde{\lambda}_{IM}(x) = \nu \cdot \left\{ \sum_{m} \widetilde{\Pr}(IM > x \mid M = m) \Pr(M = m) \right\} \tag{3.14}$$

For example, suppose $\widetilde{\Pr}(IM > x \mid M = m)$ is a lognormal CCDF with the median obtained from the solid black curve in Figure 3.6b and the standard deviation obtained from σ_{binned}. Applying Equation 3.14 to this model leads to the dashed curve in Figure 3.7a.

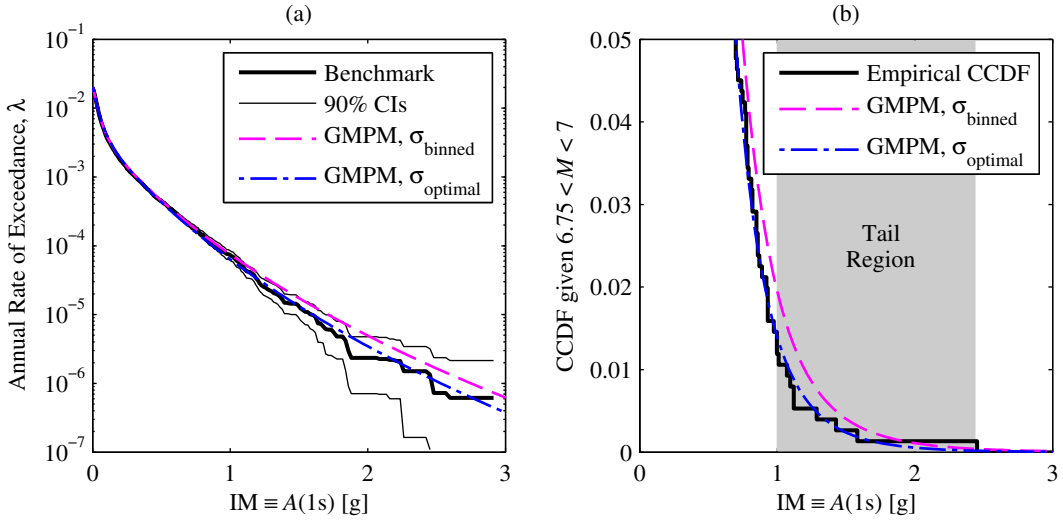

Figure 3.7: Example of enforcing benchmark-consistency on GMPMs developed from ground motions simulated by Yamamoto's stochastic model; comparison of: (a) IMHCs; (b) CCDFs at small probabilities.

The GMPMs based on σ_{binned} may not be benchmark-consistent. For example, the model for $A(1s)$ mentioned in the preceding paragraph is not benchmark-consistent because its corresponding IMHC differs from the associated benchmark IMHC at intensity levels greater than 1g (Figure 3.7a). By comparing Equation 3.14 against Equation 3.4, we see that the discrepancy between $\widetilde{\lambda}_{IM}(x)$ and $\lambda_{IM}(x)$ is due primarily to the discrepancy between

$\widetilde{\Pr}(IM > x \mid M = m)$ and $\Pr(IM > x \mid M = m)$ at small exceedance probabilities (Figure 3.7b). For other IMs and other ground motion simulation models, this issue will introduce an additional source of bias to the GMSM-based estimate of the SDHC.

Since we wish to isolate the effects of a GMSM procedure on its resulting SDHC estimate, $\widetilde{\lambda}_{IM^*}(x)$ in Equation 3.2 must agree as closely as possible with $\lambda_{IM^*}(x)$ in Equation 3.1. To achieve this goal, σ is determined for each magnitude bin such that its resulting lognormal CCDF agrees most closely with the empirical CCDF at the 'tails'; this standard deviation is denoted as $\sigma_{optimal}$. An example of the tail region is presented as the shaded area in Figure 3.7b. The right boundary of this region corresponds to the largest value of the observed IM within the magnitude bin whereas the left boundary corresponds to the intensity level at which the IMHC from σ_{binned} begins to differ from the benchmark IMHC (Figure 3.7a) [6]; if the latter is larger than the former (or if there is only one ground motion within this tail region), then the tail region is undefined and $\sigma_{optimal}$ is specified as σ_{binned}. To quantify the discrepancy between $\widetilde{\Pr}(IM > x \mid M = m)$ and $\Pr(IM > x \mid M = m)$ at small exceedance probabilities, we introduce the following metric:

$$\Delta = \sum_{x \in \Omega} \left[\frac{\widetilde{G}(x, \sigma) - G(x)}{G(x)} \right]^2 \tag{3.15}$$

where Ω denotes the tail region, $G(x)$ is a shorthand notation for the empirical CCDF, and $\widetilde{G}(x, \sigma)$ is a shorthand notation for the lognormal CCDF corresponding to a trial value of σ. The value of σ that minimizes Δ is the desired $\sigma_{optimal}$. Determined using $\sigma_{optimal}$, the IMHC for $A(1s)$ agrees closely with the benchmark IMHC, confirming that the corresponding GMPM is benchmark-consistent (Figure 3.7a). Such benchmark-consistent GMPMs were developed for 21 periods of vibration that are logarithmically spaced between 0.05s and 10s; for other vibration periods, linear interpolation on the logarithmic scale was employed. This process of determining $\sigma_{optimal}$ may also be employed when developing benchmark-consistent GMPMs for other IMs.

Correlation between Intensity Measures

Correlations between IMs are needed to specify the joint distribution of a vector IM (see e.g., [Bradley, 2010a, Jayaram et al., 2011]). Derived subsequently are new correlations that are consistent with the database of synthetic ground motions.

For a given stochastic model, the correlation between two IMs is determined from the correlation between the residuals of each IM, defined as the differences between the observed and predicted values of each synthetic ground motion; e.g., the residuals for $A(1s)$, under Rezaeian's model, are the vertical deviations between each circle and the black solid curve in Figure 3.6a. For both stochastic models, the correlations between spectral accelerations

[6] In this study, the left boundaries of the tail regions for all IMs were determined from visual comparison of the IMHCs. Alternatively, the left boundary of the tail region for an IM may be determined from its benchmark IMHC as the intensity level that corresponds to a single user-defined exceedance rate (e.g., 4×10^{-4}).

at vibration periods from 0.05 sec to 10 sec are presented in Figure 3.8. The significant differences between the correlations from the two stochastic models indicate the need for benchmark-consistent correlations.

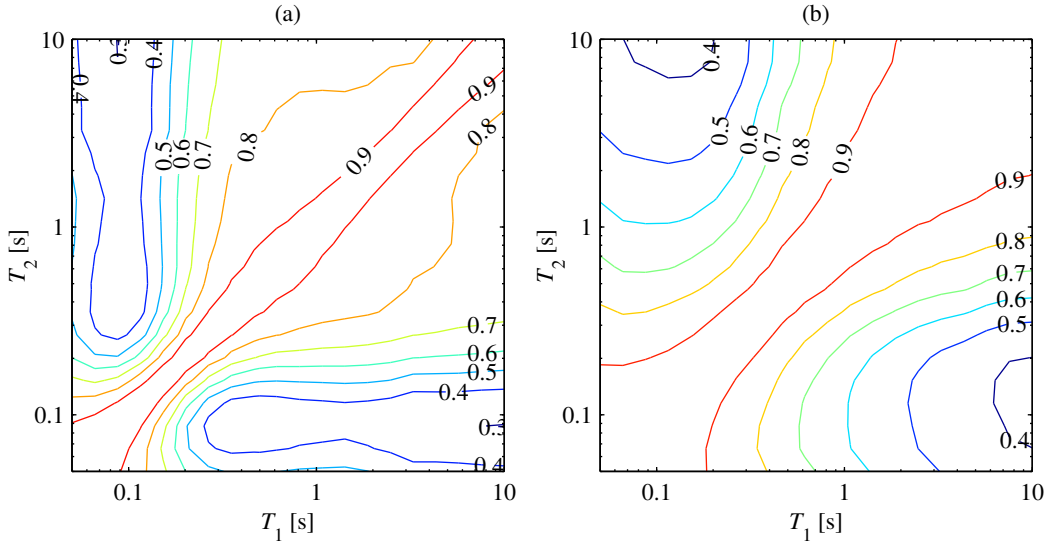

Figure 3.8: Correlations between spectral accelerations at periods from 0.05 to 10 sec observed in 10^4 ground motions simulated by: (a) Rezaeian's stochastic model; and (b) Yamamoto's stochastic model.

For both stochastic models, the correlation between two IMs appears to be magnitude-dependent. To examine this magnitude dependence, we used the approach outlined in Appendix B of [Baker, 2006]. For each IM, the associated 10^4 residuals are partitioned into the 12 magnitude bins shown in Figure 3.6. A correlation is then computed for each magnitude bin and compared against the correlation from all bins. From such comparisons, we observed magnitude dependence for many pairs of IMs. For generality, the correlation between two IMs is modeled herein as a function of magnitude by providing a correlation value for each of the 12 magnitude bins.

3.7 Illustrative Evaluation of GMSM Procedures

With a large database of synthetic ground motions obtained for the given site (Section 3.4), benchmark SDHCs determined for the given structures (Section 3.5), and benchmark-consistent prediction models developed (Section 3.6), we are now ready to illustrate the evaluation of GMSM procedures in their ability to accurately estimate the SDHC (Figure 3.1). For each of the two GMSM procedures mentioned in Section 3.4, an estimate of the SDHC is computed from Equation 3.2. The conditioning IM is defined as spectral acceleration at 1 sec and $N_{IM^*} = 12$ intensity levels are chosen, which correspond to: 50%, 20%, 10%, 5%, 2%, 1%, 0.5%, 0.2%, 0.1%, 0.05%, 0.02%, and 0.01% probability of exceedance in 50 years. At each

intensity level, a subset of $n = 44$ synthetic ground motions are selected by the GMSM procedure, as excitations for RHAs of the structure, and the lognormal distribution is employed to determine $\widehat{\Pr}(EDP > z \mid IM^* = x_i)$; in total, $N_{IM^*} \times n = 528$ RHAs are performed to compute a single estimate of the SDHC.

In this study, the seed ensemble for IDA is selected in a manner that is inspired by the approach taken to develop the Far-Field record set in [Applied Technology Council, 2009]. As described in Appendix A.7 of [Applied Technology Council, 2009], the Far-Field record set for use in IDA was determined by preferentially selecting intense ground motions that were likely to induce structural collapse. To mimic this practical approach, we first filtered the database of 10^4 synthetic ground motions according to the following criteria: (1) $6.5 < M < 7.5$, (2) PGA greater than 0.2g, and (3) PGV greater than 15 cm/sec. Among the remaining ground motions, the 44 motions with the largest values of PGV are chosen as the seed ensemble. Unlike Appendix A.7 of [Applied Technology Council, 2009], an upper limit for magnitude is provided in the first selection criterion because records from earthquakes with $M > 7.5$ are rare whereas over 2000 synthetic ground motions satisfied the three criteria above.

The selection of ground motions in GCIM-SA is significantly more sophisticated than that in IDA. In this case, 44 ground motions are re-selected at each of the 12 intensity levels. For a particular intensity level, deaggregation is performed and the target GCIM-SA spectrum is constructed using the prediction models developed in Section 3.6. For example, the target spectrum for the MCE level is presented in Figure 3.9a, which is defined at 11 vibration periods: $\mathbf{T}_{IM} = \{0.05, 0.1, 0.2, 0.3, 0.5, 0.75, 1, 2, 3, 5, 10\}$. From such a target spectrum, n response spectra may be simulated by methods presented in [Bradley, 2010a, Bradley, 2012a]; for example, two simulated spectra are illustrated by markers in Figure 3.9b. For each of the n simulated spectra, the synthetic ground motion whose response spectrum agrees most closely with the simulated one is selected (see solid and dashed curves in Figure 3.9b).

RHAs of each system, subjected to the same selection of ground motions from a GMSM procedure, are performed to compute the corresponding SDHCs. For example, the results from RHAs of the degrading system due to ground motions selected by both GMSM procedures are presented in Figure 3.10. At each intensity level, the 44 results are classified either as non-collapsed or collapsed. The non-collapsed results, which are shown in the top row of Figure 3.10, are used in conjunction with the lognormal distribution to estimate $\widehat{\Pr}(EDP > z \mid \text{NC}, IM^* = x_i)$ in Equation 3.3. On the other hand, the fragility function, $\widehat{p}_C(x_i)$ in Equation 3.3, is determined from all 44 results, using the maximum likelihood fitting procedure described by Baker in [Baker, 2015]. For each GMSM procedure, $\widehat{\Pr}(EDP > z \mid \text{NC}, IM^* = x_i)$ and $\widehat{p}_C(x_i)$ are combined via Equation 3.3 and the resulting estimate of the SDHC is computed from Equation 3.2.

The GMSM-based SDHCs for the two EDPs – peak deformation, u_m, and peak total acceleration, $\ddot{u}_o^t$ – are presented in Figure 3.11. For a particular EDP, the SDHCs from both GMSM procedures are essentially identical at exceedance rates above the DBE level but become increasingly different below the MCE level. Since N_{IM^*} and $\widetilde{\lambda}_{IM^*}(x_i)$ in Equation 3.2

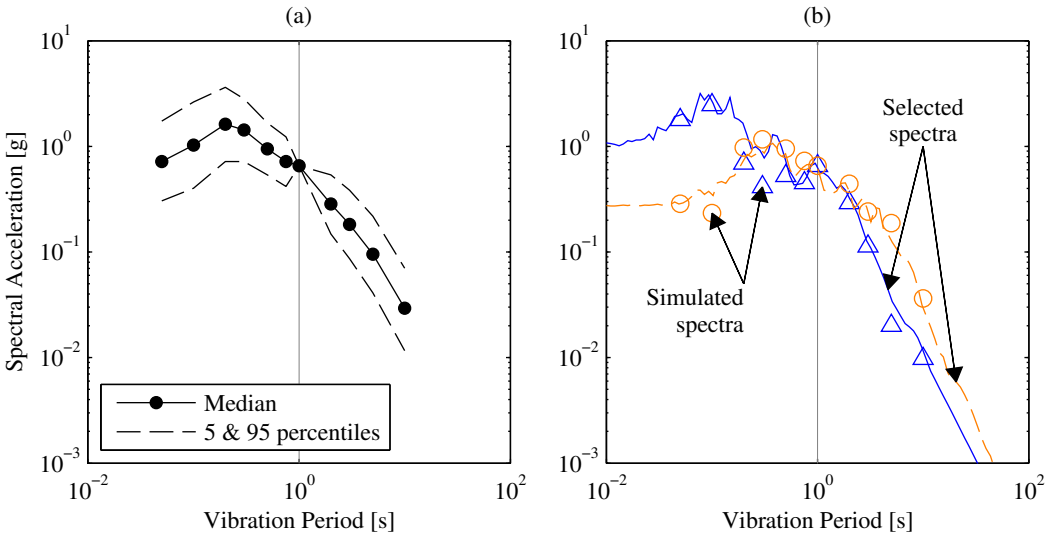

Figure 3.9: Illustration of ground motion selection via GCIM-SA for $A(1s)$ at the MCE level using Rezaeian's stochastic model: (a) target spectrum; and (b) simulated spectra from the target spectrum versus selected spectra from the database of synthetic ground motions.

are identical in both GMSM procedures, the two resulting SDHCs differ because the ground motions selected in the two cases are not the same. Thus the natural question is: which of the two SDHCs is more accurate and by how much?

To answer this question, we compare both GMSM-based SDHCs against the benchmark SDHCs from Figure 3.5; these comparisons reveal two important observations. First, the bias in an estimate of the SDHC depends on the exceedance rate. Using the two EDPs of the degrading system as an example (Figure 3.11c-d), the SDHCs from both GMSM procedures are unbiased at exceedance rates above the DBE level; at exceedance rates below the MCE level however, the SDHC from GCIM-SA remains unbiased whereas that from IDA overestimates the demand. Second, the accuracy of a SDHC from a GMSM procedure depends on the structure considered. For example, the SDHCs from GCIM-SA are unbiased for the degrading system (Figure 3.11c-d) but they underestimate the demand for the bilinear system at exceedance rates below 10^{-4} (Figure 3.11a-b). These observations may be explained using the concepts of "hazard consistency" and "IM sufficiency" [Kwong et al., 2014], which are introduced next.

We define an ensemble of ground motions to be *hazard consistent for some IM* if its resulting estimate of the IMHC, denoted by $\widehat{\lambda}_{IM}(x)$, is essentially equal to the benchmark IMHC, $\lambda_{IM}(x)$ (Equation 3.7). The former hazard curve is estimated from

$$\widehat{\lambda}_{IM}(y) = \sum_{i=1}^{N_{IM^*}} \widehat{\Pr}(IM > y \mid IM^* = x_i) \cdot |\Delta\widetilde{\lambda}_{IM^*}(x_i)| \tag{3.16}$$

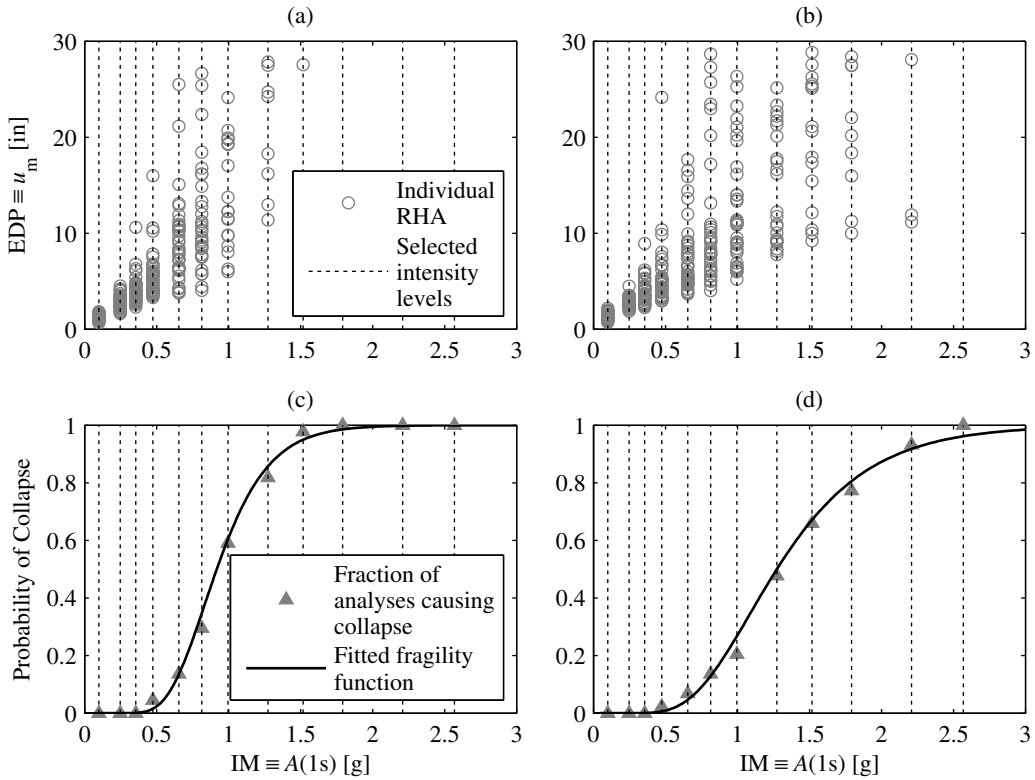

Figure 3.10: RHA results of the degrading system subjected to ground motions selected from Rezaeian's database for PSDA: (a-b) non-collapse data from IDA and GCIM-SA, respectively; (c-d) collapse data from IDA and GCIM-SA, respectively.

where $\widehat{\Pr}(IM > y \mid IM^* = x_i)$ is the empirical CCDF of IM corresponding to all ground motions scaled to intensity x_i; for example, applying Equation 3.16 to the ground motions from IDA leads to the IMHC estimates shown as dashed curves in Figure 3.12. In previous research, hazard consistency was defined relative to the IMHC computed from a GMPM in PSHA, $\widetilde{\lambda}_{IM}(x)$ in Equation 3.14, because the benchmark IMHC, $\lambda_{IM}(x)$, could not be obtained from recorded ground motions [Lin et al., 2013b, Kwong et al., 2014]. Since the latter may now be determined from synthetic motions, (1) hazard consistency is defined herein relative to the benchmark IMHC, and (2) the issue of benchmark-consistency arises for the first time (Section 3.6).

Conceptually, hazard consistency is a property of the selected ground motions: it indicates whether or not the 'intensity' of a particular ensemble is representative of that assumed in PSHA (i.e., assumed via GMPMs, stochastic models of ground motions, etc.). For example, suppose the intensity is measured by $IM^* \equiv A(1s)$. The ground motions from both GMSM procedures are hazard consistent for this IM because each GMSM-based estimate of the hazard curve agrees closely to the benchmark (Figure 3.12c). This is to be expected since for each GMSM procedure, all ground motions were deliberately scaled such that the

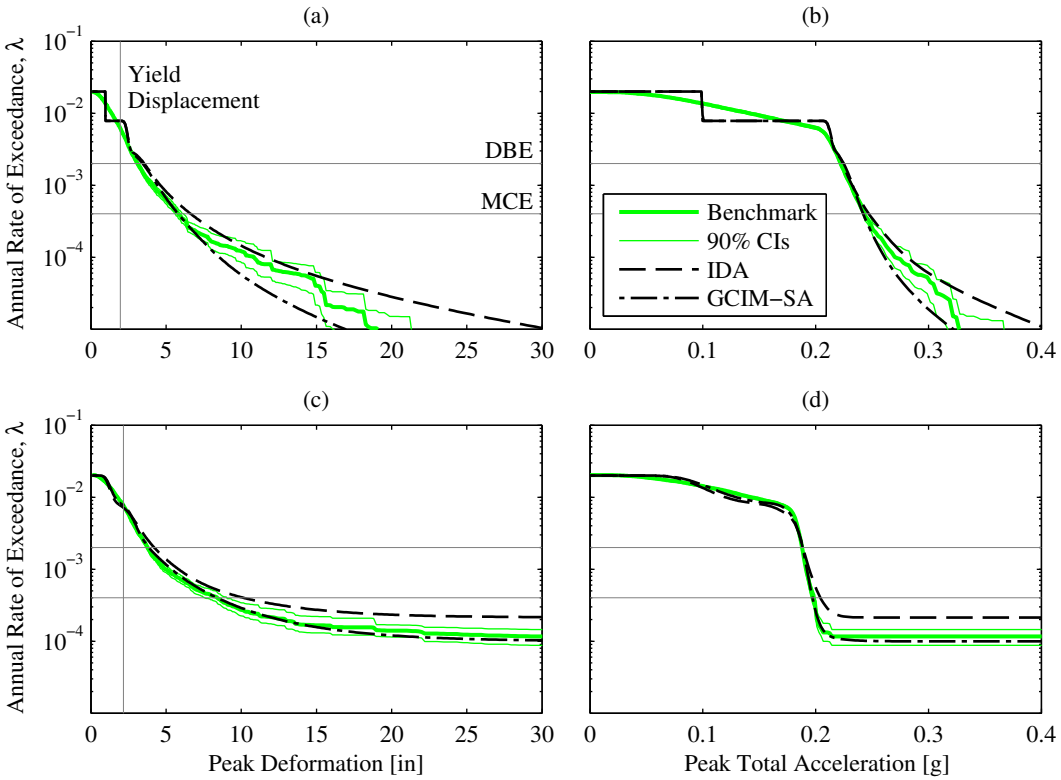

Figure 3.11: Comparison of GMSM-based SDHCs against the benchmark SDHC using Rezaeian's stochastic model: (a-b) u_m and $\ddot{u}_o^t$ of bilinear system, respectively; (c-d) u_m and $\ddot{u}_o^t$ of degrading system, respectively.

estimated hazard curve for IM^*, $\widehat{\lambda}_{IM^*}(x)$, is essentially identical to that computed from a GMPM, $\widetilde{\lambda}_{IM^*}(x)$ (see Equation 3.16), and the latter is in turn practically equal to the associated benchmark, $\lambda_{IM^*}(x)$ (see Section 3.6). However, such scaling distorts other aspects of the ground motion, potentially leading to hazard inconsistencies with respect to other IMs. For instance, Figure 3.12e demonstrates that the ground motions from IDA are hazard *inconsistent* with respect to $IM \equiv A(3s)$ whereas those from GCIM-SA are indeed hazard consistent for this IM. It is to be expected that ground motions from GCIM-SA are hazard consistent for spectral accelerations at many vibration periods, because they have been selected to deliberately match the target spectra (see Figure 3.9). However, they are potentially hazard inconsistent with respect to IMs that are not included in the selection process (e.g., cumulative absolute velocity, significant duration, etc.).

An IM, which may be scalar or vector-valued, is defined to be *sufficient* with respect to an EDP when, given a fixed value of this IM, the EDP does not depend on any other aspects of the ground motion [Shome et al., 1998, Luco and Cornell, 2007]. Put differently, a sufficient IM completely controls the response of the system. For example, the peak response of a linear-elastic MDF structure is essentially controlled by spectral acceleration at its modal

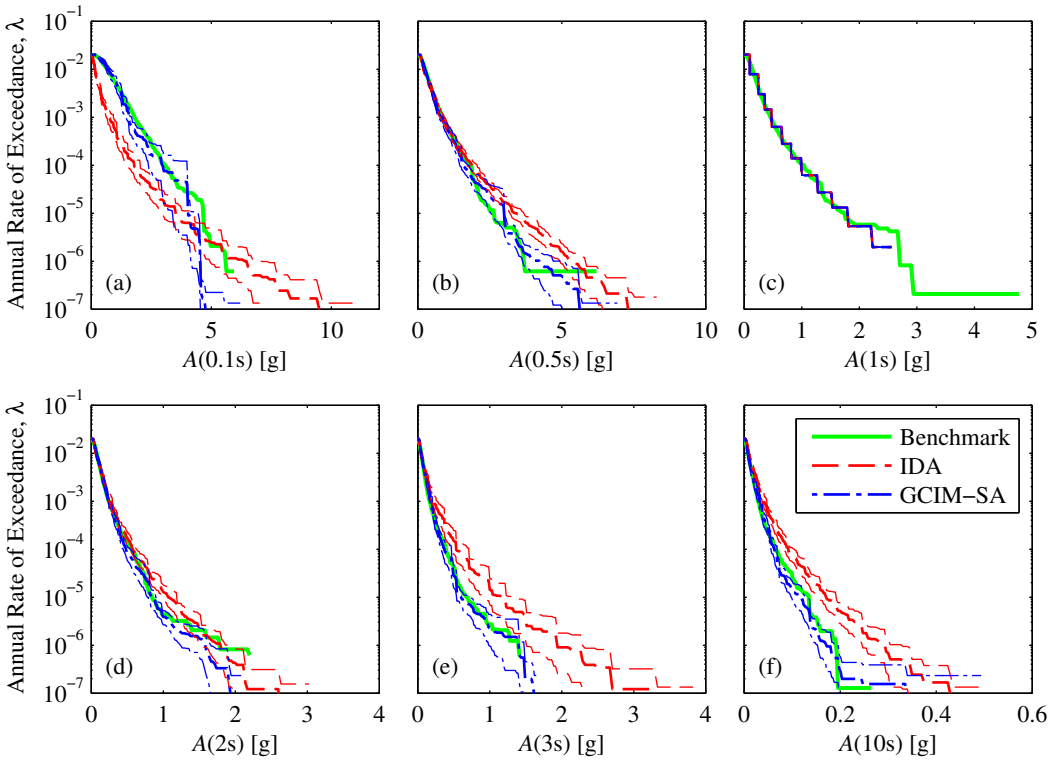

Figure 3.12: Hazard consistency of ground motions selected by both GMSM procedures in PSDA, for spectral accelerations at six periods of vibration: (a) 0.1 sec; (b) 0.5 sec; (c) 1 sec; (d) 2 sec; (e) 3 sec; and (f) 10s.

periods of vibration; therefore, this vector IM is expected to be sufficient with respect to such EDPs.

The concepts of sufficiency and hazard consistency may be used to explain why the bias in an estimate of the SDHC depends on the exceedance rate. For instance, consider the SDHCs for the degrading system in Figure 3.11c-d. At exceedance rates above the DBE level, the system responds linearly and hence $A(1s)$ is sufficient. Because ground motions from both GMSM procedures are hazard consistent for this IM (Figure 3.12c), the resulting SDHCs are unbiased at this range of linear elastic behavior. At exceedance rates below the MCE level however, the system deforms in the inelastic range and we know from structural dynamics that $A(1s)$ alone no longer controls the peak deformation. Consequently, the hazard consistency of the selected ground motions, with respect to IMs other than $A(1s)$, determines the accuracy of the resulting SDHCs. Because the ground motions from IDA are hazard inconsistent with respect to spectral accelerations at vibration periods longer than 2 sec (Figure 3.12e-f), the resulting SDHCs overestimate the demand.

The accuracy of a SDHC from a GMSM procedure depends on the structure and EDP of interest because an IM that is insufficient for one structure or EDP may turn out to

be sufficient for another. For example, consider the ground motions from GCIM-SA that were deliberately selected to be hazard consistent with respect to the vector IM, comprising spectral accelerations at vibration periods from 0.05 to 10 sec. This vector IM, or spectral shape, is insufficient for the two EDPs of the bilinear system at exceedance rates below 10^{-4}. This conclusion may be deduced as follows: if the vector IM is indeed sufficient for the EDP at exceedance rates below 10^{-4}, then the fact that the ground motions are hazard consistent with respect to this IM (Figure 3.12) should have resulted in an unbiased estimate of the SDHC at such exceedance rates [Kwong et al., 2014]; since this is not the case however (Figure 3.11a-b), the IM must not be sufficient. At such extreme levels of nonlinearity, the EDPs of the bilinear system are controlled by aspects of the ground motion other than spectral shape; in particular, the duration of the ground motion seems to affect the system's peak response because the system is able to experience many cycles of vibration, as its strength is unlimited. In contrast, the degrading system would have collapsed for exceedance rates below 10^{-4}. As a result, spectral shape appears to be sufficient for the degrading system at all exceedance rates of interest whereas it is only sufficient for the bilinear system at exceedance rates above 10^{-4}.

In general, estimates of the SDHC will be unbiased as long as the corresponding ground motions are hazard consistent with respect to an IM that is sufficient [Kwong et al., 2014]. However, sufficient IMs may not exist for EDPs of a complex, realistic structure as its response is sensitive to many details of the ground motion. Therefore, any modification of ground motions may result in biased SDHCs for such systems. The approach proposed in Figure 3.1 makes it possible to quantify potential biases and assess the sufficiency of IMs employed for ground motion selection.

To further test the proposed approach for evaluating GMSM procedures, it was reimplemented for the database of 10^4 ground motions from Yamamoto's stochastic model. Using this new database, new benchmark hazard curves were computed (Section 3.5), new benchmark-consistent prediction models were developed (Section 3.6), and new GMSM-based estimates of the SDHC were obtained; in total, this effort required an additional 11056 more RHAs of each structure. The results from utilizing Yamamoto's stochastic model are summarized in Figure 3.13.

We expect similar observations regarding bias in the SDHCs resulting from Yamamoto's stochastic model because the proposed approach aims to isolate the effects of a GMSM procedure on its resulting estimates of the SDHC. This expectation is confirmed in Figure 3.13; observe that although the benchmark SDHCs in this figure differ from those in Figure 3.11, the GMSM-based SDHCs are *also different* between the two figures. The SDHCs from GCIM-SA again underestimate the demand of the bilinear system at exceedance rates below 10^{-4}; this confirms that the response of the bilinear system is controlled by aspects of the ground motion other than spectral shape at such extreme levels of nonlinearity. For the degrading system, the SDHCs from GCIM-SA are again unbiased and those from IDA again overestimate the demand at exceedance rates below the MCE level. The fact that the SDHCs from GCIM-SA are unbiased for the degrading system in both stochastic models strongly suggests that spectral shape is indeed a sufficient IM for this system.

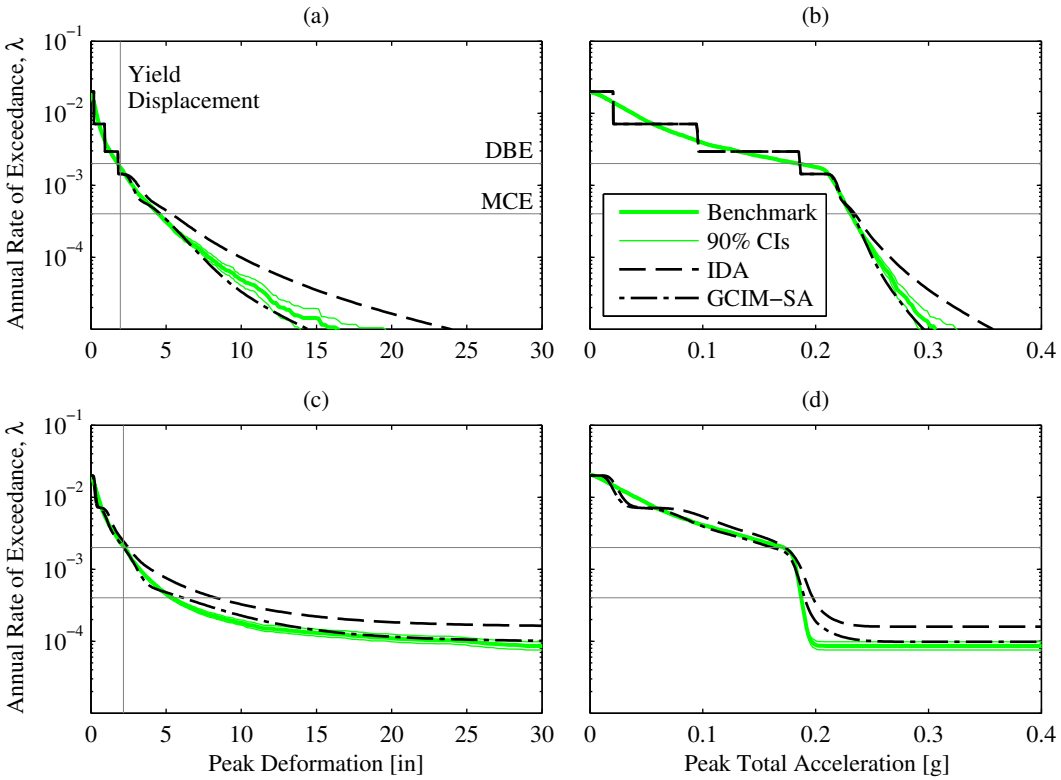

Figure 3.13: Comparison of GMSM-based SDHCs against the benchmark SDHC using Yamamoto's stochastic model: (a-b) u_m and $\ddot{u}_o^t$ of bilinear system, respectively; (c-d) u_m and $\ddot{u}_o^t$ of degrading system, respectively.

However, we observe a few minor differences between the results from the two stochastic models. First, both structures yield at different rates of exceedance (e.g., the bilinear system yields at 6×10^{-3} in Rezaeian's model but yields at the DBE level in Yamamoto's model); this is expected since the benchmark SDHC differs in each stochastic model (Section 3.3). Second, the SDHCs from IDA are unbiased for the bilinear system at exceedance rates between 2×10^{-4} and 5×10^{-5} in Rezaeian's model (Figure 3.11a-b) but overestimate the demand at this range of exceedance rates in Yamamoto's model (Figure 3.13a-b). The latter difference regarding IDA arises because ground motions from this procedure are hazard consistent with respect to $A(2s)$ in Rezaeian's model (Figure 3.12d) but are hazard *inconsistent* with respect to $A(2s)$ in Yamamoto's model (not shown). Aside from such differences, the overall similarity between the relationships depicted in Figures 3.11 and 3.13 indicates that the proposed approach for evaluating GMSM procedures is robust.

3.8 Comparison with Previous Research

In previous research, a GMSM-based estimate of the SDHC was considered unbiased if different choices of the conditioning IM led to essentially the same estimate [Bradley, 2012c,

Lin et al., 2013b]. This approach is illustrated in Figure 3.14 where estimates of the SDHC for the peak deformation of the degrading system, computed from Equation 3.2 for four choices of the conditioning period, T^*, are presented. The fact that the four SDHCs are closer to each other for GCIM-SA than for IDA suggests that SDHC estimates from GCIM-SA are less biased – or more accurate – than those from IDA.

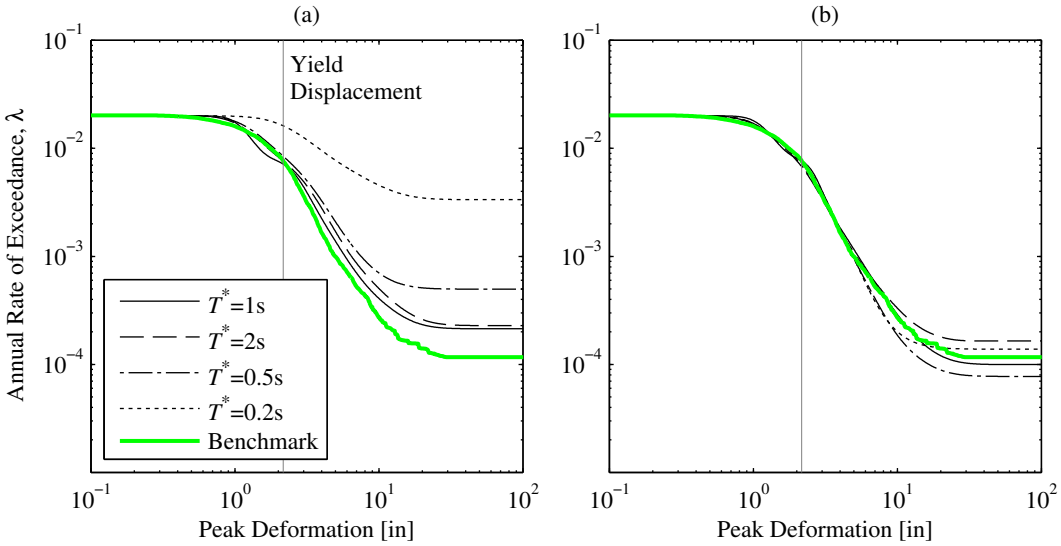

Figure 3.14: Comparison of GMSM-based SDHCs from different definitions of the conditioning IM for $EDP \equiv u_m$ of the degrading system, using ground motions simulated by Rezaeian's stochastic model: (a) IDA; (b) GCIM-SA.

This existing approach has two limitations. First, it is not possible to quantify the bias in any GMSM-based SDHC for lack of a benchmark. Second, several significantly different definitions of the conditioning IM are typically needed to draw definitive conclusions from the existing approach. For example, if only 1 s and 2 s were considered as definitions for T^*, then Figure 3.14 may erroneously suggest that the SDHCs from IDA are less biased than those from GCIM-SA.

These two limitations are overcome by the approach presented in this work. First, the bias in any SDHC estimate can be quantified by comparing the estimate against the benchmark SDHC in a controlled setting (Figure 3.1). For example, the benchmark SDHC in Figure 3.14 verifies that the SDHCs from GCIM-SA are more accurate than those from IDA. For each GMSM procedure, the SDHC corresponding to 1 sec is most accurate among the four conditioning periods considered; this confirms the conclusion by Lin et al [Lin et al., 2013b] that the choice of the conditioning period is important for accurate estimation of SDHCs in PSDA. Moreover, the ability to quantify bias enables the analyst to assess the sufficiency of IMs for an EDP of interest (Section 3.7). Second, the need to choose several definitions of the conditioning IM is avoided in the proposed approach since the benchmark SDHC is developed only once, regardless of the number of GMSM procedures considered

(see Sections 3.5 and 3.5). For a more comprehensive comparison of hazard curves in Figures 3.11-3.14, a bootstrap confidence interval may also be provided for each GMSM-based hazard curve, which is useful when the total number of ground motions used for each hazard curve is less than that in this study ($N_{IM^*} \times n = 528$).

These two limitations were also overcome in [Kwong et al., 2014], where benchmark SDHCs for the peak deformation of a bilinear SDF system were developed from prediction models based on recorded ground motions. However, the benchmark SDHC in the current study may be computed for *any* EDP of interest and the bias in a SDHC estimated from a particular GMSM procedure may be isolated more completely with the aid of synthetic ground motions. Note that the models for simulating ground motions should be appropriate for the site considered.

Applying the proposed approach for other structures and other sites can be much more complicated and computationally demanding. For example, computation of the benchmark SDHC (Section 3.5) for complex, realistic structures would require enormous effort because a large number of RHAs is necessary. For sites with multiple earthquake sources and earthquakes occurring at random locations, the methods for developing a database of ground motions and benchmark-consistent prediction models will be slightly different than those presented in this study. When developing the database of ground motions (Section 3.4), the ground motion simulation models will require randomly generated rupture scenarios from all earthquake sources as input for simulating ground motions. When developing benchmark-consistent GMPMs (Section 3.6), the probability distribution of IMs will depend on seismological parameters (e.g., distance, style-of-faulting, etc.) in addition to magnitude, increasing the complexity of the functional forms (Equation 3.13).

3.9 Conclusions

This investigation of employing synthetic ground motions to evaluate GMSM procedures has led to the following conclusions:

1. A novel approach for evaluating GMSM procedures, in the context of PSDA, is presented. In essence, synthetic ground motions are employed to: (1) derive the benchmark SDHC, for the structure and response quantity of interest, and (2) establish the causal relationship between a GMSM procedure and the bias in its resulting estimate of the SDHC. To achieve the latter goal, new benchmark-consistent prediction models are developed.

2. A case study is presented to illustrate the proposed approach. For two simple systems at a simple site, two GMSM procedures – IDA and GCIM-SA – are evaluated, leading to the following observations:

    a) The bias in an estimate of the SDHC depends on the exceedance rate. At exceedance rates above (or greater than) the DBE level, SDHCs from both pro-

cedures are unbiased for both systems and both EDPs; below the MCE level however, SDHCs from GCIM-SA are generally more accurate than those from IDA.

b) The accuracy of a SDHC from a GMSM procedure depends on the structure and EDP of interest. At exceedance rates below the MCE level, SDHCs from GCIM-SA are unbiased for the degrading system but not for the bilinear system.

c) Spectral shape appears to be sufficient for the degrading system at all exceedance rates of interest; however, it is insufficient for the bilinear system at exceedance rates below 10^{-4}. Below this exceedance rate, the response of the bilinear system is influenced by aspects of the ground motion other than spectral shape because the system is able to experience many cycles of vibration, as its strength is unlimited; in contrast, the degrading system would have already collapsed.

d) For the degrading system and for both GMSM procedures, the peak deformation hazard curve that corresponds to the system's fundamental period is most accurate among the four conditioning periods considered.

3. The proposed approach is demonstrated to be robust, as similar conclusions are obtained from two significantly different stochastic models for simulating ground motions.

4. Unlike previous research, the current approach offers the ability to quantify bias in SDHCs for *any* structure and EDP of interest, avoids the need to choose several different conditioning IMs, and isolates the bias in the SDHC estimate from a GMSM procedure more completely with synthetic ground motions.

5. In general, estimates of the SDHC will be unbiased as long as the corresponding ground motions are hazard consistent with respect to an IM that is sufficient. However, sufficient IMs may not exist for EDPs of a complex, realistic structure. Therefore, any modification of ground motions may result in biased SDHCs for such systems. The proposed approach makes it possible to quantify potential biases and assess the sufficiency of IMs employed for ground motion selection.

Chapter 4

A Ground Motion Selection Procedure for Enforcing Hazard Consistency and Estimating Seismic Demand Hazard Curves

4.1 Preview

This chapter develops a procedure to select unscaled ground motions for estimating seismic demand hazard curves (SDHCs) in performance-based earthquake engineering (PBEE). Currently, SDHCs are estimated from a probabilistic seismic demand analysis (PSDA), where several ensembles of ground motions are selected and scaled to a user-specified conditioning intensity measure (IM). In contrast, the procedure developed herein provides a way to select a *single* ensemble of *unscaled* ground motions for estimating the SDHC. In the context of unscaled motions, the proposed procedure requires three inputs: (i) database of unscaled ground motions, (ii) **IM**, the vector of IMs for selecting ground motions, and (iii) sample size, n; in the context of scaled motions, two additional inputs are needed: (i) a maximum acceptable scale factor, SF_{max}, and (ii) a target fraction of scaled ground motions, γ. Using a recently developed approach for evaluating ground motion selection and modification procedures, the proposed procedure is evaluated for a variety of inputs and is demonstrated to provide accurate estimates of the SDHC when ground motions are unscaled, or when the vector of IMs chosen to select ground motions is sufficient for the response quantity of interest.

4.2 Introduction

In performance-based earthquake engineering (PBEE), response history analyses (RHAs) of structural models are typically performed for three different contexts: (i) intensity-based assessment, (ii) scenario-based assessment, and (iii) risk-based assessment [Applied Technology Council, 2012, NEHRP Consultants Joint Venture, 2011]. This chapter focuses on a

risk-based assessment, or a probabilistic seismic demand analysis (PSDA), which is the most comprehensive context among the three. The primary output of a PSDA is a plot of the annual rate of exceedance, λ, as a function of the seismic demand, or engineering demand parameter (EDP); such a plot is referred to as a seismic demand hazard curve (SDHC), which is unique for a given structure at a given site [Bradley, 2012c]. In essence, a SDHC is computed from a PSDA by selecting several ensembles [1] of ground motions and scaling each ensemble to a user-specified conditioning intensity measure (IM); a detailed explanation of this approach may be found elsewhere (e.g., Section 2 of [Kwong et al., 2014], among others).

The objective of performing RHAs in this study is to estimate the SDHCs of a given structure at a particular site. Once constructed, the SDHC may be used to determine the seismic demand for a given annual rate of exceedance, or conversely, the exceedance rate for a given structural capacity. Furthermore, the SDHC may be integrated with fragility and consequence functions to estimate damage and loss, respectively (Chapter 9 of [Bozorgnia and Bertero, 2004]).

There are three limitations to the existing approach for computing SDHCs from a PSDA. First, the choice of the conditioning IM may not be obvious for some structures and yet it determines the influence from other IMs on the EDP [Lin et al., 2013b]. Second, ground motions selected from a PSDA are almost always amplitude scaled to various levels of the conditioning IM, potentially causing bias in the resulting demands. Third, several ensembles of scaled ground motions are typically needed to determine the SDHC for a wide range of exceedance rates.

The choice of the conditioning IM and the effects of amplitude scaling are relatively unimportant when ground motions are carefully selected to be consistent with the hazard [Bradley, 2012c, Lin et al., 2013b]. Specifically, the SDHCs are unbiased – irrespective of the extent of record scaling – when the corresponding ground motions are hazard-consistent with respect to IMs that are sufficient for the EDP in question [Kwong et al., 2014, Kwong et al., 2015b]. An IM, which may be scalar or vector-valued, is defined to be *sufficient with respect to an EDP* when the EDP is essentially controlled only by this IM and no other features of the ground motion [Shome et al., 1998, Luco and Cornell, 2007]. Since sufficient IMs may not exist for EDPs of a complex, realistic structure, a method that permits selection of unscaled ground motions is desirable.

The procedure developed herein permits selection of a single ensemble of unscaled ground motions, without the need to choose a conditioning IM. First, a vector of IMs is selected on the basis of the structure and EDPs considered. Next, the theoretical probability distribution of this vector, derived from probabilistic seismic hazard analysis (PSHA), is employed as the target for ground motion selection. By selecting a single ensemble of unscaled ground motions to be consistent with this target, hazard consistency at high exceedance rates (or short return periods) is directly enforced. To enforce hazard consistency of ground motions at low exceedance rates (or long return periods), the concept of Importance Sampling is

[1] In this study, an "ensemble" refers to a collection of single horizontal components of ground motion.

utilized. Finally, a case study is chosen to illustrate the proposed procedure, evaluate its ability in providing accurate estimates of the SDHC, and develop recommendations for user-defined inputs to the procedure.

4.3 Theoretical Background

Target for Ground Motion Selection

The target is defined by **IM**, a vector of IMs, and its probability distribution from PSHA of the particular site; although a scalar IM may also be considered, this chapter focuses on a vector of IMs for generality. Examples of such IMs include peak ground acceleration (PGA), spectral accelerations at various vibration periods, $A(T)$, and significant duration, D_{5-75}, which are explicit measures of the ground motion [Bradley, 2012a]. The number of IMs in the vector, denoted by N_{IM}, is referred to as its *dimension*. The IMs should be specified based on structural dynamics and on the analyst's experience with structures that are similar to the one in question. For example, spectral acceleration at vibration periods between the system's fundamental period, T_1, and twice the fundamental period, $2T_1$, might control inter-story drift ratios [Haselton and Baker, 2006] whereas PGA might control floor accelerations [Lin et al., 2013b].

The proposed procedure aims to select an ensemble of ground motions that is consistent with respect to the hazard curves of the IMs specified in the preceding paragraph. An ensemble of ground motions is said to be *hazard-consistent with respect to an IM* when its resulting estimate of the intensity measure hazard curve (IMHC), $\widehat{\lambda}_{IM}(x)$, is practically the same as [2] the target IMHC, $\lambda_{IM}(x)$ (see Section 4.4). The latter IMHC is given by PSHA of the site:

$$\lambda_{IM}(x) = \sum_{i=1}^{N_{Rup}} \nu(rup_i) \cdot \Pr(IM > x \mid rup_i) \tag{4.1}$$

where N_{Rup} refers to the total number of rupture scenarios considered in the PSHA [3], $\nu(rup_i)$ refers to the rate of the ith scenario, and $\Pr(IM > x \mid rup_i)$ refers to the complementary cumulative distribution function (CCDF) of the IM for a given rupture scenario. An estimate of the IMHC from an ensemble of ground motions will be defined later in this section.

In addition to hazard curves, a PSHA also provides the ingredients to determine the multivariate probability distribution of a vector of IMs. The marginal CCDF of each IM for a given earthquake (with unknown magnitude and location) near the site, $\Pr(IM > x)$, may be obtained by normalizing its corresponding hazard curve:

$$\Pr(IM > x) = \frac{\lambda_{IM}(x)}{\nu_0} = \sum_{i=1}^{N_{Rup}} \frac{\nu(rup_i)}{\nu_0} \cdot \Pr(IM > x \mid rup_i) \tag{4.2}$$

[2] Due to the presence of epistemic uncertainty, the comparison of hazard curves requires judgment.

[3] A rupture scenario is defined by the magnitude and location of rupture at the earthquake source.

where $\nu_0 = \sum_{i=1}^{N_{Rup}} \nu(rup_i)$ refers to the annual rate of earthquake occurrence; by definition of ν_0, the sum of all normalized activity rates in the first term of the summation in Equation 4.2 is unity. The marginal probability density function (PDF) of each IM, $f_{IM}(x)$, may be derived from such CCDFs. For example, Figure 4.1a shows an example IMHC from PSHA; its corresponding PDF is depicted in Figure 4.1b. Assuming the distribution of ln(**IM**) for a given rupture scenario is multivariate normal [Bradley, 2010a], where marginal means and standard deviations are given by ground-motion-prediction models (e.g., [Campbell and Bozorgnia, 2008], [Bommer et al., 2009]), and correlations among the IMs are given by correlation models (e.g., [Baker and Jayaram, 2008], [Bradley, 2012b]), Equation 4.2 indicates that the target distribution of **IM** is a *finite mixture of multivariate lognormals*:

$$f_{\mathbf{IM}}(\mathbf{x}) = \sum_{i=1}^{N_{Rup}} \frac{\nu(rup_i)}{\nu_0} \cdot f_{\mathbf{IM}|Rup}(\mathbf{x} \mid rup_i) \tag{4.3}$$

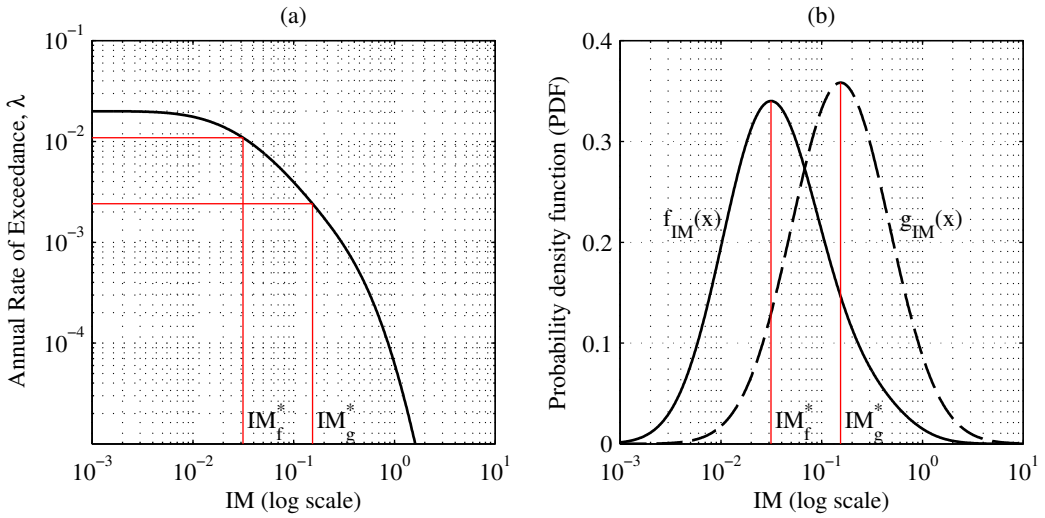

Figure 4.1: Output from PSHA: (a) example hazard curve; (b) target PDF, $f_{IM}(x)$, that corresponds to the example hazard curve (an example of an Importance Function, $g_{IM}(x)$, is also shown). The modes of the two PDFs are denoted by IM_f^* and IM_g^*.

Assuming the N_{Rup} rupture scenarios are mutually exclusive and collectively exhaustive, Equations 4.2-4.3 may be derived from the total probability theorem [Benjamin and Cornell, 1970]. First, note that all events associated with Equation 4.2 are conditioned on the fact that an earthquake, with unknown magnitude and location, has occurred near the site. Second, the normalized activity rate, $\nu(rup_i) \div \nu_0$, may be interpreted as the probability of the ith rupture occurring near the site, given occurrence of an earthquake. The probabilities expressed in Equation 4.2 are unconventional because they are *not* based on a specified assumption of earthquake occurrence in time (e.g., Poisson assumption, etc.).

The simple relationship between an IMHC and its CCDF, as stated by the equality in the left part of Equation 4.2, permits the estimation of hazard curves using a *single* ensemble of unscaled ground motions [4]. Figure 4.2 illustrates one such ensemble of n ground motions, where each data point corresponds to a unique, unscaled ground motion; the values of IM and EDP from the ensemble are quantified on the horizontal and vertical axes, respectively. Combining the empirical CCDF of each variable – IM or EDP – with the annual rate of earthquake occurrence leads to the following estimates of the hazard curves:

$$\widehat{\lambda}_{IM}^{(\mathrm{MC})}(x) = \frac{\nu_0}{n}\sum_{i=1}^{n} I(x_i > x) \qquad \widehat{\lambda}_{EDP}^{(\mathrm{MC})}(z) = \frac{\nu_0}{n}\sum_{i=1}^{n} I(z_i > z) \tag{4.4}$$

where the superscript MC denotes "Monte Carlo", and $I(\cdot)$ refers to the indicator function, which is equal to unity when the event inside the parenthesis occurs and zero otherwise. The observed values of IM and EDP from the ith ground motion are denoted by x_i and z_i, respectively. When an IMHC estimate from, say Equation 4.4a, is practically the same as the theoretical one in Equation 4.1, the corresponding ground motions are said to be hazard-consistent with respect to that particular IM; otherwise, the ground motions are hazard-inconsistent. Similarly, an SDHC estimate from, say Equation 4.4b, is said to be *unbiased*, or *accurate*, when it is essentially equal to the theoretical SDHC from PSHA, denoted by $\lambda_{EDP}(z)$.

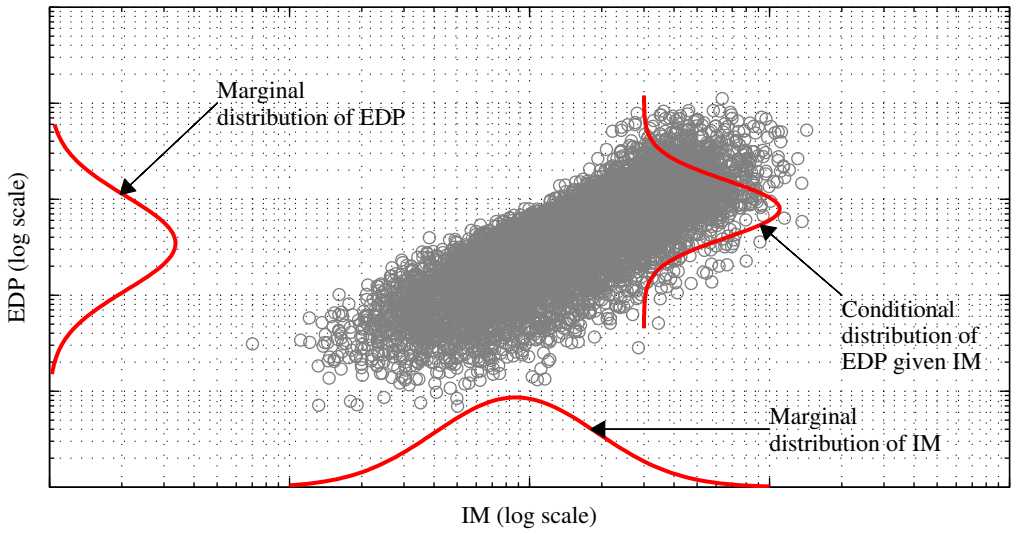

Figure 4.2: Schematic illustration of PDFs related to scattergrams of results from RHAs.

In order to enforce hazard consistency and obtain unbiased SDHCs, ground motions should be selected such that their empirical joint distribution of IM and EDP is essentially the same as the theoretical joint distribution, which is depicted in Figure 4.2 by its

[4]Equation 4.2 is also applicable to the EDPs of a given structure under the assumption of ergodicity in time, which is implicitly assumed in many applications of PBEE [Der Kiureghian, 2005].

corresponding marginal distributions and conditional distribution of $EDP \mid IM$. The agreement between the two joint distributions can be achieved by randomly sampling IM-EDP pairs directly from the theoretical joint distribution; that is, randomly sampling first from the marginal distribution of IM and then from the conditional distribution of $EDP \mid IM$. In practice, this two-step approach is equivalent to (i) randomly generating vectors of IMs from Equation 4.3, and then (ii) selecting ground motions whose IMs agree well with those generated from Equation 4.3. However, direct sampling from Equation 4.3 leads to ground motions that are relatively weak, as suggested by the exceedance rate in Figure 4.1a corresponding to the modal value of the target PDF in Figure 4.1b. Consequently, such motions will be hazard-consistent at high exceedance rates (i.e., frequent events) and are useful for computing linear response. In order to obtain ground motions that are hazard-consistent at small exceedance rates (i.e., rare events) and are useful for computing nonlinear response, the concept of Importance Sampling is introduced next.

Importance Sampling

Importance Sampling is a standard technique from statistics that is commonly used to estimate probabilities of rare events, among other applications (e.g., see [Ross, 2013]); in this study, we employ Importance Sampling to estimate hazard curves at small exceedance rates. First, the theoretical PDF given by Equation 4.3 is replaced by another PDF that samples the tail region more frequently; this new PDF is called an *Importance Function* (IF) and denoted by $g_{IM}(\cdot)$. An example of an IF is illustrated in Figure 4.1b, where its mode corresponds to an exceedance rate that is smaller than that corresponding to the mode of the theoretical PDF. Then, the IF is used to randomly generate vectors of IMs that are ultimately used to estimate hazard curves. When computing hazard curves from such data, the data are weighted in order to account for the bias introduced by replacing the target PDF with the IF.

After vectors of IMs have been randomly generated from the IF, there are three deterministic steps in computing hazard curves. First, the vectors are used to identify ground motions whose corresponding vector-valued IMs agree most closely to those from the IF (Section 4.4). Second, the selected ground motions are analyzed to determine any feature of interest, including IMs excluded from **IM** and EDPs of any structural model (through RHA). Third, the features from the selected motions are employed to compute hazard curves:

$$\widehat{\lambda}_{IM}(x) = \frac{\nu_0}{n} \sum_{i=1}^{n} [I(x_i > x) \cdot w_i] \qquad \widehat{\lambda}_{EDP}(z) = \frac{\nu_0}{n} \sum_{i=1}^{n} [I(z_i > z) \cdot w_i] \tag{4.5}$$

where x_i and z_i refer, respectively, to the observed values of IM and EDP from the ith ground motion. The *Importance Sampling weight* for the ith ground motion, w_i, is defined as the ratio between the values of the two PDFs:

$$w_i = f(\mathbf{x}_i) \div g(\mathbf{x}_i) \tag{4.6}$$

where $\mathbf{x}_i$ refers to the computed value of **IM** from the ith ground motion, $f(\cdot)$ refers to the PDF given by Equation 4.3, $g(\cdot)$ refers to the IF, and the subscript "IM" has been

dropped henceforth for brevity. Note that implementing Equation 4.6 involves the rates for all rupture scenarios considered in the PSHA, along with the target probability distribution of $\mathbf{IM} \mid Rup$ from ground-motion-prediction models (see Equation 4.3). When the ith ground motion leads to collapse, the resulting value of the EDP can be modified before Equation 4.5b is implemented; for example, the displacement may be set to infinity and the acceleration may be set to PGA after collapse has been observed [Yamamoto, 2011, Lin et al., 2013b].

There is epistemic uncertainty in the estimates of hazard curves in Equation 4.5, implying that two estimates from independent executions of the proposed procedure will not be perfectly identical. The expected values of the estimates in Equation 4.5 are (see derivations in Sections A.1 and A.2)

$$\mathbb{E}\left[\widehat{\lambda}_{IM}(x)\right] = \lambda_{IM}(x) \qquad \mathbb{E}\left[\widehat{\lambda}_{EDP}(z)\right] = \lambda_{EDP}(z) \tag{4.7}$$

where $\mathbb{E}[\cdot]$ denotes expectation [5]. These expectations imply that the estimates from the proposed procedure with unscaled ground motions are, on average, hazard-consistent and unbiased; however, this might not be the case when ground motions are scaled (see Section 4.7). The epistemic uncertainty of the estimates in Equation 4.5 is quantified by their variances (see derivations in Sections A.3 and A.4):

$$\mathbb{V}\left[\widehat{\lambda}_{IM}(x)\right] = \frac{1}{n}\left\{\nu_0^2\left[\int\limits_{\mathbf{s}:s>x} \frac{f^2(\mathbf{s})}{g(\mathbf{s})}\,\mathrm{d}\mathbf{s}\right] - \lambda_{IM}^2(x)\right\} \tag{4.8}$$

and

$$\mathbb{V}\left[\widehat{\lambda}_{EDP}(z)\right] = \frac{1}{n}\left\{\nu_0^2\left[\int_{\mathbf{s}} \Pr(EDP > z \mid \mathbf{IM} = \mathbf{s}) \cdot \frac{f^2(\mathbf{s})}{g(\mathbf{s})}\,\mathrm{d}\mathbf{s}\right] - \lambda_{EDP}^2(z)\right\} \tag{4.9}$$

where $\mathbb{V}[\cdot]$ denotes variance, $\Pr(EDP > z \mid \mathbf{IM} = \mathbf{s})$ refers to the CCDF of EDP for a given test value of $\mathbf{IM}$, and the integrals in both variances are multidimensional. Equations 4.7-4.9 suggest theoretically that as the number of unscaled ground motions increases, the hazard curve estimates become increasingly repeatable, converging to the theoretical values.

Equation 4.9 permits several observations regarding the epistemic uncertainty of the SDHC estimate from the proposed procedure. First, the epistemic uncertainty is influenced by two user-specified inputs: (i) sample size, n; and (ii) the IF, $g(\cdot)$, which appears only in the integrand; the rest of the expression is fixed for a given structure at a given site. Second, both $\Pr(EDP > z \mid \mathbf{IM} = \mathbf{s})$ and $\lambda_{EDP}(z)$ are unknown; therefore, one cannot analytically determine the IF by minimizing the variance in Equation 4.9. Third, the variance increases as the dimension of $\mathbf{IM}$ increases because the integrand is always nonnegative. Fourth, the SDHC estimate can become meaningless when $g(\cdot) = 0$. Fifth, $\Pr(EDP > z \mid \mathbf{IM} = \mathbf{s})$ is close to zero when $\mathbf{s}$ is small and close to unity when $\mathbf{s}$ is large, under two assumptions that

[5] In the case of $\mathbf{IM}$, the expectation is with respect to $g(\mathbf{x})$, and in the case of EDP, the expectation is with respect to $f_{EDP|\mathbf{IM}}(z \mid \mathbf{x}) \cdot g(\mathbf{x})$, where $f_{EDP|\mathbf{IM}}(z \mid \mathbf{x})$ refers to the theoretical conditional distribution of $EDP \mid \mathbf{IM}$.

are commonly satisfied in earthquake engineering: (i) large demand levels, z, are of interest, and (ii) the EDP is positively correlated with **IM**.

The observations from the preceding paragraph provide insight for choosing an Importance Function. In theory, many different IFs may be chosen but the desirable ones are those that minimize the first summand of the variance in Equation 4.9. In particular, the dimension of **IM** (Section 4.3) should not be too large and hence, IMs for ground motion selection should be judiciously chosen. To avoid the possibility of infinite variance, the value of the IF must not be zero within the domain of Equation 4.3. Furthermore, the ratio $f^2(\cdot) \div g(\cdot)$ should be less than unity at the tails of the target distribution (see e.g., Figure 4.1b). The theory in this section facilitates the preceding discussion of desirable IFs in a general, qualitative manner; specific recommendations, which are derived from practical considerations, are provided in Section 4.4.

4.4 Ground Motion Selection Procedure

Overview

Figure 4.3 presents a block diagram of the proposed ground motion selection procedure. First, the analyst specifies inputs to the procedure and then performs PSHA of the given site to determine the target for ground motion selection (Equation 4.3). Based on the inputs, an IF is constructed (Section 4.4) and is then employed to select an ensemble of ground motions (Section 4.4). Next, the Importance Sampling weights, computed from the selected ground motions, are used to confirm hazard consistency; if hazard consistency is judged to be unsatisfactory, then new ground motions may be reselected from the proposed procedure (Section 4.4). Finally, nonlinear RHAs of the structural model, subjected to the selected ground motions, are performed and the results are combined with the Importance Sampling weights to compute the SDHC.

There are five inputs to the proposed procedure: (i) a database of prospective ground motions, (ii) **IM**, a vector of IMs, (iii) a maximum acceptable scale factor, SF_{max}, (iv) a target fraction of scaled ground motions, γ, and (v) a sample size, n. The database of prospective ground motions should contain unscaled motions that originate from tectonic environments and soil conditions that are similar to those for the site under consideration [Bommer and Acevedo, 2004]. This study applies the proposed procedure to synthetic ground motions in order to preliminarily evaluate its ability to estimate SDHCs (Sections 4.5-4.8); a more comprehensive explanation of the procedure's application to recorded motions is in preparation by the authors. The vector of IMs should be chosen based on our understanding of the dynamics of the structure; to reflect higher-mode, inelastic, and duration-sensitive response, we recommend using the vector $\mathbf{IM} = \{A(T_k), A(T_1), A(2T_1), D_{5-75}\}$, where T_1 and T_k refer, respectively, to the first and kth mode of the structure (Section 4.6). One possibility for identifying the kth mode is through the concept of modal contribution factors [Chopra, 2011]. The parameters SF_{max} and γ should be chosen based on the sufficiency of **IM**: if **IM** is deemed sufficient, then large scale factors may be employed; otherwise, the degree of

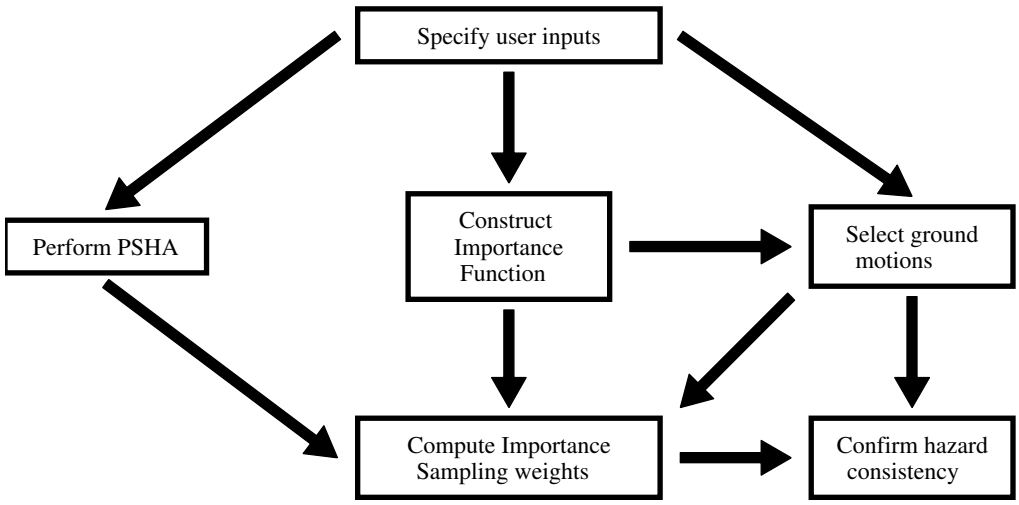

Figure 4.3: Block diagram of proposed ground motion selection procedure.

scaling should be minimized (Section 4.7). Finally, the parameter n should be chosen based on a tolerable level of epistemic uncertainty in the SDHC estimates (Section 4.8).

Database-Driven Importance Function

The purpose of the IF in Figure 4.3 is to select ground motions that are intense while simultaneously consistent with the target defined by Equation 4.3. The proposed procedure achieves this goal in two steps: (i) randomly generate a vector of IMs from the IF, and (ii) select the ground motion whose corresponding vector of IMs agrees most closely to the one from the IF. Since ground motions are selected from a user-specified database of prospective motions, this database plays a major role in fulfilling the purpose of the IF. For example, when the largest observed value of $A(1s)$ in the database is, say $1g$, there would be no point in specifying an IF whose probability density is nonzero at intensities greater than $1g$. Because the database of prospective motions may be effectively enlarged by allowing ground motions to be scaled, we recommend an IF that is controlled by three inputs: (i) the specified database of unscaled ground motions, (ii) SF_{max}, and (iii) γ.

If ground motions are restricted to be unscaled, the proposed IF is a multivariate lognormal distribution whose parameters are determined from the database of unscaled ground motions; this IF is denoted by $g_u(\mathbf{x})$. To determine the parameters of this multivariate distribution – μ_{IF} and $\mathbf{\Sigma}_{IF}$ – we first consider the corresponding marginal distributions. The marginal distribution of the jth IM within **IM** is lognormal; its two parameters – μ_j and σ_j – are computed from the mean and standard deviation of the observed values of $\ln(IM_j)$ in the database. An example of this lognormal distribution is shown in Figure 4.4a, where the fitted CCDF is compared to the empirical CCDF from the database of ground motions. Repeating such calculations for all IMs gives the mean vector of $g_u(\mathbf{x})$:

$$\mu_{IF} = [\mu_1 \quad \mu_2 \quad \dots \quad \mu_{N_{IM}}] \tag{4.10}$$

Next, the correlation between the jth and kth IM, denoted by $\rho_{j,k}$, is computed from the correlation between the observed values of $\ln(IM_j)$ and $\ln(IM_k)$ in the database. Combining such correlations with all σ_j provides the covariance matrix of $g_u(\mathbf{x})$:

$$\boldsymbol{\Sigma}_{IF} = \begin{bmatrix} \sigma_1^2 & \rho_{1,2}\sigma_1\sigma_2 & \cdots & \rho_{1,N_{IM}}\sigma_1\sigma_{N_{IM}} \\ \rho_{2,1}\sigma_2\sigma_1 & \sigma_2^2 & \cdots & \rho_{2,N_{IM}}\sigma_2\sigma_{N_{IM}} \\ \vdots & \vdots & \ddots & \vdots \\ \rho_{N_{IM},1}\sigma_{N_{IM}}\sigma_1 & \rho_{N_{IM},2}\sigma_{N_{IM}}\sigma_2 & \cdots & \sigma_{N_{IM}}^2 \end{bmatrix} \tag{4.11}$$

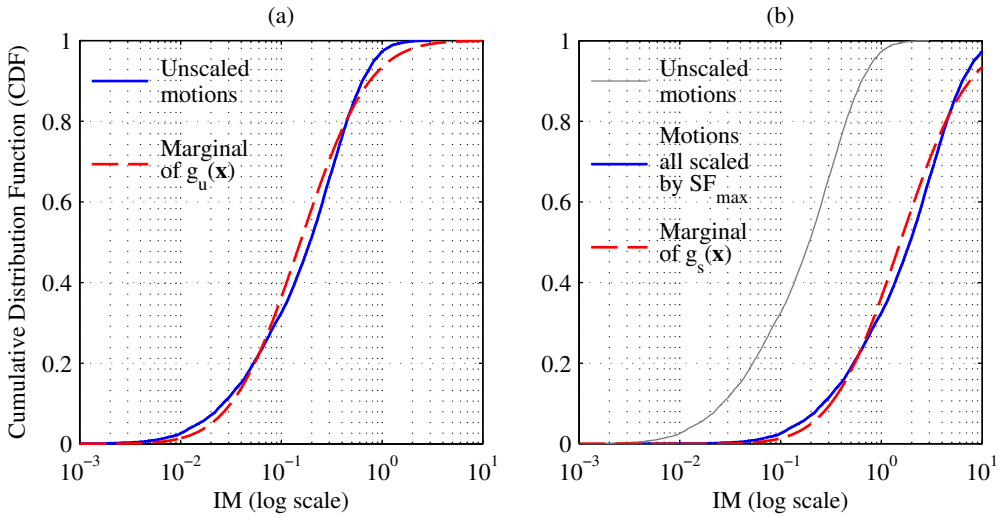

Figure 4.4: Illustration of Importance Functions derived from a database of prospective ground motions that are all: (a) unscaled, $g_u(\mathbf{x})$; or (b) scaled by SF_{max}, $g_s(\mathbf{x})$.

The approach described in the preceding paragraph may also be applied to determine an IF when ground motions are all scaled by the same scale factor. When the given database of ground motions is deemed to lack an adequate number of strong ground motions, judged by comparing $g_u(\cdot)$ against $f(\cdot)$ (Figure 4.1b), it is natural to consider scaling the motions upwards. For example, suppose it is desired to scale all the motions in the database by a factor of SF_{max} in order to create a new database of prospective motions. The IMs computed from scaled ground motions may be different, depending on the type of IM (e.g., spectral acceleration increases linearly with scale factor whereas many common measures of duration are unaffected by scaling) [Bradley, 2012a]. Applying the approach in the preceding paragraph to the new database of scaled ground motions leads to the IF denoted by $g_s(\mathbf{x})$, which is illustrated in Figure 4.4b. Observe that $g_s(\mathbf{x})$ differs from $g_u(\mathbf{x})$ only in its mean vector; the covariance matrices (and σ_j) are the same in both cases.

In general, the recommended IF is a two-component mixture of multivariate lognormals:

$$g(\mathbf{x}) = [1-\gamma] \cdot g_u(\mathbf{x}) + \gamma \cdot g_s(\mathbf{x}) \tag{4.12}$$

where $0 \leq \gamma \leq 1$ may be interpreted as the fraction of scaled ground motions in the ensemble of n selected motions. An example of this IF is shown by the solid curve in Figure 4.5a; for comparison, the target PDF (Equation 4.3) and its two individual components – $g_u(x)$ and $g_s(x)$ – are also shown. This two-component mixture distribution permits the selection of ground motions that are scaled by factors between unity and SF_{max}, where the fraction of scaled motions is roughly controlled by γ (Figure 4.5b). For instance, when $\gamma = 0$, the general two-component IF reduces to $g_u(\cdot)$ whereas when $\gamma = 1$, it reduces to $g_s(\cdot)$. Note that when $SF_{max} = 1$, the general two-component IF also reduces to $g_u(\cdot)$, irrespective of γ.

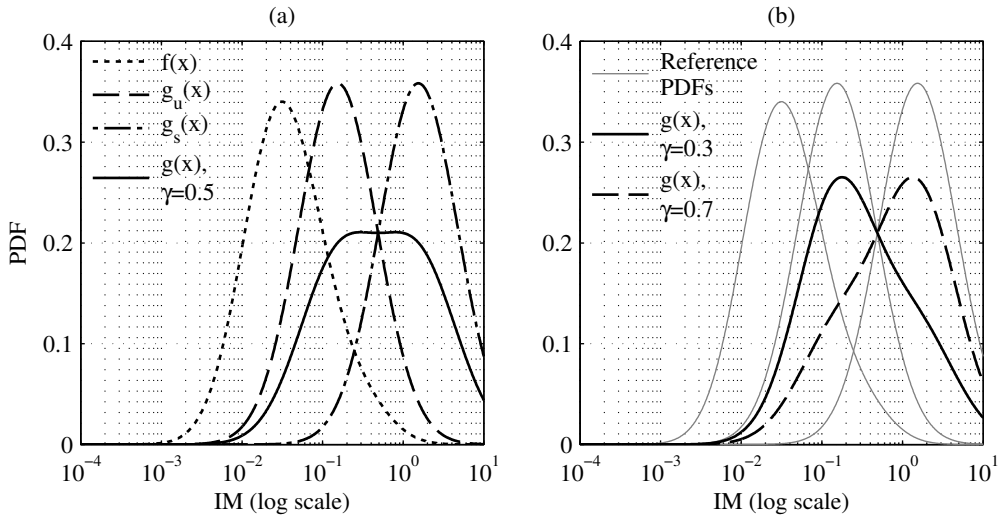

Figure 4.5: Illustration of the recommended two-component Importance Function, $g(x) = [1-\gamma] \cdot g_u(x) + \gamma \cdot g_s(x)$: (a) comparison of $g(x)$, with $\gamma = 0.5$, against its two individual components and the target PDF; (b) the effect of γ on $g(x)$.

Selection and Scaling of Ground Motions from Randomly Generated Intensity Measures

The IF is used to randomly generate n vectors of IMs, which are in turn used to select a corresponding ensemble of n ground motions. Consequently, the ability to randomly generate a vector of IMs is an important consideration in choosing the IF. When the IF is specified as either $g_u(\mathbf{x})$ or $g_s(\mathbf{x})$, a vector of IMs can be readily generated from the multivariate lognormal distribution. When the IF is the two-component IF given by Equation 4.12, a vector of IMs can be obtained in two steps: (i) identify one of the two components by randomly sampling from the Bernoulli distribution with probability γ, and (ii) randomly generate a vector of IMs from the component identified.

After a collection of n vectors is randomly generated from the IF, denoted by $\mathbf{IM}_{IF}$, a corresponding ensemble of ground motions is selected. For each successive $\mathbf{IM}_{IF}$, the database of prospective ground motions is searched for the optimal match while ensuring that no motion is duplicated. The optimal ground motion is defined as the one whose

computed vector of (potentially scaled) IMs, denoted by $\mathbf{IM}_P$, agrees most closely with the current $\mathbf{IM}_{IF}$. The misfit between $\mathbf{IM}_{IF}$ and $\mathbf{IM}_P$ is quantified by Δ [6]:

$$\Delta = \sum_{j=1}^{N_{IM}} \left[\frac{\ln(IM_{IF,j}) - \ln(IM_{P,j})}{\sigma_j} \right]^2 \tag{4.13}$$

where N_{IM} refers to the dimension of $\mathbf{IM}$ (Section 4.3) and σ_j refers to the standard deviation of $\ln(IM_j)$ from the IF (Section 4.4). Thus, for a given $\mathbf{IM}_{IF}$, the selected ground motion (and corresponding scale factor) is the one whose value of Δ is the smallest among all prospective motions. To avoid selection of duplicate motions, the selected motion is removed from the database before proceeding to the next $\mathbf{IM}_{IF}$.

When scaled ground motions are of interest, the optimal scale factor for each prospective ground motion must be determined before computing Δ. To determine the optimal scale factor for a given $\mathbf{IM}_{IF}$, we first note the relationship between the scaled and unscaled values of the jth IM:

$$IM_{P,j} = IM_{U,j} \times SF^{\alpha_j} \tag{4.14}$$

where $IM_{P,j}$ and $IM_{U,j}$ refer, respectively, to the scaled and unscaled values of the jth IM, SF refers to a scale factor, and α_j denotes how the jth IM changes with record scaling (e.g., $\alpha_j = 1$ for spectral acceleration, $\alpha_j = 0$ for significant duration, etc.). Substituting Equation 4.14 into Equation 4.13 shows that, for a given $\mathbf{IM}_{IF}$, Δ is a quadratic function of the scale factor. By minimizing Δ with respect to SF, the optimal scale factor may be derived for each prospective ground motion (see derivation in Section A.5):

$$SF_{optimal} = \exp\left\{ \frac{\sum_{j=1}^{N_{IM}} \left(\frac{\alpha_j}{\sigma_j^2}\right) \ln\left(\frac{IM_{IF,j}}{IM_{U,j}}\right)}{\sum_{j=1}^{N_{IM}} \left(\frac{\alpha_j}{\sigma_j}\right)^2} \right\} \tag{4.15}$$

where $IM_{IF,j}$ refers to the jth IM within the current $\mathbf{IM}_{IF}$ under consideration. When $SF_{optimal}$ is greater than SF_{max} (or less than SF_{max}^{-1}), its value is replaced by SF_{max} (or SF_{max}^{-1}), before Δ is computed.

Estimating Hazard Curves

The ground motions selected from the proposed procedure should be examined for hazard consistency with respect to $\mathbf{IM}$ before proceeding with RHAs. In other words, the 95% confidence interval (CI) of an IMHC estimate (Equation 4.5a) should cover the target IMHC (Equation 4.1). Such CIs may be readily computed by applying the bootstrap procedure [Efron and Tibshirani, 1993] to the selected ground motions, generating a different IMHC estimate from Equation 4.5a per bootstrap sample. The concept of hazard consistency is illustrated in Figure 4.6. The ground motions in Figure 4.6a are hazard-consistent with

[6] Each IM in the vector may be weighted based on its importance relative to the other IMs; however, this is omitted herein for the sake of simplicity.

respect to $A(1s)$, at exceedance rates greater than 10^{-6}, because the 95% bootstrap CI covers the target IMHC in this range. In contrast, the bootstrap CIs in Figure 4.6b do not cover the target IMHC at exceedance rates less than 10^{-5} and therefore, the corresponding ground motions are hazard-*inconsistent* with respect to PGA in this range of exceedance rates.

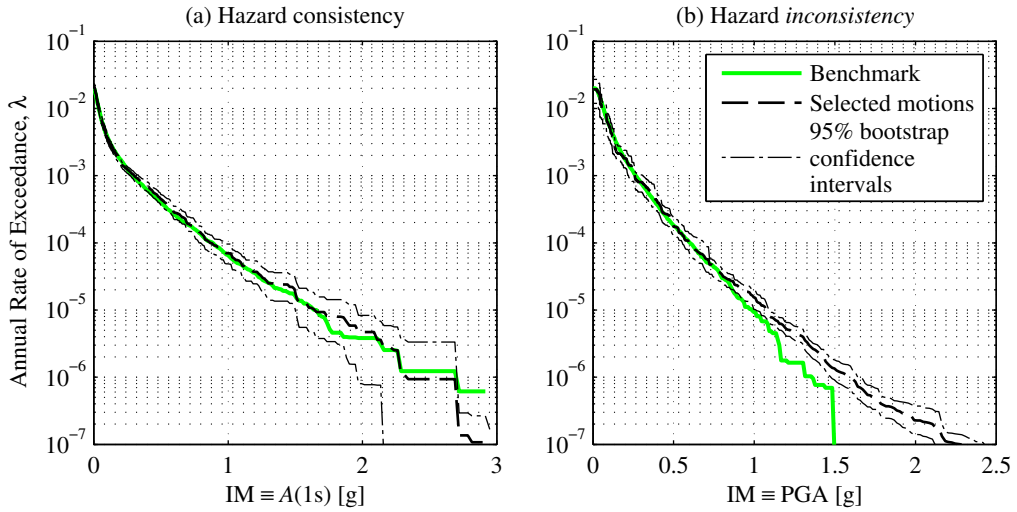

Figure 4.6: The concept of hazard consistency. An example of ground motions that are: (a) hazard-consistent with respect to $A(1s)$ at exceedance rates greater than 10^{-6}; (b) hazard-*inconsistent* with respect to PGA at exceedance rates less than 10^{-5}.

When hazard consistency is judged to be unsatisfactory at a particular range of exceedance rates, there are two options to explore for improving hazard consistency. First, ground motions may be re-selected by randomly generating another collection of n vector-valued IMs from the IF. If the re-selected motions remain hazard-inconsistent, then the next option is to vary the sample size, n. By decreasing n, the CI of the IMHC estimate widens and the likelihood of satisfying hazard consistency increases; however, the epistemic uncertainty in the SDHC estimate also increases. By increasing n, the CI of the IMHC estimate shrinks, converging to the target IMHC (Section 4.3); however, the maximum value of n may be limited by the number of prospective motions in the database or by time constraints associated with performing RHAs.

When the preceding two options are inadequate to satisfy hazard consistency, the next option to consider is modifying the IF. First, we recommend changing SF_{max} and γ to experiment with different IFs (Figure 4.5). With each IF, new ground motions may be selected and checked for hazard consistency with respect to **IM**. When changing SF_{max} and γ is inadequate, then the database of prospective ground motions can be enlarged (e.g., adding synthetic ground motions to a database of recorded motions).

There are four steps to estimate SDHCs from an ensemble of hazard-consistent ground

motions. First, RHA of the structural model is performed for all n ground motions. Second, the results from RHAs are partitioned into collapse and noncollapse cases. Third, the EDPs corresponding to the collapsed cases are replaced by appropriate values (e.g., drifts may be replaced by infinity and floor accelerations by PGA). Applying Equation 4.5b to the latter values of EDP – where the Importance Sampling weights are identical to those for the IMHC estimates (Equation 4.5a) – leads to the desired estimate of the SDHC.

4.5 An Illustrative Example

A 4-story reinforced concrete frame is chosen to demonstrate the applicability of the proposed procedure to realistic buildings. This well-vetted frame has been studied by past researchers in various contexts (e.g., [Yamamoto, 2011], [PEER GMSM Working Group, 2009], [Goulet et al., 2007]) and consequently, details regarding its geometry and material properties may be found in such references. In essence, the frame satisfies the strong column-weak beam philosophy and is modeled in OpenSEES [Mazzoni et al., 2006], where the inelasticity is captured by plastic hinges at the ends of beam-column elements; its four modal periods of vibration are: $T_1 = 0.94$ sec, $T_2 = 0.30$ sec, $T_3 = 0.17$ sec, $T_4 = 0.12$ sec. The frame is classified as collapsed when its displacement increases without bounds. We consider two EDPs: (i) maximum inter-story drift ratio (MIDR), defined as the largest peak inter-story drift ratio among the four stories, and (ii) maximum floor acceleration (MFA), defined as the largest peak floor acceleration among the four stories and the ground.

The selected site and earthquake rupture forecast are identical to those shown in Fig 2 of [Kwong et al., 2015b]. A single strike-slip fault, with an activity rate of $\nu_0 = \nu = 0.02$ earthquakes per year, is located 10 km away from the site. Each earthquake is assumed to occur at a fixed distance of 10 km but with different magnitudes that are characterized by the Youngs & Coppersmith PDF shown in Fig 2b of [Kwong et al., 2015b]; the database of prospective ground motions is specified as 10^4 synthetic motions that are simulated from the stochastic model by Yamamoto and Baker [Yamamoto and Baker, 2013, Yamamoto, 2011], with input magnitudes from the uniform distribution shown in Fig 2b of [Kwong et al., 2015b]. This example is chosen because benchmark SDHCs may be readily computed from synthetic ground motions to evaluate the proposed ground motion selection procedure [Kwong et al., 2015b].

Assuming in this section that no **IM** is perfectly sufficient for the response of this complex, realistic frame, the proposed selection procedure is applied to only unscaled ground motions; that is, $SF_{max} = 1$ and $\gamma = 0$. Since the first and fourth mode periods of the 4-story frame are $T_1 = 0.94$ sec and $T_4 = 0.12$ sec, respectively, the vector of IMs is specified as $\mathbf{IM} = \{A(0.1s), A(1s), A(2s), D_{5-75}\}$; thus, $N_{IM} = 4$. In order to minimize the effects of epistemic uncertainty on the accuracy of the SDHC estimate (Section 4.3), n is specified as 1000.

For our example site, the target probability distribution of **IM** from PSHA (Equation 4.3)

reduces to

$$f_{\mathbf{IM}}(\mathbf{x}) = \sum_{m} \Pr(M = m) \cdot f_{\mathbf{IM}|M}(\mathbf{x} \mid m) \tag{4.16}$$

where the summation is over the number of magnitude bins chosen to discretize the Youngs & Coppersmith magnitude PDF, $\Pr(M = m)$ refers to the probability of an earthquake with magnitude m occurring, and $f_{\mathbf{IM}|M}(\mathbf{x} \mid m)$ denotes the multivariate lognormal distribution of $\mathbf{IM} \mid M$ whose parameters are given by the benchmark-consistent prediction models. Since $SF_{max} = 1$ in this example, the general two-component IF in Equation 4.12 reduces to $g_u(\mathbf{x})$; its parameters are derived from the 10^4 unscaled ground motions (Figure 4.4a). With the IF constructed, a subset of n motions is selected from the specified database (Section 4.4).

Before proceeding with RHAs, the selected motions are checked for hazard consistency with respect to **IM**. First, the Importance Sampling weights are determined by applying Equation 4.6 to all IMs computed from the selected motions, where $f(\cdot)$ is given by Equation 4.16 and $g(\cdot)$ is given by $g_u(\mathbf{x})$ as mentioned in the preceding paragraph. Then, a hazard curve is estimate for each IM, using Equation 4.5a, and compared against the corresponding benchmark. In this example, ground motions were re-selected a few times in order to achieve hazard consistency for a wide range of exceedance rates. This consistency is confirmed in Figure 4.7, where each benchmark hazard curve falls within the 95% bootstrap CIs, for a wide range of exceedance rates.

After hazard consistency is confirmed, SDHCs are estimated for both EDPs of the 4-story frame. Since the selected motions are unscaled in this example, each motion corresponds to a unique value of the EDP that was already computed when determining the benchmark SDHC. As a result, selecting ground motions becomes equivalent to selecting a subset of EDPs from the specified database. The SDHC estimates, obtained by applying Equation 4.5b to the selected values of EDP, are shown by dashed black curves in Figure 4.8. In order to convey the epistemic uncertainty of the SDHCs, 95% bootstrap CIs are also shown in this figure, which were obtained by applying the bootstrap procedure to the selected motions.

Figure 4.8 demonstrates that the SDHC estimates from the proposed procedure, using a large number of unscaled ground motions, are accurate because the benchmark SDHCs are approximately covered by the 95% CIs. The agreement between the proposed estimate and the associated benchmark is excellent for both EDPs, at a wide range of exceedance rates. Such excellent agreement is likely due to the fact that the selected motions are hazard-consistent with respect to many different features of the ground motion, even though only four IMs were chosen to select ground motions. The selected motions in this example are consistent with the hazard for a wide range of IMs because (i) the motions are unscaled, and (ii) the chosen **IM** is strongly correlated with many other IMs. Alternatively, the excellent agreement in the SDHCs may also be due to the fact that the chosen **IM** is sufficient; this possibility is investigated in the next two sections of this chapter.

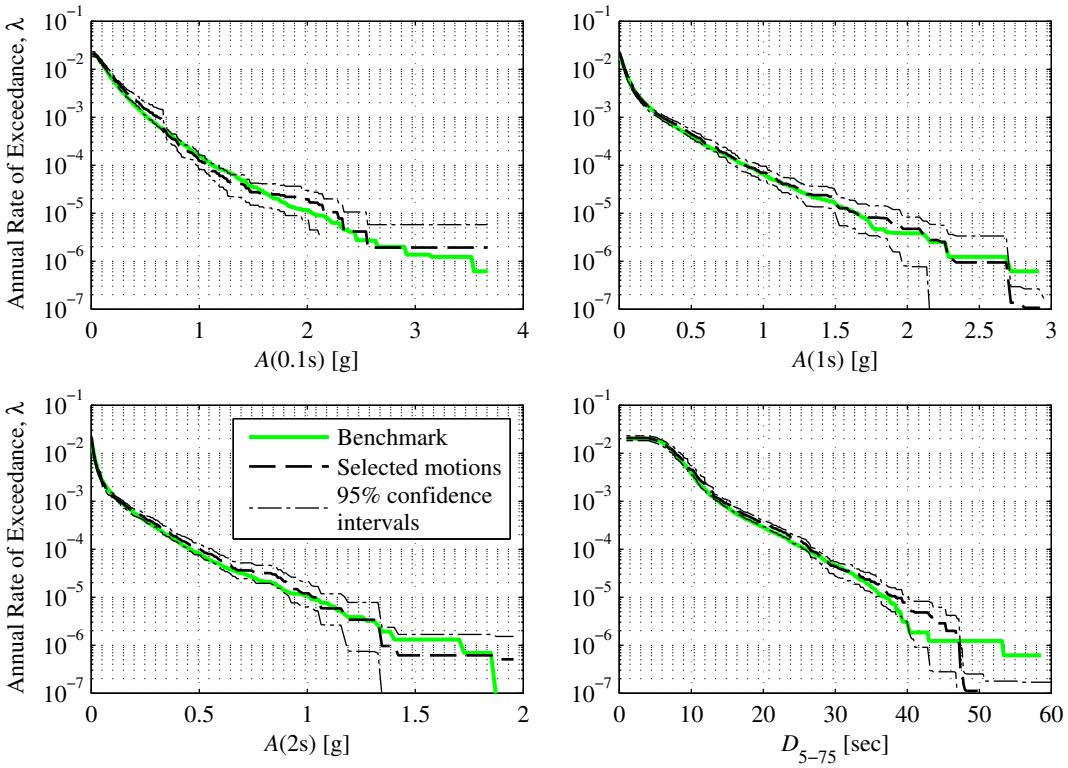

Figure 4.7: Hazard consistency of 1000 unscaled ground motions selected from $g(\mathbf{x}) = g_u(\mathbf{x})$; Confidence intervals (CIs) from 100 bootstrap samples of the selected motions.

4.6 Minimum Number of Intensity Measures To Be Considered

The results from the preceding section demonstrate that accurate SDHC estimates may be obtained from the proposed procedure when a large number of unscaled motions are selected using four IMs: (i) $A(T_1)$, (ii) $A(2T_1)$, (iii) $A(T_k)$, and (iv) D_{5-75}. At the same time, Equation 4.9 suggests that as the dimension of **IM** decreases, the epistemic uncertainty in the SDHC estimate also decreases because the integrand within the multidimensional integral is nonnegative. Consequently, the natural question is: can accurate SDHC estimates be obtained with fewer than four IMs?

To answer this question, four different choices of **IM** are considered: (i) "bestIM", (ii) "SAonly", (iii) "T1plus2T1", and (iv) "T1only"; these denote, respectively, (i) vector comprising $A(0.1s)$, $A(1s)$, $A(2s)$, and D_{5-75}, (ii) vector comprising $A(0.1s)$, $A(1s)$, and $A(2s)$, (iii) vector comprising $A(1s)$ and $A(2s)$, and (iv) $A(1s)$ alone. To investigate the effects of **IM** on the resulting SDHC estimate, other inputs to the procedure are fixed and SDHC estimates from different choices of **IM** are compared against the benchmark. The SDHC estimate for a given choice of **IM** is obtained by selecting a subset of $n = 1000$, unscaled mo-

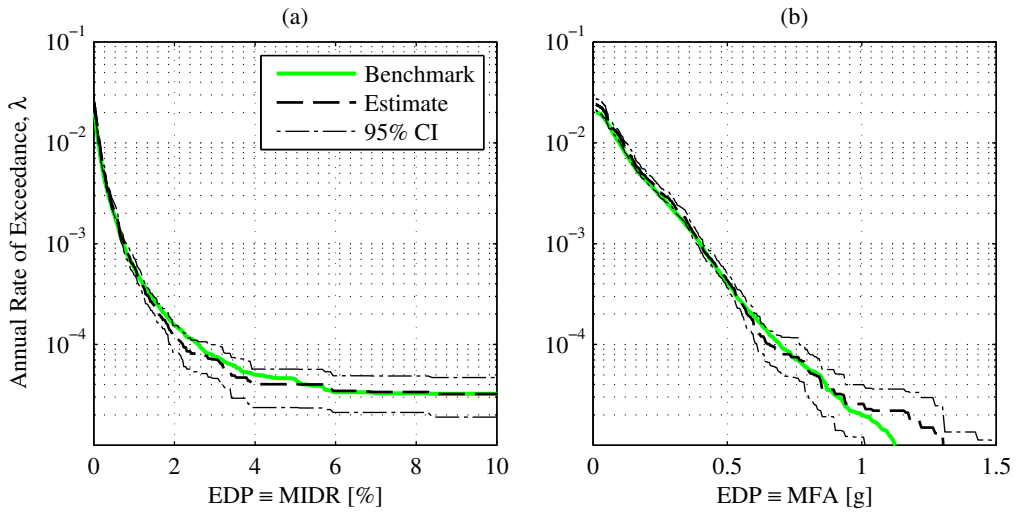

Figure 4.8: SDHC estimates from proposed procedure with $n = 1000$ unscaled ground motions selected using $\mathbf{IM} = \{A(0.1s), A(1s), A(2s), D_{5-75}\}$: (a) MIDR; (b) MFA. CIs from 100 bootstrap samples.

tions from the database of synthetic motions described in Section 4.5. This estimate varies with each execution of the procedure because each execution produces a different selection of ground motions from the IF (Section 4.4); thus, it is desirable to consider the epistemic uncertainty of the SDHC estimate when comparing results from different choices of **IM**. Since ground motions are unscaled, no additional RHAs are required in each execution of the procedure and therefore, the epistemic uncertainty for a given choice of **IM** may be rigorously quantified through many executions of the procedure.

The MIDR hazard curves from different choices of **IM** are presented in Figure 4.9. For each choice of **IM**, 100 SDHCs were obtained from 100 independent executions of the procedure; these SDHCs are summarized by the mean and 95% CI. This figure shows that the epistemic uncertainty is similar across the four choices of **IM**, since the width of CIs are similar. Comparing the CIs against the benchmark indicates that the SDHC from "bestIM" is unbiased at all exceedance rates whereas those from the other three choices of **IM** are unbiased only at exceedance rates greater than 10^{-4}; this implies that D_{5-75}, or duration, should not be excluded when estimating MIDR hazard curves, especially near collapse. Note that the differences between the results from "T1only" and "SAonly" are small because the corresponding ground motions are unscaled and any inconsistencies in the hazard with respect to IMs beyond **IM** are typically less pronounced for unscaled motions than for scaled motions.

Figure 4.10 shows the MFA hazard curves from different choices of **IM**. Consistent with the results for MIDR, the epistemic uncertainty is again similar across the four choices of **IM**; this suggests that, as long as ground motions are unscaled, more than four IMs

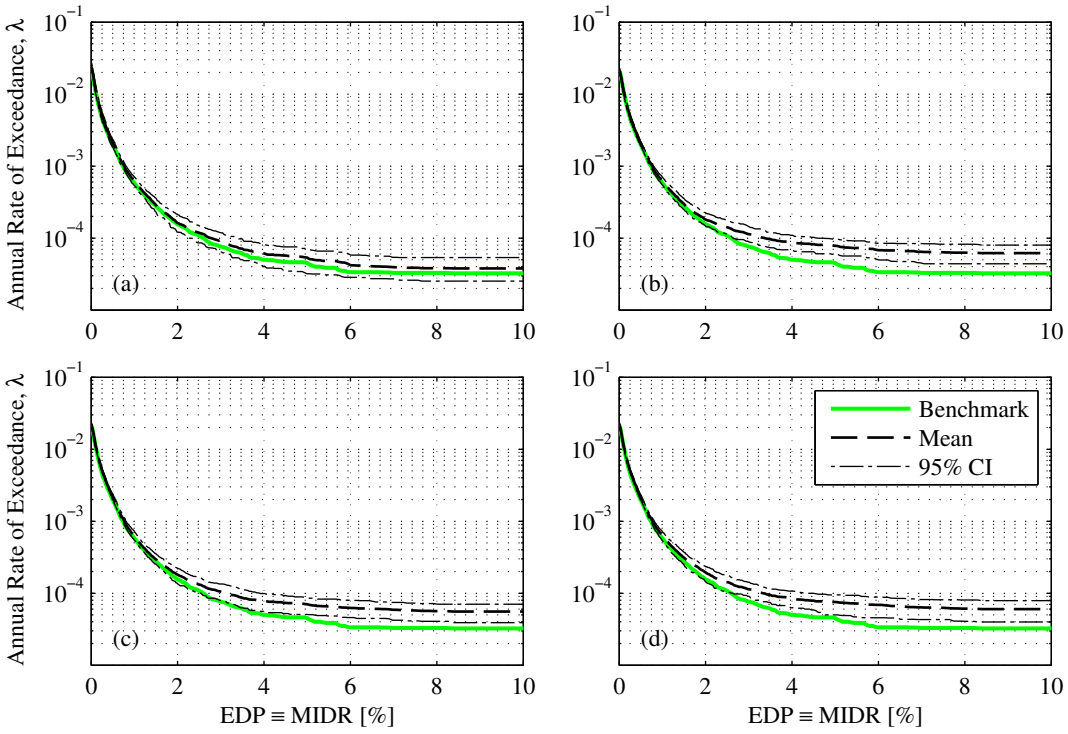

Figure 4.9: MIDR hazard curves from proposed procedure with four different choices for **IM**: (a) "bestIM" $\equiv \{A(0.1s), A(1s), A(2s), D_{5-75}\}$; (b) "SAonly" $\equiv \{A(0.1s), A(1s), A(2s)\}$; (c) "T1plus2T1" $\equiv \{A(1s), A(2s)\}$; and (d) "T1only" $\equiv A(1s)$. CIs from 100 independent executions of the proposed procedure with 1000 unscaled motions per execution.

may be specified in the proposed procedure without significantly increasing the epistemic uncertainty in the resulting SDHC estimates. Unlike the results for MIDR, the SDHCs from *both* "bestIM" and "SAonly" are unbiased at a wide range of exceedance rates, implying that duration may be excluded when estimating MFA hazard curves. On the other hand, spectral accelerations at short vibration periods are important for the accurate prediction of MFA, because slight biases at rates between $5 \cdot 10^{-4}$ to 10^{-2} are observed for choices of **IM** that exclude $A(0.1s)$; this conclusion is consistent with the findings from Lin et al [Lin et al., 2013b]. The results from Figures 4.9-4.10 suggest collectively that, as long as ground motions are unscaled, the sufficiency of **IM** plays a lesser role in determining the accuracy of the SDHC estimate than when ground motions are scaled.

4.7 Maximum Scaling of Ground Motions

In general, scaling distorts ground motions and causes inconsistencies with respect to the hazard. However, such hazard inconsistencies may be deliberately avoided for some IMs through sophisticated ground motion selection procedures [Lin et al., 2013b, Bradley, 2012c]. For example, by using the probability distribution of **IM** from PSHA (Equation 4.3) as

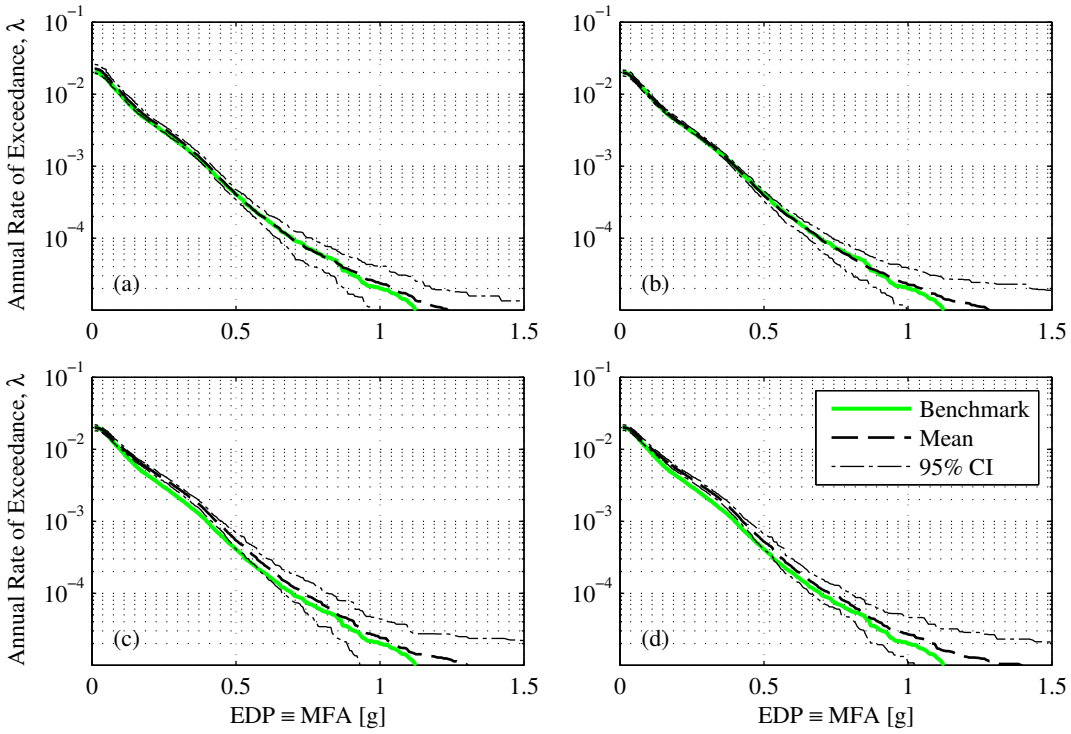

Figure 4.10: MFA hazard curves from proposed procedure with four different choices for **IM**: (a) "bestIM" $\equiv \{A(0.1s), A(1s), A(2s), D_{5-75}\}$; (b) "SAonly" $\equiv \{A(0.1s), A(1s), A(2s)\}$; (c) "T1plus2T1" $\equiv \{A(1s), A(2s)\}$; and (d) "T1only" $\equiv A(1s)$. CIs from 100 independent executions of the proposed procedure with 1000 unscaled motions per execution.

the target to select scaled ground motions, the resulting motions will be, not surprisingly, consistent with the hazard for this particular vector of IMs. Nevertheless, inconsistencies with respect to features of the ground motion beyond **IM** will become increasingly pronounced as the level of record scaling increases.

Are hazard inconsistencies with respect to IMs excluded from **IM** practically significant? The answer to this question depends strongly on the sufficiency of **IM** with respect to the EDP at hand. If **IM** is insufficient (i.e., the EDP depends appreciably on other features of the ground motion besides **IM**), then such inconsistencies are significant, leading to biased SDHCs. On the other hand, if **IM** is sufficient (i.e., the EDP depends primarily on **IM** only), then by definition, such inconsistencies are immaterial and do not cause bias.

Comparing the complexity of the ground motion time series against the simplicity of IMs, it seems unlikely for an IM to be simultaneously sufficient with respect to several EDPs of a realistic structural model [Bradley, 2012c]. As a result, ground motions selected for RHAs should, ideally speaking, not be scaled, which can be achieved using the selection procedure developed herein. When ground motions must be scaled, the vector of IMs for selecting ground motions should be chosen judiciously. Based on the results presented in Sections 4.5

and 4.6, the vector $\mathbf{IM} = \{A(0.1s), A(1s), A(2s), D_{5-75}\}$, denoted by "bestIM", appears to be sufficient for both EDPs of the 4-story frame; however, how sufficient is this vector and what degree of scaling can be combined with it?

To answer these questions, n is again fixed as 1000, and four different combinations of SF_{max} and γ, which represent increasing levels of scaling (see Figure 4.5), are considered: (i) 5 and 0.5; (ii) 5 and 0.9; (iii) 10 and 0.5; and (iv) 10 and 0.9. For each combination, an estimate of the SDHC is determined and compared against the benchmark. Unlike Section 4.6, each implementation of the procedure with a different combination of scaling requires additional RHAs because EDPs corresponding to scaled ground motions have *not* been computed previously; in total, 4000 RHAs of the 4-story frame were performed to obtain the results presented in this section. Since additional RHAs are needed for each implementation of the procedure, the epistemic uncertainty in the SDHC estimate is approximately quantified by a bootstrap CI. To make meaningful comparisons among the four cases of scaling, each of the four ensemble of ground motions was carefully checked for hazard consistency with respect to **IM**; this is demonstrated in Figure 4.11, where the CIs of each IMHC estimate have been omitted for clarity. With hazard consistency satisfied for all four cases of scaling, the degree of bias in the resulting SDHCs indicates the degree to which "bestIM" is insufficient for this 4-story frame.

The SDHCs from the four combinations of scaling are presented in Figures 4.12-4.13. Taking into account the epistemic uncertainty depicted in Figure 4.12, the MIDR hazard curve from $SF_{max} = 5$ and $\gamma = 0.5$ is least biased and that from $SF_{max} = 10$ and $\gamma = 0.9$ is most biased, among the four combinations considered. With the exception of Figure 4.12d at exceedance rates less than $4 \cdot 10^{-5}$, the biases are generally conservative in the sense that for a given level of exceedance rate, the demand is overestimated. For fixed γ, the bias in the MIDR hazard curve increases with increasing SF_{max}. Similarly, for fixed SF_{max}, the bias in the MIDR hazard curve increases with increasing γ. In contrast, the MFA hazard curves from all four combinations are practically unbiased.

Since ground motions are hazard-consistent with respect to **IM** (Fig 4.11), the bias observed in Figure 4.12b suggests that "bestIM" is insufficient for MIDR. Relative to MIDR, "bestIM" appears to be less insufficient with respect to MFA, as suggested by the excellent agreement among the four cases shown in Figure 4.13. This can be explained partially by the fact that unlike drifts or displacements, accelerations are limited by the strength of the system and thus, MFA is less sensitive to scaling than MIDR. Considering the epistemic uncertainty and the extent of scaling, the biases shown in Figures 4.12-4.13 suggest that "bestIM" is still a useful, practical vector for selecting ground motions with the proposed procedure.

When **IM** is sufficient with respect to EDP, the conditional probability distribution of $EDP \mid \mathbf{IM}$ is essentially independent of record scaling; that is, the conditional distribution from scaled ground motions, $f(EDP \mid \mathbf{IM}, \text{scaled})$, is nearly the same as that from unscaled motions, $f(EDP \mid \mathbf{IM}, \text{unscaled})$. In contrast, an insufficient **IM** implies that the two conditional distributions are different, with the difference increasingly significant as the degree of

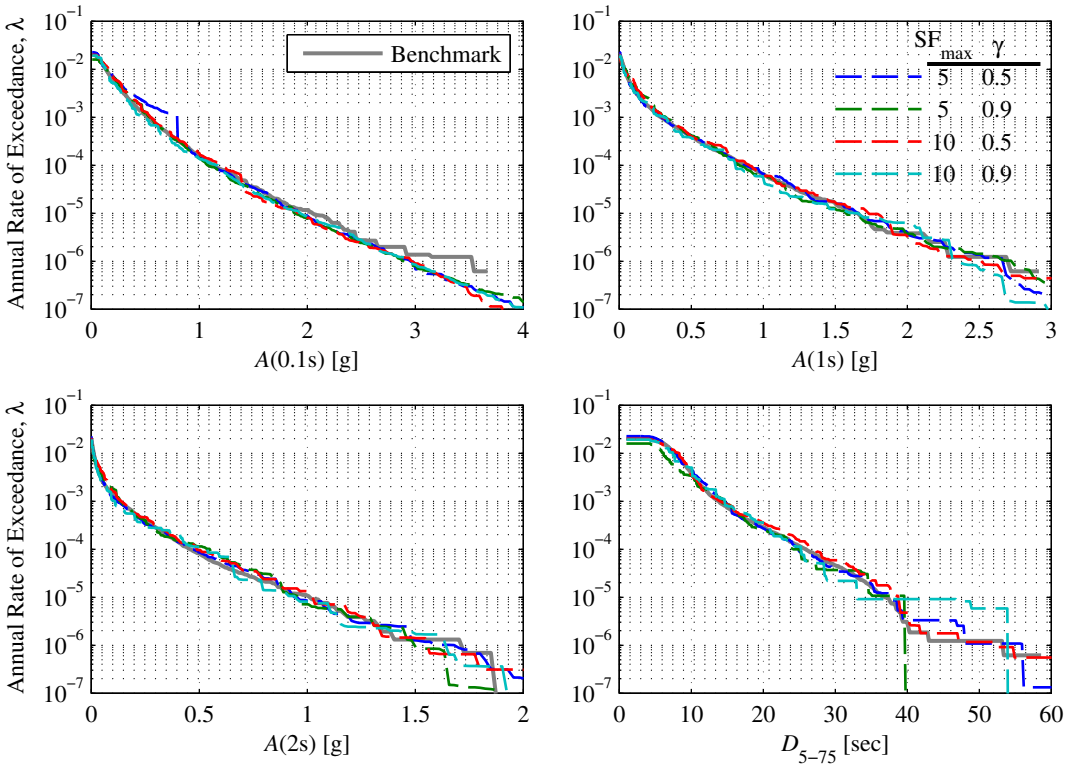

Figure 4.11: Hazard consistency of ground motions, scaled to various degrees, with respect to IMs employed for ground motion selection: (a) $A(0.1s)$; (b) $A(1s)$; (c) $A(2s)$; and (d) D_{5-75}.

scaling increases; in this case, the expectation in Equation 4.7b no longer holds, which can be seen in Figure 4.12. Given the relationship between scaling and bias, ground motions should not be scaled (i.e., $SF_{max} = 1$ or $\gamma = 0$) but if scaling is necessary, then some bias in the SDHC should be anticipated, depending on the sufficiency of the vector-valued IM chosen to select ground motions. Based on the results shown in Figures 4.12-4.13, the optimal values of SF_{max} and γ depend on the EDP of interest and on the specified **IM**; when **IM** consists of $A(T_1)$, $A(2T_1)$, $A(T_k)$, and D_{5-75}, we recommend $SF_{max} \leq 5$ and $\gamma \leq 0.5$.

The lack of sufficiency in "bestIM" with respect to MIDR implies that hazard inconsistencies with respect to other features of the ground motion cause bias in MIDR hazard curves. In Figure 4.14, the ground motions from the four combinations of scaling are examined for hazard consistency with respect to four IMs that are excluded from "bestIM": (i) peak ground acceleration (PGA), (ii) peak ground velocity (PGV), (iii) peak ground displacement (PGD), and (iv) cumulative absolute velocity (CAV). These IMs are chosen to represent the frequency content (at short, moderate, and long periods) and duration of the ground motion. The differences between the four ensembles are most pronounced for PGD; in fact, many other IMs were also examined and the differences are most pronounced for spectral accelerations at periods longer than 2 sec. Therefore, the MIDR of the 4-story

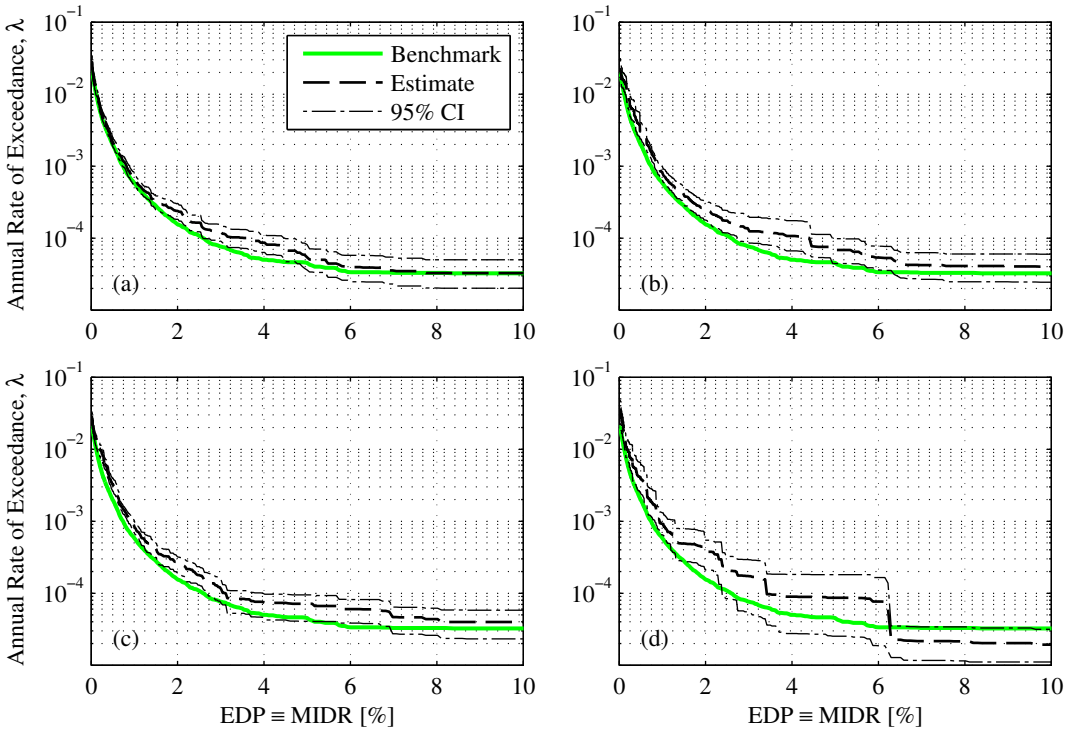

Figure 4.12: MIDR hazard curves from proposed procedure with four different combinations of SF_{max} and γ: (a) 5 and 0.5; (b) 5 and 0.9; (c) 10 and 0.5; and (d) 10 and 0.9. CIs from 100 bootstrap samples with "bestIM" and $n = 1000$ per bootstrap sample.

frame appears to be sensitive to the long period content of the ground motion.

The motions from the four combinations of scaling are similar to each other in that they are hazard-consistent with respect to PGA, PGV, and CAV (Figure 4.14). This is the case because such IMs are strongly correlated with "bestIM": PGA and PGV are correlated with spectral accelerations at vibration periods between 0.1 and 2 sec while CAV is correlated with D_{5-75}. On the other hand, PGD is correlated with spectral accelerations at periods longer than 2 sec, which were excluded from "bestIM". At the same time, we know from Figure 4.10 that the MFA is sensitive to spectral accelerations at short periods. Therefore, the excellent agreement in Figure 4.13, despite extensive scaling, is likely due to the fact that all four ensembles are hazard-consistent with respect to spectral accelerations at short periods of vibration.

The degree of scaling also affects the epistemic uncertainty of the SDHC estimates because different values of SF_{max} and γ lead to different IFs (Figure 4.5). For $EDP \equiv MIDR$, the widths of the CIs from Figures 4.12a-c are similar to each other and differ with those from Figure 4.12d. For $EDP \equiv MFA$ however, the widths of the CIs from all four cases shown in Figure 4.13 are similar to each other. These observations imply that the effect of scaling on the epistemic uncertainty varies with the type of EDP. From Equation 4.9, we see that the

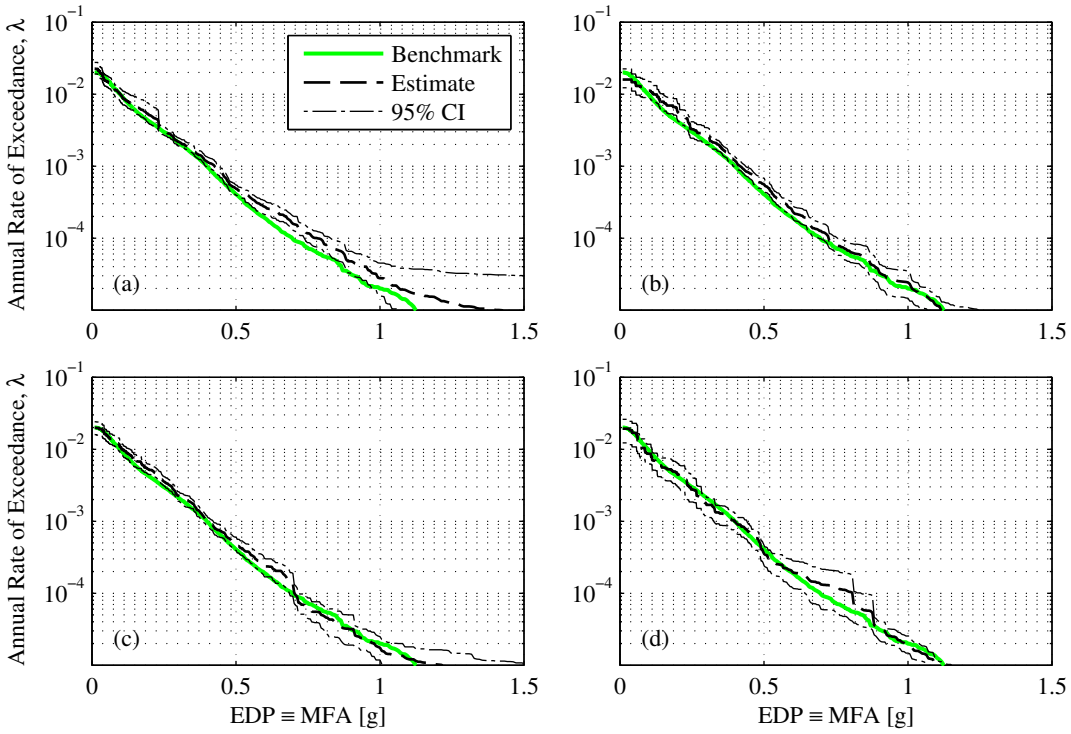

Figure 4.13: MFA hazard curves from proposed procedure with four different combinations of SF_{max} and γ: (a) 5 and 0.5; (b) 5 and 0.9; (c) 10 and 0.5; and (d) 10 and 0.9. CIs from 100 bootstrap samples with "bestIM" and $n = 1000$ per bootstrap sample.

epistemic uncertainty is affected by two quantities that depend on the EDP and are unknown *a-priori*: (i) $\Pr(EDP > z \mid \mathbf{IM} = \mathbf{s})$ and (ii) $\lambda_{EDP}(z)$. In order to approximately quantify the epistemic uncertainty contained in any particular SDHC estimate from the proposed procedure, we recommend supplying the estimate with a bootstrap CI (e.g., Figure 4.8). In addition to varying the IF (through SF_{max}, γ, and the database of prospective motions), the epistemic uncertainty may also be reduced by increasing the sample size, which is discussed next.

4.8 Minimum Number of Selected Motions

How many ground motions should be specified for the proposed procedure (see Figure 4.3)? In general, a large sample size is desirable because as the value of n increases, the epistemic uncertainty in the SDHC decreases (Equation 4.9) and consequently, the estimate becomes more repeatable. Furthermore, when scaling is not permitted and **IM** is sufficient, the SDHC estimate converges to the theoretical value (Equation 4.7b) with increasing values of n. However, the maximum value of n that can be specified is limited by the total number of prospective ground motions in the specified database. Hence, small values of n are also of interest and for a given site, EDP, and IF, the desirable value of n depends on the tolerable

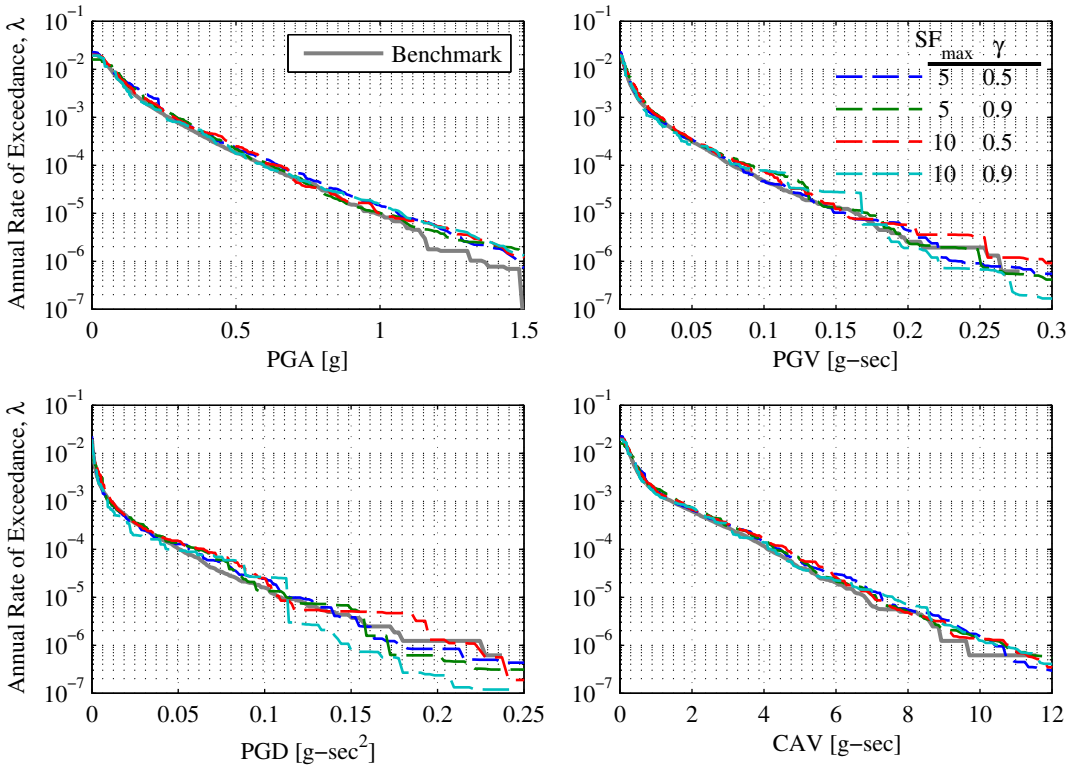

Figure 4.14: Hazard consistency of ground motions, scaled to various degrees, with respect to four miscellaneous IMs: (a) PGA; (b) PGV; (c) PGD; and (d) CAV.

level of epistemic uncertainty.

We investigate the effects of different sample sizes for $SF_{max} = 1$ and "bestIM" (Section 4.6). Unscaled ground motions are considered in this section because when ground motions are scaled significantly and **IM** is insufficient, the resulting SDHC estimate is biased, regardless of the sample size (see Section 4.7). Four different values of n are considered: (i) 100, (ii) 250, (iii) 500, and (iv) 1000. For each value of n, the procedure was executed 100 times, yielding 100 independent estimates of the SDHC; these SDHCs, summarized by the mean and 95% CI, are compared against the benchmark.

The MIDR hazard curves from different sample sizes are presented in Figure 4.15. As indicated by the mean, the estimate from the proposed procedure is, on average, unbiased regardless of the sample size, which is consistent with Equation 4.7b. For a given value of n, the epistemic uncertainty in the SDHC estimate increases for decreasing exceedance rates and is largest at collapse. As n decreases from 1000 to 100, the epistemic uncertainty increases. In particular, the relatively wide CIs near collapse in Figure 4.15a indicate that the SDHC estimate from a single execution with $n = 100$ is not very repeatable; that is, another execution with $n = 100$ will likely produce a different estimate of the SDHC. The repeatability of an SDHC estimate is measured by the standard deviation of the logarithm

of the collapse rate, denoted by σ_C, since exceedance rates may be considered to be approximately lognormally distributed [Bradley, 2009]; the values of σ_C for each choice of sample size are displayed in Figure 4.15.

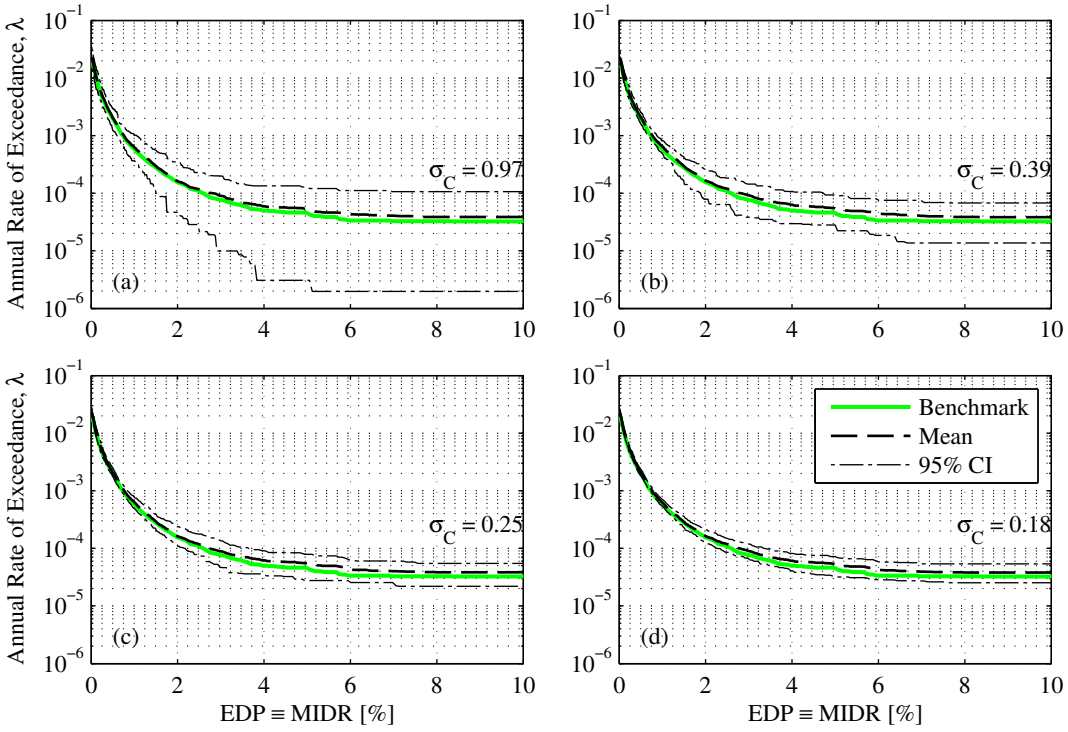

Figure 4.15: MIDR hazard curves from proposed procedure with four different choices for n: (a) 100; (b) 250; (c) 500; and (d) 1000. CIs from 100 independent executions of the procedure with unscaled motions selected using "bestIM" per execution.

Assuming a σ_C value of 0.4 is tolerable, values of n between 250 to 500 are recommended for the proposed procedure with $SF_{max} = 1$ and "bestIM"; this recommended range appears to be also applicable to scaled ground motions, but more research is needed to confirm this tentative conclusion. If smaller values of σ_C are desired, then n should be increased. To provide some context for such values of σ_C, note that the epistemic uncertainty in seismic hazard and seismic response is on the order of 0.5-1.5 and 0.4, respectively [Bradley, 2012c, Bradley, 2009]. The recommended range of $250 \leq n \leq 500$ is tantamount to performing 25 to 50 RHAs at 10 intensity levels in a PSDA, except that a non-parametric approach is employed in the proposed procedure (Equation 4.5) whereas a parametric approach is typically employed in PSDA. Consequently, the required sample size for the proposed procedure may be reduced if the estimates from Equation 4.5 are fitted with a parametric probability distribution.

4.9 Conclusions

A novel ground motion selection procedure is developed in this chapter. For a given structure at a given site, the procedure provides a single ensemble of ground motions and a corresponding collection of Importance Sampling weights for estimating SDHCs. The procedure requires five inputs: (i) database of prospective ground motions, (ii) **IM**, a vector of IMs for selecting ground motions, (iii) maximum acceptable scale factor, SF_{max}, (iv) a target fraction of scaled ground motions, γ, and (v) sample size, n. This procedure provides the following advantages:

1. The ability to estimate SDHCs from a *single* ensemble of ground motions;
2. The option to select ground motions that are scaled to varying degrees, including the important case of selecting *only* unscaled ground motions; and
3. The means to achieve hazard consistency with respect to a specified vector of IMs.

Using a recently developed method for evaluating ground motion selection procedures, the proposed procedure is evaluated in its ability to estimate SDHCs of a 4-story reinforced concrete frame, leading to the following conclusions:

1. The proposed procedure provides accurate estimates of the SDHC when ground motions are unscaled, or when the vector of IMs chosen to select ground motions is sufficient for the response quantity of interest.
2. If ground motions are restricted to be unscaled, then the sufficiency of the vector-valued IM comprising $A(0.1s)$, $A(1s)$, $A(2s)$, and D_{5-75}, denoted by "bestIM", plays a lesser role in determining the accuracy of the SDHC estimate than when ground motions are scaled. When ground motions are unscaled, "bestIM" is sufficient for both MIDR and MFA of the 4-story frame; in fact, D_{5-75} may be excluded for estimating MFA hazard curves.
3. If scaling of ground motions is permitted, the sufficiency of "bestIM" plays a major role in determining the accuracy of the SDHC estimate. When ground motions are scaled by factors as large as 10, "bestIM" remains sufficient for MFA but not for MIDR; the latter EDP seems to be influenced also by spectral acceleration at vibration periods longer than $2T_1$. The bias in MIDR hazard curves caused by amplitude scaling is generally conservative.
4. The epistemic uncertainty of the SDHC estimate, which increases for decreasing exceedance rates, is influenced by both the IF and the sample size n. For a given IF, the desired sample size depends on the level of epistemic uncertainty that can be tolerated.
5. Based on the exploratory analyses in this study, inputs for the proposed procedure are recommended as:

- **IM** $= \{A(T_k), A(T_1), A(2T_1), D_{5-75}\}$, where T_1 and T_k refer, respectively, to the first and kth mode of the structure;
- $SF_{max} \leq 5$ and $\gamma \leq 0.5$ when **IM** $= \{A(T_k), A(T_1), A(2T_1), D_{5-75}\}$;
- $250 \leq n \leq 500$ when **IM** $= \{A(T_k), A(T_1), A(2T_1), D_{5-75}\}$, $SF_{max} \leq 5$, and $\gamma \leq 0.5$.

The application of these recommendations, which are based on analyses of a 4-story frame, should be tested for taller buildings.

Chapter 5

Evaluation of the Exact Conditional Spectrum and Generalized Conditional Intensity Measure Methods for Ground Motion Selection

5.1 Preview

Two existing, contemporary GMSM procedures – (i) CS-exact, and (ii) GCIM – are evaluated in their ability to accurately estimate seismic demand hazard curves (SDHCs) of a given structure at a specified site. The amount of effort involved in implementing these procedures to compute a single SDHC is studied and a case study is chosen where rigorous benchmark SDHCs can be determined for evaluation purposes. By comparing estimates from GMSM procedures against the benchmark, we conclude that estimates from CS-exact are unbiased in many of the cases considered. The estimates from GCIM are even more accurate, as they are unbiased for most – but not all – of the cases where estimates from CS-exact are biased. We find that it is possible to obtain biased SDHCs from GCIM, even after employing a very diverse collection of intensity measures (IMs) to select ground motions and implementing its bias-checking feature, because it is usually difficult to identify IMs that are truly 'sufficient' for the response of a complex, multi-degree-of-freedom system.

5.2 Introduction

Several ground motion selection and modification (GMSM) procedures have been proposed in the past to select ground motions for conducting intensity-based assessments. The goal of an intensity-based assessment is to estimate the probability distribution of a response quantity, or engineering demand parameter (EDP), for a specified value of the intensity measure (IM) [NEHRP Consultants Joint Venture, 2011, Applied Technology Council, 2012]. A common example of this type of assessment is when the IM is defined as the spectral acceleration at the fundamental period of the structure, $A(T_1)$, and the intensity level is determined from a

specified return period (e.g., 475 years, 2475 years, etc.) or annual rate of exceedance (e.g., 2.1×10^{-3} events per year, 4.04×10^{-4} events per year, etc.).

In the context of intensity-based assessments, Baker and Cornell [Baker and Cornell, 2006b] investigated four different approaches to select ground motions and concluded that when matching parameters to select ground motions, spectral shape is a more important parameter to match than causal parameters such as earthquake magnitude, M, and source-to-site distance, R. Based on this finding, the Conditional Mean Spectrum (CMS) was proposed as the target spectrum for selecting ground motions [Baker and Cornell, 2006b, Baker, 2011]. However, the CMS, by definition, does not provide the proper aleatory variability in the response spectrum and as a result, extensions of the CMS have been developed by Jayaram et al. [Jayaram et al., 2011] and Lin et al. [Lin et al., 2013a]; these new spectra are known respectively as the Conditional Spectrum (CS), and the "exact" CS. Moreover, the CMS (again by definition) does not account for IMs that are unrelated to spectral accelerations and to overcome this limitation, the Generalized Conditional Intensity Measure (GCIM) approach was developed by Bradley [Bradley, 2010a], which may be interpreted as a generalization of the CMS.

The previously mentioned methods for selecting ground motions are sophisticated in the sense that explicit measures of the ground motion (e.g., spectral acceleration, significant duration, etc.) are carefully accounted for in the selection process through knowledge from probabilistic seismic hazard analysis (PSHA) of the site. Despite this sophistication, the accuracy of the results from such procedures is unclear because ground motions are almost always amplitude scaled and record scaling remains a subject of debate [Der Kiureghian and Fujimura, 2009]. For example, Grigoriu [Grigoriu, 2010] argues (on the basis of analyzing stochastic processes) that scaled ground motions provide "limited if any information on the seismic performance of structural systems". On the other hand, Bradley [Bradley, 2012c] argues that scaling will not cause bias in the EDP (due to a scalar IM), as long as either (i) the EDP is not dependent on the IM, or (ii) the probability distribution of the IM from the selected ground motions is consistent with the theoretical distribution.

In this chapter, we evaluate the accuracy of the results from sophisticated, contemporary GMSM procedures. Specifically, we evaluate two procedures – (i) "exact" CS (henceforth denoted as CS-exact for brevity) [1], and (ii) GCIM – in their ability to accurately estimate seismic demand hazard curves (SDHCs) for a given structure at a specified site. This context is chosen in order to draw definitive conclusions, since the SDHC of a given structure at a given site is unique [Bradley, 2013a]. In order to evaluate these procedures, we employ the notion of a 'benchmark' [Kwong et al., 2014] and apply the methodology described in Section 2 of [Kwong et al., 2015b]. Before evaluating these two GMSM procedures, let us first understand how they may be implemented for estimating SDHCs.

[1] More precisely, the special case that involves only a single ground-motion-prediction model is studied herein.

5.3 Step-By-Step Summaries of Ground Motion Selection Procedures for Estimating Seismic Demand Hazard Curves

Probabilistic Seismic Demand Analysis

Both CS-exact and GCIM employ probabilistic seismic demand analysis (PSDA) to estimate SDHCs of a given structure at a given site. In essence, several intensity-based assessments are conducted and the results from such assessments are combined with the hazard curve for the scalar conditioning IM to produce the SDHC. This commonality among CS-exact and GCIM, which is embodied by PSDA, is summarized for a single EDP as follows:

1. Specify the scalar conditioning IM, IM^*, for scaling ground motions [2].
2. Determine the hazard curve for IM^* from PSHA of the site and select N_{IM^*} intensity levels for conducting intensity-based assessments (see e.g., Fig 1a of [Kwong et al., 2014]).
3. For each of the N_{IM^*} intensity levels of IM^*, scale and select n ground motions from a master database.
4. Perform response history analyses (RHAs) of the structure due to all $N_{IM^*} \times n$ ground motions.
5. Estimate the SDHC using Eqs 2-3 of [Kwong et al., 2015b]; when the EDP is a measure of total acceleration (i.e., the acceleration at a specific floor or over all floors), replace the values of the EDP corresponding to collapse by peak ground acceleration (PGA) and apply Eq 2 of [Kwong et al., 2015b] (see also Section 5 of [Lin et al., 2013b]).

As seen in the above summary, the primary difference between CS-exact and GCIM in the context of estimating SDHCs is in the selection of ground motions (Step 3). The subsequent summaries of CS-exact and GCIM refer extensively to publications on CS [Baker, 2011, Jayaram et al., 2011, Lin et al., 2013a] and GCIM [Bradley, 2010a, Bradley, 2012a, Bradley, 2012c]; in the interest of brevity, they are not presented as stand-alone descriptions.

The "Exact" Conditional Spectrum Approach (CS-Exact)

In CS-exact, the scalar conditioning IM is typically specified as the spectral acceleration at a conditioning period of vibration, T^*; i.e., $IM^* \equiv A(T^*)$. For the ith intensity level of $A(T^*)$, denoted by x_i, the CS-exact approach to selecting n ground motions is summarized as follows:

[2] The scalar conditioning IM must change with amplitude scaling (e.g., significant duration cannot be chosen).

1. Perform deaggregation to determine the percent contribution of each rupture scenario to $A(T^*) = x_i$ (see e.g., Fig 3a of [Kwong et al., 2014]).

2. Scale all ground motions from the master database so that $A(T^*) = x_i$; optionally reduce the size of this database of scaled, prospective ground motions with a user-specified maximum scale factor, SF_{max}.

3. Specify a range of vibration periods over which the target spectrum is defined (e.g., $0.2T_1$ to $2T_1$ [Baker, 2011], 0.05 to 10 sec [Jayaram et al., 2011], etc.); see shaded region in Fig 3b of [Kwong et al., 2014].

4. Determine the "exact" CS, as described by Method 4 in [Lin et al., 2013a] (specialized for a single ground-motion-prediction model).

5. Randomly simulate n response spectra from the target spectrum in Step 4, using the approach discussed in Section 3.2 of [Bradley, 2012a] (specialized for the case where all IMs are spectral accelerations).

6. Select n ground motions (from the database developed in Step 2) whose response spectra most closely agree with those simulated from Step 5, using the approach discussed in Section 3.3 of [Bradley, 2012a] (specialized for the case where all IMs are equally weighted spectral accelerations).

7. Confirm that the selected ground motions are consistent with the target spectrum: apply Kolmogorov-Smirnov (KS) tests on the selected motions for spectral acceleration at each of the vibration periods specified in Step 3.

    a) If the selected motions pass the KS tests for all vibration periods, then proceed to the next intensity level of $A(T^*)$; otherwise, repeat Steps 5-6 to reselect another set of n ground motions.

    b) If the KS tests cannot be satisfied for all vibration periods after N_{Iter} attempts, then reselect another set of n ground motions by applying the greedy optimization procedure (as described on Pages 800-801 in [Jayaram et al., 2011]) to the latest set with the target means and standard deviations at each period given by Eqs 14-15 in [Lin et al., 2013a], specialized for a single ground-motion-prediction model.

The preceding summary of CS-exact differs from the CS approach described by Jayaram et al. [Jayaram et al., 2011] in two ways: (i) the target spectrum (Step 4), and (ii) the selection process (Steps 5-7). In [Jayaram et al., 2011], the target spectrum is a multivariate lognormal distribution for the mean rupture scenario whereas in this study, the target spectrum is a finite mixture of multivariate lognormal distributions (see e.g., page 143 of [Wasserman, 2004]), where the mixing weights are obtained from deaggregation (see Eq 8 in [Bradley, 2010a]). Because the target spectrum in the CS approach considers a single rupture scenario whereas that in CS-exact considers all rupture scenarios, the dispersion [3] of $A(T)$ from

[3]The term dispersion refers to the standard deviation of the natural logarithm of $A(T)$.

CS is typically less than that from CS-exact. This difference in dispersion is illustrated in Figure 5.1a, where the dispersion from CS-exact is given by Eq 15 in [Lin et al., 2013a], specialized for a single ground-motion-prediction model.

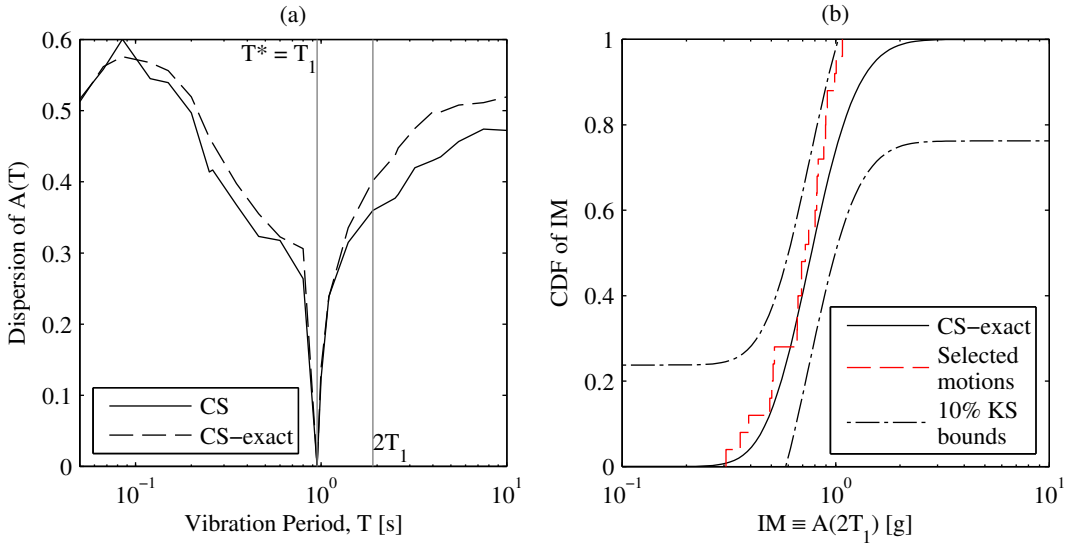

Figure 5.1: (a) Dispersion of $A(T)$ from CS versus that from CS-exact for a given level of $A(T^*)$; (b) example of applying a KS test to ground motions selected for the same level of $A(T^*)$.

Ground motions are selected in [Jayaram et al., 2011] by matching the target mean vector and covariance matrix with a greedy optimization technique whereas in this study, ground motions are selected so that they pass the KS tests at all vibration periods. For example, Figure 5.1b depicts the KS test for $A(2T_1)$, as applied to the ground motions selected to match the target spectrum from CS-exact (Steps 5-6). The target cumulative distribution function (CDF) of $A(2T_1)$ from CS-exact (solid black) is compared against the empirical CDF of $A(2T_1)$ from the selected motions (dashed red); the selected motions are deemed to be consistent with the target at this period when the empirical CDF falls within the KS bounds at a specified significance level (chained black). The KS test is preferred over the greedy optimization technique in this study (see Step 7b) because the mean vector and covariance matrix from CS-exact are inadequate to completely characterize its target spectrum, as it is not multivariate lognormal.

The choice of CS-exact is motivated by the desire to select ground motions that are *hazard-consistent* with respect to spectral accelerations at T_1, T_2, T_3, and $2T_1$ of the structure while simultaneously avoiding the need to inflate standard deviations [Lin et al., 2013b], where T_1, T_2, and T_3 refer respectively to the first, second, and third modal period of the structure. In this study, an ensemble of $N_{IM^*} \times n$ ground motions, which may be obtained by repeating the above summary for all N_{IM^*} intensity levels, is said to be *hazard-consistent with respect to an IM* when its resulting estimate of the hazard curve (from Eq 16 in [Kwong et al., 2015b]) is essentially equal to the target hazard curve. For example, the ground motions

portrayed in Figure 5.2a are hazard-consistent with respect to $A(2T_1)$ at exceedance rates greater than 4×10^{-6}, because the 95% bootstrapped [Efron and Tibshirani, 1993] confidence intervals (CI) of the hazard curve estimate essentially cover the benchmark hazard curve. If the motions are judged to be hazard-inconsistent (e.g., see exceedance rates less than 4×10^{-6} in Figure 5.2a), then ground motions may be reselected for one or more intensity levels of $A(T^*)$.

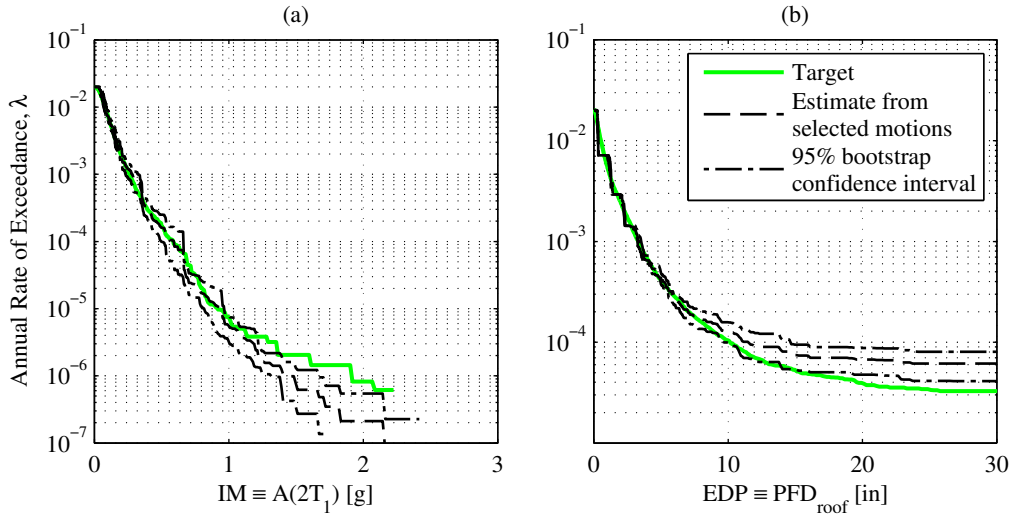

Figure 5.2: Illustration of (a) hazard consistency; (b) SDHC bias.

An SDHC estimate from a GMSM procedure is said to be unbiased when it is practically the same as the target SDHC. For example, an SDHC estimate is shown by the dashed black curve in Figure 5.2b, whereas the target SDHC is shown by the solid green curve. By applying the bootstrap procedure to the EDPs determined by RHAs of the structure, 95% CIs can be developed to portray the epistemic uncertainty in the SDHC estimate. Because the CIs in Figure 5.2b essentially cover the benchmark SDHC at exceedance rates greater than 5×10^{-5}, the SDHC estimate is said to be unbiased in this range.

The Generalized Conditional Intensity Measure Approach (GCIM)

For the ith intensity level of IM^*, denoted by x_i, the GCIM approach to selecting n ground motions is summarized as follows:

1. Perform deaggregation to determine the percent contribution of each rupture scenario to $IM^* = x_i$ (see e.g., Fig 3a of [Kwong et al., 2014]).
2. Scale all ground motions from the master database so that $IM^* = x_i$.
3. Specify a large number of IMs for selecting ground motions, collectively denoted by **IM**, using a weight vector as discussed in Section 5.2 of [Bradley, 2012c].

4. Compute the multivariate GCIM distribution of **IM** | IM^*, using the vector version of Eqs 8-12 in [Bradley, 2010a].

5. Randomly simulate n vectors of **IM** from the multivariate GCIM distribution in Step 4, using the approach discussed in Section 3.2 of [Bradley, 2012a].

6. Select n ground motions (from the database developed in Step 2) whose computed values of **IM** most closely agree with those simulated from Step 5, using the approach discussed in Section 3.3 of [Bradley, 2012a].

7. Confirm that the selected ground motions are consistent with the target from GCIM: apply KS tests on the selected motions for each of the IMs specified in Step 3.

    a) If the selected motions pass the KS tests for all IMs, then proceed to the next intensity level of IM^*; otherwise, repeat Steps 5-6 to reselect another set of n ground motions.

    b) If the KS tests cannot be satisfied for all IMs after N_{Iter} attempts, then check whether or not such IM inconsistencies will cause EDP biases.

        i. Perform RHA of the structure due to the latest selection of ground motions.

        ii. Specify an EDP (e.g., floor displacement, story drift ratio, etc.) for checking.

        iii. For each inconsistent IM identified in Step 7b, check whether or not it is important to the current EDP considered by applying the approach shown schematically in Fig 7a of [Bradley, 2010a].

        iv. For each IM that is *both* inconsistent and important to the current EDP considered, estimate the potential bias in the EDP caused by that particular IM, following the approach outlined on pages 1337-1340 of [Bradley, 2010a]; note the IM that caused the largest estimated EDP bias, along with its bias estimate.

        v. Repeat Steps 7(b)iii-7(b)iv for all other EDPs of interest.

        vi. If all inconsistent IMs are unimportant to all EDPs, or all estimated EDP biases are judged to be acceptable, then proceed to the next intensity level of IM^*; otherwise, repeat Steps 3-6 to reselect another set of n ground motions, with a potentially different weight vector based on the information from Step 7(b)v.

The GCIM approach summarized above differs from the CS-exact approach (Section 5.3) in two major aspects: (i) any IM (in addition to spectral acceleration) can be incorporated and weighted to select ground motions (Step 3), and (ii) any potential biases in EDPs due to IM inconsistencies can be examined in a practical manner (Step 7b). Note that unlike Step 2 of the summary for CS-exact, scale factors are not limited in GCIM because GCIM aims to capture many more IMs than in CS-exact when selecting ground motions. With these differences, the GCIM approach is holistic but can be quite involved. For example, the bias-checking procedure requires RHAs of the structure to be performed first (Step 7(b)i), before

scattergrams of EDP versus IM can be developed (see e.g., Fig 7a of [Bradley, 2010a], Fig 3 of [Kwong et al., 2015a]). In addition, as the number of EDPs (Step 7(b)ii) and IMs (Step 3) increases, the number of checks and ground motion reselections may become cumbersome (Step 7b).

5.4 Methodology for Evaluation

Both CS-exact and GCIM scale ground motions but differ in the IMs chosen for selection. If the IMs chosen are indeed 'sufficient' for all EDPs of interest and the selected ground motions are also hazard-consistent with respect to such IMs, then scaling should not cause any bias in the resulting SDHC estimates [Kwong et al., 2014]. An IM, which is considered vector-valued for generality, is formally defined to be *sufficient with respect to* EDP, and denoted as $\mathbf{IM}_s$, when it satisfies the following equation:

$$\Pr(EDP > z \mid \mathbf{IM}_s, IM_1, IM_2, \ldots, IM_\infty) \approx \Pr(EDP > z \mid \mathbf{IM}_s) \tag{5.1}$$

where "$IM_1, IM_2, \ldots, IM_\infty$" characterizes features of the ground motion time series other than those in $\mathbf{IM}_s$ such as duration, M, R, etc. (see Appendix A of [Luco and Cornell, 2007]); otherwise, it is *insufficient with respect to this particular EDP*. Put differently, a sufficient IM allows the analyst to focus on a subset of the infinitely many different features of the time series, thus simplifying the problem considerably.

In many situations, because the degree of sufficiency of an IM is unknown, potential EDP biases may occur. One way to investigate whether or not such biases exist is to determine the sensitivity of the SDHC estimate from the GMSM procedure to the choice of the scalar conditioning IM [Lin et al., 2013b, Bradley, 2012c]. Although this approach is straightforward and can expose potential biases (assuming enough choices of the scalar conditioning IM are considered), the actual bias due to insufficiency of **IM** cannot be quantified for lack of a benchmark [Kwong et al., 2015b, Kwong et al., 2014]. Another way to explicitly quantify potential EDP biases is to implement the bias-checking procedure in GCIM [Bradley, 2010a]. Although this approach provides estimates of potential EDP biases in a practical fashion, such biases are caused by a single scalar IM, which may be significantly different from that caused by multiple IMs (see Section 5.7 of this chapter).

In order to quantify the potential bias in an EDP due to simultaneous inconsistencies with respect to multiple IMs, we propose to compare SDHC estimates from GMSM procedures against a *benchmark*. Such benchmark SDHCs can be determined from the approach described in Section 2 and schematically illustrated in Fig 1 of [Kwong et al., 2015b]. In essence, this approach involves three main steps. First, a universe of synthetic ground motions is generated such that they are consistent with the earthquake rupture forecast of the site. Second, benchmark hazard curves are computed using Eqs 5, 9, and 12 of [Kwong et al., 2015b]. Third, all GMSM procedures are applied to a subset of this universe of synthetic ground motions when estimating SDHCs; this is important for isolating the biases caused by a GMSM procedure on its resulting SDHC estimates. For nonlinear multi-degree-of-freedom

systems, identifying IMs that are truly sufficient (i.e., Equation 5.1 with an equality) is difficult but with a benchmark, one can definitively identify IMs that are *insufficient* for a given EDP. A case study is presented next to illustrate these ideas.

5.5 Case Study Considered

Structural Models and Response Quantities

Two reinforced concrete frames – 4-story and 20-story – are considered. These well-vetted frames have been studied by past researchers in various contexts (e.g., [Yamamoto, 2011], [PEER GMSM Working Group, 2009], [Goulet et al., 2007]) and consequently, details regarding geometry and material properties may be found in such references. In essence, both frames satisfy the strong-column, weak-beam philosophy and are modeled in OpenSEES [Mazzoni et al., 2006], where the inelasticity is captured by plastic hinges at the ends of beam-column elements; each frame is classified as collapsed when its displacement increases without bounds. The four modal periods of vibration for the 4-story frame are: $T_1 = 0.94$ sec, $T_2 = 0.30$ sec, $T_3 = 0.17$ sec, $T_4 = 0.12$ sec; for the 20-story frame, the four modal periods are: $T_1 = 2.6$ sec, $T_2 = 0.85$ sec, $T_3 = 0.46$ sec, $T_4 = 0.32$ sec.

Many EDPs are considered for the multistory frames. For each frame, the EDPs considered are: (i) peak (over time) floor displacements (PFD), (ii) peak story drift ratios (PSDR), (iii) peak floor accelerations (PFA), (iv) maximum of peak story drift ratios over all stories (MSDR), and (v) maximum of peak floor accelerations over all floors (MFA). Thus, a total of 14 EDPs are considered for the 4-story frame and a total of 62 EDPs are considered for the 20-story frame.

Specific Implementation of GMSM Procedures

Both CS-exact and GCIM share the same inputs to PSDA. In this study, the conditioning IM, IM^*, is defined as spectral acceleration at the fundamental period of the structure, $A(T_1)$; i.e., $T^* = T_1$. Six sources of error in computing SDHCs were identified by Bradley on page 1430 of [Bradley, 2012c]; in order to minimize these errors, $N_{IM^*} = 12$ intensity levels are chosen to discretize the hazard curve for $A(T_1)$, $n = 25$ ground motions are selected at each intensity level, and the probability distribution of EDP for a given intensity level is estimated with a non-parametric approach. The $N_{IM^*} = 12$ intensity levels correspond to: 50%, 20%, 10%, 5%, 2%, 1%, 0.5%, 0.2%, 0.1%, 0.05%, 0.02%, and 0.01% probability of exceedance in 50 years [4]. Moreover, 95% CIs are provided for each GMSM-based estimate of the SDHC using the bootstrap technique with 100 bootstrap samples.

In order to be as faithful as possible to the original intentions behind the CS-exact method, the following parameters were chosen for implementation. First, the scale factors for all ground motions were limited by $SF_{max} = 4$ (Step 2). Second, 25 vibration periods, logarithmically spaced between 0.05 to 10 sec, were chosen to compute the target spectrum.

[4] The Poisson assumption is used here.

Third, each KS test was conducted at the 10% significance level, and ground motions were reselected up to $N_{Iter} = 10$ times per intensity level, before resorting to the greedy optimization technique. (The greedy technique is treated as a last resort here because it matches only the first two statistical moments and not the complete probability distribution of the "exact" CS.)

In order to be as faithful as possible to the original intentions behind the GCIM method, the following parameters were chosen for implementation. First, 24 IMs were considered for selecting ground motions: peak ground acceleration (PGA), peak ground velocity (PGV), peak ground displacement (PGD), acceleration spectrum intensity (ASI), spectrum intensity (SI), displacement spectrum intensity (DSI), cumulative absolute velocity (CAV), 5-95% significant duration (D_{5-95}), 5-75% significant duration (D_{5-75}), and spectral accelerations at 15 vibration periods: 0.05, 0.1, 0.2, 0.25, 0.3, 0.5, 0.75, 0.95, 1, 2, 2.6, 3, 4, 5, and 10 sec. Second, following [Bradley, 2012c], weights for each IM were assigned by giving 85% to amplitude-based IMs and 15% to the cumulative-based IMs (see Table I in [Bradley, 2012c]). Third, all KS tests (and t-tests from Step 7(b)iii) were conducted at the 10% significance level, and ground motions were reselected up to $N_{Iter} = 10$ times per intensity level, before proceeding with RHAs and resorting to the bias-checking procedure.

Site, Ground Motions, and Ground-Motion-Prediction Models

The site chosen is identical to that depicted in Fig 2a and described in Section 3.1 of [Kwong et al., 2015b]. In essence, the seismicity of the site is controlled by a single strike-slip fault that is located 10 km away. Earthquakes occur randomly with magnitudes following the Youngs & Coppersmith probability density function, at an activity rate of $\nu = 0.02$ earthquakes per year.

Two stochastic models were utilized to generate two universes of 10^4 ground motions. These ground motion simulation models are described in Section 3.1 of [Kwong et al., 2015b] and are referred to as Rezaeian's GM model [Rezaeian and Der Kiureghian, 2008] and Yamamoto's GM model [Yamamoto and Baker, 2013]. An example ground motion time series with $M \approx 7$ from Rezaeian's GM model is presented in Figure 5.3a and an example ground motion time series with $M \approx 7$ from Yamamoto's GM model is illustrated in Figure 5.3b. With two GM models and two multistory frames, at least 4×10^4 RHAs of multistory frames were performed for this study.

In order to apply CS-exact and GCIM to a database of synthetic ground motions, ground-motion-prediction models that are "consistent with the benchmark" must be available. Such benchmark-consistent GMPMs were developed for 120 IMs and for each GM model, following the approach outlined in Section 5 of [Kwong et al., 2015b]. The selection of functional forms, determination of optimal standard deviations, and consideration of correlations, are documented in Appendix B. With these benchmark-consistent prediction models developed, CS-exact is evaluated first, followed by GCIM.

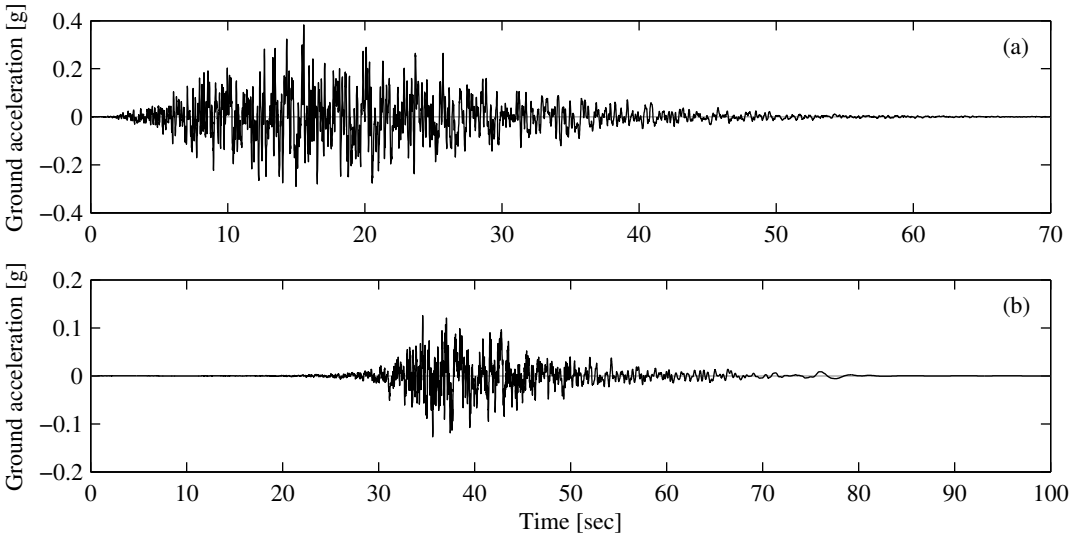

Figure 5.3: Example ground motion time series with $M \approx 7$ from: (a) Rezaeian's GM model; and (b) Yamamoto's GM model.

5.6 Evaluation of CS-Exact

The CS-exact procedure (Section 5.3) is implemented first for the 20-story frame, using ground motions from Rezaeian's GM model. The ground motions are carefully selected to be hazard-consistent with respect to spectral accelerations at vibration periods between 0.05 to 10 sec (Section 5.5). The only intensity levels of $IM^* = A(T_1)$ where $N_{Iter} = 10$ attempts to reselect ground motions were inadequate to satisfy the KS tests at all vibration periods are those corresponding to 0.02% and 0.01% probability of exceedance in 50 years. As a result, the selection of ground motions for each of these two intensity levels is finalized by applying the greedy optimization technique to the latest set (Step 7b) before proceeding with RHAs.

Hazard consistency of the preceding selected ensemble of $N_{IM^*} \times n$ ground motions is summarized in Figure 5.4. As expected, the selected motions are generally hazard-consistent with respect to spectral accelerations at the first three modal periods and twice the fundamental period of the 20-story frame, because CS-exact aims to select motions that are consistent with the target spectra at all intensity levels of $A(T_1)$, for a wide range of vibration periods. However, the selected motions are hazard-inconsistent with respect to $A(T_2)$ and $A(2T_1)$ at exceedance rates less than 10^{-5}; as discussed in Section 2 of [Kwong et al., 2015a], these inconsistencies arise from the fact that the selection of ground motions at a particular intensity level (Section 5.3) does not account for the 'tail' of the probability distribution of $IM \mid A(T^*)$. Because SDHC biases at low exceedance rates are controlled by hazard inconsistencies at low exceedance rates (e.g., consider the case where $IM \equiv EDP$ in Figure 5.2a), it is generally more important to enforce hazard consistencies at low exceedance rates than to satisfy KS tests at individual levels of IM^*.

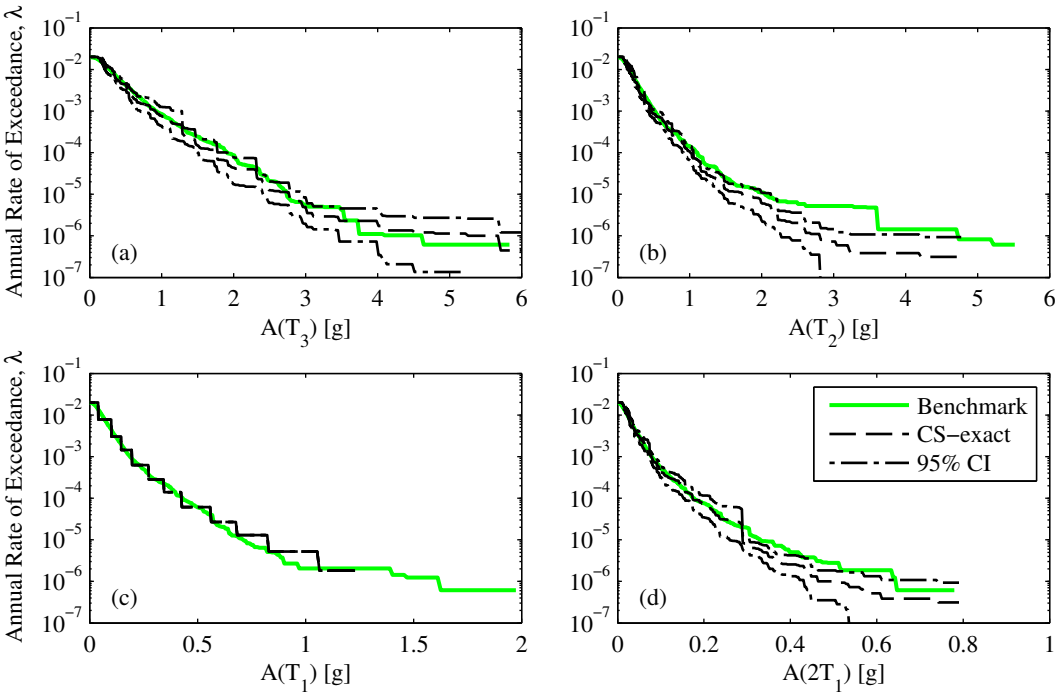

Figure 5.4: Hazard consistency of ground motions, selected by CS-exact for the 20-story frame, with respect to spectral accelerations at four vibration periods (Rezaeian's GM model).

Figure 5.5 presents the SDHC estimates of the 20-story frame, resulting from the ground motions summarized in Figure 5.4, along with the benchmark SDHCs, which are determined from 10^4 RHAs of this frame. A subset of four EDPs is chosen to summarize results for the 62 EDPs considered (Section 5.5): (i) roof displacement, PFD_{20}, (ii) first-story drift ratio, $PSDR_1$, (iii) roof acceleration, PFA_{20}, and (iv) maximum floor acceleration over all floors, MFA. These EDPs are chosen to illustrate responses at specific floors/stories that are often of interest in loss assessments in performance-based earthquake engineering. For PFD_{20}, $PSDR_1$, and PFA_{20}, the SDHC estimate from CS-exact is unbiased at exceedance rates greater than 10^{-5} (Figure 5.5a-c). The SDHC estimate from CS-exact is also generally unbiased for MFA, but slightly underestimates the benchmark at a few ranges of exceedance rates (Figure 5.5d). The difference between the observations for PFA_{20} against those for MFA highlights the importance of considering response quantities at individual floors. Overall, the SDHCs from CS-exact are unbiased at exceedance rates greater than 10^{-5} for nearly all of the 62 EDPs considered for the 20-story frame, with MFA and PFA_2 as the only exceptions.

The benchmark SDHCs shown in Figure 5.5 enable biases in the SDHC estimates to be quantified and insufficient IMs to be identified. Note that without the benchmark, a concept developed in [Kwong et al., 2014] and in [Kwong et al., 2015b], it would be difficult to identify biases such as those shown in Figure 5.5d by varying conditioning periods as in Fig 11 of [Lin et al., 2013b], where a nearly identical 20-story frame was studied. The

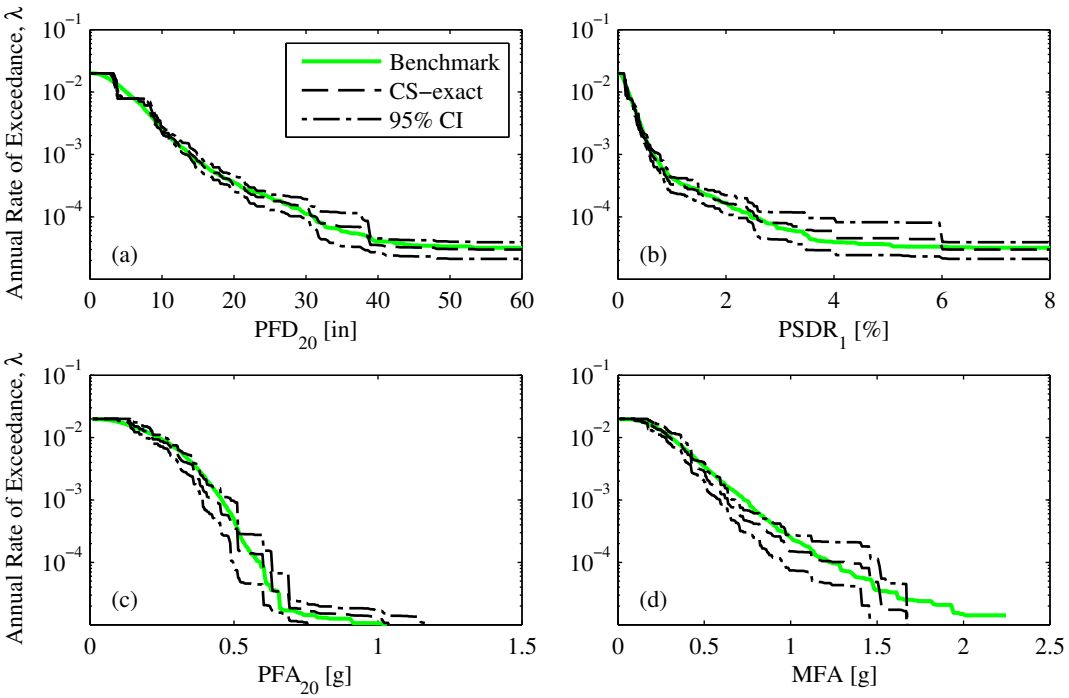

Figure 5.5: Comparison of SDHC estimates for several EDPs of the 20-story frame from CS-exact against benchmark (Rezaeian's GM model).

biases shown in Figure 5.5d imply that $A(T_1)$ is insufficient relative to MFA because ground motions are deliberately scaled in CS-exact to achieve hazard consistency with respect to $A(T_1)$ (Figure 5.4c). Do the biases shown in Figure 5.5d *also* imply that $A(T_2)$ is insufficient relative to MFA? Strictly speaking, the answer is no because the selected motions are hazard-inconsistent with respect to $A(T_2)$ at exceedance rates less than 10^{-5} (Figure 5.4b) and hence, the biases in MFA could have been caused by either such inconsistencies or insufficiency. If ground motions were somehow selected to be hazard-consistent at such low exceedance rates (e.g., using the procedure developed in Chapter 4), then more definitive statements can be made with regard to insufficiency. This subtle point should be kept in mind when interpreting all subsequent results.

The evaluation of CS-exact for the 20-story frame is repeated for Yamamoto's GM model. An additional 10^4 RHAs of the 20-story frame are performed to compute benchmark SDHCs and an additional subset of $N_{IM^*} \times n = 300$ ground motions is selected via CS-exact. As in Rezaeian's GM model (Figure 5.4), the motions from Yamamoto's GM model are again selected so that hazard consistency is generally achieved with respect to spectral accelerations over a wide range of vibration periods. The SDHCs resulting from such motions are presented in Figure 5.6. Similar to the results from Rezaeian's GM model (Figure 5.5), the SDHCs from CS-exact are unbiased for many of the EDPs considered for the 20-story frame. However, unlike the MFA hazard curve from Rezaeian's GM model (Figure 5.5d), that from Yamamoto's GM model is unbiased at all exceedance rates greater than 10^{-5} (Figure 5.6d).

This observation implies that strictly speaking, SDHC biases are caused *directly* by the hazard inconsistencies of the specific selection of ground motions and *indirectly* by the GMSM procedure in question; the GMSM procedure is only a tool for achieving hazard consistencies. From a pragmatic standpoint however, Figures 5.5 and 5.6 collectively suggest that the vector of spectral accelerations at vibration periods between 0.05 to 10 sec (Section 5.5), or spectral shape, is sufficient for the 20-story frame studied in this chapter, because the SDHC biases are small for nearly all of the EDPs considered.

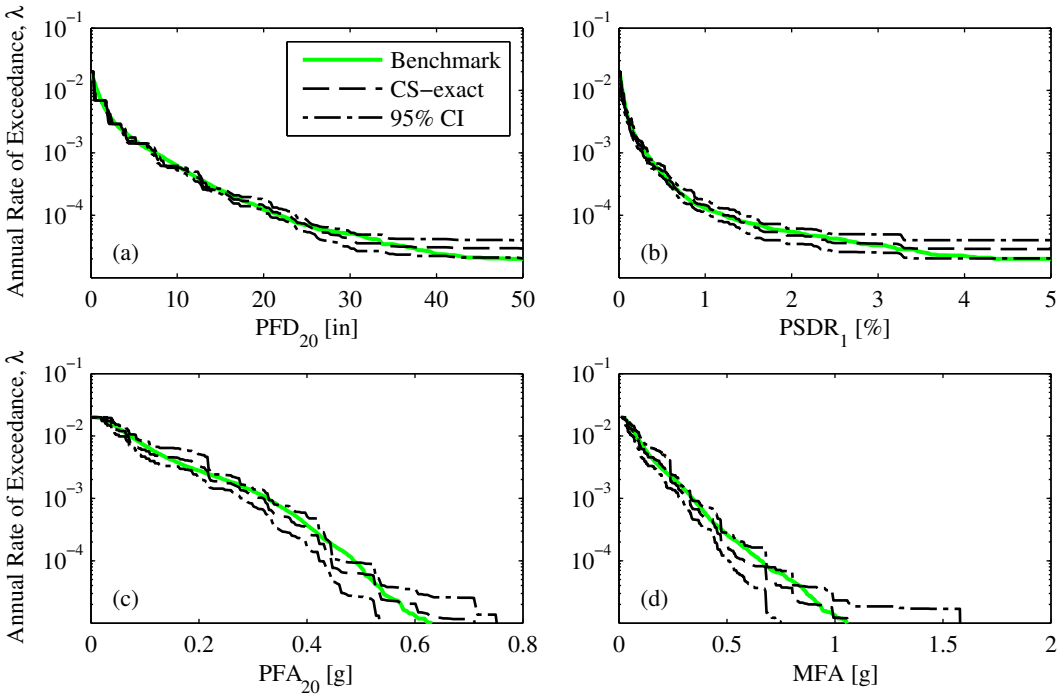

Figure 5.6: Comparison of SDHC estimates for several EDPs of the 20-story frame from CS-exact against benchmark (Yamamoto's GM model).

The CS-exact procedure is also evaluated with the 4-story frame (Section 5.5). A total of 2×10^4 RHAs of this frame were conducted to develop the benchmark SDHCs for both GM models. In each of the two models, the ground motions were again carefully selected to be hazard-consistent with respect to spectral accelerations at vibration periods between 0.05 to 10 sec. The SDHC estimates of the 4-story frame for Rezaeian's GM model are presented in Figure 5.7 whereas those for Yamamoto's GM model are presented in Figure 5.8. A subset of four EDPs is chosen to summarize results for the 14 EDPs considered: (i) roof displacement, PFD_4, (ii) first-story drift ratio, $PSDR_1$, (iii) roof acceleration, PFA_4, and (iv) maximum floor acceleration over all floors, MFA.

In contrast to the SDHCs from CS-exact for the 20-story frame (Figures 5.5 and 5.6), those for the 4-story frame are generally more biased. Specifically, (i) the roof acceleration hazard curves from CS-exact underestimate the benchmark for both GM models (Figures 5.7c and 5.8c), and (ii) in Yamamoto's GM model, the annual rate of collapse is overestimated

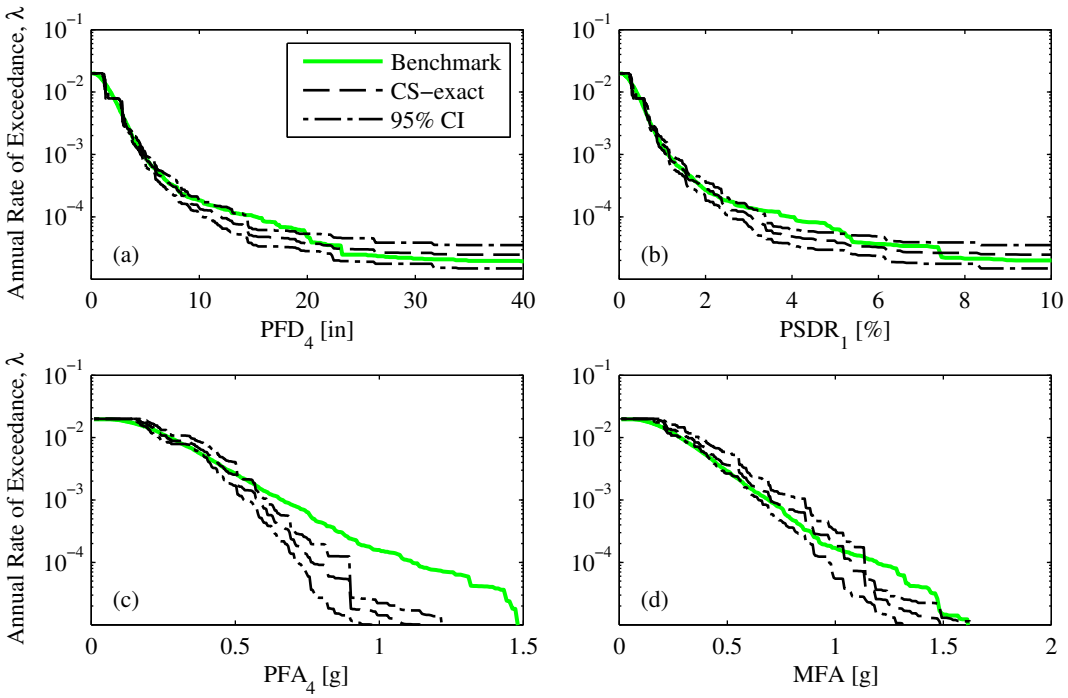

Figure 5.7: Comparison of SDHC estimates for several EDPs of the 4-story frame from CS-exact against benchmark (Rezaeian's GM model).

(Figures 5.8a-b). To some readers, the biases observed in the roof acceleration hazard curves (Figures 5.7c and 5.8c) may appear surprising because the selected ground motions are hazard-consistent with respect to spectral accelerations at all modal periods of the frame and at the same time, one might expect roof acceleration to be sensitive to higher modes (see e.g., Appendix A.1 of [Lin, 2012]). This finding suggests that roof acceleration depends on a feature of the ground motion time series that has not been considered in the analysis thus far, pointing out the importance of developing a rigorous benchmark when evaluating results from GMSM procedures. Overall, the biases documented in Figures 5.7-5.8 indicate that spectral shape is generally *insufficient* for the response of the 4-story frame, although it may be considered to be sufficient for the 20-story frame.

The magnitude of biases in the SDHCs indicate the degree to which the vector of IMs chosen for ground motion selection is sufficient. Recall that the ground motions selected via CS-exact for both frames are generally hazard-consistent with respect to spectral accelerations over a wide range of vibration periods (or loosely speaking, spectral shape). Since less bias is observed for the 20-story frame (Figures 5.5-5.6) than for the 4-story frame (Figures 5.7-5.8), we conclude that spectral shape is less insufficient for the 20-story frame than for the 4-story frame; i.e., this IM does a better job of satisfying Equation 5.1 for EDPs of the 20-story frame than for those of the 4-story frame. Furthermore, based on the biases noted in Figures 5.7 and 5.8, spectral shape is less insufficient for displacements and drift ratios than for floor accelerations of the 4-story frame. The phrase 'less insufficient' is uti-

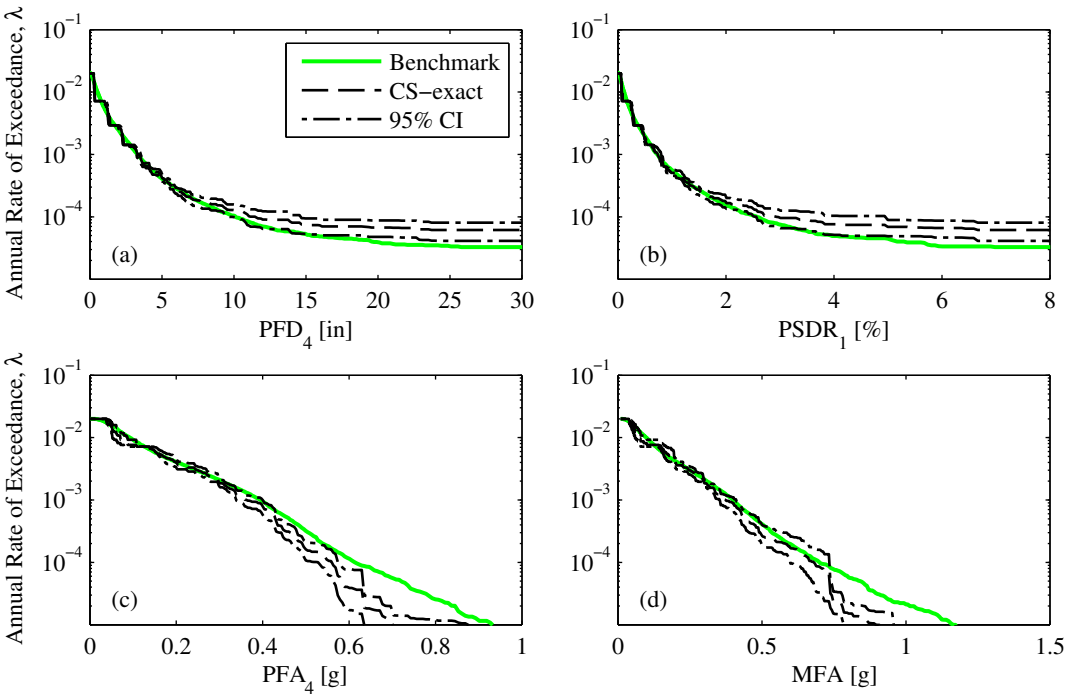

Figure 5.8: Comparison of SDHC estimates for several EDPs of the 4-story frame from CS-exact against benchmark (Yamamoto's GM model).

lized because it is difficult to prove that an IM is truly sufficient; i.e., the good agreement in SDHCs does *not* necessarily imply that the IM satisfies Equation 5.1 with an equality because the selected motions may happen to be hazard-consistent with respect to other IMs by chance.

In general, the bias in the SDHC from CS-exact depends on the particular EDP considered because an IM that is insufficient for one case may appear to be sufficient for another. For instance, the roof displacement hazard curve from CS-exact using Yamamoto's GM model (Figure 5.8a) overestimates the annual rate of collapse whereas that using Rezaeian's GM model (Figure 5.7a) is unbiased for nearly all exceedance rates. The overestimation in Yamamoto's GM model arises from the fact that spectral shape is insufficient for the estimation of the collapse rate of the 4-story frame.

To illustrate this fact, let us consider Figure 5.9, where hazard consistency of the ground motions selected via CS-exact for this frame, is examined with respect to two IMs that are not employed in the selection of ground motions: (i) PGV, and (ii) D_{5-75}. In both GM models, the selected motions are generally hazard-consistent with respect to PGV even though this IM is not utilized in the selection of ground motions (Figure 5.9a and c), because PGV is highly correlated with the response spectrum at moderate vibration periods [5] and at the

[5]The correlation, ρ, between PGV and $A(1s)$ in Yamamoto's GM model is 0.85; in Rezaeian's GM model, it is 0.90.

same time, hazard consistency for this range of periods is enforced in CS-exact. In contrast, the selected motions are far more hazard-*inconsistent* with respect to D_{5-75} in Yamamoto's GM model (Figure 5.9b) than in Rezaeian's GM model (Figure 5.9d), because the correlation between PGV and D_{5-75} is much weaker in Yamamoto's GM model ($\rho = -0.06$) than in Rezaeian's GM model ($\rho = -0.34$). Therefore, spectral shape *appears* to be sufficient in Rezaeian's GM model for estimating the collapse rate (Figure 5.7a) because in this model, D_{5-75} happens to be somewhat correlated with the response spectrum at moderate periods of vibration. In order to control IMs in addition to spectral accelerations, the GCIM approach was developed, which is evaluated next.

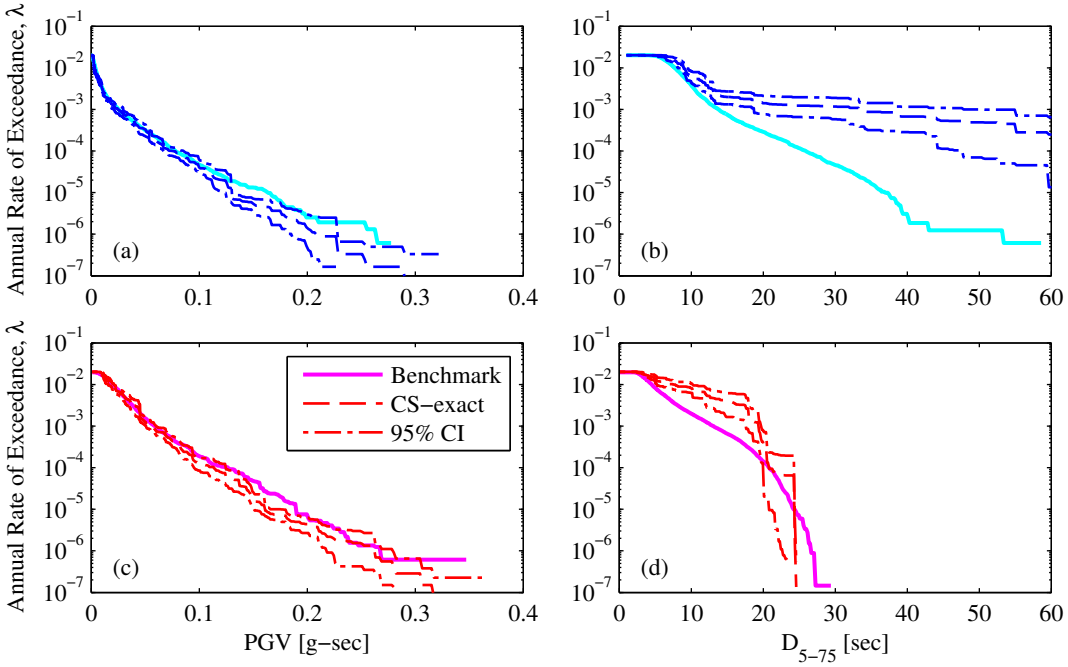

Figure 5.9: Hazard consistency of ground motions selected for the 4-story frame via CS-exact from Yamamoto's master database, with respect to: (a) PGV and (b) D_{5-75}; hazard consistency of ground motions selected for the 4-story frame via CS-exact from Rezaeian's master database, with respect to: (c) PGV and (d) D_{5-75}.

5.7 Evaluation of GCIM

The GCIM procedure (Section 5.3) is implemented first for the 4-story frame and for Rezaeian's GM model. For a given intensity level of $A(T_1)$, ground motions are iteratively selected so that they satisfy the KS tests for the 24 IMs mentioned in Section 5.5, which include measures of duration in addition to spectral accelerations. Figure 5.10a presents an example of applying the KS test to the ground motions selected for the 0.02% probability of exceedance in 50 years level. The KS test indicates whether or not the difference between the two CDFs of $A(0.1)$ – empirical (dashed black) and GCIM (solid green) – is statistically significant. At the 10% significance level, both the KS bounds (chained green) and p-value in Figure 5.10a

indicate that the selected motions are *inconsistent* with respect to $A(0.1)$, because the empirical CDF falls outside of the KS bounds and the p-value is less than the significance level. Such an inconsistency prompted several more reselections of ground motions (via Steps 5-6 of Section 5.3), until the selected motions pass the KS tests for all 24 IMs.

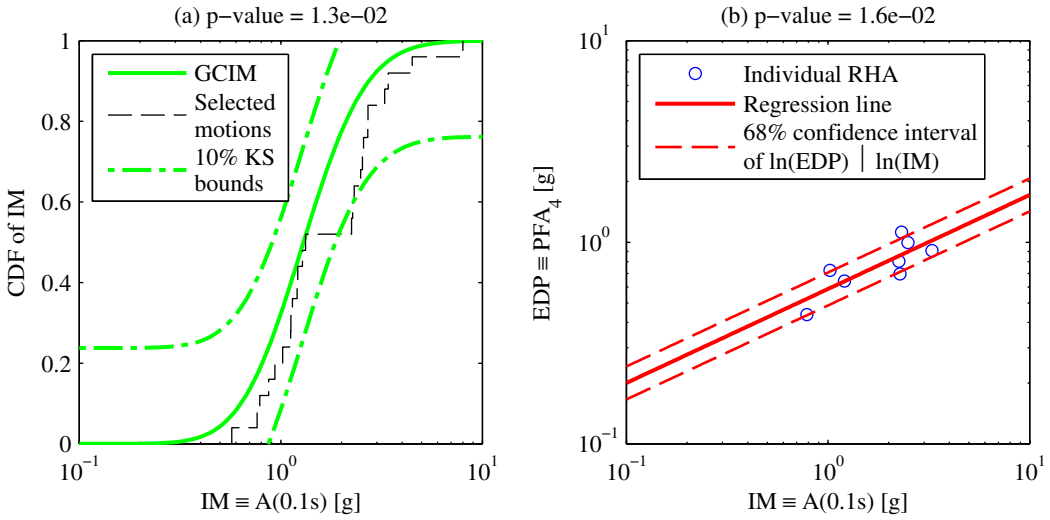

Figure 5.10: Examples of applying: (a) KS tests, and (b) t-tests to ground motions selected for $A(T_1)$ at 0.02% probability of exceedance in 50 years (Rezaeian's GM model).

When IM inconsistencies remain after $N_{Iter} = 10$ reselections, the bias-checking procedure in GCIM (Step 7b) is implemented, where the first step is to examine the potential significance of such inconsistencies relative to an EDP of interest. This is done by (i) performing $n = 25$ RHAs of the 4-story frame, (ii) creating a scattergram of the EDP versus each IM in log-log space, (iii) determining the regression line, and (iv) applying the t-test to determine whether or not the slope of the regression line is statistically significant (Step 7(b)iii). For example, the potential significance of the inconsistency shown in Figure 5.10a, relative to roof acceleration of the 4-story frame, is examined in Figure 5.10b; in this figure, only 8 out of the $n = 25$ RHA results are shown (blue circles) because the rest of the ground motions led to collapse. From this subset of the RHA results, the regression line is determined (solid red) and its slope is tested for statistical significance via the t-test. Because the p-value from the t-test (which is 1.6×10^{-2}) is less than the significance level, the inconsistency of the selected motions with respect to $A(0.1)$ is deemed to be statistically significant for PFA_4 and hence the potential bias in PFA_4 due to $A(0.1)$ should be estimated next in order to decide whether or not ground motions should be reselected with a potentially different weighting of the 24 IMs. If the slope had turned out to be statistically *insignificant*, then the inconsistency in Figure 5.10a would have been deemed unimportant and hence reselection of ground motions would not be necessary.

In order to determine whether or not ground motion reselection is necessary for the example intensity level considered in Figure 5.10, the potential biases in PFA_4 caused by each individual inconsistent IM are estimated (Step 7(b)iv). For the 0.02% probability of

exceedance in 50 years level of $A(T_1)$, the selected motions are *also inconsistent* with respect to $A(0.5)$, in addition to $A(0.1)$ (Figure 5.10a). Figure 5.11a presents the potential bias in PFA_4 due to $A(0.1)$, whereas Figure 5.11b presents the potential bias in PFA_4 due to $A(0.5)$. For each scalar IM, the estimated bias is indicated by the discrepancy between the "uncorrected" (dashed black) and "corrected" (chained red) CDFs of roof acceleration for the 0.02% probability of exceedance in 50 years level. The "uncorrected" CDF is obtained by fitting a lognormal distribution to the values of EDP where collapse did not occur (solid grey); on the other hand, the "corrected" CDF is obtained by applying Eq 17 in [Bradley, 2010a] to the non-collapse cases of the RHA results. Since the potential biases due to $A(0.5)$ are smaller than those due to $A(0.1)$, the bias due to $A(0.1)$ dictates whether or not ground motion reselection is necessary for this intensity level (Step 7(b)iv).

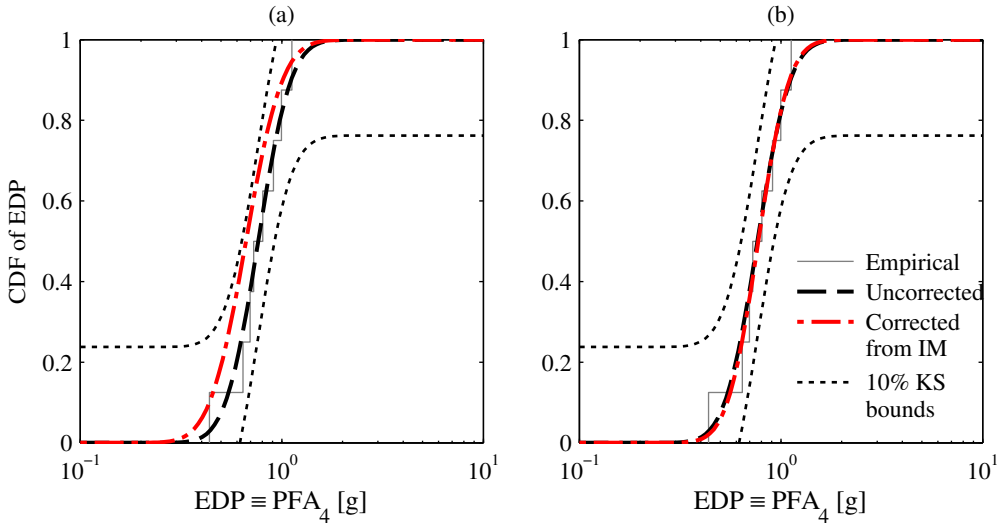

Figure 5.11: Estimates of bias in PFA_4 from GCIM due to: (a) $IM \equiv A(0.1)$, and (b) $IM \equiv A(0.5)$, for $A(T^*)$ at 0.02% probability of exceedance in 50 years (Rezaeian's GM model).

It is up to the analyst to decide whether or not such EDP biases estimated from GCIM are acceptable. In this study, we adopt an approach that is inspired by the KS test illustrated in Figure 5.10a. Specifically, the difference between the empirical CDF (solid grey) and the "corrected" CDF (chained red) is quantified by the KS test. Since the "corrected" CDF falls within the 10% KS bounds (Figure 5.11a), the bias in PFA_4 due to $A(0.1)$ is deemed acceptable; hence, the current selection of ground motions and corresponding RHA results are considered to be final.

By reselecting ground motions at each intensity level of $A(T_1)$ up to $N_{Iter} = 10$ times, the selected motions for the 4-story frame with Rezaeian's GM model passed almost all of the KS tests. This is demonstrated in Figure 5.12a, where only three out of the $N_{IM^*} \times 24 = 288$ KS tests led to inconsistencies (shown in magenta); these three IMs, denoted by numbers 2, 4, and 6, correspond respectively to spectral accelerations at vibration periods of 0.1, 0.25, and 0.5 sec. Among these three cases, only those corresponding to 0.02% probability of

exceedance in 50 years led to statistically significant slopes from regression analyses for roof acceleration, as illustrated in Figure 5.12b. Therefore, 0.02% probability of exceedance in 50 years is the only intensity level in which ground motion reselection might be necessary; i.e., the selected motions for all other intensity levels is finalized at this point. Based on the estimated biases presented in Figure 5.11, ground motion reselection for this intensity level does not seem necessary.

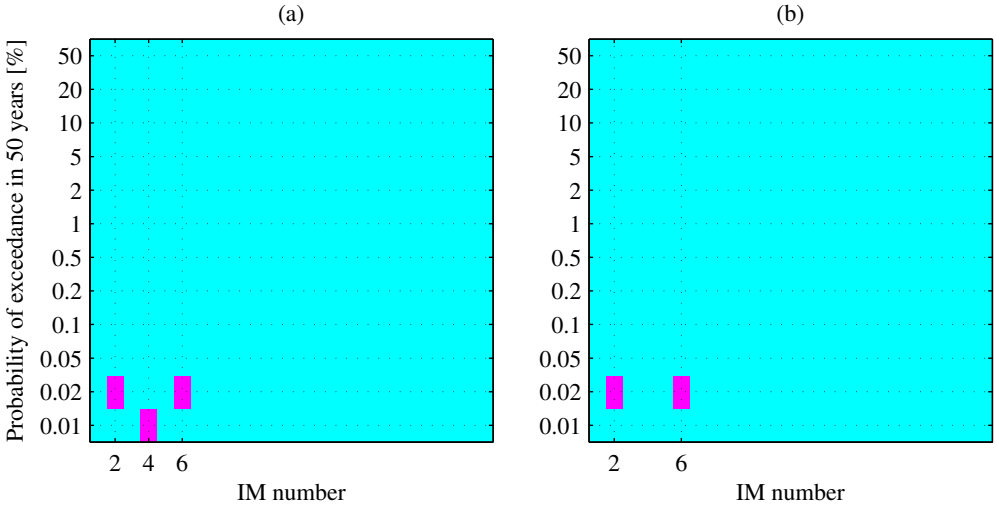

Figure 5.12: (a) Summary of results from KS tests for all 24 IMs employed in GCIM, at all intensity levels of $A(T^*)$ (magenta indicates inconsistency with respect to GCIM distribution); (b) cases where IM is *both* inconsistent and important to PFA_4, as measured by t-tests (magenta indicates slope from linear regression is statistically significant, given IM is inconsistent). Results for Rezaeian's GM model.

The bias-checking procedure in GCIM offers several benefits for selecting ground motions. First, the p-values from KS tests permit ground motions to be selected in a somewhat automated fashion (Figure 5.12a). Second, the p-values from t-tests allow users to identify intensity levels of IM^* that require potential reselection of ground motions (e.g., Figure 5.12b). Third, decisions regarding the reselection of ground motions at a particular intensity level are better informed with estimates of the "corrected" CDF of EDP (Figure 5.11).

However, the bias-checking procedure in GCIM has several limitations. First, RHAs of the multistory frame must be performed before scattergrams can be constructed (e.g., Figure 5.10b). Second, the treatment of collapses in the bias-checking procedure is unclear. One option is to exclude collapses, as shown in Figure 5.10b; however, this can lead to questionable results as the number of collapses approaches the total number of ground motions selected for the particular intensity level, n (i.e., in the limit, no data would be available to construct the scattergram). Another option is to include the collapses; however, this may also lead to questionable results because one is utilizing the numerical values of EDP corresponding to collapse. Third, the application of t-tests can become cumbersome as the number of EDPs increases (e.g., 14 EDPs are considered for the 4-story frame and 62 EDPs

are considered for the 20-story frame) and as the number of IM inconsistencies increases (e.g., Figure 5.12a); therefore, it is advantageous to minimize the number of such inconsistencies from KS tests. Fourth, the estimated EDP biases from GCIM are approximate, as they depend on the particular scalar IM considered (see Figure 5.11).

Figure 5.13 presents the SDHCs of the 4-story frame resulting from the ground motions summarized in Figure 5.12a. Figure 5.13 demonstrates that the SDHCs from GCIM are unbiased for many of the EDPs, from linear-elastic behavior to collapse. Moreover, the epistemic uncertainty in the SDHC estimates is relatively small, implying excellent repeatability of the estimates. However, the SDHCs from GCIM are biased for some of the floor accelerations; in particular, the roof acceleration hazard curve from GCIM underestimates the benchmark at exceedance rates less than 2×10^{-3}, as shown in Figure 5.13c. This bias in floor accelerations indicates that there is no guarantee that the resulting SDHC estimates from GCIM are unbiased, even after (i) enforcing hazard consistency of the selected motions with respect to a very diverse collection of IMs (i.e., spectral accelerations, spectrum intensities, significant duration, etc.), and (ii) implementing the bias-checking procedure.

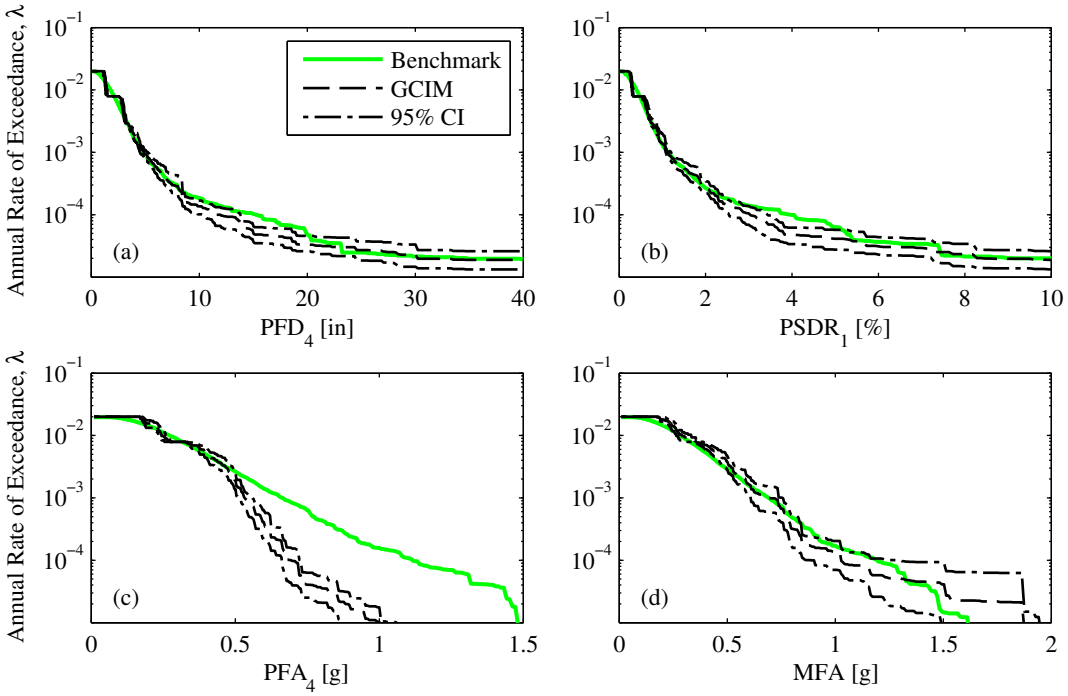

Figure 5.13: Comparison of SDHC estimates for several EDPs of the 4-story frame from GCIM against benchmark (Rezaeian's GM model).

The biases in roof acceleration were not detected by implementing the bias-checking procedure in GCIM. Although the bias-checking procedure enables potential EDP biases to be estimated in a practical fashion, the bias estimates of roof acceleration (Figure 5.11) are significantly different from the actual bias. Specifically, the "corrected" CDF in Figure 5.11a indicates that the roof acceleration hazard curve from the current selection of ground motions

will *overestimate* the 'true' roof acceleration hazard curve by a *slight* amount, because it is 'to the left' of the "uncorrected" CDF. In contrast, the benchmark SDHC in Figure 5.13c demonstrates that the current SDHC estimate from GCIM *underestimates* the benchmark by a *significant* amount.

The preceding limitation of the bias-checking procedure does *not* arise from the fact that bias estimates in Figure 5.11 were judged to be acceptable. Instead of assuming the EDP biases are acceptable, ground motions at the 0.02% probability of exceedance in 50 years level are reselected with a different weight vector (85% is now given to PGA, ASI, and spectral accelerations at periods from 0.05 to 0.95 sec, while 15% is given to the rest of the original 24 IMs) so that the remaining IM inconsistencies ($A(3s)$ and CAV) are demonstrated to be unimportant for roof acceleration of the 4-story frame, via t-tests such as that illustrated in Figure 5.10b. This new selection of ground motions is employed to revise the SDHCs of the 4-story frame; these revised SDHCs are shown in Figure 5.14. As demonstrated in Figure 5.14c, the underestimation in the GCIM estimate of the roof acceleration hazard curve remains present, even when ground motions are reselected with a different weight vector for the 0.02% probability of exceedance in 50 years level. Therefore, the discrepancy between conclusions from the benchmark (Figure 5.13c) and from the bias-checking procedure in GCIM (Figure 5.11) does *not* arise from the fact that bias estimates in Figure 5.11 were judged to be acceptable. Note that the SDHCs are nearly identical in Figures 5.13 and 5.14 because: (i) ground motions are reselected for only one out of $N_{IM^*} = 12$ intensity levels; (ii) the SDHCs for displacements and drift ratios at low exceedance rates are controlled by the annual rate of collapse, which is insensitive to the RHA results from the revised selection of ground motions; and (iii) the SDHCs for floor accelerations are sensitive to the revised RHA results only at exceedance rates less than 10^{-6}.

The GCIM procedure is also applied to the 4-story frame using Yamamoto's GM model. Ground motions are again iteratively selected at each intensity level of $A(T_1)$ until all IM inconsistencies from KS tests are demonstrated to be statistically insignificant for all EDPs considered (Figure 5.12). As in the case for Rezaeian's GM model, difficulties are encountered at the two largest intensity levels of $A(T_1)$ and hence, the bias-checking procedure is implemented for these levels. Specifically, $n = 25$ RHAs of the 4-story frame were conducted and ground motions were reselected with a different weighting of the 24 IMs. This reselection of ground motions was then considered as finalized because after another round of $n = 25$ RHAs of the frame was conducted with this reselection, the remaining IM inconsistencies were demonstrated to be unimportant for all EDPs of the 4-story frame (Step 7(b)iii).

The SDHCs of the 4-story frame, resulting from the preceding ground motions from Yamamoto's GM model, are presented in Figure 5.15. As in the case of Rezaeian's GM model, the SDHCs from GCIM are again unbiased for the majority of the EDPs considered (i.e., floor displacements, story drift ratios, etc.). Furthermore, the epistemic uncertainty in the estimates from GCIM is again relatively small. Since GCIM accounts for cumulative effects of the ground motion (e.g., CAV, D_{5-75}, etc.) in addition to spectral accelerations over a wide range of vibration periods, the good agreement near the annual rate of collapse suggests that such cumulative effects are important for estimating the collapse rate of this

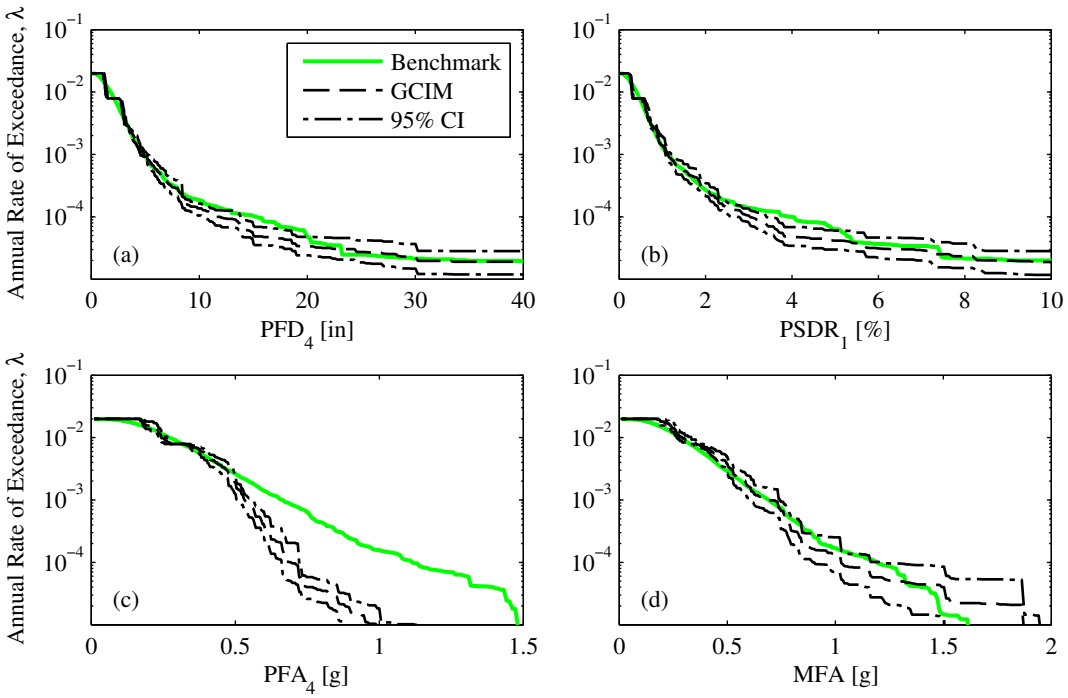

Figure 5.14: Comparison of the benchmark against SDHC estimates for several EDPs of the 4-story frame from GCIM, with ground motions reselected at the 0.02% probability of exceedance in 50 years level via a new weight vector (Rezaeian's GM model).

frame (compare e.g., Figure 5.15a against Figure 5.8a).

As in the case of Rezaeian's GM model, the GCIM estimate of the roof acceleration hazard curve again underestimates the benchmark (Figure 5.15c). The larger underestimation in Figure 5.13c, relative to that in Figure 5.15c, arises from differences in correlation of IMs between the two GM models (see Figure 5.9). As demonstrated by comparing Figure 5.15c against Figure 5.8c, even the inclusion of cumulative effects of the ground motion does not improve the estimate of the roof acceleration hazard curve. Because ground motions are carefully selected in GCIM to be hazard-consistent with respect to a diverse collection of 24 IMs in both GM models (see Section 5.5), the biases in Figures 5.13c and 5.15c reveal that this specific collection of IMs is *insufficient with respect to roof acceleration of the 4-story frame*. In other words, this EDP depends on a feature of the ground motion time series that has not been considered thus far in the analysis, pointing out the importance of developing a rigorous benchmark when evaluating results from GMSM procedures.

The GCIM method was also implemented for the 20-story frame and for both GM models. In both models, ground motions were again carefully selected to ensure hazard consistency with respect to all 24 IMs. Similar to the 4-story frame, it is difficult to satisfy all KS tests at the two largest intensity levels of $A(T_1)$. For these intensity levels, ground motions were examined for potential biases in EDPs; fortunately, reselection of ground motions was

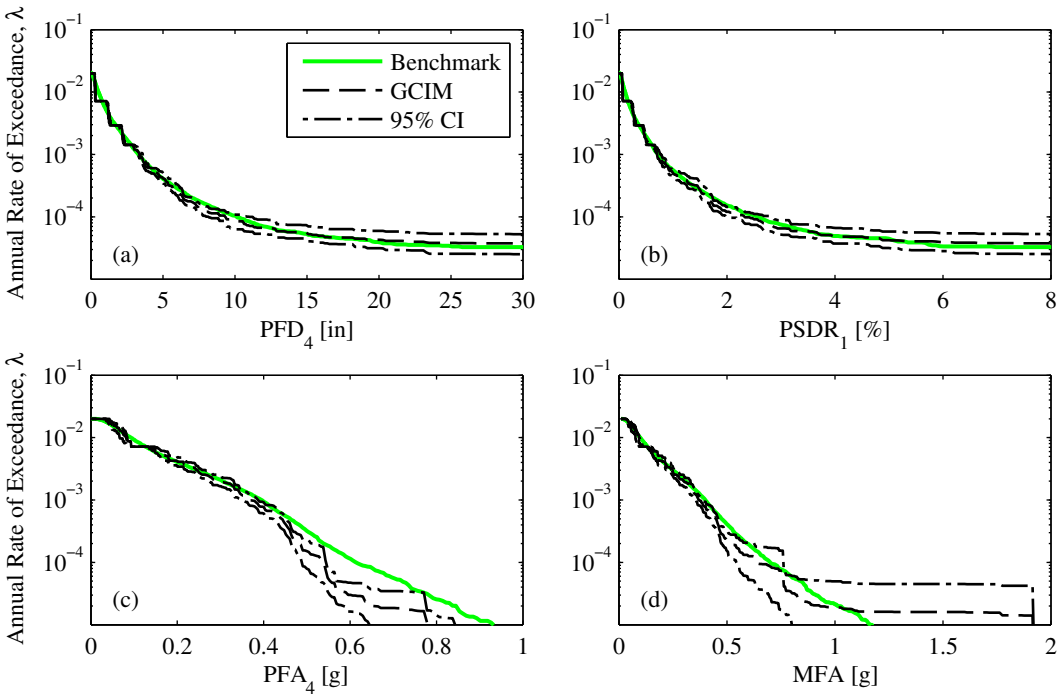

Figure 5.15: Comparison of SDHC estimates for several EDPs of the 4-story frame from GCIM against benchmark (Yamamoto's GM model).

not necessary for these levels because all IM inconsistencies from the initial selection of ground motions were demonstrated to be unimportant for the EDPs of the 20-story frame (Step 7(b)iii). In the interest of brevity, the SDHC estimates of the 20-story frame from GCIM are not presented in this chapter; instead, they are provided in Appendix C. Based on those results, the agreement between the GCIM-based SDHCs of the 20-story frame and the benchmark is excellent for all EDPs considered. This is expected because (i) a comparable level of good agreement was observed from CS-exact for the same frame (see Figures 5.5 and 5.6), and at the same time, (ii) GCIM captures even more aspects of the ground motion than in CS-exact when selecting ground motions (Section 5.5); i.e., the vector of 24 IMs employed in GCIM is less insufficient than the collection of spectral accelerations employed in CS-exact (see Equation 5.1).

5.8 Comparative Summary of CS-Exact and GCIM

Table 5.1 compares the implementation of CS-exact and GCIM in this study for computing SDHCs of a given structure at a specified site. The two procedures are similar in that (i) a scalar conditioning IM is chosen to scale ground motions (attributes 1-2), (ii) a relatively large number of IMs is employed to select ground motions (attribute 5), and (iii) KS tests are employed at each intensity level of IM^* to ensure hazard consistency of the selected motions (attribute 8). In addition, the two procedures are similar in that $N_{IM^*} = 12$ intensity-based assessments are conducted and hence determining a single estimate of the SDHC requires:

(i) performing $N_{IM^*} = 12$ deaggregations, (ii) computing $N_{IM^*} = 12$ target multivariate distributions, and (iii) selecting $N_{IM^*} = 12$ sets of ground motions (attributes 6-7).

Table 5.1: Summary of effort involved in using CS-exact and GCIM in this study to compute SDHCs of a given structure at the specified site.

Attribute	CS-exact	GCIM
1. Conditioning IM	$A(T^*) = A(T_1)$	$IM^* = A(T_1)$
2. Can all ground motions be unscaled?	Usually not	Usually not
3. Limits on scaling of ground motions	$SF_{max} = 4$	Not typically used
4. Type of IMs considered	Spectral accelerations	Spectral accelerations, peak ground measures, spectrum intensities, cumulative effects
5. Number of IMs used to select ground motions	25 vibration periods	24 IMs
6. Total number of PSHA-based calculations for selecting ground motions	$N_{IM^*} = 12$ deaggregations and conditional spectra	$N_{IM^*} = 12$ deaggregations and GCIM distributions of **IM**
7. Total number of ground motions used	$N_{IM^*} = 12$ sets of $n = 25$ ground motions	$N_{IM^*} = 12$ sets of $n = 25$ ground motions
8. How hazard consistency is enforced	KS tests and greedy optimization	KS tests and bias-checking procedure

Table 5.1 also highlights two major differences between GCIM and CS-exact. First, other features of the ground motion time series in addition to spectral accelerations (e.g., cumulative effects, etc.) are incorporated in the ground motion selection process of GCIM whereas only spectral accelerations are incorporated in that of CS-exact (attribute 4). Because scale factors in GCIM can be indirectly limited with a judicious choice of **IM** [Bradley, 2012a], no scale factor threshold is specified for GCIM in this study; in contrast, scale factors in CS-exact are directly limited by $SF_{max} = 4$ (attribute 3). Second, potential EDP biases due to hazard inconsistencies are explicitly examined for all EDPs in GCIM whereas in CS-exact, such potential EDP biases are implicitly assumed to be satisfactory after implementing the greedy optimization technique (attribute 8).

Finalizing the selection of ground motions in GCIM (Step 7b in Section 5.3) can involve much more effort than in CS-exact (Step 7b in Section 5.3), depending on the level of EDP bias that is acceptable to the analyst when implementing the bias-checking procedure in GCIM. If only very small EDP biases are acceptable at a particular intensity level of IM^*, then finalizing the selection of ground motions in GCIM tends to necessitate more RHAs of the structure than in CS-exact. For example, if the estimated EDP biases for the 4-story frame in Figure 5.11 are deemed unacceptable, then an additional n RHAs of the frame must be performed (Step 7(b)i in Section 5.3) before EDP biases can be re-estimated for all 14

EDPs to finalize the selection of ground motions (Step 7(b)vi in Section 5.3). On the other hand, if larger EDP biases are acceptable, then no additional RHAs are necessary before proceeding to compute SDHCs in GCIM.

The two major differences between GCIM and CS-exact (attributes 4 and 8) may lead to SDHC estimates that are more accurate than those from CS-exact. For example, by accounting for the cumulative effects of the ground motion in the selection process and employing the bias-checking procedure, the overestimation in the annual rate of collapse for the 4-story frame from CS-exact (Figure 5.8) is eliminated in GCIM (Figure 5.15). As elaborated in Section 5.7 however, the bias-checking procedure can become quite involved, depending on the number of IMs and EDPs considered (Figure 5.12) and on the level of accuracy desired by the analyst (Figure 5.11).

Including more IMs in the ground motion selection process (attribute 4) and explicitly checking for potential EDP biases (attribute 8) in GCIM may not necessarily lead to improved estimates of the SDHC. For example, since the SDHCs from CS-exact for the 20-story frame are generally unbiased (Figures 5.5 and 5.6), inclusion of additional IMs does not lead to significantly improved SDHC estimates for the 20-story frame. Furthermore, it is demonstrated in Section 5.7 that even after implementing the bias-checking procedure, for a wide range of IMs and EDPs (see Figures 5.10-5.11), the SDHCs resulting from the finalized selection of ground motions may still be biased (e.g., Figure 5.13c).

5.9 Conclusions

In this study, two existing, contemporary GMSM procedures – CS-exact and GCIM – were evaluated for their ability to accurately estimate seismic demand hazard curves (SDHCs) of a given structure at a specified site. A case study was chosen where rigorous benchmark SDHCs were determined for evaluation purposes. The amount of effort involved in implementing these procedures to compute a single SDHC is summarized in Table 5.1. In essence N_{IM^*} intensity-based assessments are conducted where for each assessment, ground motions are scaled but selected to be consistent with respect to the target defined by PSHA for a user-specified collection of IMs. The results from implementing these procedures are compared against the benchmark, leading to the following conclusions:

1. In general, whether or not the estimate from a particular GMSM procedure is biased depends on the particular problem (i.e., structure, EDP, and database of ground motions), because the underlying cause of SDHC bias involves two important aspects of the particular selection of ground motions: (i) hazard consistency, and (ii) IM sufficiency. A GMSM procedure is only a tool for achieving hazard consistency with respect to a user-specified collection of IMs; whether or not the resulting SDHC is biased depends on how sufficient the vector of IMs is, relative to the EDP of interest.

2. Good agreement between the benchmark SDHC and the estimate from CS-exact is observed for all of the EDPs considered for the 20-story frame.

3. Good agreement between the benchmark SDHC and the estimate from GCIM is observed for all of the EDPs considered for the 20-story frame and for all floor displacements and all story drift ratios of the 4-story frame.

4. The SDHC estimate from CS-exact underestimates some of the floor accelerations and overestimates the annual rate of collapse of the 4-story frame.

5. The SDHC estimate from GCIM underestimates some of the floor accelerations, indicating that it is possible to obtain significantly biased SDHCs from GCIM, even after (i) enforcing hazard consistency for a diverse collection of IMs, and (ii) implementing the bias-checking procedure to approximate potential EDP biases arising from improper ground motion selection.

6. If hazard consistency is enforced with respect to a collection of IMs, the benchmark SDHCs enable us to identify IMs that are insufficient; two examples:

    a) The vector of spectral accelerations at 25 vibration periods from 0.05 to 10 sec, employed herein for CS-exact, is insufficient for estimating the collapse rate of the 4-story frame; in this case, cumulative effects of the ground motion appear to be important.

    b) The vector of 24 IMs employed herein for GCIM, which captures amplitude, frequency content, and duration of the ground motion, is insufficient for estimating roof acceleration of the 4-story frame.

Finally, we note that the above conclusions are based on synthetic ground motions and on a relatively simple site. For recorded ground motions and a realistic site with many earthquake sources and uncertainty in source-to-site distance, the insufficiency of the IMs considered herein may be even more pronounced than what has been documented herein.

Chapter 6

Evaluation of the Importance Sampling-Based Method for Ground Motion Selection

6.1 Preview

An Importance Sampling (IS) based ground motion selection procedure was proposed for estimating seismic demand hazard curves (SDHCs) of structures at a specified site. This procedure enables us to estimate SDHCs from unscaled yet intense ground motions, through various choices of the Importance Function (IF). More importantly, it enables us to directly enforce hazard consistency of the selected motions with respect to a given set of intensity measures (IMs), and to estimate SDHCs with a single ensemble of ground motions. In this chapter, we evaluate the IS procedure in its ability to accurately estimate SDHCs of structures at a specified site. For a case study where rigorous benchmark SDHCs can be determined, we find that SDHCs from this procedure are typically unbiased, especially when all ground motions are unscaled. The epistemic uncertainty of the SDHCs from the procedure is controlled primarily by the IF, and secondarily by the number of ground motions to be selected. Finally, we demonstrate that SDHCs of multiple structures can be estimated accurately from a single ensemble of ground motions by applying the procedure with a non-structure-specific vector of IMs.

6.2 Introduction

Seismic demand hazard curves (SDHCs) for a given structure at a given site, which are important for assessing the structure's risk (i.e., damage and loss) in performance-based earthquake engineering, are typically estimated in practice via probabilistic seismic demand analysis (PSDA) [Shome et al., 1998]. In this analysis, multiple intensity-based assessments [NEHRP Consultants Joint Venture, 2011, Applied Technology Council, 2012] of the structure are conducted and the results are combined with the hazard curve of the chosen conditioning scalar intensity measure (IM), which is determined by probabilistic seismic hazard

analysis (PSHA) of the given site. More details about PSDA can be found in Section 2 of [Kwong et al., 2014], among others.

Since recorded ground motions (GMs) [1] are often distorted by scaling in PSDA, it is natural to question the value of the information derived from such scaled GMs (e.g., [Grigoriu, 2010, Corigliano et al., 2012]). As pointed out in Section 6 of [Kwong et al., 2014] however, inaccuracies or biases of the SDHCs are not caused directly by GM record scaling but rather, by hazard inconsistencies of the selected GMs with respect to IMs that influence the response quantity, or engineering demand parameter (EDP); such IMs are said to be *sufficient for the EDP* [Luco and Cornell, 2007]. In other words, the bias in an estimate of the SDHC is directly related to two important aspects of the corresponding selection of GMs: (i) IM sufficiency, and (ii) hazard consistency [2].

If GMs are selected such that they are hazard-consistent with respect to a sufficient IM, which may be scalar or vector-valued, then the resulting SDHCs are unbiased, irrespective of the degree of record scaling. For example, suppose the conditioning scalar IM is defined as spectral acceleration at the fundamental vibration period of the structure, $A(T_1)$. By scaling GMs to the hazard curve of $A(T_1)$ that is determined from PSHA, the motions are deliberately ensured to be hazard-consistent with respect to this IM. If the EDP of interest is sensitive to *only* $A(T_1)$ and to no other features of the GM (i.e., this IM is sufficient for the EDP), then the resulting SDHC is unbiased, independent of the degree to which GMs were scaled and regardless of whether or not all GMs were selected from the same earthquake event (such is the case for all EDPs of a linear-elastic SDF system).

In many situations however, the response of a structure is sensitive to many more features of the GM besides $A(T_1)$ alone and consequently, it is important to ensure that the selected GMs are *also* hazard-consistent with respect to such features. This can be achieved with the Generalized Conditional Intensity Measure (GCIM) approach [Bradley, 2010a], where Kolmogorov-Smirnov tests are employed to identify GMs that are consistent with the GCIM distributions for a wide range of user-specified IMs. However, such tests do not necessarily ensure hazard consistency at low exceedance rates because such rates may be controlled by the 'tails' of GCIM distributions (see Section 2 of [Kwong et al., 2015a]). Furthermore, the typical use of GM scaling in PSDA suggests that hazard inconsistencies may still exist for IMs that have not been considered by the analyst in the selection of GMs; such IMs can be important for certain EDPs (see Sections 6.8 and 6.10 below). Since hazard inconsistencies appear to be more pronounced when GMs are scaled (e.g., compare Fig 12 against Fig 9a in [Kwong et al., 2015c]), one possible solution for minimizing such hazard inconsistencies is to minimize the degree of record scaling.

Supposing that we are interested in avoiding record scaling altogether when estimating

[1] The phrase "ground motion" refers herein to ground acceleration as a function of time.

[2] In this study, a SDHC estimate is said to be unbiased or accurate when its 95% bootstrapped confidence interval [Efron and Tibshirani, 1993] covers the benchmark SDHC; otherwise, it is biased or inaccurate. Similarly, a set of GMs is said to be hazard-consistent with respect to IM when the 95% bootstrapped confidence interval of the hazard curve estimate covers the benchmark; otherwise, it is hazard-inconsistent.

SDHCs, how can we best utilize a database of unscaled GMs for this purpose? The GM selection method based on Importance Sampling (IS), which is developed in [Kwong et al., 2015c], answers this question. In this chapter, we evaluate this procedure in its ability to accurately estimate SDHCs for a given structure at a specified site, using the concepts and methodologies developed in publications [Kwong et al., 2014] and [Kwong et al., 2015b]. Before doing so, let us first take a closer look at this selection procedure.

6.3 Step-By-Step Summary of the IS Procedure

The IS-based method for selecting n number of GMs and estimating SDHCs is summarized as follows (see Fig 3 in [Kwong et al., 2015c] for a block diagram):

1. Specify **IM**, a vector of N_{IM} number of IMs, to be utilized for selecting GMs.

2. Determine the target probability distribution of **IM** from PSHA of the site, $f_{\mathbf{IM}}(\mathbf{x})$:

$$f_{\mathbf{IM}}(\mathbf{x}) = \sum_{i=1}^{N_{Rup}} \frac{\nu(rup_i)}{\nu_0} \cdot f_{\mathbf{IM}|Rup}(\mathbf{x} \mid rup_i) \tag{6.1}$$

   where N_{Rup} is the total number of rupture scenarios considered in the PSHA, $\nu(rup_i)$ is the rate of the ith scenario, ν_0 is the annual rate of earthquake occurrence, and $f_{\mathbf{IM}|Rup}(\mathbf{x} \mid rup_i)$ is the multivariate density of **IM** given the ith rupture scenario (usually assumed multivariate lognormal whose parameters are given by empirical prediction models).

3. Choose an Importance Function (IF), $g_{\mathbf{IM}}(\mathbf{x})$, for selecting GMs (see Section 6.4).

4. Randomly sample n vectors of **IM** from $g_{\mathbf{IM}}(\mathbf{x})$; each vector is denoted by $\mathbf{IM}_{IF}$.

5. Select n GMs from a specified database whose computed values of **IM**, each denoted by $\mathbf{IM}_P$, most closely agree with those simulated from Step 4, where closeness for each (potentially scaled) GM is quantified by a misfit, Δ:

$$\Delta = \sum_{j=1}^{N_{IM}} \left[\frac{\ln(IM_{IF,j}) - \ln(IM_{P,j})}{\sigma_j} \right]^2 \tag{6.2}$$

   and σ_j refers to the standard deviation of $\ln(IM_j)$ from the IF; if scaled GMs are desired, then each value of $\mathbf{IM}_P$ in the database is determined by Eqs 14-15 in [Kwong et al., 2015c].

6. Compute the IS weights for all selected GMs, where the IS weight for the ith GM, w_i, is:

$$w_i = f(\mathbf{x}_i) \div g(\mathbf{x}_i) \tag{6.3}$$

   and $\mathbf{x}_i$ refers to $\mathbf{IM}_P$ for the ith GM.

7. Check hazard consistency of the selected GMs with respect to any IM of interest. The estimated hazard curves from the selected GMs are given by:

$$\widehat{\lambda}_{IM}(x) = \frac{\nu_0}{n}\sum_{i=1}^{n}\left[I(x_i > x)\cdot w_i\right] \qquad \widehat{\lambda}_{EDP}(z) = \frac{\nu_0}{n}\sum_{i=1}^{n}\left[I(z_i > z)\cdot w_i\right] \tag{6.4}$$

where x_i and z_i refer, respectively, to the computed values of IM and EDP from the ith (potentially scaled) GM. If deemed hazard-inconsistent, then reselect GMs (Steps 4-6), following the guidance provided in Section 3.4 of [Kwong et al., 2015c].

8. Perform response history analyses (RHAs) of the structure due to the n selected GMs.

9. Estimate the SDHC by applying Equation 6.4b to the n computed values of EDP.

When implementing Step 1, the number of IMs in the vector **IM** should be relatively small (i.e., four to six) because a large number of IMs leads to large epistemic uncertainty in the resulting estimates of hazard curves (see Equation 6.5 below), which is undesirable. In addition, a small number of IMs reduces the computational time involved in computing IS weights (Step 6) because the evaluation of Equation 6.3 requires the evaluation of multiple multivariate lognormal probability density functions (PDFs), as shown by Equation 6.1. Furthermore, with a finite number of GMs in the database to select from (Step 5), it is possible to obtain a selection of GMs that does not agree closely with the values of **IM** that are randomly simulated from the IF. Consequently, it is very important to check hazard consistency of the selected motions (Step 7) before proceeding with any RHAs of the structure; if the selected motions are hazard-inconsistent, then GMs should be reselected. Finally, the choice of IF (Step 3) is a critical step in the IS procedure, which is discussed more thoroughly next.

6.4 Choice of Importance Function

In general, the selected IF should possess three desirable characteristics. First, one must be able to easily randomly sample a vector of IMs from such an IF (see Step 4 of the summary above). Second, the chosen IF should produce randomly sampled values of **IM** that facilitate selection of GMs from a given database; e.g., when the largest observed value of $A(1s)$ in the database is $1g$, there would be no point in specifying an IF whose mode is located at intensities greater than $1g$. Third, the chosen IF should minimize the epistemic uncertainty of the resulting SDHC estimates; this epistemic uncertainty is quantified by Eq 9 of [Kwong et al., 2015c], which is repeated here for convenience:

$$\mathbb{V}\left[\widehat{\lambda}_{EDP}(z)\right] = \frac{1}{n}\left\{\nu_0^2\left[\int_{\mathbf{s}}\Pr(EDP > z \mid \mathbf{IM} = \mathbf{s})\cdot\frac{f^2(\mathbf{s})}{g(\mathbf{s})}\,\mathrm{d}\mathbf{s}\right] - \lambda_{EDP}^2(z)\right\} \tag{6.5}$$

where $\mathbb{V}[\cdot]$ denotes variance, $\Pr(EDP > z \mid \mathbf{IM} = \mathbf{s})$ denotes the complementary cumulative distribution function of EDP for a given test value of **IM**, $\lambda_{EDP}(z)$ denotes the theoretical SDHC, and the subscript "**IM**" in both f and g is dropped henceforth for brevity. We see

from this equation that for a given site and number of GMs, the epistemic uncertainty of the SDHC estimate varies with both the EDP and the level of demand, in addition to the choice of the IF.

To facilitate random sampling of **IM** from the IF, its form is chosen as either a multivariate lognormal (MVLN) distribution or a mixture of such MVLNs. Using a vector of four IMs as an example, Figure 6.1 illustrates two examples of the MVLN form, denoted by g_1 (chained blue) and g_2 (dashed red). Although their mean vector and covariance matrices are different, it is relatively easy to generate a random value of **IM** in each case (see e.g., Section 6.2 of [Ross, 2013]). Figure 6.1 also illustrates an example of the mixture form, denoted by g_3. This IF is a mixture of the previous two MVLNs:

$$g_3(\mathbf{x}) = [1 - \eta] \cdot g_1(\mathbf{x}) + \eta \cdot g_2(\mathbf{x}) \tag{6.6}$$

where $0 \leq \eta \leq 1$ refers to the *mixing proportion*. In this case, values of **IM** can be randomly generated from g_3 via two steps: (i) identify one of the two components by randomly sampling from the Bernoulli distribution with probability η, and (ii) randomly generate a value of **IM** from the component identified. Such mixture distributions are useful for minimizing the epistemic uncertainty of the resulting estimates of hazard curves [Hesterberg, 2003].

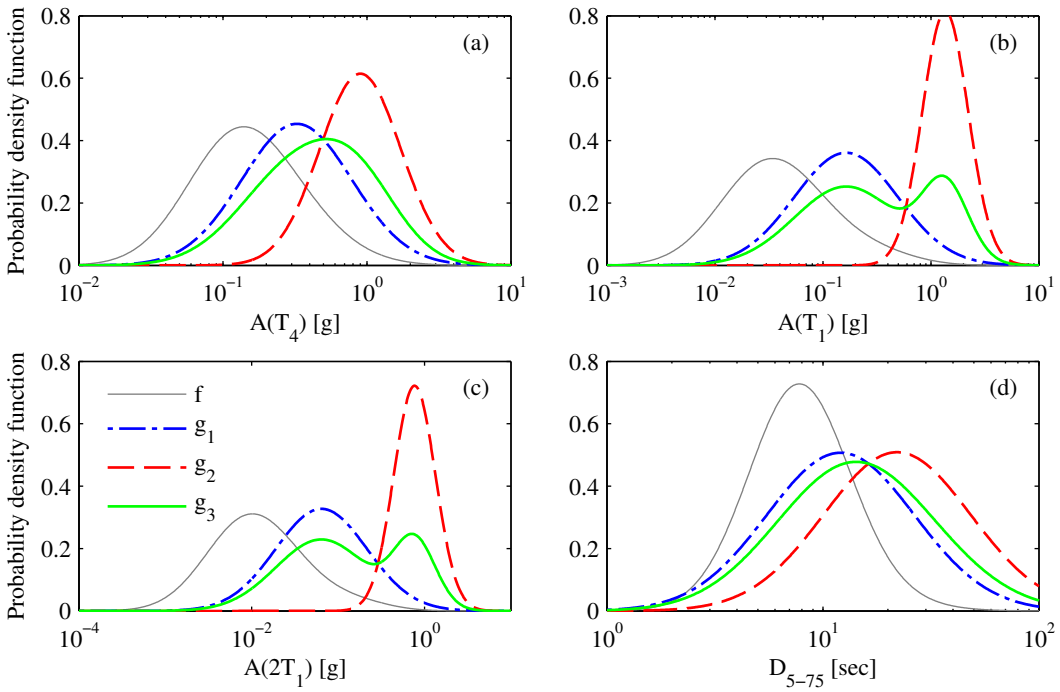

Figure 6.1: Marginal distribution for (a) $A(T_4)$, (b) $A(T_1)$, (c) $A(2T_1)$, (d) D_{5-75}, derived for three database-driven IFs with reference to target PDFs from PSHA, f (solid thin grey): (i) g_1 (chained blue), (ii) g_2 (dashed red), (i) g_3 (solid green).

To facilitate the selection of GMs among a given database of N motions, we propose to derive the parameters of the IF from the database. Such IFs are called database-driven

IFs, which were first introduced in Section 3.2 of [Kwong et al., 2015c]. In essence, after **IM** is identified (see Step 1 of the above summary), the N observed values of **IM** in the GM database may be used to estimate the mean vector and covariance matrix of a MVLN distribution; an example of this approach is shown as g_1 in Figure 6.1. However, not all values of **IM** in the database may be of interest. For instance, one might be interested in only unscaled GMs where $A(T_1) \geq 1g$ and $A(2T_1) \geq 0.5g$. In this case, another possible IF can be obtained by first filtering the database of N GMs according to the latter criteria before determining the mean vector and covariance matrix of the IF; an example of this approach is depicted as g_2 in Figure 6.1. By mixing such IFs via Equation 6.6, more choices of the IF become available.

Ideally, the single, "optimal" IF is the one that minimizes the epistemic uncertainty of the resulting SDHC estimate, which is given by Equation 6.5. However, the IF cannot be determined from minimizing Equation 6.5 because the term $\Pr(EDP > z \mid \mathbf{IM} = \mathbf{s})$ in this equation is unknown.

To overcome this problem, we propose to choose the IF by minimizing the epistemic uncertainty in the hazard curves for influential IMs, instead of for EDPs. Specifically, given a set of EDPs and corresponding demand levels of interest, one first specifies a set of IMs (Step 1) and corresponding intensity levels that are deemed most influential to the demands. Then, the IF is chosen by minimizing the epistemic uncertainty of the hazard curves for such IMs. This approach assumes that when the epistemic uncertainty from influential IMs is minimized, the epistemic uncertainty for EDPs is also minimized. We summarize this approach as follows:

1. For each prospective IF:
    a) Randomly sample n values of **IM** from the IF.
    b) Compute the hazard curve for each of the N_{IM} elements in **IM**, by applying Equation 6.4a to the n randomly sampled values of **IM**.
    c) Repeat the latter two steps until N_{HC} number of hazard curves (e.g., $N_{HC} = 100$) have been computed for each element of **IM**.
    d) Construct a 95% confidence interval (CI) of the hazard curve for each element of **IM**.
2. Choose the IF that leads to the smallest 95% CI for the IMs and exceedance rates of interest.

This approach is illustrated in Figure 6.2 for g_1 and g_3 from Figure 6.1. For each of the two IFs and for each of the four IMs, the 95% CI of the hazard curve is presented. As expected, the CIs of the hazard curves for $A(T_1)$ and $A(2T_1)$ from g_3 are smaller than those from g_1, at exceedance rates less than 10^{-5}, because g_3 concentrates on the tail regions of $A(T_1)$ and $A(2T_1)$ more so than g_1 (compare densities at large intensity levels in Figures 6.1b-c). If one assumed that the nonlinear response of the system is most sensitive to $A(T_1)$ and

$A(2T_1)$ at exceedance rates less than 10^{-5}, then g_3 would be chosen over g_1. In this chapter, the IS-based method for selecting GMs is evaluated for several choices of the IF.

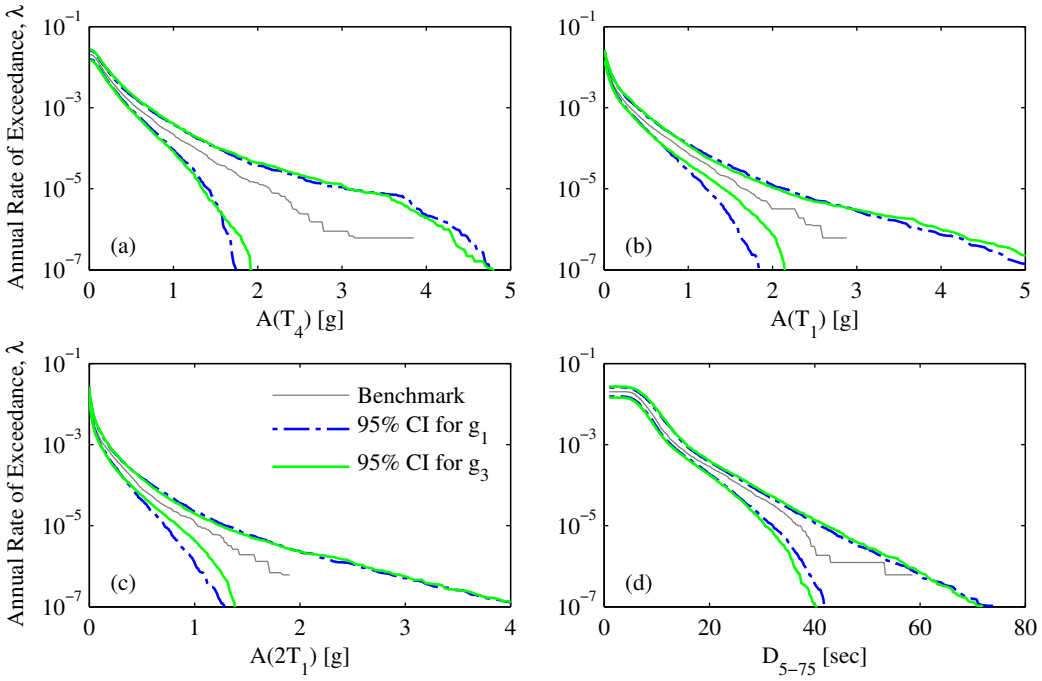

Figure 6.2: Illustration of proposed approach for choosing IF among several possibilities; $N_{HC} = 10^3$. Hazard curves for (a) $A(T_4)$; (b) $A(T_1)$; (c) $A(2T_1)$; (d) D_{5-75}.

6.5 Methodology for Evaluation

In order to evaluate the IS-based method in its ability to accurately estimate SDHCs for a given structure at a specified site, we employ the methodology that has been described comprehensively in [Kwong et al., 2015b]. In essence, this methodology involves three main steps. First, a universe of synthetic GMs is generated such that they are consistent with the earthquake rupture forecast of the site. Second, benchmark hazard curves are computed using Eqs 5, 9, and 12 of [Kwong et al., 2015b]. Third, SDHCs are estimated by applying the IS-based procedure to a subset of this universe of synthetic GMs; this is important for isolating the biases caused by the ground motion selection and modification (GMSM) procedure on its resulting SDHC estimates. By comparing the SDHC estimates from the IS-based method against the respective benchmarks in this context, the potential bias from the GM selection procedure can be quantified. Furthermore, if the selected GMs are hazard-consistent with respect to a particular collection of IMs, then such comparisons also permit identification of insufficient IMs.

6.6 Case Study Considered

A case study is chosen where most of the tools needed in the evaluation methodology (i.e., benchmark hazard curves, benchmark-consistent prediction models, etc.) are readily available. The site chosen is identical to that depicted in Fig 2a and described in Section 3.1 of [Kwong et al., 2015b]; in essence, the seismicity of the site is controlled by a single strike-slip fault that is located 10 km away, and earthquakes occur randomly with magnitudes following the Youngs & Coppersmith PDF, at an activity rate of $\nu = 0.02$ earthquakes per year. Two GM simulation models were utilized to generate two universes of 10^4 GMs; these models are described in Section 3.1 of [Kwong et al., 2015b] and are referred to as Rezaeian's GM model [Rezaeian and Der Kiureghian, 2008] and Yamamoto's GM model [Yamamoto and Baker, 2013]. In the interest of brevity, most results in this chapter are shown for Rezaeian's GM model; other results may be found in Appendix D.

In order to apply the IS-based selection procedure to a database of synthetic GMs, GM prediction models (GMPMs) that are "consistent with the benchmark" must be available. Such benchmark-consistent GMPMs were developed for 120 IMs and for each GM model, following the approach outlined in Section 5 of [Kwong et al., 2015b]. The selection of functional forms, determination of optimal standard deviations, and consideration of correlations, are documented in Appendix B.

Two well-vetted reinforced concrete frames – 4-story and 20-story – are considered. These frames were studied in many past publications (e.g., [Yamamoto, 2011], [PEER GMSM Working Group, 2009], etc.) and have been modeled in OpenSEES [Mazzoni et al., 2006]. The four modal periods of vibration for the 4-story frame are: $T_1 = 0.94$ sec, $T_2 = 0.30$ sec, $T_3 = 0.17$ sec, $T_4 = 0.12$ sec; for the 20-story frame, the four modal periods are: $T_1 = 2.6$ sec, $T_2 = 0.85$ sec, $T_3 = 0.46$ sec, $T_4 = 0.32$ sec. For each frame, the EDPs considered are: (i) peak (over time) floor displacements (PFD), (ii) peak story drift ratios (PSDR), (iii) peak floor accelerations (PFA), (iv) maximum of peak story drift ratios over all stories (MSDR), and (v) maximum of peak floor accelerations over all floors (MFA). Thus, a total of 14 EDPs are considered for the 4-story frame and a total of 62 EDPs are considered for the 20-story frame.

6.7 Estimating SDHCs without Scaling Ground Motions

In this section, we evaluate the IS procedure in its ability to estimate SDHCs without scaling GMs and with different choices of the IF. In order to facilitate comparison between the results from this procedure against those from a typical application of PSDA, $n = 300$ GMs are selected herein for computing SDHCs of each system. For each multistory frame, four IMs are chosen to select GMs (Step 1): spectral accelerations at the fundamental vibration period of the structure, $A(T_1)$, twice the fundamental period, $A(2T_1)$, and the fourth-mode period, $A(T_4)$, and 5-75% significant duration, D_{5-75}. The periods $2T_1$ and T_4 were chosen to roughly consider period lengthening during inelastic response and higher-mode effects.

With **IM** specified, two choices of the IF were considered for selecting unscaled GMs. The first IF, denoted by g_1, is a MVLN distribution whose parameters are determined from all 10^4 unscaled, GMs in the database. The second IF, denoted by g_3, is a two-component mixture of MVLN distributions developed via Equation 6.6; the first component is identical to g_1 whereas the second component is a MVLN distribution whose parameters are determined from only those motions in the database that satisfy the following criteria: (i) $A(T_1) \geq 1g$ and (ii) $A(2T_1) \geq 0.5g$. These two IFs were discussed in Section 6.4 with reference to Figures 6.1-6.2. With these inputs to the IS-based method specified, g_1 is evaluated first, followed by g_3.

The IS-based method offers a direct means of enforcing hazard consistency with respect to **IM**. Using Rezaeian's GM model and the 4-story frame as an example, $n = 300$ values of **IM** were randomly generated from g_1 (Step 4), which were in turn used to select $n = 300$ GMs from the database of size 10^4 (Step 5). Applying Equations 6.3 and 6.4a to the selected GMs leads to estimates of hazard curves for any IM. In particular, Figure 6.3 presents hazard curves from these selected motions for nine different IMs: $A(T_4)$, $A(T_1)$, $A(2T_1)$, $A(4T_1)$, peak ground acceleration (PGA), peak ground velocity (PGV), peak ground displacement (PGD), cumulative absolute velocity (CAV), and D_{5-75}. As expected, the selected motions are hazard-consistent with respect to the four IMs considered in selecting GMs (highlighted in red) since for each of these IMs, the 95% CI of the hazard curve estimate covers the benchmark. Observe that by design of the IS-based selection procedure, hazard consistency for D_{5-75} at exceedance rates down to approximately 10^{-6} can be directly enforced.

More importantly, Figure 6.3 demonstrates that the GMs selected by the IS-based method are also hazard-consistent with respect to many other IMs, even though only four IMs are chosen to select GMs. This is the case because (i) the specified **IM** is strongly correlated with many other features of the GM, and (ii) record scaling is avoided, which preserves the inter-dependence structure among all IMs. Thus, the IS procedure offers the ability to enforce hazard consistency over a wide range of IMs and exceedance rates (through various choices for **IM** and the IF). Based on the hazard consistency of the selected motions depicted in Figure 6.3, the resulting SDHCs of the 4-story frame are expected to be unbiased.

This expectation is confirmed in Figure 6.4, where the resulting SDHCs of the 4-story frame are presented together with the respective benchmarks for four EDPs: (i) peak roof displacement, PFD_4, (ii) peak first story drift ratio, $PSDR_1$, (iii) peak roof acceleration, PFA_4, and (iv) MSDR. The SDHCs from IS are unbiased because the 95% CI of each SDHC (from bootstrapping [Efron and Tibshirani, 1993]) essentially covers the benchmark over a wide range of exceedance rates. However, the epistemic uncertainty of such SDHC estimates near collapse (i.e., around 2×10^{-5}) is relatively large. These observations regarding bias and epistemic uncertainty are also valid for all other EDPs considered for this frame, even though only four IMs are utilized in selecting a single ensemble of $n = 300$ GMs to estimate such SDHCs.

The preceding evaluation of the IS-based method with g_1 for the 4-story frame is repeated for the 20-story frame. Ground motions are again selected (with g_1 as the IF) to be hazard-

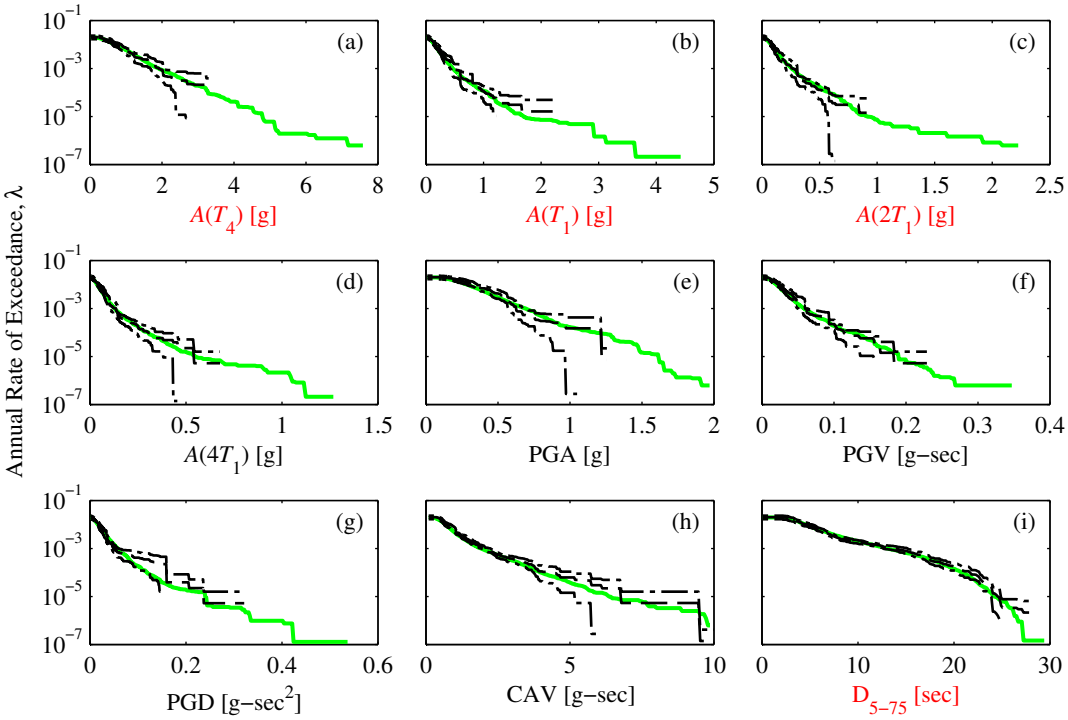

Figure 6.3: Hazard consistency of the motions selected with g_1 for the 4-story frame, with respect to: (a) $A(T_4)$; (b) $A(T_1)$; (c) $A(2T_1)$; (d) $A(4T_1)$; (e) PGA; (f) PGV; (g) PGD; (h) CAV; and (i) D_{5-75}. Benchmark in solid green, estimate from IS in dashed black, and 95% CI of estimate from IS in chained black (Rezaeian's GM model).

consistent for four IMs: (i) $A(T_4)$, (ii) $A(T_1)$, (iii) $A(2T_1)$, and (iv) D_{5-75}. As in the case of the 4-story frame, the selected GMs are hazard-consistent with respect to many more IMs than the four used in the selection process. Consequently, we expect the resulting SDHCs of the 20-story frame to be unbiased.

This expectation is confirmed in Figure 6.5. In this figure, the SDHCs of the 20-story frame resulting from the GMs selected by g_1 are presented together with the respective benchmarks for four EDPs: peak roof displacement, PFD_{20}, peak first story drift ratio, $PSDR_1$, peak roof acceleration, PFA_{20}, and MSDR. As in the case of the 4-story frame, the IS-based SDHCs of the 20-story frame are again unbiased for all EDPs considered. The epistemic uncertainty of the SDHC estimates at low exceedance rates is again relatively large for displacements and drifts but not for accelerations of this frame. These conclusions are supported by results from analyses starting with Yamamoto's GM model (see Appendix D).

How would the results change if a different IF was chosen for the IS-based method? Recall from Equation 6.5 that for a given site, structure, and number of GMs n, the epistemic uncertainty in the SDHCs from IS is dictated by the IF. Thus, different choices of the IF lead to different degrees of epistemic uncertainty in the resulting SDHC estimates. As mentioned in Section 6.4, the IF cannot be determined by minimizing Equation 6.5 because the term

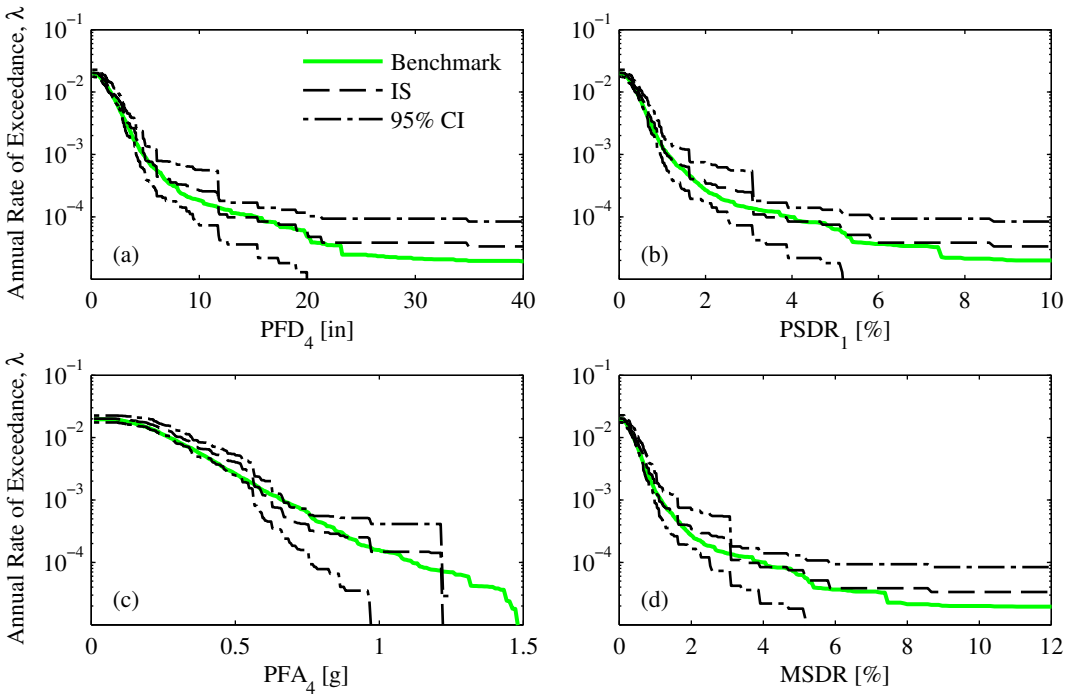

Figure 6.4: Comparison of SDHC estimates for several EDPs of the 4-story frame from IS, with g_1 as the IF, against benchmark (Rezaeian's GM model).

$\Pr(EDP > z \mid \mathbf{IM} = \mathbf{s})$ is unknown. Nevertheless, perhaps we can minimize the epistemic uncertainty associated with EDPs by minimizing the epistemic uncertainty associated with influential IMs. This seems reasonable because if **IM** is perfectly sufficient for the EDP, then by definition, the EDP is a function of only **IM** and hence, minimizing uncertainty for **IM** is tantamount to minimizing uncertainty for the EDP.

To test this idea, we evaluate the IS-based method with g_3 as the IF. Specifically, η and g_2 in Equation 6.6 were chosen so that at exceedance rates less than 10^{-4}, the resulting g_3 led to a reduction (relative to g_1) in epistemic uncertainty of the hazard curves for $A(T_1)$ and $A(2T_1)$; see Figure 6.2. Consequently, by choosing g_3 as the IF, one is assuming that the nonlinear response at such exceedance rates is influenced primarily by these two IMs.

Figure 6.6 examines hazard consistency of the GMs selected from g_3 for the 4-story frame in Rezaeian's GM model, with respect to the same nine IMs shown in Figure 6.3. Comparing this figure against Figure 6.3, we observe that the GMs selected from g_3 are hazard-consistent for *lower* exceedance rates than those from g_1. Moreover, we observe in this figure that at exceedance rates less than 10^{-5}, the epistemic uncertainty in the hazard curves for $A(T_1)$ and $A(2T_1)$ is smaller than that for IF=g_1. In fact, a similar reduction in epistemic uncertainty at low exceedance rates is observed for all nine IMs except for $A(T_4)$ and PGA. These observations were expected because g_3 places more probability density than g_1 at large intensity levels of $A(T_1)$ and $A(2T_1)$ (Figure 6.1), and such IMs are in turn well

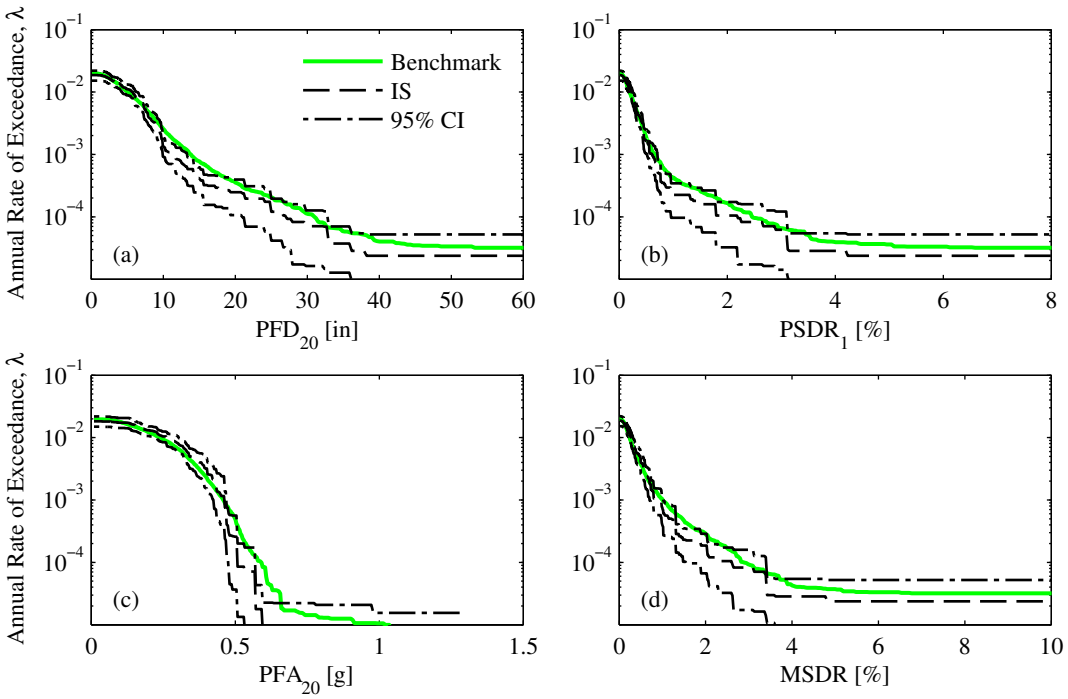

Figure 6.5: Comparison of SDHC estimates for several EDPs of the 20-story frame from IS, with g_1 as the IF, against benchmark (Rezaeian's GM model).

correlated with many other IMs. If the nonlinear response of the 4-story frame is indeed primarily influenced by intense levels of $A(T_1)$ and $A(2T_1)$, then the reduction in epistemic uncertainty of the hazard curves, as shown in Figure 6.6, suggests that a similar reduction will be obtained for the SDHCs.

With g_3 as the IF, Figure 6.7 presents the SDHCs for the 4-story frame. Comparing this figure against Figure 6.4, we observe that the SDHCs from both choices of the IF are unbiased but the epistemic uncertainty in the SDHCs differ. At low annual rates of exceedance, the choice of g_3 as the IF leads to smaller epistemic uncertainty in the displacement and drift hazard curves but slightly larger epistemic uncertainty in the acceleration hazard curves. These observations suggest that intense levels of $A(T_1)$ and $A(2T_1)$ have dominant influence on large displacements and drifts but not on large accelerations of the building.

The evaluation of IS with g_3 as the IF was repeated for three other cases: the 20-story frame with Rezaeian's GM model, and both frames starting with GMs from Yamamoto's model (see Appendix D). In all cases, the choice of g_3 as the IF leads to unbiased SDHCs with smaller (relative to g_1) epistemic uncertainty in the displacement and drift hazard curves and slightly larger epistemic uncertainty in the acceleration hazard curves, thus confirming the conclusions reached earlier for the 4-story frame in Rezaeian's model. These results suggest that: (i) SDHCs from IS with unscaled GMs are usually unbiased, and (ii) the IF should be chosen such that at low exceedance rates, the epistemic uncertainty of hazard curves is

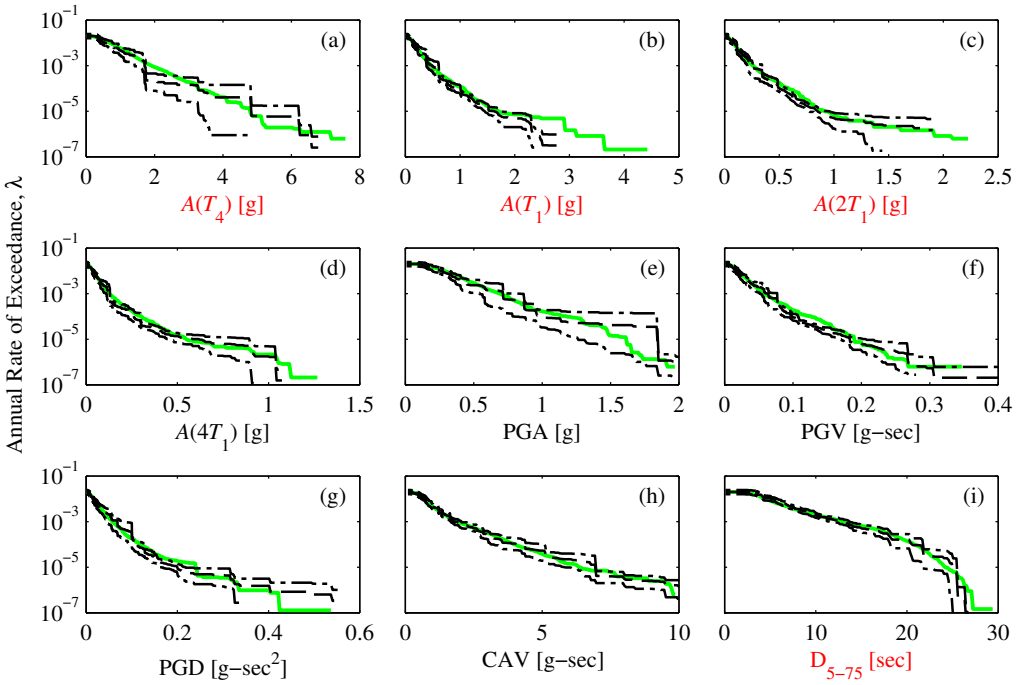

Figure 6.6: Hazard consistency of the motions selected with g_3 for the 4-story frame, with respect to: (a) $A(T_4)$; (b) $A(T_1)$; (c) $A(2T_1)$; (d) $A(4T_1)$; (e) PGA; (f) PGV; (g) PGD; (h) CAV; and (i) D_{5-75}. Benchmark in solid green, estimate from IS in dashed black, and 95% CI of estimate from IS in chained black (Rezaeian's GM model).

minimized for all IMs that are deemed influential to all EDPs of interest.

6.8 Estimating SDHCs with Scaled Ground Motions

In practice, GM records that are intense enough may be lacking. For example, the largest observed value of $A(T_1)$ in a given database might conceivably be less than the mode of the target PDF shown in Figure 6.1b. In this case, the IFs for $A(T_1)$ that are derived from purely unscaled GMs would no longer concentrate on intense levels of this IM; i.e., the IFs shown in Figure 6.1b would be shifted towards the left. As a result, the hazard curve estimates from the IS-based method will exhibit a relatively large degree of epistemic uncertainty at low exceedance rates, despite the fact that they may be unbiased. This problem can be overcome by either: (i) adding more synthetic GMs to the database that are also intense and unscaled, or (ii) scaling the motions in the existing database; we investigate the latter option next.

By allowing GMs to be scaled, the effective size of the database increases and hence, more prospective IFs can be developed. For instance, a two-component mixture of MVLNs was introduced via Eq 12 in [Kwong et al., 2015c], where the IF is controlled by three inputs: (i) the specified database of unscaled GMs, (ii) the maximum acceptable scale factor, SF_{max}, and (iii) a target fraction of scaled GMs, γ. Through varying the parameters SF_{max} and γ,

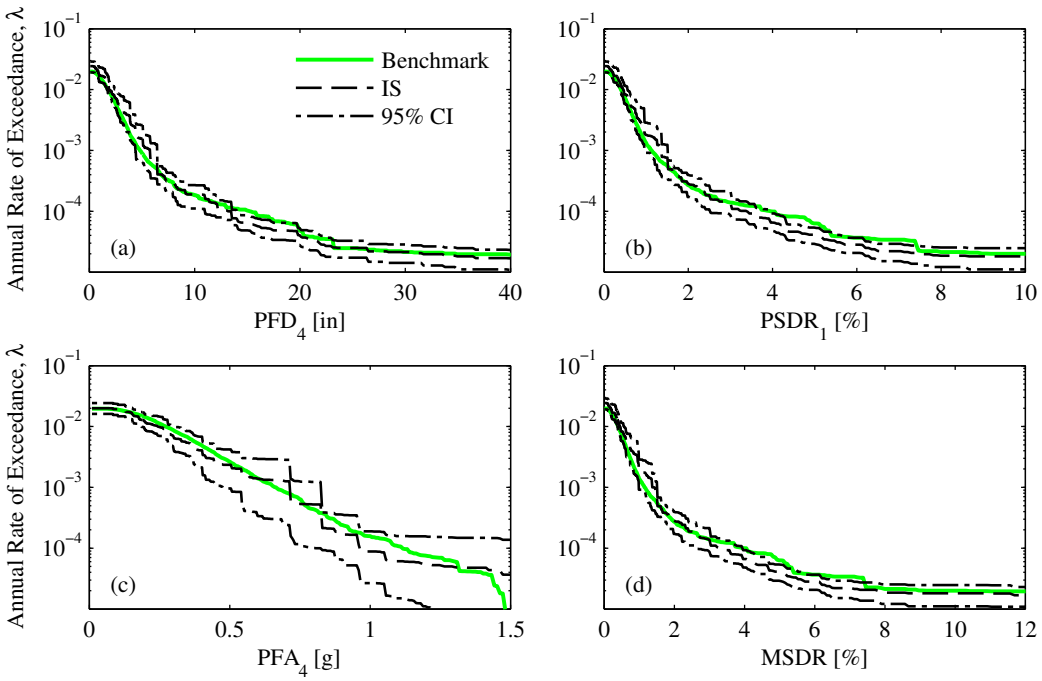

Figure 6.7: Comparison of SDHC estimates for several EDPs of the 4-story frame from IS, with g_3 as the IF, against benchmark (Rezaeian's GM model).

different IFs can be constructed for minimizing the epistemic uncertainty of hazard curve estimates.

However, record scaling also potentially introduces bias into the hazard curve estimates, depending on the sufficiency of **IM** relative to the EDP (and seismic demand level, z) of interest. This issue was investigated in Section 6 of [Kwong et al., 2015c], where the relationship between various levels of record scaling and bias in SDHCs of the (same) 4-story frame was explored. The results from that study suggest that the inelastic response of the 4-story frame is sensitive to the long-period content and duration of the GM. Furthermore, it was concluded that a vector of IMs becomes increasingly insufficient as the extent of record scaling increases, leading to the recommendation that when employing the IS-based method with scaled GMs, (i) SF_{max} should be less than or equal to 5, and (ii) γ should be less than or equal to 0.5.

In this section, we evaluate the IS-based method with scaled GMs by first choosing inputs that are based on knowledge gained from the study mentioned in the preceding paragraph. First, in order to minimize potential biases caused by record scaling, six IMs are chosen for **IM** to select GMs: $A(T_4)$, $A(T_1)$, $A(3T_1)$, displacement spectrum intensity (DSI) [Bradley, 2011], CAV, and D_{5-75}. The IMs $A(3T_1)$ and DSI are chosen because as previously mentioned, the nonlinear response of the 4-story frame is judged to be sensitive to the long period content of the GM. Second, the IF is chosen as the two-component mixture defined by Eq 12 in [Kwong et al., 2015c], with $SF_{max} = 5$ and $\gamma = 0.5$.

With **IM** and the IF defined, we first examine the GMs selected and scaled for the 4-story frame in Rezaeian's model. Figure 6.8 presents the hazard curves computed from these scaled GMs, with respect to the same nine IMs used in Figure 6.3. Comparing these two figures against each other, we observe that the scaled GMs are generally hazard-consistent at lower exceedance rates (or equivalently, larger intensity levels) than the unscaled GMs selected by g_1. For instance, the scaled GMs are hazard-consistent with respect to $A(T_4)$ for almost all exceedance rates down to 10^{-7} (Figure 6.8a) whereas the unscaled motions are hazard-consistent for exceedance rates down to only 10^{-4} (Figure 6.3a). Furthermore, at low exceedance rates, the epistemic uncertainty of the hazard curves from the scaled motions tends to be less than that from the unscaled motions. These observations are expected because the IF with $SF_{max} = 5$ and $\gamma = 0.5$ puts more probability density around large values of **IM** than g_1.

However, the use of record scaling implies that the inter-dependence structure among IMs is modified and as a result, scaled GMs tend to be less hazard-consistent than unscaled GMs. For example, the scaled motions depicted in Figure 6.8g are hazard-consistent with respect to PGD only at exceedance rates down to about 10^{-4}, even though six IMs are utilized in the selection process; in contrast, the unscaled motions depicted earlier in Figure 6.3g are hazard-consistent with respect to PGD at exceedance rates down to about 10^{-6}, even though four IMs are utilized in the selection process. Whether or not such hazard inconsistencies of scaled motions lead to bias in the resulting SDHCs depends on the sufficiency of **IM** with respect to the EDPs of interest.

Computed by applying Equation 6.4b to the RHA results from the scaled GMs, the SDHCs for the 4-story frame are presented in Figure 6.9. Comparing this figure against Figure 6.4 for unscaled GMs selected by g_1, we see that scaling GMs leads to smaller epistemic uncertainty of the SDHCs. Compared to the benchmark SDHCs however, the SDHCs from scaled GMs are more biased than those from unscaled GMs selected by g_1; in particular, we observe a significant underestimation of the roof acceleration hazard curve at exceedance rates less than 10^{-3}. This bias indicates that the vector of six IMs employed in selecting GMs is insufficient for estimating large roof accelerations of this frame; put differently, large levels of this response quantity are influenced by hazard inconsistencies with respect to IMs that have not been utilized to select GMs. One way to minimize such hazard inconsistencies is to minimize record scaling, which preserves the inter-dependence structure among IMs.

The IS-based method with $SF_{max} = 5$ and $\gamma = 0.5$ is also evaluated for the 20-story frame with Rezaeian's model. The same six IMs used in selecting GMs for the 4-story frame are also used to select GMs for the 20-story frame: $A(T_4)$, $A(T_1)$, $A(3T_1)$, DSI, CAV, and D_{5-75}. By design of the IS-based procedure, the GMs selected for the 20-story frame are ensured to be hazard-consistent with respect to these six IMs over a relatively wide range of exceedance rates, despite the fact that they have been scaled.

The resulting SDHCs for the 20-story frame are presented in Figure 6.10. Comparing this figure against Figure 6.5 for unscaled GMs selected by g_1, we observe that the epistemic uncertainty in the SDHCs from scaled GMs is not appreciably less than that from the un-

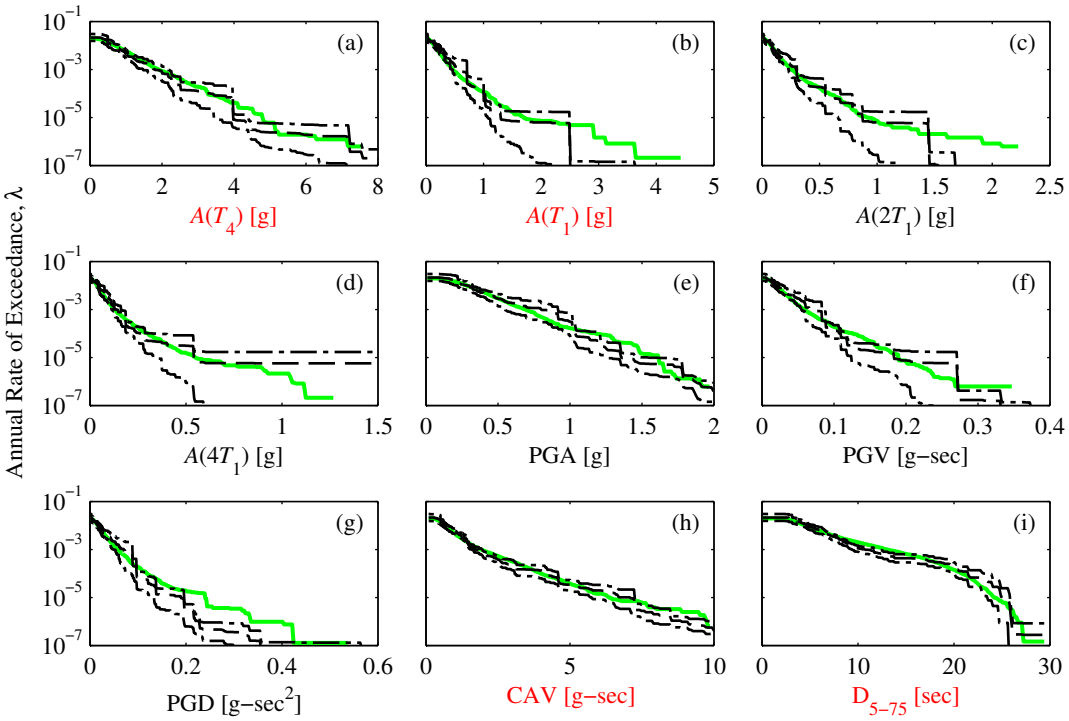

Figure 6.8: Hazard consistency of the motions selected with $SF_{max} = 5$ and $\gamma = 0.5$ for the 4-story frame, with respect to: (a) $A(T_4)$; (b) $A(T_1)$; (c) $A(2T_1)$; (d) $A(4T_1)$; (e) PGA; (f) PGV; (g) PGD; (h) CAV; and (i) D_{5-75}. Benchmark in solid green, estimate from IS in dashed black, and 95% CI of estimate from IS in chained black (Rezaeian's GM model).

scaled GMs. This is because the IF for scaled GMs is chosen herein by specifying SF_{max} and γ to be respectively, 5 and 0.5, instead of specifying these values on the basis of minimizing the epistemic uncertainty in hazard curves for IMs, as described at the end of Section 6.4 with reference to Figure 6.2. Compared to the respective benchmarks, we observe that the SDHCs from scaled GMs are essentially unbiased for this frame, unlike those shown in Figure 6.9 for the 4-story frame. This good agreement indicates two possibilities: either (i) **IM** is sufficient for the nonlinear response of the 20-story frame, or (ii) the selected GMs happen to be hazard-consistent with respect to all IMs that are influential to the response and are excluded from **IM**. To see which of these two possibilities is more plausible, we repeat the evaluation of the IS-based method with record scaling, using Yamamoto's GM model.

Starting with Yamamoto's model, GMs are selected via IS and utilized for estimating SDHCs of both frames; these SDHCs are presented in Figures 6.11-6.12. For each frame, GMs are again selected such that they are hazard-consistent with respect to the same six IMs over a wide range of exceedance rates. The resulting SDHCs for the 4-story frame are now essentially unbiased (Figure 6.11); unlike the results for Rezaeian's model where a significant underestimation of the roof acceleration hazard curve was observed (Figure 6.9c), the estimated roof acceleration hazard curve for Yamamoto's model is unbiased (Figure 6.11c). Because bias was observed in Rezaeian's model, we know that the vector of six IMs used

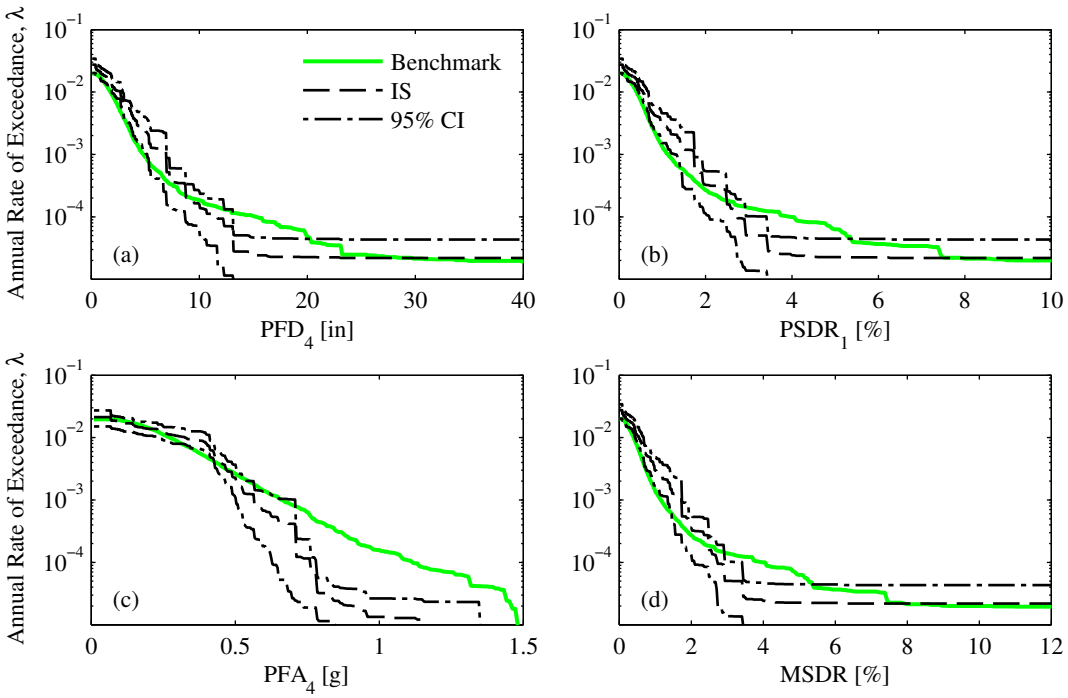

Figure 6.9: Comparison of SDHC estimates for several EDPs of the 4-story frame from IS, with $SF_{max} = 5$ and $\gamma = 0.5$, against benchmark (Rezaeian's GM model).

for selecting GMs is insufficient for estimating large roof accelerations of this frame; hence, the good agreement observed in Yamamoto's model indicates that the particular selection of GMs in this model happen to be hazard-consistent with respect to IMs that are influential to roof acceleration. Without the benchmark SDHCs in Rezaeian's GM model (Figure 6.9), one could have erroneously concluded that the vector of six IMs is sufficient for this frame on the sole basis of the good agreement observed in Yamamoto's model (Figure 6.11).

The results for the 20-story frame tell a slightly different story. Comparing Figure 6.12 for Yamamoto's model against Figure 6.10 for Rezaeian's model, we observe that the SDHC estimates for this frame from scaled GMs are essentially unbiased in both models. Although the good agreement observed in both models could have been caused by the fact that in each model, the particular selection of GMs is hazard-consistent with respect to all influential IMs, the consistent observation from both models suggests that, for the extent of record scaling considered herein, the vector of six IMs used in selecting GMs is indeed sufficient for the nonlinear response of the 20-story frame.

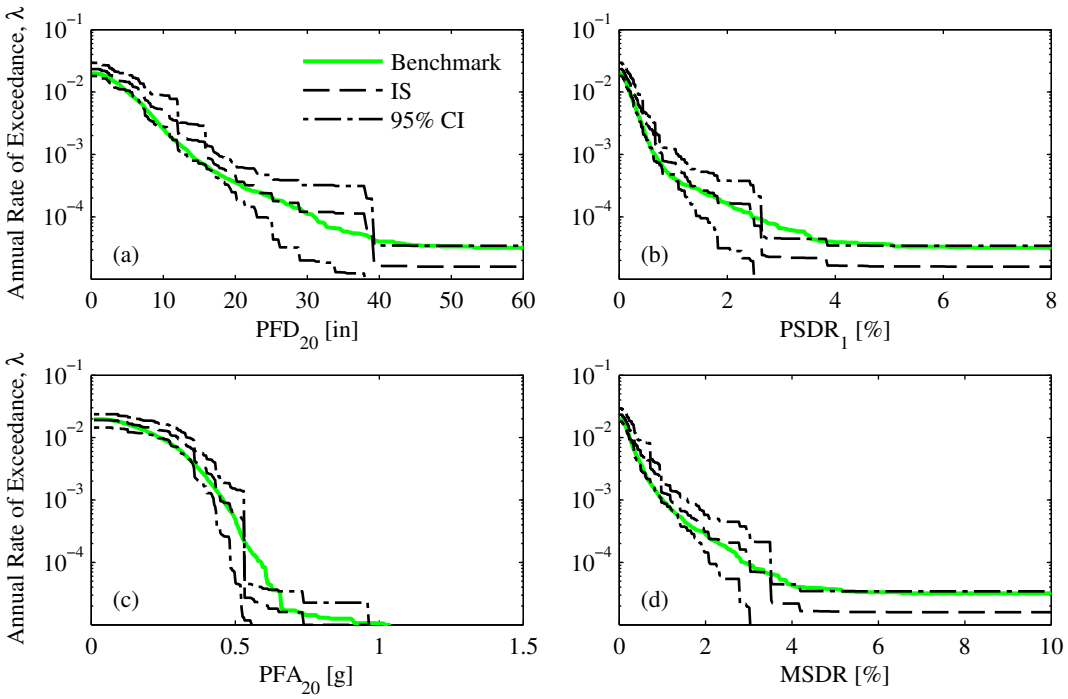

Figure 6.10: Comparison of SDHC estimates for several EDPs of the 20-story frame from IS, with $SF_{max} = 5$ and $\gamma = 0.5$, against benchmark (Rezaeian's GM model).

6.9 Estimating SDHCs of Multiple Systems from a Single Ensemble of Ground Motions

When designing a new structure or retrofitting an existing structure, it is common to consider several alternative designs. For evaluating designs, SDHCs can be developed for each alternative by PSDA. When the fundamental period of each alternative design is different however, PSDA typically requires GMs to be re-selected (and scaled) for each system, which can be cumbersome when many systems are considered for the site. By using a single ensemble of GMs instead, we can more readily take advantage of high-performance computing resources (e.g., XSEDE machines) that are becoming increasingly available for performing nonlinear RHAs in OpenSEES [Ventura et al., 2015, McKenna and Fenves, 2008]. Consequently, the ability to select a single ensemble of GMs for accurately estimating SDHCs of multiple systems at the same site seems like an attractive proposition; in this section, we evaluate the IS-based method in its ability to achieve this goal.

We saw earlier that the bias in SDHCs is dictated directly by the particular selection of GMs. Specifically, as long as the motions are hazard-consistent with respect to a set of IMs that is sufficient, then the resulting SDHC estimates are unbiased. However, for general, complex MDF systems, it is difficult to identify (*a priori*) IMs that are sufficient. To overcome this problem, one can employ a large number of IMs in the selection of GMs, as in the GCIM method [Bradley, 2010a]. Another solution is to select GMs based on fewer

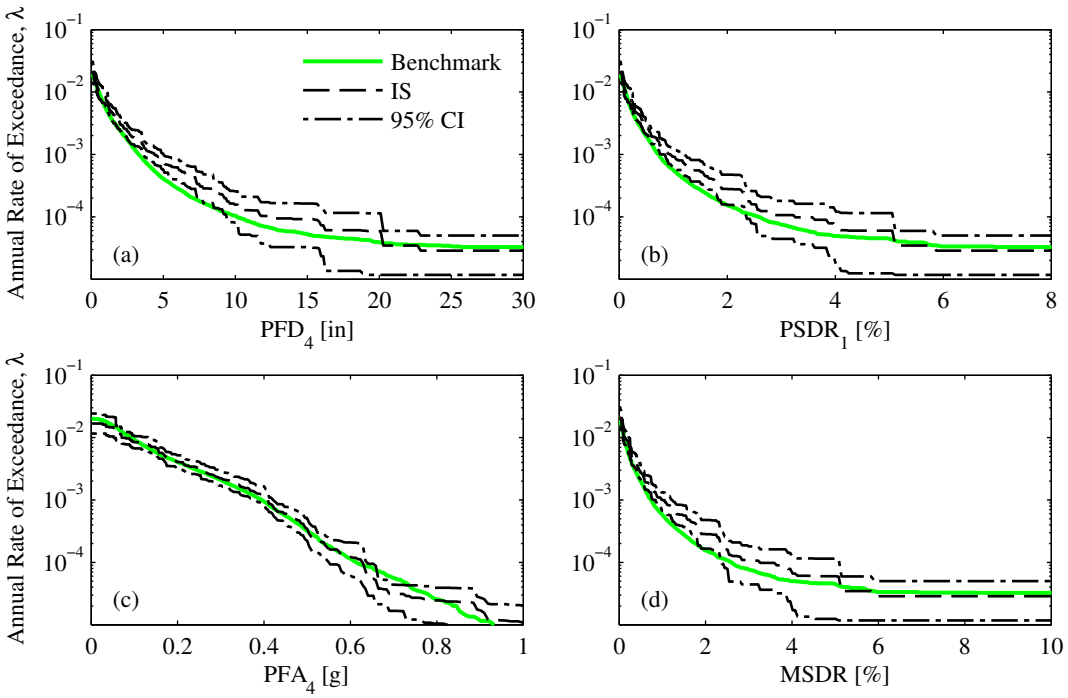

Figure 6.11: Comparison of SDHC estimates for several EDPs of the 20-story frame from IS, with $SF_{max} = 5$ and $\gamma = 0.5$, against benchmark (Yamamoto's GM model).

IMs, but at the same time, minimize the degree of record scaling.

This alternative is motivated by previous results demonstrating that unscaled GMs can be hazard-consistent with respect to a large number of IMs, even when a small number of IMs was employed in the IS-based selection process. For example, Figure 6.3 demonstrates that the motions selected by g_1 are hazard-consistent with respect to all nine IMs at exceedance rates greater than 10^{-4}, despite the fact that only four IMs were employed in selecting GMs. Such is the case because the four IMs are well correlated with many other IMs and simultaneously, the inter-dependence structure among IMs is preserved by avoiding record scaling altogether.

To obtain a single ensemble of GMs that results in accurate SDHCs for several systems, one would need a vector of IMs that: (i) covers the most important aspects of the GM, and (ii) is not specific to a particular structure. The three characteristics of far-fault GMs that are most influential to structural response are: amplitude, frequency content, and duration [Kramer, 1996]. Motivated by this idea, we selected GMs with four non-structure-specific IMs: PGA, PGV, PGD, and D_{5-75}.

Using these four IMs as **IM**, g_3 as the IF (see Figure 6.1 and Equation 6.6), and Rezaeian's GM model, a single ensemble of $n = 300$ unscaled GMs was selected by the IS-based method. The hazard consistency of these selected motions was examined in Figure 6.13,

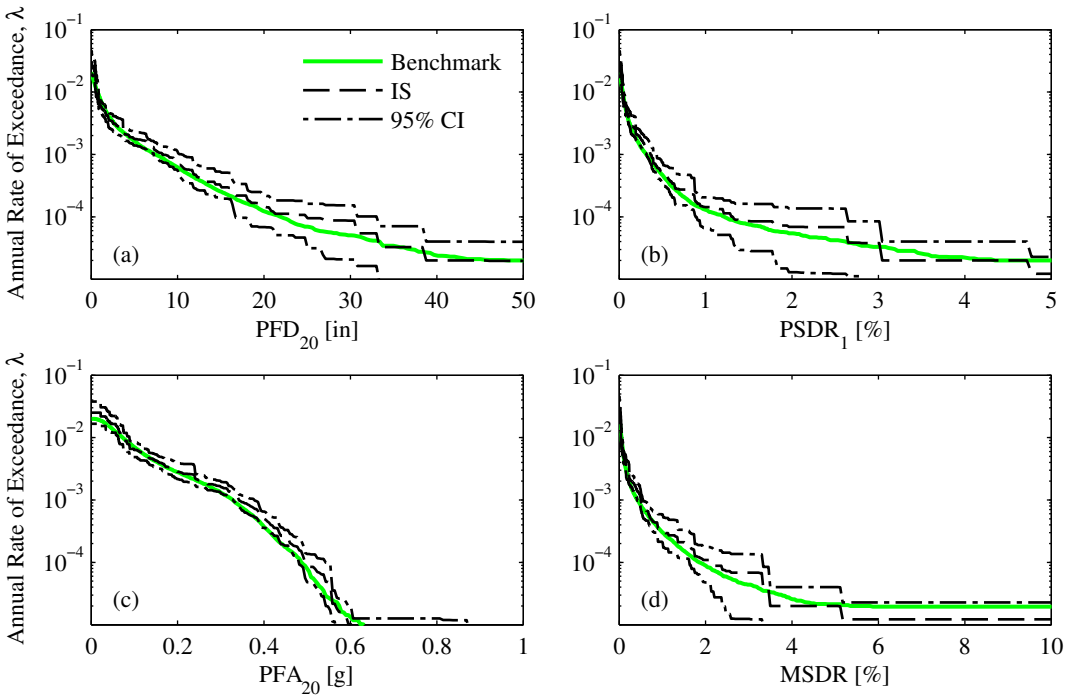

Figure 6.12: Comparison of SDHC estimates for several EDPs of the 20-story frame from IS, with $SF_{max} = 5$ and $\gamma = 0.5$, against benchmark (Yamamoto's GM model).

with respect to nine IMs: $A(0.1s)$, $A(1s)$, $A(5s)$, $A(10s)$, PGA, PGV, PGD, CAV, and D_{5-75}. As expected from the design of the IS-based procedure, the selected motions are hazard-consistent with respect to all four IMs (highlighted in red) at exceedance rates down to 10^{-6}. In addition to the IMs that were chosen for the selection process, the selected motions are also hazard-consistent with respect to IMs such as CAV and spectral accelerations at various vibration periods. Such hazard consistency suggests that the resulting SDHC estimates will be unbiased for many systems.

To explore this expectation, RHAs were performed for both multistory frames, subjected to the *same* set of $n = 300$ GMs mentioned in the preceding paragraph. The resulting SDHCs of the 4-story and 20-story frames are presented in Figures 6.14 and 6.15, respectively. We observe that the SDHCs for both frames are practically unbiased for all EDPs and demand levels considered, even though only a single ensemble of GMs has been utilized. If one desires to reduce the epistemic uncertainty in the SDHCs at low exceedance rates, one can increase the number of GMs n and/or choose a different IF (Section 6.4). Repeating this evaluation for Yamamoto's GM model led to similar observations. Therefore, these results suggest that *accurate* SDHC estimates of *multiple* systems can be obtained from a *single* ensemble of GMs by applying the IS-based method with **IM** specified as PGA, PGV, PGD, and D_{5-75}.

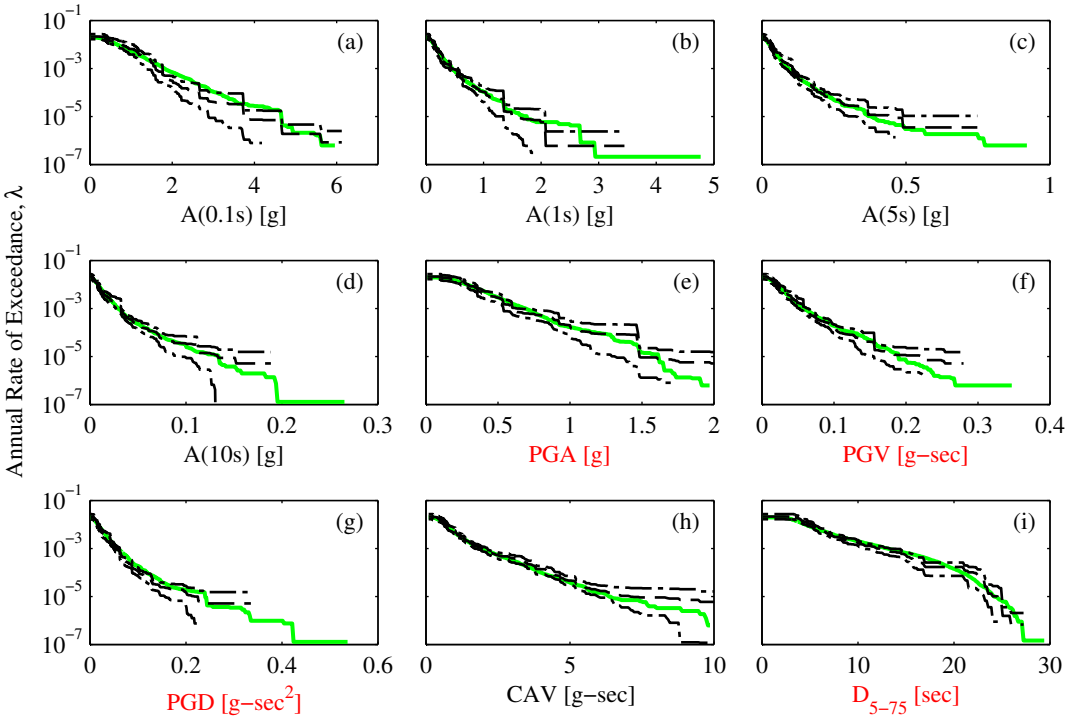

Figure 6.13: Hazard consistency of the motions selected from a non-structure-specific **IM**, with respect to: (a) $A(0.1s)$; (b) $A(1s)$; (c) $A(5s)$; (d) $A(10s)$; (e) PGA; (f) PGV; (g) PGD; (h) CAV; and (i) D_{5-75}. Benchmark in solid green, estimate from IS in dashed black, and 95% CI of estimate from IS in chained black (Rezaeian's GM model).

6.10 Comparison with the GCIM Method

It is of interest to compare the IS-based method against the GCIM approach to GM selection [Bradley, 2010a]. The latter method can be viewed as the state-of-the-art procedure in selecting GMs, in the sense that any IM can be employed to select GMs and potential biases caused by improper GM selection can be estimated in a practical fashion. Despite this holistic nature, estimating SDHCs with GCIM typically requires record scaling [3] and several ensembles of GMs.

Table 6.1 compares the two methods for estimating SDHCs for a given structure at a specified site. The two methods are similar in that a wide variety of IMs can be chosen to select GMs, so long as GMPMs are available for such IMs. However, IS differs from GCIM in several ways. First, it is not necessary in IS to choose a conditioning scalar IM, IM^*, and as a result, unscaled GMs can be readily selected. Note that the choice of IM^* can appreciably affect the resulting SDHCs, even when a large number of IMs are utilized for selecting GMs (see e.g., Fig 11 of [Bradley et al., 2015]). Second, if scaling is desired in IS, the degree of record scaling can be controlled by two parameters: (i) the maximum scale factor, SF_{max},

[3] By utilizing a lognormal weighting kernel, GCIM can be used to estimate SDHCs without record scaling [Bradley et al., 2015].

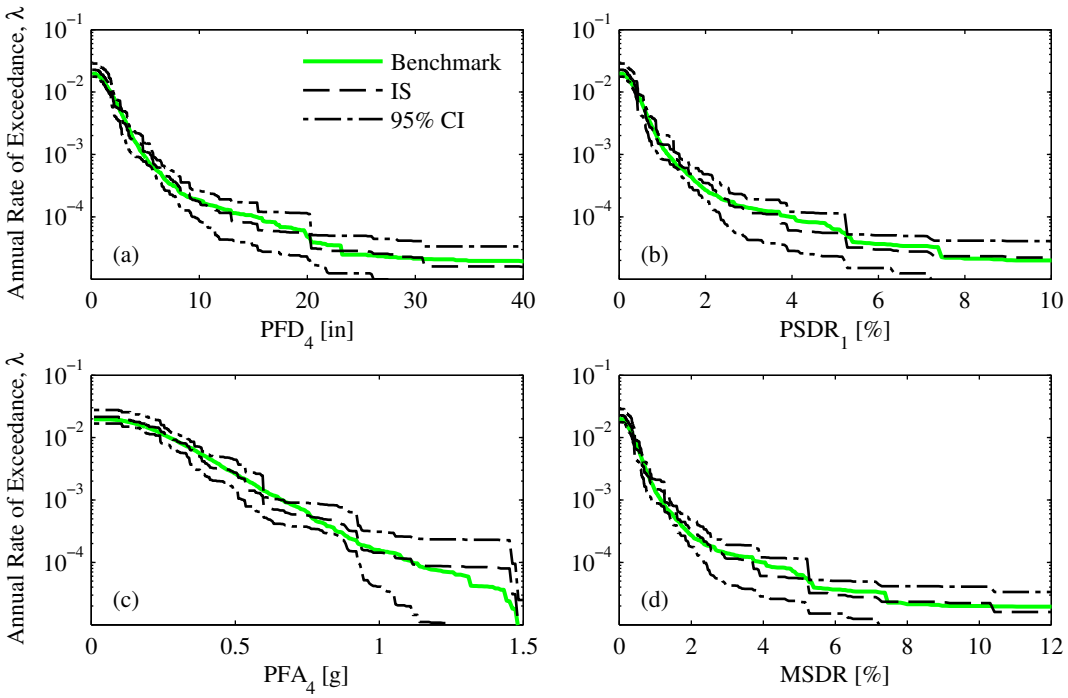

Figure 6.14: Comparison of SDHC estimates for several EDPs of the 4-story frame from a single non-structure-specific set of GMs, against benchmark (Rezaeian's GM model).

and (ii) the target fraction of scaled motions in the ensemble, $0 \leq \gamma \leq 1$; by minimizing the degree of scaling, fewer IMs may be utilized to select GMs without causing excessive bias in the demands [Kwong et al., 2015c]. Third, by using a single target distribution of **IM** from PSHA in IS (Equation 6.1), a single set of GMs can be developed for directly enforcing hazard consistency and computing SDHCs of multiple systems. Finally, unlike GCIM, a practical approach for estimating potential bias in demands caused by improper GM selection is unavailable in IS; however, such estimates of bias from GCIM can be significantly different from the actual bias, as demonstrated in Chapter 5.

The inputs for GCIM are chosen to facilitate comparison against the SDHC from the IS-based method with a non-structure-specific vector of IMs. To control for the epistemic uncertainty in a SDHC estimate arising from a finite number of GMs, $N_{GM} = 25$ motions were selected for each of the $N_{IM^*} = 12$ intensity levels of IM^* leading to a total of $25 \times 12 = 300$ GMs for each GCIM-based SDHC estimate. Moreover, the four IMs in the IS-based method – PGA, PGV, PGD, and D_{5-75} – were also employed to select motions in GCIM. Finally, PGV was chosen as IM^* for scaling GMs for the 4-story frame, since the fundamental period of the frame, which is 0.95 sec, lies in the velocity-sensitive region of the response spectrum, and D_{5-75} does not vary with record scaling.

Figure 6.16 examines hazard consistency of the GMs selected by GCIM, with respect to the same nine IMs presented in Figure 6.13. By scaling motions to intensity levels of PGV,

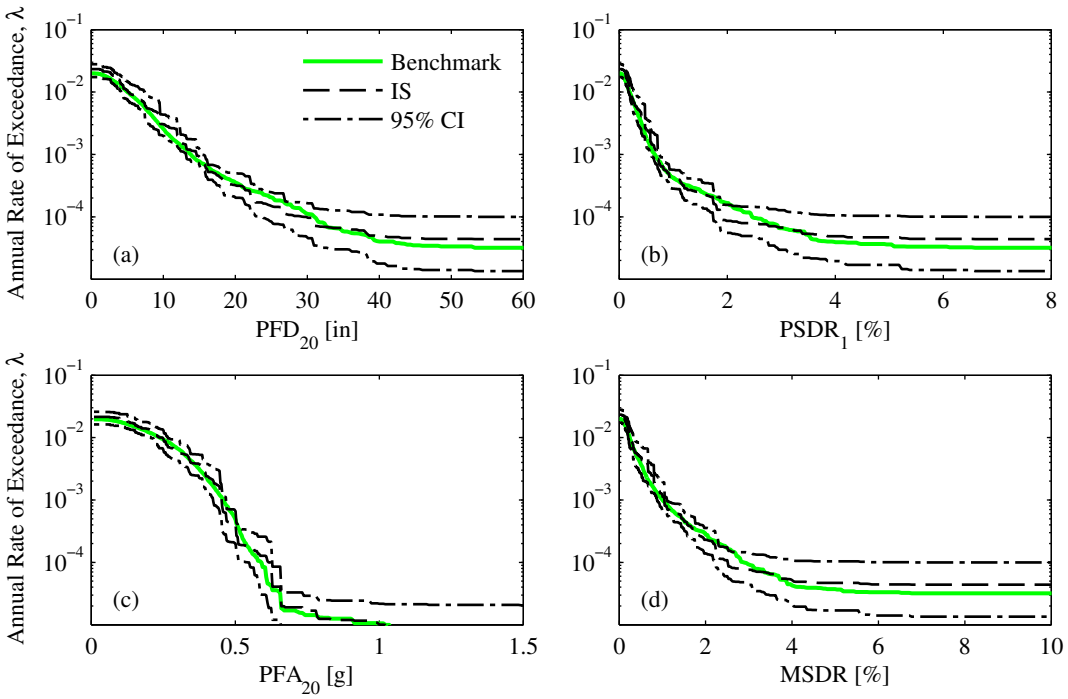

Figure 6.15: Comparison of SDHC estimates for several EDPs of the 20-story frame from the same set of GMs utilized in Figures 6.13-6.14, against benchmark (Rezaeian's GM model).

the selected motions are, as expected, hazard-consistent with respect to PGV at exceedance rates down to about 10^{-6}. Because PGA, PGD, and D_{5-75} were also considered in the selection of GMs, the selected GMs are also hazard-consistent with respect to these three IMs; specifically, the motions are hazard-consistent down to an exceedance rate of 10^{-7} for PGA and PGD but only down to 10^{-4} for D_{5-75}. The hazard consistency for D_{5-75} does not extend to lower exceedance rates because the Kolmogorov-Smirnov test in GCIM does not capture the tails of the GCIM distributions for D_{5-75} [Kwong et al., 2015a]. In contrast, the selected motions from IS are hazard-consistent with respect to D_{5-75} at exceedance rates down to 10^{-6} (Figure 6.13i) because IS aims to directly satisfy hazard consistency at low exceedance rates through various choices of the IF. Whether or not such large values of D_{5-75} are influential to the nonlinear response of the structure is unknown until the resulting SDHC estimate is compared against the benchmark SDHC. As in IS, the selected motions from GCIM are also hazard-consistent with respect to other IMs such as CAV and spectral accelerations at various periods, even though only four IMs are employed in the selection process. This suggests that the resulting GCIM-based SDHC estimates should be unbiased.

The SDHC estimates resulting from the motions selected by GCIM are presented in Figure 6.17. Despite extensive record scaling, the SDHCs are unbiased for all displacements and drifts. In fact, the epistemic uncertainty of the SDHC estimates is even smaller than that from IS (Figure 6.14). However, the SDHC estimates from GCIM could also be significantly biased for some EDPs. For instance, Figure 6.17c demonstrates that the GCIM-based es-

Table 6.1: Comparison of using GCIM and IS (without scaling GMs) to compute SDHCs of a given structure at the specified site.

Attribute	GCIM	IS
Need to choose conditioning scalar IM?	Yes	No
Can all selected GMs be unscaled?	Possibly (see [Bradley et al., 2015])	Yes
Limits on scaling of GMs	Not typically used	Controlled by parameters SF_{max} & γ
Type of IMs considered	Spectral accelerations, peak ground measures, spectrum intensities, cumulative effects	Spectral accelerations, peak ground measures, spectrum intensities, cumulative effects
Number of IMs used to select GMs	Many (e.g., more than 14)	Few (e.g., 4-6)
Total number of PSHA-based calculations for selecting GMs	N_{IM^*} deaggregations and N_{IM^*} GCIM distributions	1 target distribution for **IM** (Eq 6.1) and 1 choice of Importance Function
Total number of GMs used	N_{IM^*} sets of N_{GM} GMs	1 ensemble of $n = N_{IM^*} \times N_{GM}$ GMs
How hazard consistency is enforced	Kolmogorov-Smirnov tests	Direct comparison of hazard curves
Is sub-procedure available for checking bias in demands?	Yes	No
Can 1 set of motions be used to compute SDHCs for several systems?	No	Yes

timate significantly underestimates the roof acceleration hazard curve at exceedance rates less than 10^{-3}. In fact, such underestimation is observed for accelerations at all floors of the building. Furthermore, the GCIM-based estimate of floor acceleration hazard curves remained biased even when the number of IMs employed to select motions was increased from four to 24 (see Chapter 5).

The biases in floor accelerations are caused indirectly by record scaling and directly by hazard inconsistencies of the selected GMs with respect to IMs that are influential to floor accelerations. When record scaling is avoided altogether, hazard inconsistencies of the selected GMs tend to be minimized and hence, the resulting SDHCs tend to be unbiased; for example, the IS-based method with unscaled GMs leads to unbiased estimates of roof acceleration hazard curves for the 4-story frame (see Figures 6.14c, 6.7c, and 6.4c). In contrast, when GMs are scaled in IS, an underestimation in floor accelerations that is similar to that from GCIM is also observed (Figure 6.9c). Because the scaled motions from both IS and GCIM are hazard-consistent with respect to many IMs and exceedance rates (see

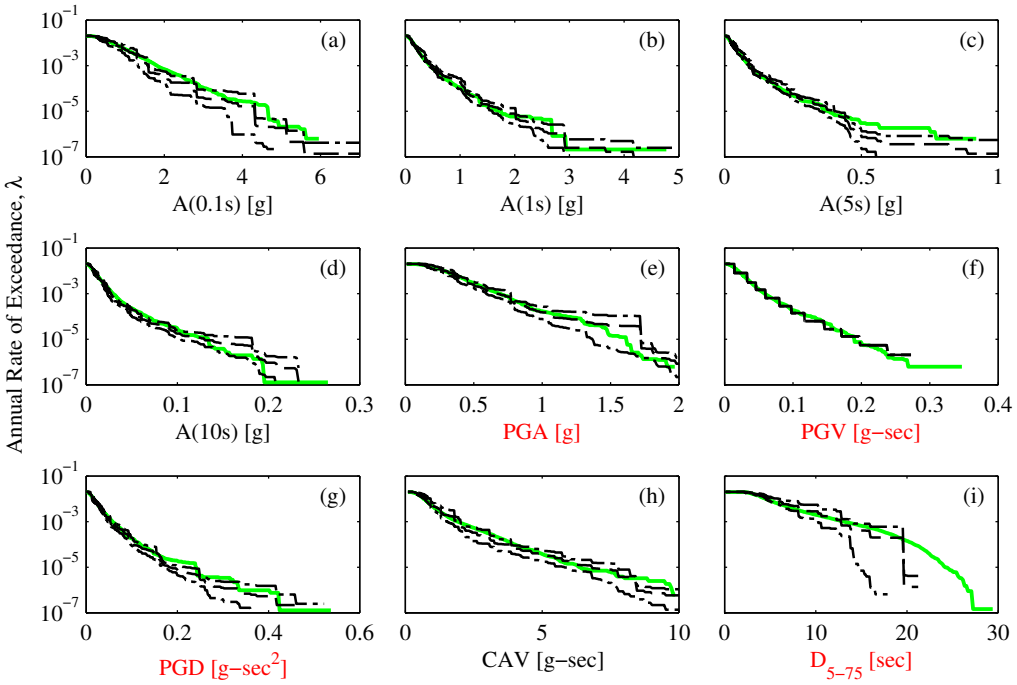

Figure 6.16: Hazard consistency of the motions selected and scaled to PGV from GCIM with the same four non-structure-specific IMs employed in IS, with respect to: (a) $A(0.1s)$; (b) $A(1s)$; (c) $A(5s)$; (d) $A(10s)$; (e) PGA; (f) PGV; (g) PGD; (h) CAV; and (i) D_{5-75}. Benchmark in solid green, estimate from GCIM in dashed black, and 95% CI of estimate from GCIM in chained black (Rezaeian's GM model).

Figures 6.8 and 6.16), these biases imply that the scaled motions in each method are hazard-*inconsistent* with respect to IMs that are influential to floor accelerations; put differently, the IMs for which the scaled motions are hazard-consistent are insufficient for estimating floor accelerations.

Besides offering the ability to directly enforce hazard consistency and readily select GMs without record scaling, the IS-based method also offers the ability to select a *single* set of GMs, which differs from the use of N_{IM^*} sets in GCIM for a single SDHC estimate. Although it is possible to utilize a relatively few number of GM sets (e.g., ≥ 3) in GCIM to estimate SDHCs [Bradley, 2013b], the results from such an approximation depend on how $EDP \mid IM$ is parameterized and how the integral in the PSDA equation is evaluated [Bradley et al., 2015]. With multiple ensembles of GMs in GCIM, it is necessary to repeat the selection process multiple times. Furthermore, each selection involves: (i) performing deaggregation for IM^*, (ii) determining the target GCIM distributions for **IM**, and (iii) randomly sampling values of **IM** from the GCIM distributions. In contrast, these three steps are done only once in IS: (i) determine the target distribution for **IM** from PSHA (Equation 6.1), (ii) choose an IF (Section 6.4), and (iii) randomly sample values of **IM** from the IF. As mentioned previously, a single set of GMs facilitates the use of high-performance computing resources that are becoming increasingly available for performing nonlinear RHAs

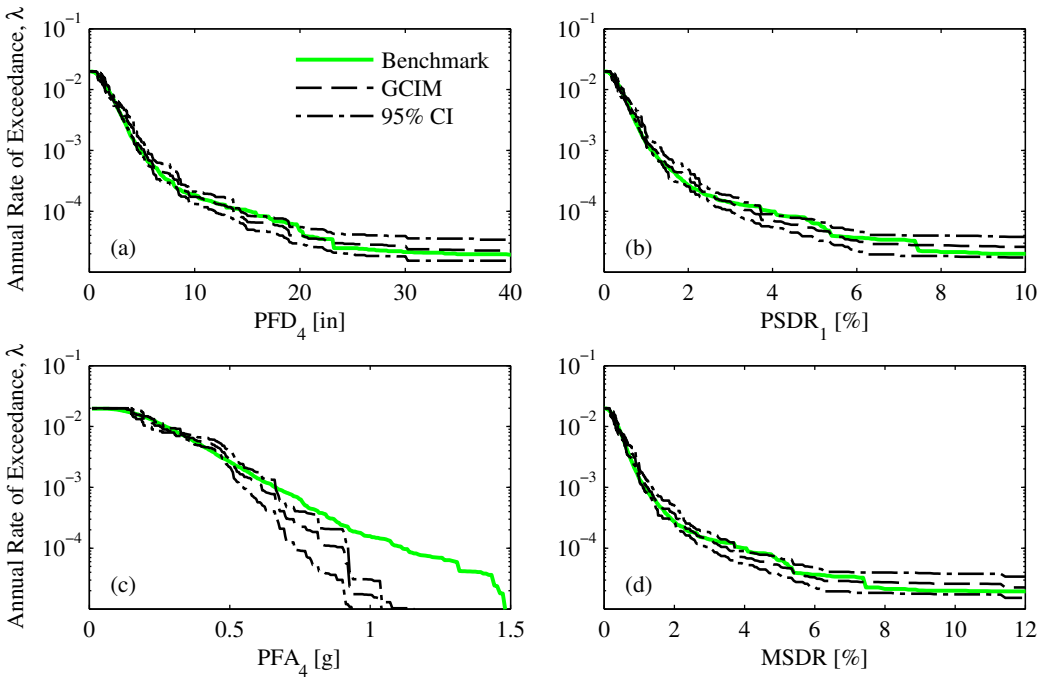

Figure 6.17: Comparison of SDHC estimates for several EDPs of the 4-story frame, from GCIM with the same four non-structure-specific IMs employed in IS, against benchmark (Rezaeian's GM model).

in OpenSEES [Ventura et al., 2015, McKenna and Fenves, 2008].

6.11 Conclusions

The IS based GM selection procedure developed earlier for estimating SDHCs of structures at a specified site [Kwong et al., 2015c] enables us to take advantage of unscaled yet intense GMs for estimating SDHCs, through various choices of the IF. Moreover, it enables us to directly enforce hazard consistency of the selected motions with respect to a given set of IMs and to estimate SDHCs with a single ensemble of GMs. In this chapter, we evaluated the IS-based method in its ability to accurately estimate SDHCs of multistory building frames, leading to the following conclusions:

1. The method simplifies the selection of GMs for estimating SDHCs, by reducing the number of: (i) sets of GMs for RHAs, (ii) IMs chosen to select GMs, and (iii) target distributions of **IM** to be computed from PSHA.

2. When implementing the method without scaling GMs:

    a) The resulting SDHCs are unbiased for all EDPs, systems, and GM simulation models considered.

b) The epistemic uncertainty of the resulting SDHCs varies, depending on the choice of the IF.

3. When implementing the method with scaled GMs (up to $SF_{max} = 5$):

   a) The SDHCs remain unbiased for all cases except for the peak floor accelerations of the 4-story frame in Rezaeian's GM model.

   b) The vector-valued IM consisting of $A(T_4)$, $A(T_1)$, $A(3T_1)$, DSI, CAV, and D_{5-75} is insufficient for estimating large floor accelerations of the 4-story frame but appears to be sufficient for estimating the nonlinear response of the 20-story frame.

   c) The scaled GMs tend to be hazard-*inconsistent* with respect to more IMs than when scaling is avoided.

4. When implementing the method with a non-structure-specific vector of IMs, accurate SDHC estimates of multiple systems can be obtained from a single ensemble of GMs.

5. The potential bias and epistemic uncertainty of the hazard curve estimates depend on the choice of the IF and hence, the IF must be carefully chosen, following the guidelines presented in Section 6.4. In essence, the IF should be chosen such that at low exceedance rates, the epistemic uncertainty of the resulting hazard curves is minimized for all IMs that are deemed influential to all EDPs of interest.

6. Unlike the GCIM method of selecting GMs, which can be considered as the state-of-the-art in GM selection, the IS-based method:

   a) avoids the need to choose a conditioning scalar IM, facilitating the selection of unscaled GMs;

   b) directly enforces hazard consistency of GMs at low exceedance rates, through various choices of the IF;

   c) utilizes fewer IMs to select GMs (e.g., 4-6);

   d) reduces the number of ensembles of GMs required for a single SDHC estimate from N_{IM^*} ensembles down to one (where N_{IM^*} is chosen to satisfactorily approximate the integration in PSDA); and

   e) offers the ability to accurately estimate SDHCs of multiple structures with a single ensemble of GMs.

7. With the same number of IMs and GMs in both GCIM and IS, the IS-based method without scaling leads to less bias but larger epistemic uncertainty in the SDHC estimates.

The preceding conclusions are based on SDHCs for structures at an idealized site. For a realistic site with several earthquake sources and aleatory variability in source-to-site distance, the target probability distribution of **IM** from PSHA, f from Equation 6.1, and the lack of recorded GMs may collectively render it difficult to obtain a database-driven IF, g, that concentrates on intense levels of the IMs while simultaneously avoiding record scaling.

Chapter 7

Conclusions

In this report, the issue of selecting and scaling ground motions for estimating seismic demand hazard curves (SDHCs) of structures is investigated. The key contributions are summarized as follows:

1. An approach to rigorously quantify potential biases in SDHC estimates from ground-motion selection and modification (GMSM) procedures is developed, leading to the important notion of a *benchmark SDHC*;
2. Based on the concept of Importance Sampling, a novel ground motion selection procedure is developed that allows: (i) hazard consistency to be directly enforced for a user-specified collection of IMs, and (ii) SDHCs of a structure to be estimated from a single ensemble of ground motions, with the option of avoiding record scaling altogether; and
3. Contemporary GMSM procedures are evaluated for a variety of structures and response quantities in their ability to accurately estimate SDHCs at a given site.

This investigation has led to the following major conclusions:

1. Biases in SDHC estimates are caused *directly* by hazard inconsistencies of the specific selection of ground motions with respect to intensity measures (IMs) that are influential to the response and *indirectly* by GMSM procedures; such procedures are only a means for enforcing hazard consistency of a particular selection of ground motions, with respect to a user-specified collection of IMs;
2. As long as ground motions are selected to be hazard-consistent with respect to an IM that is sufficient, the resulting estimates of the SDHC are unbiased, irrespective of the level of record scaling;
3. Given that a particular selection of ground motions is hazard-consistent with respect to a vector of IMs, any bias observed in the resulting estimate of the SDHC implies that

the vector of IMs is *insufficient* for that particular response quantity. The concept of a benchmark, developed in Chapters 2-3, enables such biases to be directly determined and hence, insufficient IMs to be identified; and

4. Based on the evaluation of three contemporary GMSM procedures – (i) "exact" Conditional Spectrum (CSexact), (ii) Generalized Conditional Intensity Measure (GCIM), and (iii) Importance Sampling (IS) – the following can be concluded:

    a) The SDHCs from CS-exact are unbiased for many systems and response quantities, but in some cases, the annual rate of collapse is overestimated and floor accelerations are underestimated. The epistemic uncertainty in the SDHCs is relatively small;

    b) The SDHCs from GCIM are unbiased for many systems and response quantities, but in few cases, the floor accelerations are underestimated. The epistemic uncertainty in the SDHCs is relatively small; and

    c) The SDHCs from IS are unbiased for all systems and response quantities considered when record scaling is avoided altogether; however, the epistemic uncertainty in the SDHCs depends on the Importance Function chosen to select ground motions. When ground motions are scaled in IS, both the SDHC bias and epistemic uncertainty depend on the IMs and the Importance Function chosen to select ground motions.

The work in this report is limited in that:

1. Only two multistory frames were studied.
2. Although representative of the Bay Area in Northern California, the site considered is idealized.
3. Only a single horizontal component of ground motion was investigated herein.
4. Near-fault effects of ground motions were not considered.

Future research should consider more structural systems and sites to confirm the generality of the conclusions presented in this report.

Bibliography

[Abrahamson et al., 2008] Abrahamson, N., Atkinson, G., Boore, D., Bozorgnia, Y., Campbell, K., Chiou, B., Idriss, I., Silva, W., and Youngs, R. (2008). Comparisons of the NGA ground-motion relations. *Earthquake Spectra*, 24(1):45–66.

[Abrahamson and Silva, 2008] Abrahamson, N. and Silva, W. (2008). Summary of the Abrahamson & Silva NGA ground-motion relations. *Earthquake Spectra*, 24(1):67–97.

[Akkar and Özen, 2005] Akkar, S. and Özen, Ö. (2005). Effect of peak ground velocity on deformation demands for SDOF systems. *Earthquake engineering & structural dynamics*, 34(13):1551–1571.

[American Society of Civil Engineers, 2010] American Society of Civil Engineers (2010). *Minimum design loads for buildings and other structures*. American Society of Civil Engineers : Structural Engineering Institute, Reston, Va.

[Applied Technology Council, 2009] Applied Technology Council (2009). Quantification of building seismic performance factors, FEMA P695. Technical report, Federal Emergency Management Agency, Washington D.C.

[Applied Technology Council, 2012] Applied Technology Council (2012). Seismic performance assessment of buildings, Volume 1 - Methodology, FEMA P-58-1. Technical report, Federal Emergency Management Agency, Washington D.C.

[Baker and Cornell, 2005] Baker, J. and Cornell, C. (2005). A vector-valued ground motion intensity measure consisting of spectral acceleration and epsilon. *Earthquake Engineering & Structural Dynamics*, 34(10):1193–1217.

[Baker, 2006] Baker, J. W. (2006). *Vector-valued ground motion intensity measures for probabilistic seismic demand analysis*. PhD thesis, Department of Civil and Environmental Engineering, Stanford University, Stanford, CA.

[Baker, 2007a] Baker, J. W. (2007a). Measuring bias in structural response caused by ground motion scaling. In *8th Pacific Conference on Earthquake Engineering, Singapore*.

[Baker, 2007b] Baker, J. W. (2007b). Probabilistic structural response assessment using vector-valued intensity measures. *Earthquake Engineering & Structural Dynamics*, 36(13):1861–1883.

[Baker, 2011] Baker, J. W. (2011). Conditional mean spectrum: Tool for ground motion selection. *ASCE Journal of Structural Engineering*, 137(3):322–331.

[Baker, 2015] Baker, J. W. (2015). Efficient analytical fragility function fitting using dynamic structural analysis. *Earthquake Spectra*, 31(1):579–599.

[Baker and Cornell, 2006a] Baker, J. W. and Cornell, C. A. (2006a). Correlation of response spectral values for multicomponent ground motions. *Bulletin of the Seismological Society of America*, 96(1):215–227.

[Baker and Cornell, 2006b] Baker, J. W. and Cornell, C. A. (2006b). Spectral shape, epsilon and record selection. *Earthquake Engineering & Structural Dynamics*, 35(9):1077–1095.

[Baker and Cornell, 2006c] Baker, J. W. and Cornell, C. A. (2006c). Which spectral acceleration are you using? *Earthquake Spectra*, 22:293.

[Baker and Jayaram, 2008] Baker, J. W. and Jayaram, N. (2008). Correlation of spectral acceleration values from NGA ground motion models. *Earthquake Spectra*, 24:299.

[Bazzurro and Cornell, 1999] Bazzurro, P. and Cornell, C. A. (1999). Disaggregation of seismic hazard. *Bulletin of the Seismological Society of America*, 89(2):501–520.

[Benjamin and Cornell, 1970] Benjamin, J. R. and Cornell, C. A. (1970). *Probability, Statistics and Decision for Civil Engineers*. McGraw Hill Book Company.

[Bobadilla and Chopra, 2007] Bobadilla, H. and Chopra, A. K. (2007). Modal pushover analysis for seismic evaluation of reinforced concrete special moment resisting frame buildings. Technical report, Earthquake Engineering Research Center: University of California, Berkeley.

[Bommer and Acevedo, 2004] Bommer, J. and Acevedo, A. (2004). The use of real earthquake accelerograms as input to dynamic analysis. *Journal of Earthquake Engineering*, 8:43–91.

[Bommer et al., 2009] Bommer, J. J., Stafford, P. J., and Alarcón, J. E. (2009). Empirical equations for the prediction of the significant, bracketed, and uniform duration of earthquake ground motion. *Bulletin of the Seismological Society of America*, 99(6):3217–3233.

[Boore and Atkinson, 2008] Boore, D. M. and Atkinson, G. M. (2008). Ground-motion prediction equations for the average horizontal component of PGA, PGV, and 5%-damped PSA at spectral periods between 0.01 s and 10.0 s. *Earthquake Spectra*, 24(1):99–138.

[Bozorgnia et al., 2014] Bozorgnia, Y., Abrahamson, N. A., Atik, L. A., Ancheta, T. D., Atkinson, G. M., Baker, J. W., Baltay, A., Boore, D. M., Campbell, K. W., Chiou, B. S.-J., et al. (2014). NGA-West2 research project. *Earthquake Spectra*, 30(3):973–987.

[Bozorgnia and Bertero, 2004] Bozorgnia, Y. and Bertero, V. V. (2004). *Earthquake engineering: From engineering seismology to performance-based engineering*. CRC Press, Boca Raton, Fla.

[Bradley, 2012a] Bradley, B. (2012a). A ground motion selection algorithm based on the generalized conditional intensity measure approach. *Soil Dynamics and Earthquake Engineering*, 40:48–61.

[Bradley, 2009] Bradley, B. A. (2009). Seismic hazard epistemic uncertainty in the San Francisco Bay Area and its role in performance-based assessment. *Earthquake Spectra*, 25(4):733–753.

[Bradley, 2010a] Bradley, B. A. (2010a). A generalized conditional intensity measure approach and holistic ground-motion selection. *Earthquake Engineering & Structural Dynamics*, 39(12):1321–1342.

[Bradley, 2010b] Bradley, B. A. (2010b). Site-specific and spatially distributed ground-motion prediction of acceleration spectrum intensity. *Bulletin of the Seismological Society of America*, 100(2):792–801.

[Bradley, 2011] Bradley, B. A. (2011). Empirical equations for the prediction of displacement spectrum intensity and its correlation with other intensity measures. *Soil Dynamics and Earthquake Engineering*, 31(8):1182–1191.

[Bradley, 2012b] Bradley, B. A. (2012b). Empirical correlations between cumulative absolute velocity and amplitude-based ground motion intensity measures. *Earthquake Spectra*, 28(1):37–54.

[Bradley, 2012c] Bradley, B. A. (2012c). The seismic demand hazard and importance of the conditioning intensity measure. *Earthquake Engineering & Structural Dynamics*, 41(11):1417–1437.

[Bradley, 2013a] Bradley, B. A. (2013a). A comparison of intensity-based demand distributions and the seismic demand hazard for seismic performance assessment. *Earthquake Engineering & Structural Dynamics*, 42(15):2235–2253.

[Bradley, 2013b] Bradley, B. A. (2013b). Practice-oriented estimation of the seismic demand hazard using ground motions at few intensity levels. *Earthquake Engineering & Structural Dynamics*, 42(14):2167–2185.

[Bradley et al., 2015] Bradley, B. A., Burks, L. S., and Baker, J. W. (2015). Ground motion selection for simulation-based seismic hazard and structural reliability assessment. *Earthquake Engineering & Structural Dynamics*. (in press).

[Campbell and Bozorgnia, 2008] Campbell, K. W. and Bozorgnia, Y. (2008). NGA ground motion model for the geometric mean horizontal component of PGA, PGV, PGD and 5% damped linear elastic response spectra for periods ranging from 0.01 to 10 s. *Earthquake Spectra*, 24:139.

[Campbell and Bozorgnia, 2010] Campbell, K. W. and Bozorgnia, Y. (2010). A ground motion prediction equation for the horizontal component of cumulative absolute velocity (CAV) based on the PEER-NGA strong motion database. *Earthquake Spectra*, 26(3):635–650.

[Carlton and Abrahamson, 2014] Carlton, B. and Abrahamson, N. (2014). Issues and approaches for implementing conditional mean spectra in practice. *Bulletin of the Seismological Society of America*, 104(1):503–512.

[Chapman, 1995] Chapman, M. C. (1995). A probabilistic approach to ground-motion selection for engineering design. *Bulletin of the Seismological Society of America*, 85(3):937–942.

[Chiou and Youngs, 2008] Chiou, B.-J. and Youngs, R. R. (2008). An NGA model for the average horizontal component of peak ground motion and response spectra. *Earthquake Spectra*, 24(1):173–215.

[Chopra, 2011] Chopra, A. K. (2011). *Dynamics of structures: Theory and applications to earthquake engineering*. Pearson Prentice Hall, Upper Saddle River, NJ, 4th edition.

[Corigliano et al., 2012] Corigliano, M., Lai, C. G., Rota, M., and Strobbia, C. L. (2012). ASCONA: automated selection of compatible natural accelerograms. *Earthquake Spectra*, 28(3):965–987.

[Der Kiureghian, 2005] Der Kiureghian, A. (2005). Non-ergodicity and PEER's framework formula. *Earthquake Engineering & Structural Dynamics*, 34(13):1643–1652.

[Der Kiureghian and Fujimura, 2009] Der Kiureghian, A. and Fujimura, K. (2009). Nonlinear stochastic dynamic analysis for performance-based earthquake engineering. *Earthquake Engineering & Structural Dynamics*, 38(5):719–738.

[Douglas and Aochi, 2008] Douglas, J. and Aochi, H. (2008). A survey of techniques for predicting earthquake ground motions for engineering purposes. *Surveys in geophysics*, 29(3):187–220.

[Efron and Tibshirani, 1993] Efron, B. and Tibshirani, R. (1993). *An introduction to the bootstrap*, volume 57. Chapman & Hall/CRC.

[Field et al., 2005] Field, E. H., Gupta, N., Gupta, V., Blanpied, M., Maechling, P., and Jordan, T. H. (2005). Hazard calculations for the WGCEP-2002 earthquake forecast using OpenSHA and distributed object technologies. *Seismological Research Letters*, 76(2):161–167.

[Goulet et al., 2007] Goulet, C. A., Haselton, C. B., Mitrani-Reiser, J., Beck, J. L., Deierlein, G. G., Porter, K. A., and Stewart, J. P. (2007). Evaluation of the seismic performance of a code-conforming reinforced-concrete frame buildingfrom seismic hazard to collapse safety and economic losses. *Earthquake Engineering & Structural Dynamics*, 36(13):1973–1997.

[Grigoriu, 2010] Grigoriu, M. (2010). To scale or not to scale seismic ground-acceleration records. *ASCE Journal of Engineering Mechanics*, 137(4):284–293.

[Hancock et al., 2008] Hancock, J., Bommer, J. J., and Stafford, P. J. (2008). Numbers of scaled and matched accelerograms required for inelastic dynamic analyses. *Earthquake Engineering & Structural Dynamics*, 37(14):1585–1607.

[Haselton and Baker, 2006] Haselton, C. and Baker, J. (2006). Ground motion intensity measures for collapse capacity prediction: Choice of optimal spectral period and effect of spectral shape. In *8th National Conference on Earthquake Engineering*, pages 18–22.

[Heo et al., 2010] Heo, Y., Kunnath, S. K., and Abrahamson, N. (2010). Amplitude-scaled versus spectrum-matched ground motions for seismic performance assessment. *ASCE Journal of Structural Engineering*, 137(3):278–288.

[Hesterberg, 2003] Hesterberg, T. (2003). *Advances in Importance Sampling*. PhD thesis, Department of Statistics, Stanford University, Stanford, CA.

[Ibarra et al., 2005] Ibarra, L. F., Medina, R. A., and Krawinkler, H. (2005). Hysteretic models that incorporate strength and stiffness deterioration. *Earthquake engineering & structural dynamics*, 34(12):1489–1511.

[Iervolino and Cornell, 2005] Iervolino, I. and Cornell, C. (2005). Record selection for nonlinear seismic analysis of structures. *Earthquake Spectra*, 21(3):685–713.

[Jayaram and Baker, 2008] Jayaram, N. and Baker, J. W. (2008). Statistical tests of the joint distribution of spectral acceleration values. *Bulletin of the Seismological Society of America*, 98(5):2231–2243.

[Jayaram et al., 2011] Jayaram, N., Lin, T., and Baker, J. W. (2011). A computationally efficient ground-motion selection algorithm for matching a target response spectrum mean and variance. *Earthquake Spectra*, 27(3):797–815.

[Kalkan and Chopra, 2011] Kalkan, E. and Chopra, A. K. (2011). Modal-pushover-based ground-motion scaling procedure. *ASCE Journal of Structural Engineering*, 137(3):298–310.

[Katsanos et al., 2010] Katsanos, E. I., Sextos, A. G., and Manolis, G. D. (2010). Selection of earthquake ground motion records: A state-of-the-art review from a structural engineering perspective. *Soil Dynamics and Earthquake Engineering*, 30(4):157–169.

[Kottke and Rathje, 2008] Kottke, A. and Rathje, E. M. (2008). A semi-automated procedure for selecting and scaling recorded earthquake motions for dynamic analysis. *Earthquake Spectra*, 24(4):911–932.

[Kramer, 1996] Kramer, S. L. (1996). *Geotechnical earthquake engineering*, volume 1. Prentice-Hall Civil Engineering and Engineering Mechanics Series, Upper Saddle River, NJ.

[Kwong et al., 2014] Kwong, N. S., Chopra, A. K., and McGuire, R. K. (2014). A framework for the evaluation of ground motion selection and modification procedures. *Earthquake Engineering & Structural Dynamics*, 44(5):795–815. DOI: 10.1002/eqe.2502.

[Kwong et al., 2015a] Kwong, N. S., Chopra, A. K., and McGuire, R. K. (2015a). Authors Reply to the discussion by Brendon A. Bradley of A framework for the evaluation of ground motion selection and modification procedures. *Earthquake Engineering & Structural Dynamics*, 44(5):823–828.

[Kwong et al., 2015b] Kwong, N. S., Chopra, A. K., and McGuire, R. K. (2015b). Evaluation of ground motion selection and modification procedures using synthetic ground motions. *Earthquake Engineering & Structural Dynamics*. DOI: 10.1002/eqe.2558.

[Kwong et al., 2015c] Kwong, N. S., Chopra, A. K., and McGuire, R. K. (2015c). A ground motion selection procedure for enforcing hazard consistency and estimating seismic demand hazard curves. *Earthquake Engineering & Structural Dynamics*, 44(14):2467–2487. DOI: 10.1002/eqe.2593.

[Lin, 2012] Lin, T. (2012). *Advancement of hazard-consistent ground motion selection methodology*. PhD thesis, Department of Civil and Environmental Engineering, Stanford University, Stanford, CA.

[Lin et al., 2013a] Lin, T., Harmsen, S. C., Baker, J. W., and Luco, N. (2013a). Conditional spectrum computation incorporating multiple causal earthquakes and ground-motion prediction models. *Bulletin of the Seismological Society of America*, 103(2A):1103–1116.

[Lin et al., 2013b] Lin, T., Haselton, C. B., and Baker, J. W. (2013b). Conditional spectrum-based ground motion selection. Part I: Hazard consistency for risk-based assessments. *Earthquake Engineering & Structural Dynamics*, 42(12):1847–1865.

[Luco and Bazzurro, 2007] Luco, N. and Bazzurro, P. (2007). Does amplitude scaling of ground motion records result in biased nonlinear structural drift responses? *Earthquake Engineering & Structural Dynamics*, 36(13):1813–1835.

[Luco and Cornell, 2007] Luco, N. and Cornell, C. A. (2007). Structure-specific scalar intensity measures for near-source and ordinary earthquake ground motions. *Earthquake Spectra*, 23(2):357–392.

[Malhotra, 2003] Malhotra, P. (2003). Strong-motion records for site-specific analysis. *Earthquake Spectra*, 19(3):557–578.

[Mazzoni et al., 2006] Mazzoni, S., McKenna, F., Scott, M. H., Fenves, G. L., et al. (2006). *OpenSees command language manual*. Pacific Earthquake Engineering Research (PEER) Center at University of California, Berkeley, Berkeley, CA.

[McGuire, 1995] McGuire, R. K. (1995). Probabilistic seismic hazard analysis and design earthquakes: Closing the loop. *Bulletin of the Seismological Society of America*, 85(5):1275–1284.

[McGuire, 2004] McGuire, R. K. (2004). *Seismic hazard and risk analysis*. Earthquake Engineering Research Institute, Oakland, CA.

[McKenna and Fenves, 2008] McKenna, F. and Fenves, G. L. (2008). Using the OpenSees interpreter on parallel computers, NEESit Report No. TN-2007-16. Technical report, Network for Earthquake Engineering Simulation, National Science Foundation, Washington, D.C.

[NEHRP Consultants Joint Venture, 2011] NEHRP Consultants Joint Venture (2011). Selecting and scaling earthquake ground motions for performing response-history analyses, NIST GCR 11-917-15. Technical report, National Institute of Standards and Technology, Washington, D.C.

[PEER GMSM Working Group, 2009] PEER GMSM Working Group (2009). Evaluation of ground motion selection and modification methods: Predicting median interstory drift response of buildings. PEER Report 01, PEER Center, Berkeley, CA.

[Porter et al., 2007] Porter, K., Kennedy, R., and Bachman, R. (2007). Creating fragility functions for performance-based earthquake engineering. *Earthquake Spectra*, 23(2):471–489.

[Power et al., 2008] Power, M., Chiou, B., Abrahamson, N., Bozorgnia, Y., Shantz, T., and Roblee, C. (2008). An overview of the NGA project. *Earthquake Spectra*, 24(1):3–21.

[Rezaeian and Der Kiureghian, 2008] Rezaeian, S. and Der Kiureghian, A. (2008). A stochastic ground motion model with separable temporal and spectral nonstationarities. *Earthquake Engineering & Structural Dynamics*, 37(13):1565–1584.

[Rezaeian and Der Kiureghian, 2010] Rezaeian, S. and Der Kiureghian, A. (2010). Simulation of synthetic ground motions for specified earthquake and site characteristics. *Earthquake Engineering & Structural Dynamics*, 39(10):1155–1180.

[Riddell, 2007] Riddell, R. (2007). On ground motion intensity indices. *Earthquake Spectra*, 23:147.

[Ross, 2013] Ross, S. M. (2013). *Simulation*. Elsevier.

[Seifried, 2013] Seifried, A. E. (2013). *Response spectrum compatibilization and its impact on structural response assessment*. PhD thesis, Department of Civil and Environmental Engineering, Stanford University, Stanford, CA.

[Shome, 1999] Shome, N. (1999). *Probabilistic seismic demand analysis of nonlinear structures*. PhD thesis, Department of Civil and Environmental Engineering, Stanford University, Stanford, CA.

[Shome et al., 1998] Shome, N., Cornell, C. A., Bazzurro, P., and Carballo, J. E. (1998). Earthquakes, records, and nonlinear responses. *Earthquake Spectra*, 14(3):469–500.

[Stewart et al., 2001] Stewart, J. P., Chiou, S.-J., Bray, J. D., Graves, R. W., Somerville, P. G., and Abrahamson., N. A. (2001). Ground motion evaluation procedures for performance-based design. Technical report, PEER Center: University of California Berkeley, Berkeley, CA.

[Tothong and Cornell, 2006] Tothong, P. and Cornell, C. A. (2006). An empirical ground-motion attenuation relation for inelastic spectral displacement. *Bulletin of the Seismological Society of America*, 96(6):2146–2164.

[Tothong and Luco, 2007] Tothong, P. and Luco, N. (2007). Probabilistic seismic demand analysis using advanced ground motion intensity measures. *Earthquake Engineering & Structural Dynamics*, 36(13):1837–1860.

[Vamvatsikos and Cornell, 2002] Vamvatsikos, D. and Cornell, C. (2002). Incremental dynamic analysis. *Earthquake Engineering & Structural Dynamics*, 31(3):491–514.

[Vamvatsikos and Cornell, 2004] Vamvatsikos, D. and Cornell, C. (2004). Applied incremental dynamic analysis. *Earthquake Spectra*, 20(2):523–553.

[Ventura et al., 2015] Ventura, C. E., Bebamzadeh, A., and Fairhurst, M. (2015). Efficient performance-based design using parallel and cloud computing. *The Structural Design of Tall and Special Buildings*. (in press).

[Wasserman, 2004] Wasserman, L. (2004). *All of statistics : a concise course in statistical inference*. Springer, New York.

[Watson-Lamprey and Abrahamson, 2006] Watson-Lamprey, J. and Abrahamson, N. (2006). Selection of ground motion time series and limits on scaling. *Soil Dynamics and Earthquake Engineering*, 26(5):477–482.

[Watson-Lamprey, 2007] Watson-Lamprey, J. A. (2007). *Selection and scaling of ground motion time series*. PhD thesis, Department of Civil and Environmental Engineering, University of California Berkeley, Berkeley, CA.

[Yamamoto, 2011] Yamamoto, Y. (2011). *Stochastic model for earthquake ground motion using wavelet packets*. PhD thesis, Department of Civil and Environmental Engineering, Stanford University, Stanford, CA.

[Yamamoto and Baker, 2013] Yamamoto, Y. and Baker, J. W. (2013). Stochastic model for earthquake ground motion using wavelet packets. *Bulletin of the Seismological Society of America*, 103(6):3044–3056.

[Yang et al., 2009] Yang, D., Pan, J., and Li, G. (2009). Non-structure-specific intensity measure parameters and characteristic period of near-fault ground motions. *Earthquake Engineering & Structural Dynamics*, 38(11):1257–1280.

[Youngs and Coppersmith, 1985] Youngs, R. R. and Coppersmith, K. J. (1985). Implications of fault slip rates and earthquake recurrence models to probabilistic seismic hazard estimates. *Bulletin of the Seismological society of America*, 75(4):939–964.

Appendix A

Derivations for the Proposed Importance Sampling Procedure

A.1 Derivation for Equation 4.7a

Let a randomly generated vector of IMs from the Importance Function (IF), $g_{\mathbf{X}}(\mathbf{x})$, be denoted by $\mathbf{X}$ and let a random sample of n vector-valued IMs be denoted by $\{\mathbf{X}_1, \ldots, \mathbf{X}_n\}$. Let a single element of the vector $\mathbf{X}_i$ be denoted by X_i and the rest of its elements be denoted by $\mathbf{X}_i^c$; that is, $\mathbf{X}_i = \{X_i, \mathbf{X}_i^c\}$. The resulting estimate of the hazard curve for an IM [1] is given by Equation 4.5a, repeated here for convenience:

$$\widehat{\lambda}_{IM}(x) = \frac{\nu_0}{n} \sum_{i=1}^{n} \left[I(X_i > x) \cdot w(\mathbf{X}_i) \right] \tag{A.1}$$

where x_i is capitalized and w_i is replaced by $w(\mathbf{X}_i)$ to emphasize that the hazard curve estimate is random because the IMs generated from the IF are random.

Taking the expectation of $\widehat{\lambda}_{IM}(x)$ in Equation A.1 with respect to $g_{\mathbf{X}}(\mathbf{x})$ gives

$$\begin{aligned}
\mathbb{E}_{\mathbf{X}}\left[\widehat{\lambda}_{IM}(x)\right] &= \nu_0 \cdot \mathbb{E}_{\mathbf{X}}\left[I(X_1 > x) \cdot w(\mathbf{X}_1) \right] \\
&= \nu_0 \int_{\mathbf{s}} \left[I(s > x) \cdot w(\mathbf{s}) \right] \, g(\mathbf{s}) \, \mathrm{d}\mathbf{s} \\
&= \nu_0 \int_{s} \int_{\mathbf{s}^c} \left[I(s > x) \, f(\mathbf{s}) \right] \mathrm{d}\mathbf{s}^c \, \mathrm{d}s \\
&= \nu_0 \int_{s} I(s > x) \left(\int_{\mathbf{s}^c} f(\mathbf{s}) \, \mathrm{d}\mathbf{s}^c \right) \mathrm{d}s \\
&= \nu_0 \int_{x}^{\infty} f(s) \, \mathrm{d}s \\
&= \lambda_{IM}(x)
\end{aligned} \tag{A.2}$$

[1] Only IMs included in **IM** are considered in this section.

where each transition is obtained from:

1. Each i^{th} vector, $\mathbf{X}_i$, is independent and identically distributed, with the joint distribution as $g_{\mathbf{X}}(\mathbf{x})$.
2. Rule of the lazy statistician.
3. Definition of Importance Sampling weight and rewriting domain of integration.
4. Indicator function does not depend on $\mathbf{s}^c$.
5. Definition of the indicator function and definition of the marginal distribution, $f_X(s)$, relative to the joint distribution, $f_{\mathbf{X}}(\mathbf{s})$.
6. Definition of the complementary cumulative distribution function (CCDF) and application of Equation 4.2.

A.2 Derivation for Equation 4.7b

Let a randomly generated vector of IMs from the Importance Function (IF), $g_{\mathbf{X}}(\mathbf{x})$, be denoted by $\mathbf{X}$ and let a random sample of n vector-valued IMs be denoted by $\{\mathbf{X}_1, \ldots, \mathbf{X}_n\}$. Each vector-valued IM corresponds to a ground motion time series and hence, a random sample of vector-valued IMs corresponds to an ensemble of n ground motions. Let an arbitrary EDP of the ith ground motion be denoted by Z_i. The resulting estimate of the hazard curve for an EDP is given by Equation 4.5b, repeated here for convenience:

$$\widehat{\lambda}_{EDP}(z) = \frac{\nu_0}{n} \sum_{i=1}^{n} [I(Z_i > z) \cdot w(\mathbf{X}_i)] \tag{A.3}$$

where z_i is capitalized and w_i is replaced by $w(\mathbf{X}_i)$ to emphasize that the hazard curve estimate is random because the IMs generated from the IF are random. By introducing the IF, $g_{\mathbf{X}}(\mathbf{x})$, the joint probability distribution of Z and $\mathbf{X}$, denoted by $f_{Z,\mathbf{X}}(z, \mathbf{x}) = f_{Z|\mathbf{X}}(z \mid \mathbf{x}) \cdot f_{\mathbf{X}}(\mathbf{x})$ (see Figure 4.2), becomes $g_{Z,\mathbf{X}}(z, \mathbf{x}) = f_{Z|\mathbf{X}}(z \mid \mathbf{x}) \cdot g_{\mathbf{X}}(\mathbf{x})$.

Taking the expectation of $\widehat{\lambda}_Z(z)$ in Equation A.3 with respect to $g_{Z,\mathbf{X}}(z,\mathbf{x})$ gives

$$\begin{aligned}
\mathbb{E}_{Z,\mathbf{X}}\left[\widehat{\lambda}_{EDP}(z)\right] &= \nu_0 \cdot \mathbb{E}_{Z,\mathbf{X}}\left[I(Z_1 > z) \cdot w(\mathbf{X}_1)\right] \\
&= \nu_0 \int_t \int_{\mathbf{s}} \left[I(t > z) \cdot w(\mathbf{s})\right] \, g_{Z,\mathbf{X}}(t,\mathbf{s}) \, \mathrm{d}\mathbf{s} \, \mathrm{d}t \\
&= \nu_0 \int_t I(t > z) \int_{\mathbf{s}} w(\mathbf{s}) \left[f_{Z|\mathbf{X}}(t \mid \mathbf{s}) \, g(\mathbf{s})\right] \mathrm{d}\mathbf{s} \, \mathrm{d}t \\
&= \nu_0 \int_z^\infty \left(\int_{\mathbf{s}} f(\mathbf{s}) \, f_{Z|\mathbf{X}}(t \mid \mathbf{s}) \, \mathrm{d}\mathbf{s} \right) \mathrm{d}t \\
&= \nu_0 \int_z^\infty f_Z(t) \, \mathrm{d}t \\
&= \lambda_{EDP}(z)
\end{aligned} \tag{A.4}$$

where each transition is obtained from:

1. Each i^{th} vector $(\mathbf{X}, Z)_i$ is independent and identically distributed, with the joint distribution as $g_{Z,\mathbf{X}}(t,\mathbf{s}) = f_{Z|\mathbf{X}}(t \mid \mathbf{s}) \cdot g(\mathbf{s})$.
2. Rule of the lazy statistician.
3. Indicator function does not depend on $\mathbf{s}$ and definition of joint distribution $g_{Z,\mathbf{X}}(t,\mathbf{s})$.
4. Definitions of the indicator function and of the Importance Sampling weight.
5. Marginal distribution $f_Z(t)$ from joint distribution $f_{Z,\mathbf{X}}(t,\mathbf{s}) = f(\mathbf{s}) \cdot f_{Z|\mathbf{X}}(t \mid \mathbf{s})$ (see Figure 4.2).
6. Definition of CCDF and use of Equation 4.2.

The expected values of the hazard curve estimates for IMs that are excluded from those chosen to select ground motions (i.e., $IM \notin \mathbf{IM}$) may be derived in a fashion similar to that presented in this section.

A.3 Derivation for Equation 4.8

The variance of $\widehat{\lambda}_{IM}(x)$ in Equation A.1, with respect to the joint distribution of $\mathbf{X}$, is

$$\begin{aligned}
\mathbb{V}_{\mathbf{X}}\left[\widehat{\lambda}_{IM}(x)\right] &= \frac{\nu_0^2}{n} \cdot \mathbb{V}_{\mathbf{X}}\left[I(X_1 > x) \cdot w(\mathbf{X}_1)\right] \\
&= \frac{\nu_0^2}{n} \left\{ \mathbb{E}_{\mathbf{X}}\left[\left[I(X_1 > x) \cdot w(\mathbf{X}_1)\right]^2\right] - \left(\mathbb{E}_{\mathbf{X}}\left[I(X_1 > x) \cdot w(\mathbf{X}_1)\right]\right)^2 \right\} \\
&= \frac{1}{n} \left\{ \nu_0^2 \cdot \mathbb{E}_{\mathbf{X}}\left[\left[I(X_1 > x) \cdot w(\mathbf{X}_1)\right]^2\right] - \lambda_{IM}^2(x) \right\}
\end{aligned} \tag{A.5}$$

where each transition is obtained from:

1. Each $\mathbf{X}_i$ is independent and identically distributed with the joint distribution as $g(\mathbf{x})$.
2. Computational formula for variance.
3. Recognizing that $\nu_0 \cdot \mathbb{E}_{\mathbf{X}}\left[I(X_1 > x) \cdot w(\mathbf{X}_1)\right] = \lambda_{IM}(x)$ (see Equation A.2 in Section A.1).

The term $\mathbb{E}_{\mathbf{X}}\left[\left[I(X_1 > x) \cdot w(\mathbf{X}_1)\right]^2\right]$ in Equation A.5 may be rewritten as follows:

$$\begin{aligned}
\mathbb{E}_{\mathbf{X}}\left[\left[I(X_1 > x) \cdot w(\mathbf{X}_1)\right]^2\right] &= \int_{\mathbf{s}} \left[I(s > x) \cdot w(\mathbf{s})\right]^2 g(\mathbf{s})\, \mathrm{d}\mathbf{s} \\
&= \int_{\mathbf{s}} \left[I(s > x) \cdot w^2(\mathbf{s})\right] g(\mathbf{s})\, \mathrm{d}\mathbf{s} \\
&= \int\limits_{\mathbf{s}:s>x} \frac{f^2(\mathbf{s})}{g(\mathbf{s})}\, \mathrm{d}\mathbf{s} \qquad \text{(A.6)}
\end{aligned}$$

where each transition is obtained from:

1. Rule of the lazy statistician.
2. Square of the indicator function is the indicator function.
3. Definitions of the indicator function and of the Importance Sampling weight.

Substituting Equation A.6 into Equation A.5 gives

$$\mathbb{V}_{\mathbf{X}}\left[\widehat{\lambda}_{IM}(x)\right] = \frac{1}{n}\left\{\nu_0^2 \int\limits_{\mathbf{s}:s>x} \frac{f^2(\mathbf{s})}{g(\mathbf{s})}\, \mathrm{d}\mathbf{s} - \lambda_{IM}^2(x)\right\} \qquad \text{(A.7)}$$

A.4 Derivation for Equation 4.9

The variance of $\widehat{\lambda}_{EDP}(z)$ in Equation A.3, with respect to the joint distribution of Z and $\mathbf{X}$, is

$$\begin{aligned}
\mathbb{V}_{Z,\mathbf{X}}\left[\widehat{\lambda}_{EDP}(z)\right] &= \frac{\nu_0^2}{n} \cdot \mathbb{V}_{Z,\mathbf{X}}\left[I(Z_1 > z) \cdot w(\mathbf{X}_1)\right] \\
&= \frac{\nu_0^2}{n}\left\{\mathbb{E}_{Z,\mathbf{X}}\left[\left[I(Z_1 > z) \cdot w(\mathbf{X}_1)\right]^2\right] - \left(\mathbb{E}_{Z,\mathbf{X}}\left[I(Z_1 > z) \cdot w(\mathbf{X}_1)\right]\right)^2\right\} \\
&= \frac{1}{n}\left\{\nu_0^2 \cdot \mathbb{E}_{Z,\mathbf{X}}\left[\left[I(Z_1 > z) \cdot w(\mathbf{X}_1)\right]^2\right] - \lambda_{EDP}^2(z)\right\} \qquad \text{(A.8)}
\end{aligned}$$

where each transition is obtained from:

1. Each i^{th} vector $(\mathbf{X}, Z)_i$ is independent and identically distributed, with the joint distribution as $g_{Z,\mathbf{X}}(t, \mathbf{s}) = f_{Z|\mathbf{X}}(t \mid \mathbf{s}) \cdot g(\mathbf{s})$.
2. Computational formula for variance.
3. Recognizing that $\nu_0 \cdot \mathbb{E}_{Z,\mathbf{X}}\left[I(Z_1 > z) \cdot w(\mathbf{X}_1)\right] = \lambda_{EDP}(z)$ (see Equation A.4 in Section A.2).

The term $\mathbb{E}_{Z,\mathbf{X}}\left[\left[I(Z_1 > z) \cdot w(\mathbf{X}_1)\right]^2\right]$ in Equation A.8 may be rewritten as follows:

$$\begin{aligned}
\mathbb{E}_{Z,\mathbf{X}}\left[\left[I(Z_1 > z) \cdot w(\mathbf{X}_1)\right]^2\right] &= \int_{\mathbf{s}}\int_{t} \left[I(t > z) \cdot w(\mathbf{s})\right]^2 \, g_{Z,\mathbf{X}}(t, \mathbf{s}) \, \mathrm{d}t \, \mathrm{d}\mathbf{s} \\
&= \int_{\mathbf{s}}\int_{t} \left[I(t > z) \cdot w^2(\mathbf{s})\right] \left[f_{Z|\mathbf{X}}(t \mid \mathbf{s}) \, g(\mathbf{s})\right] \mathrm{d}t \, \mathrm{d}\mathbf{s} \\
&= \int_{\mathbf{s}}\int_{t} \left[I(t > z) \cdot \frac{f^2(\mathbf{s})}{g(\mathbf{s})}\right] f_{Z|\mathbf{X}}(t \mid \mathbf{s}) \, \mathrm{d}t \, \mathrm{d}\mathbf{s} \\
&= \int_{\mathbf{s}} \left[\int_{t} I(t > z) \cdot f_{Z|\mathbf{X}}(t \mid \mathbf{s}) \, \mathrm{d}t\right] \frac{f^2(\mathbf{s})}{g(\mathbf{s})} \, \mathrm{d}\mathbf{s} \\
&= \int_{\mathbf{s}} \Pr(Z > z \mid \mathbf{X} = \mathbf{s}) \cdot \frac{f^2(\mathbf{s})}{g(\mathbf{s})} \, \mathrm{d}\mathbf{s} \qquad \text{(A.9)}
\end{aligned}$$

where each transition is obtained from:

1. Rule of the lazy statistician.
2. Square of the indicator function is the indicator function and definition of joint distribution $g_{Z,\mathbf{X}}(t, \mathbf{s})$.
3. Definition of the Importance Sampling weight.
4. The ratio $\frac{f^2(\mathbf{s})}{g(\mathbf{s})}$ does not depend on t.
5. Definition of conditional CCDF of $Z \mid X$.

Substituting Equation A.9 into Equation A.8 gives

$$\mathbb{V}_{Z,\mathbf{X}}\left[\widehat{\lambda}_{EDP}(z)\right] = \frac{1}{n}\left\{\nu_0^2 \int_{\mathbf{s}} \Pr(Z > z \mid \mathbf{X} = \mathbf{s}) \cdot \frac{f^2(\mathbf{s})}{g(\mathbf{s})} \, \mathrm{d}\mathbf{s} - \lambda_{EDP}^2(z)\right\} \qquad \text{(A.10)}$$

The variance of the hazard curve estimates for IMs that are excluded from those chosen to select ground motions (i.e., $IM \notin \mathbf{IM}$) may be derived in a fashion similar to that presented in this section.

A.5 Derivation for Equation 4.15

Given an observed value of the vector-valued IM from the Importance Function, $\mathbf{IM}_{IF}$, and a computed value of the vector-valued IM from the scaled ground motion time series, $\mathbf{IM}_{P}$, the optimal scale factor can be derived by first rewriting Equation 4.13 to express Δ as a quadratic function of the scale factor, SF. Substituting Equation 4.14 into Equation 4.13 and rearranging terms gives

$$\Delta = \sum_{j=1}^{N_{IM}} \left[\frac{\ln\left(\frac{IM_{IF,j}}{IM_{U,j}}\right) - \alpha_j \ln(SF)}{\sigma_j} \right]^2 \tag{A.11}$$

Setting the first derivative of Δ with respect to SF to zero leads to the scale factor that minimizes Δ:

$$\frac{\partial \Delta}{\partial SF} = \sum_{j=1}^{N_{IM}} 2 \left[\frac{\ln\left(\frac{IM_{IF,j}}{IM_{U,j}}\right) - \alpha_j \ln(SF)}{\sigma_j} \right] \left(\frac{-\alpha_j}{\sigma_j \cdot SF} \right) = 0 \tag{A.12}$$

Assuming SF is never zero, Equation A.12 is equivalent to:

$$\sum_{j=1}^{N_{IM}} \left[\frac{\ln\left(\frac{IM_{IF,j}}{IM_{U,j}}\right) - \alpha_j \ln(SF)}{\sigma_j} \right] \left(\frac{\alpha_j}{\sigma_j} \right) = 0 \tag{A.13}$$

Distributing the summation in Equation A.13 and rearranging terms gives

$$\sum_{j=1}^{N_{IM}} \left(\frac{\alpha_j}{\sigma_j^2} \right) \ln\left(\frac{IM_{IF,j}}{IM_{U,j}} \right) = \ln(SF) \left[\sum_{i=j}^{N_{IM}} \left(\frac{\alpha_j}{\sigma_j} \right)^2 \right] \tag{A.14}$$

Finally, isolating SF in Equation A.14 leads to the desired optimal scale factor:

$$SF_{optimal} = \exp\left\{ \frac{\sum_{j=1}^{N_{IM}} \left(\frac{\alpha_j}{\sigma_j^2} \right) \ln\left(\frac{IM_{IF,j}}{IM_{U,j}} \right)}{\sum_{j=1}^{N_{IM}} \left(\frac{\alpha_j}{\sigma_j} \right)^2} \right\} \tag{A.15}$$

Appendix B

Documentation of Developing Benchmark-Consistent Prediction Models

This appendix documents the development of benchmark-consistent prediction models that are needed to select ground motions within a universe of synthetic ground motions generated from a stochastic model. For both stochastic models – Rezaeian's and Yamamoto's – a total of 120 intensity measures (IMs) were considered. These IMs include 5%-damped spectral accelerations at the same vibration periods utilized in the NGA West 2 project [Bozorgnia et al., 2014] (i.e., a total of 111 periods ranging from 0.01 to 20 sec), peak ground acceleration (PGA), peak ground velocity (PGV), peak ground displacement (PGD), cumulative absolute velocity (CAV), acceleration spectrum intensity (ASI), spectrum intensity (SI), displacement spectrum intensity (DSI), 5-95% significant duration (D_{5-95}), and 5-75% significant duration (D_{5-75}).

B.1 Functional Forms

To facilitate the development of functional forms, the 120 IMs were partitioned into four categories: (i) spectral accelerations, (ii) peak ground parameters (PGA, PGV, and PGD), (iii) spectrum intensity related parameters (ASI, SI, and DSI), and (iv) cumulative based measures (CAV, D_{5-95}, and D_{5-75}). For each category and each stochastic model, a polynomial-based functional form (see Equation 3.13) was determined via the approach described in Section 3.6. In Rezaeian's model, the following functional forms were employed:

1. Spectral accelerations: linear
2. Peak ground parameters: linear
3. Spectrum intensity related parameters: linear
4. Cumulative based measures: cubic

In Yamamoto's model, the following functional forms were employed:

1. Spectral accelerations: purequadratic
2. Peak ground parameters: purequadratic
3. Spectrum intensity related parameters: purequadratic
4. Cumulative based measures: cubic

Figure 3.6 illustrated the linear and purequadratic functional forms; the cubic functional form is illustrated in Figure B.1. The determination of $\sigma_{optimal}$ is discussed next.

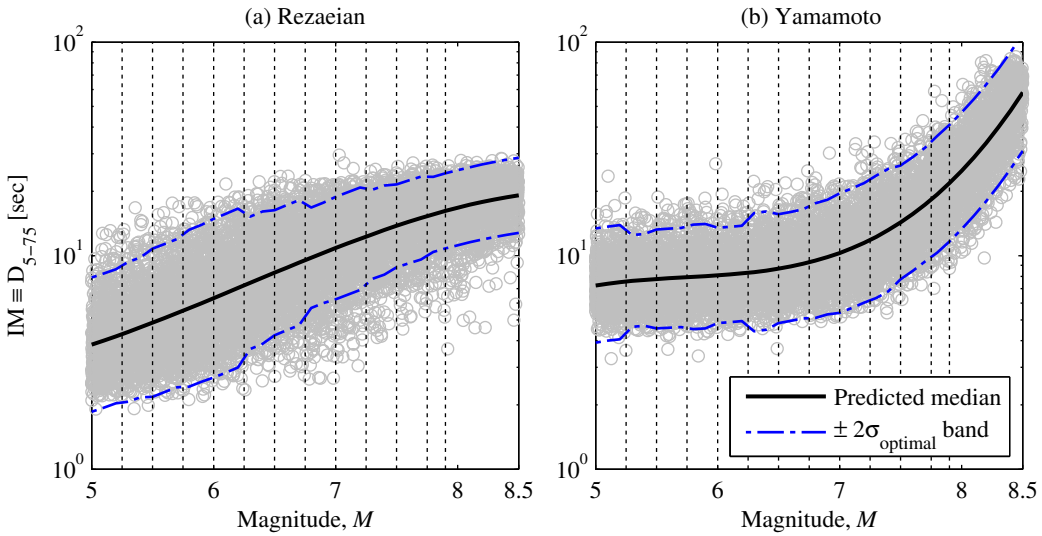

Figure B.1: Functional form for D_{5-75} under stochastic model from: (a) Rezaeian; (b) Yamamoto.

B.2 Benchmark Consistency of Ground-Motion-Prediction Models

Once the functional forms for all 120 IMs are finalized via exploratory data analysis, the standard deviations, σ, of the ground-motion-prediction models (GMPMs) were further adjusted to achieve consistency with respect to the benchmark, as elaborated in Section 3.6. In essence, the standard deviation is modeled as a nonparametric function of magnitude and at each magnitude interval, the value of σ was adjusted so that the GMPM-based estimate of the hazard curve agrees closely with the benchmark hazard curve (see Figure 3.7a). Figures B.2-B.19 document such hazard-consistent GMPMs for IMs unrelated to spectral accelerations.

B.3 Correlations between IMs

The correlation between IMs (more precisely, between the residuals of the IMs) were discussed in Section 3.6. As mentioned therein, the correlations were occasionally found to depend on the earthquake magnitude. For generality, the correlation between a pair of IMs is modeled as a function of the magnitude by computing a correlation for each magnitude interval shown schematically by the dotted lines in Figure B.1. The correlations between spectral accelerations at various vibration periods were shown in Figure 3.8; correlations between IMs that are unrelated to spectral accelerations were also computed.

B.4 Figures for Confirming Benchmark Consistency

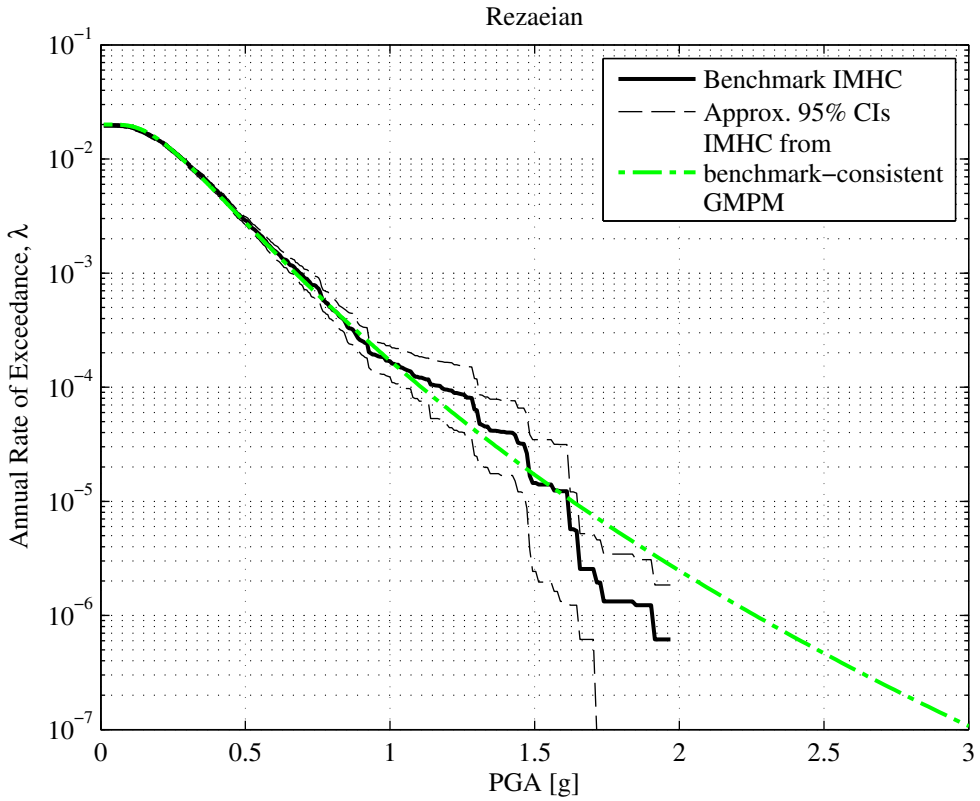

Figure B.2: Benchmark-consistency of GMPM for PGA under Rezaeian's stochastic model.

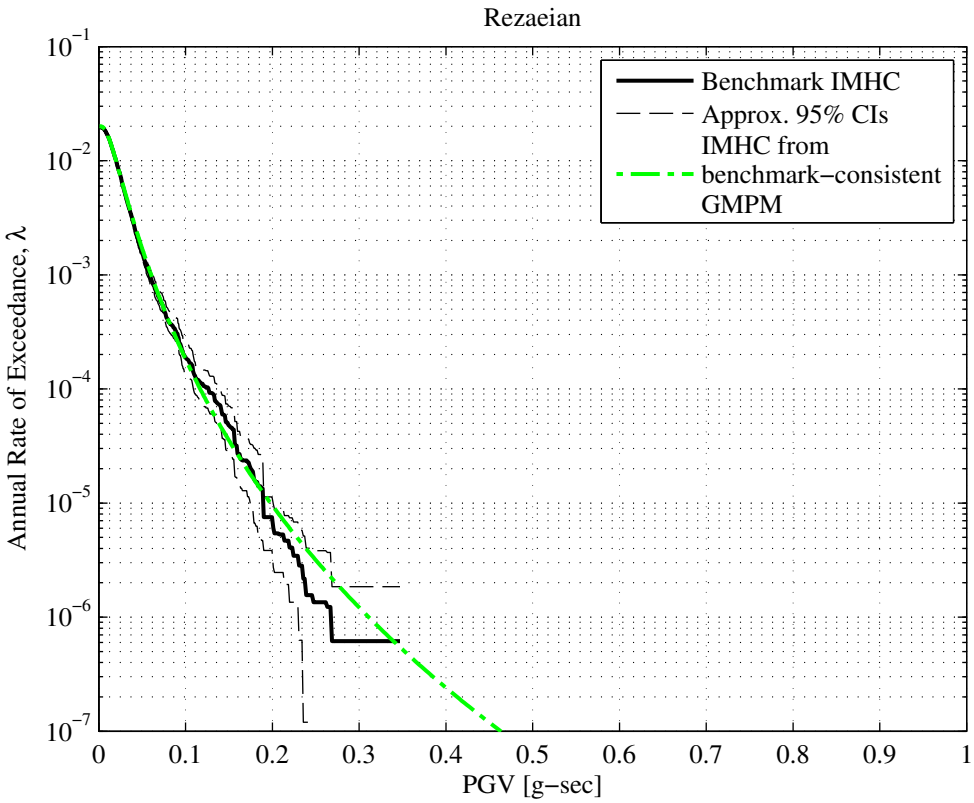

Figure B.3: Benchmark-consistency of GMPM for PGV under Rezaeian's stochastic model.

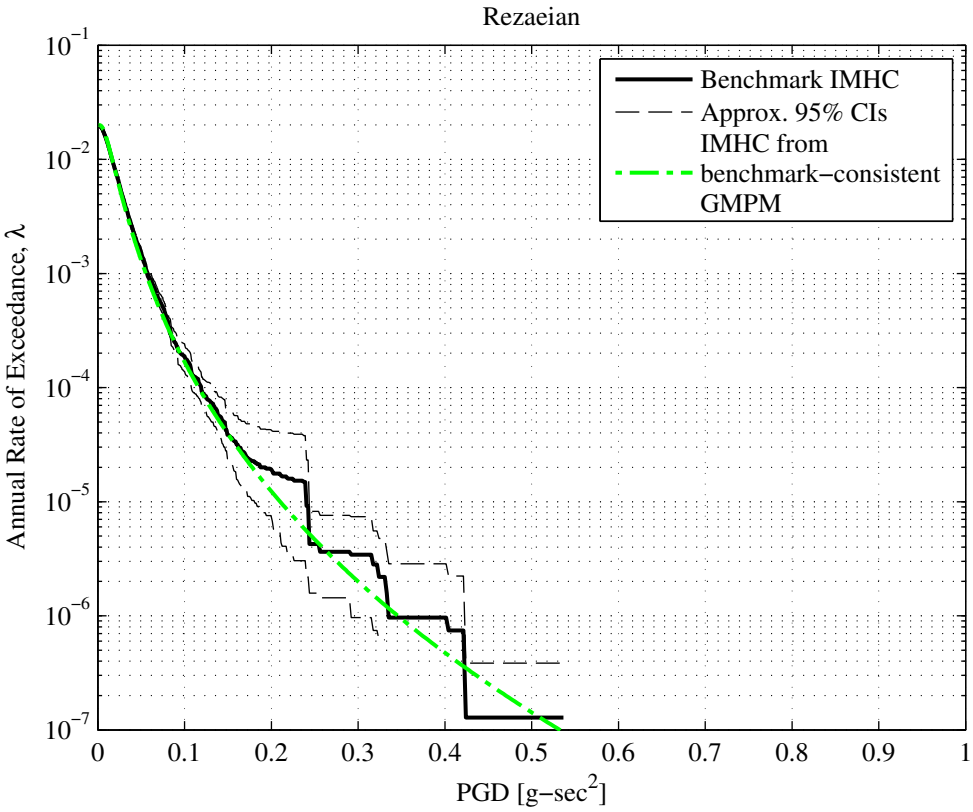

Figure B.4: Benchmark-consistency of GMPM for PGD under Rezaeian's stochastic model.

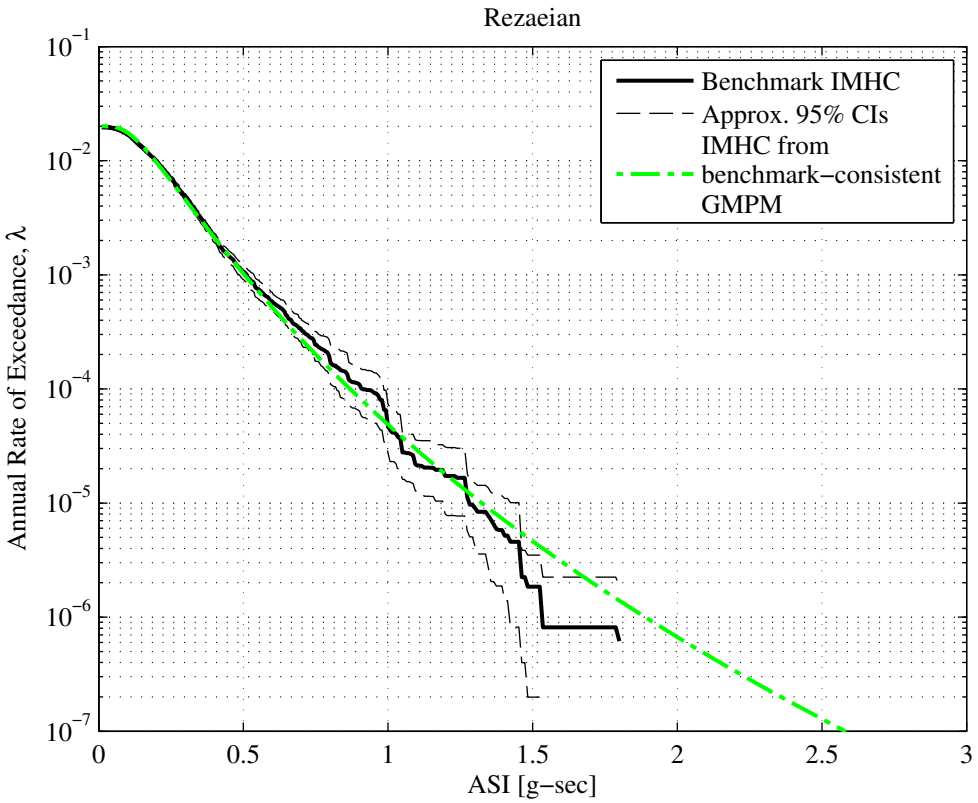

Figure B.5: Benchmark-consistency of GMPM for ASI under Rezaeian's stochastic model.

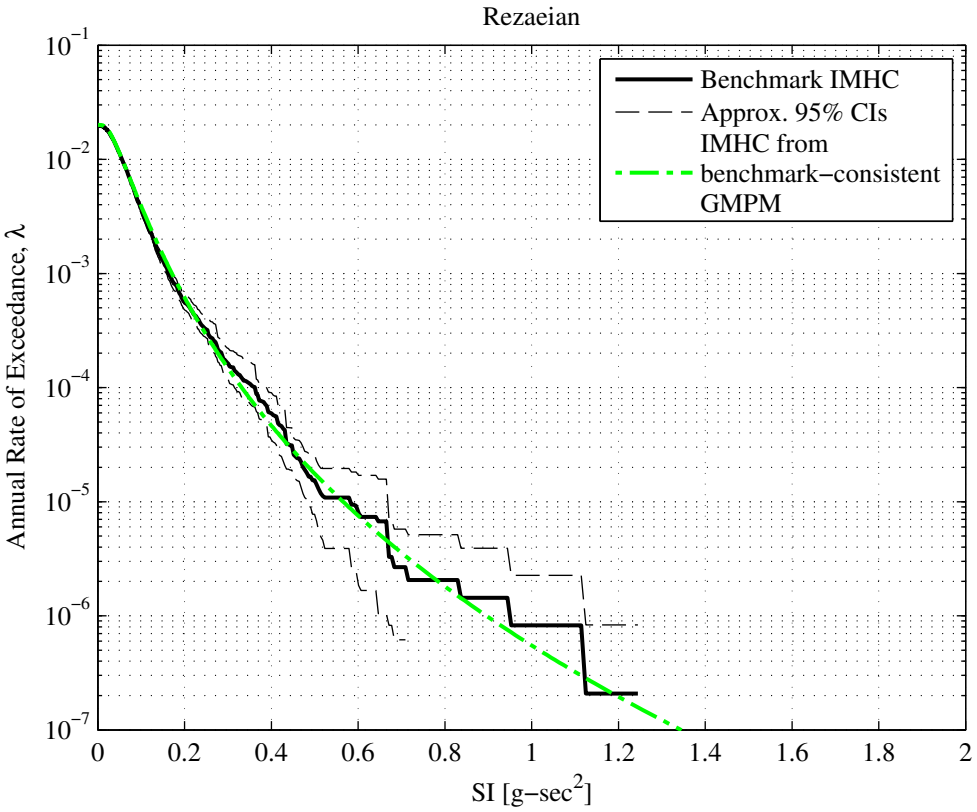

Figure B.6: Benchmark-consistency of GMPM for SI under Rezaeian's stochastic model.

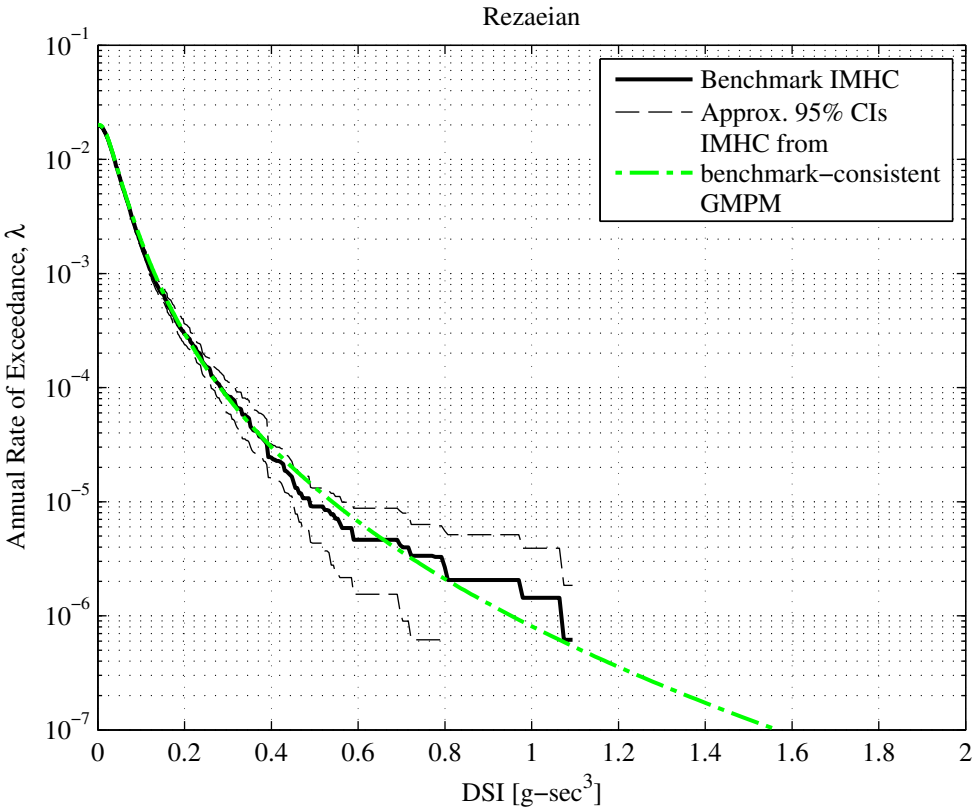

Figure B.7: Benchmark-consistency of GMPM for DSI under Rezaeian's stochastic model.

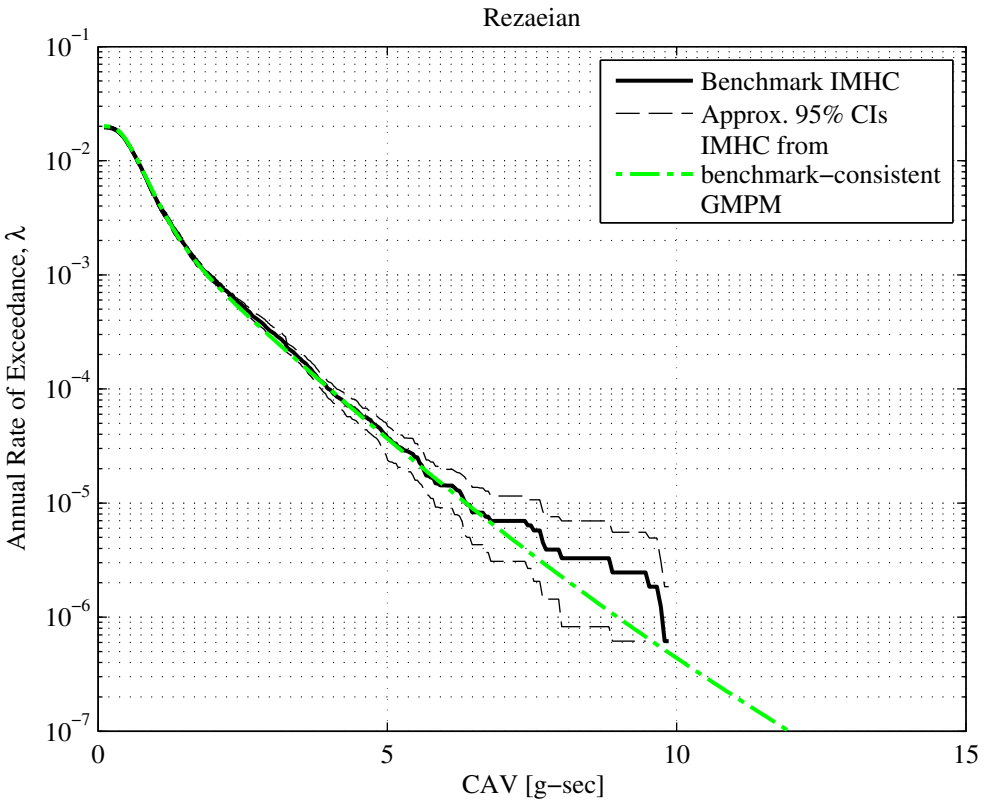

Figure B.8: Benchmark-consistency of GMPM for CAV under Rezaeian's stochastic model.

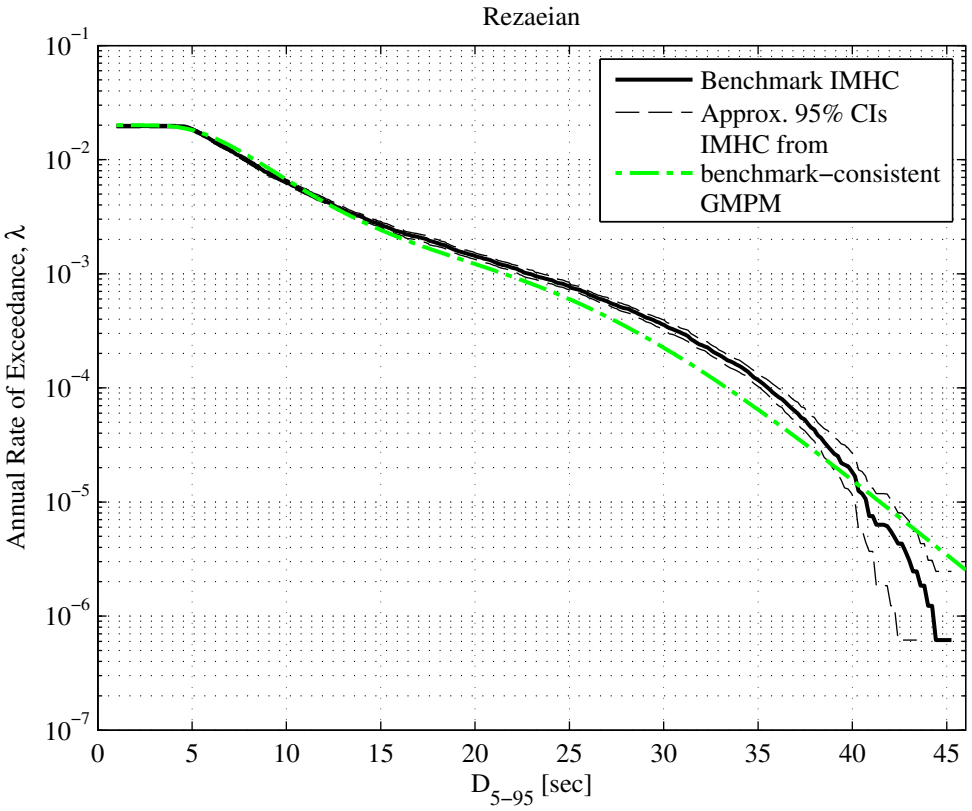

Figure B.9: Benchmark-consistency of GMPM for D_{5-95} under Rezaeian's stochastic model.

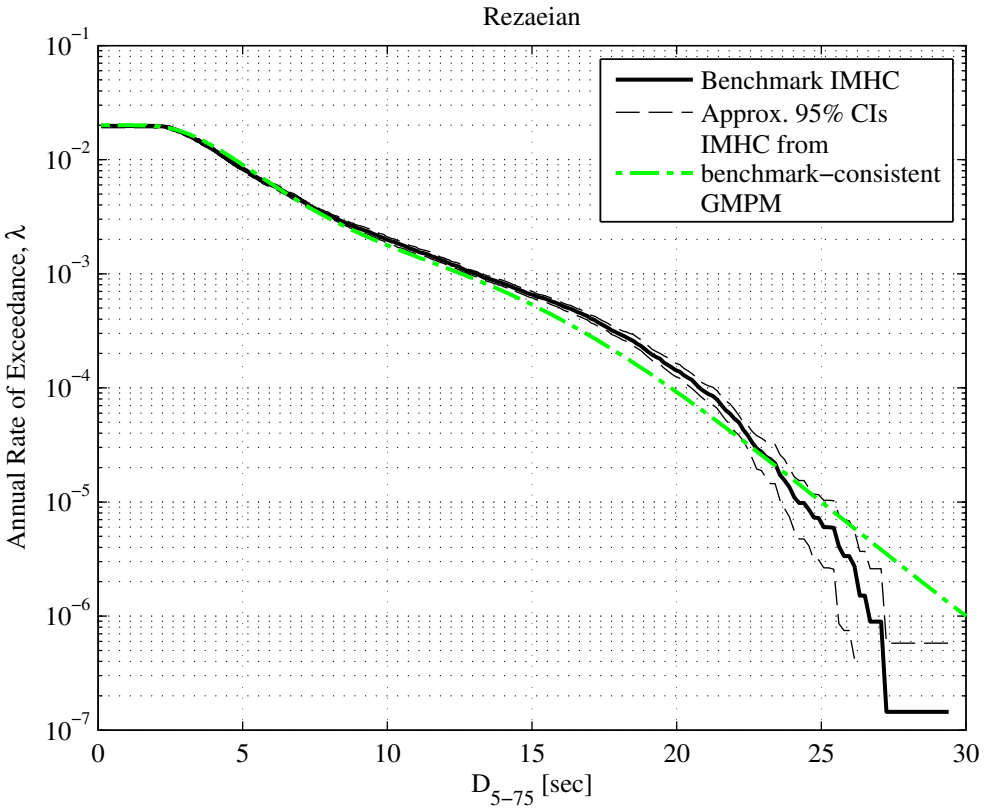

Figure B.10: Benchmark-consistency of GMPM for D_{5-75} under Rezaeian's stochastic model.

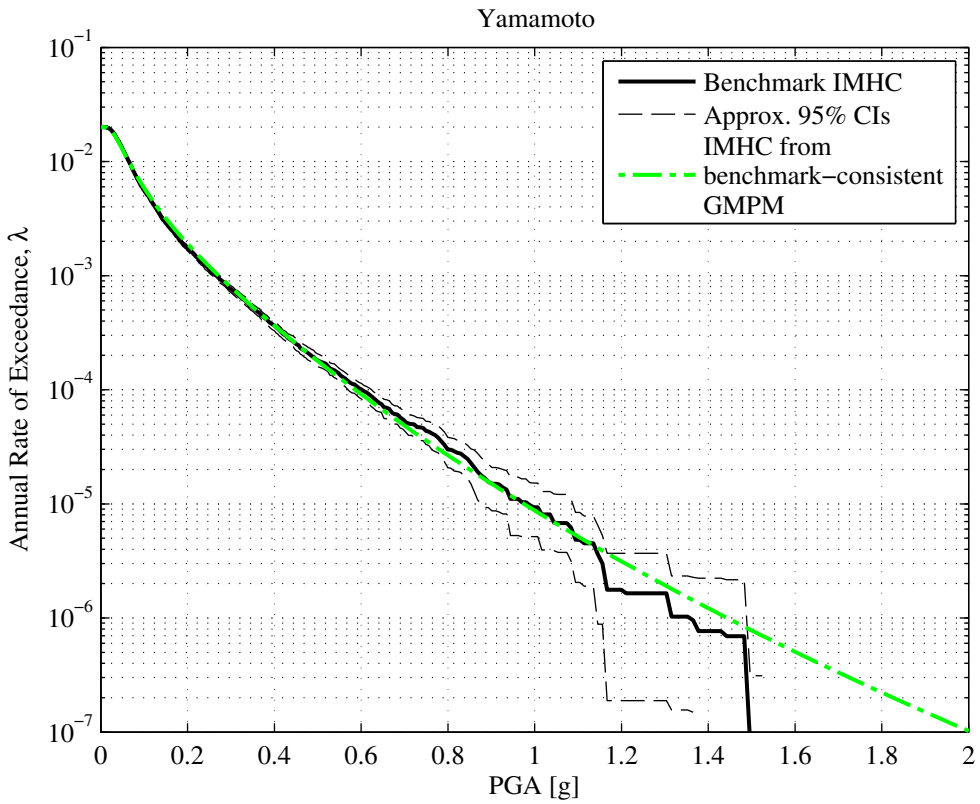

Figure B.11: Benchmark-consistency of GMPM for PGA under Yamamoto's stochastic model.

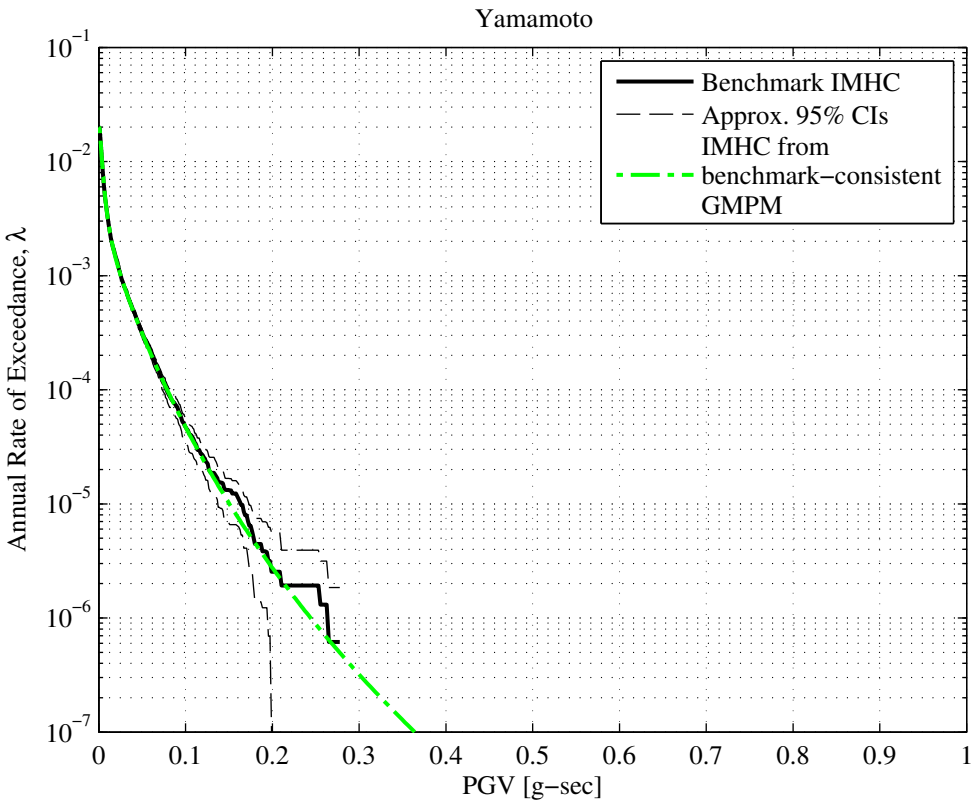

Figure B.12: Benchmark-consistency of GMPM for PGV under Yamamoto's stochastic model.

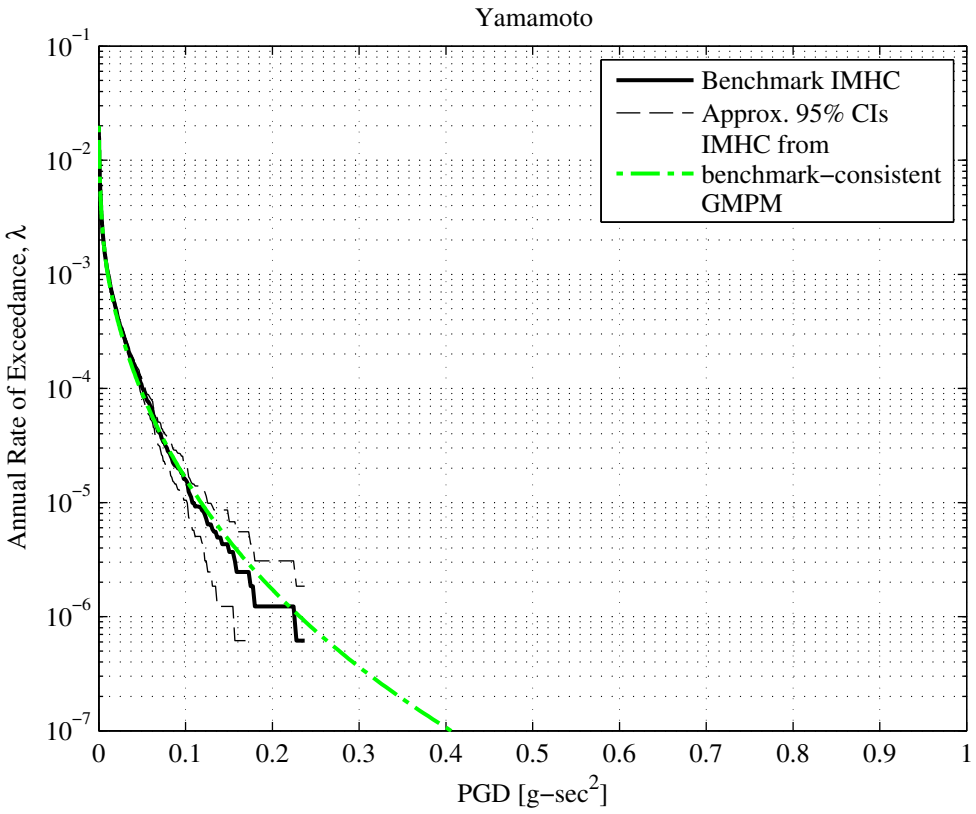

Figure B.13: Benchmark-consistency of GMPM for PGD under Yamamoto's stochastic model.

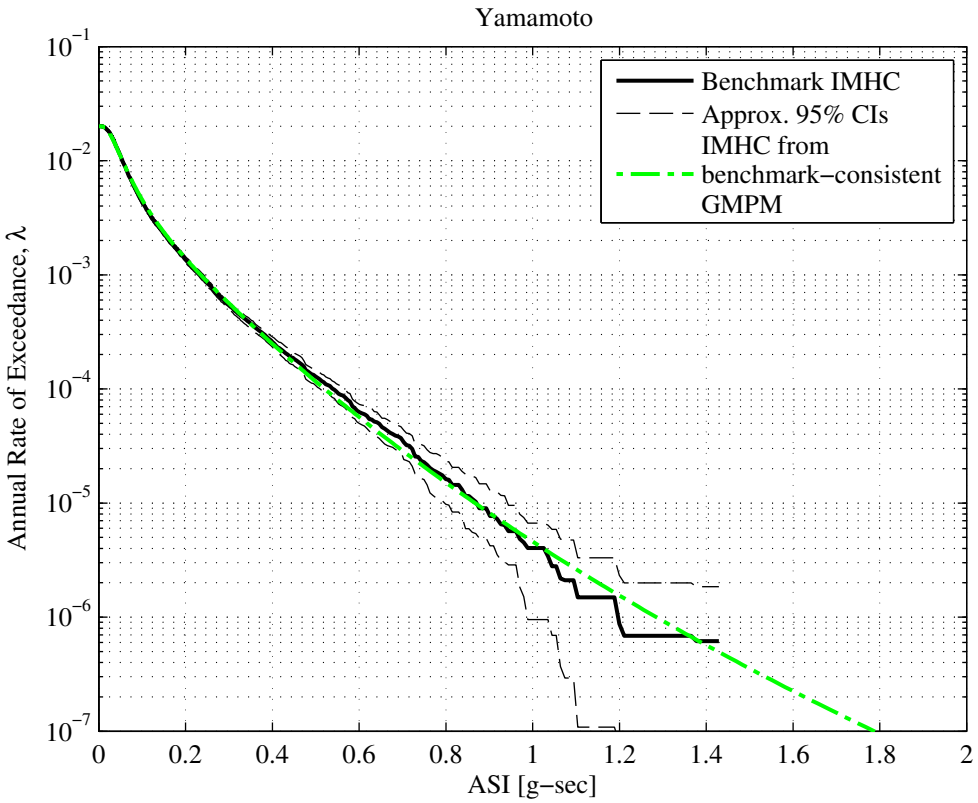

Figure B.14: Benchmark-consistency of GMPM for ASI under Yamamoto's stochastic model.

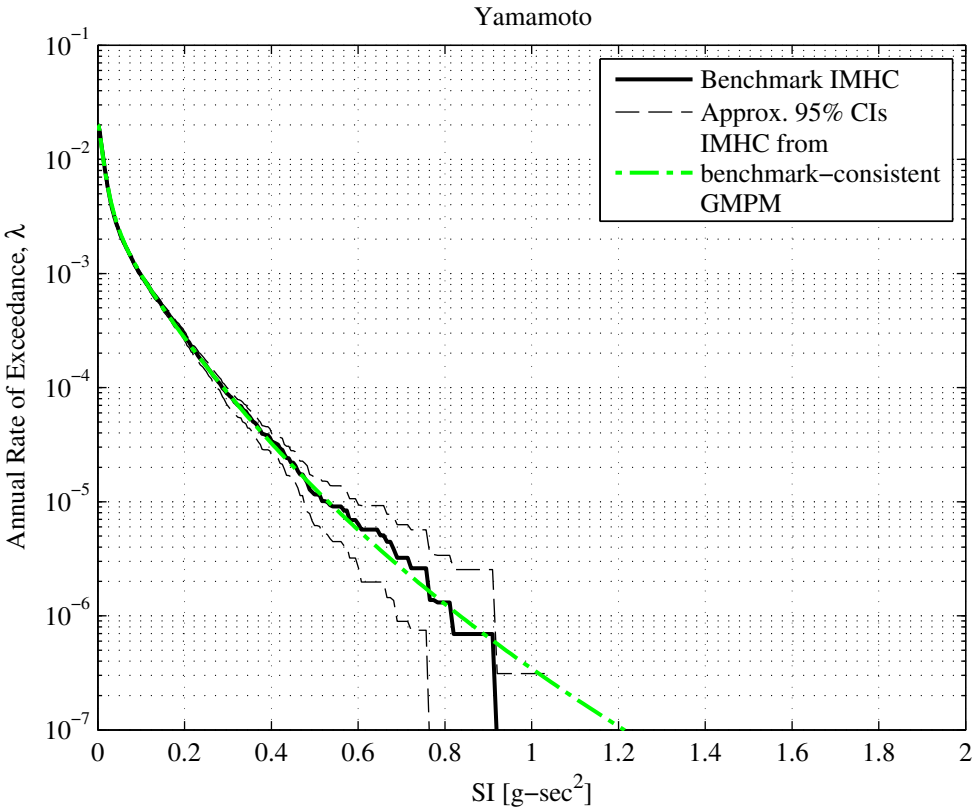

Figure B.15: Benchmark-consistency of GMPM for SI under Yamamoto's stochastic model.

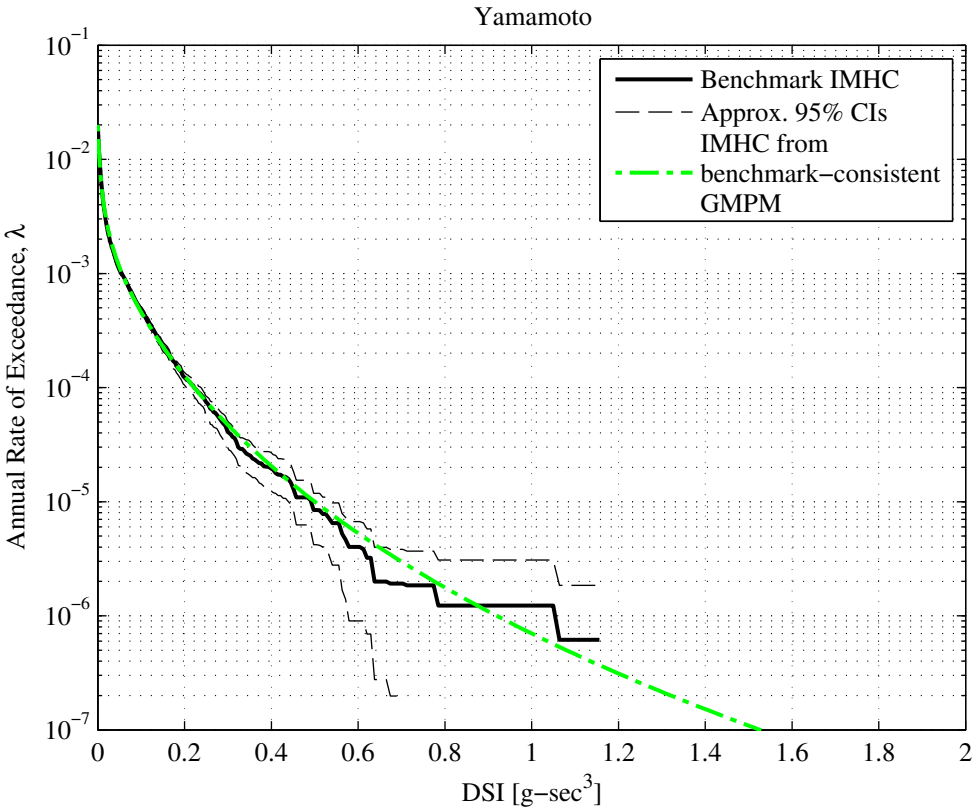

Figure B.16: Benchmark-consistency of GMPM for DSI under Yamamoto's stochastic model.

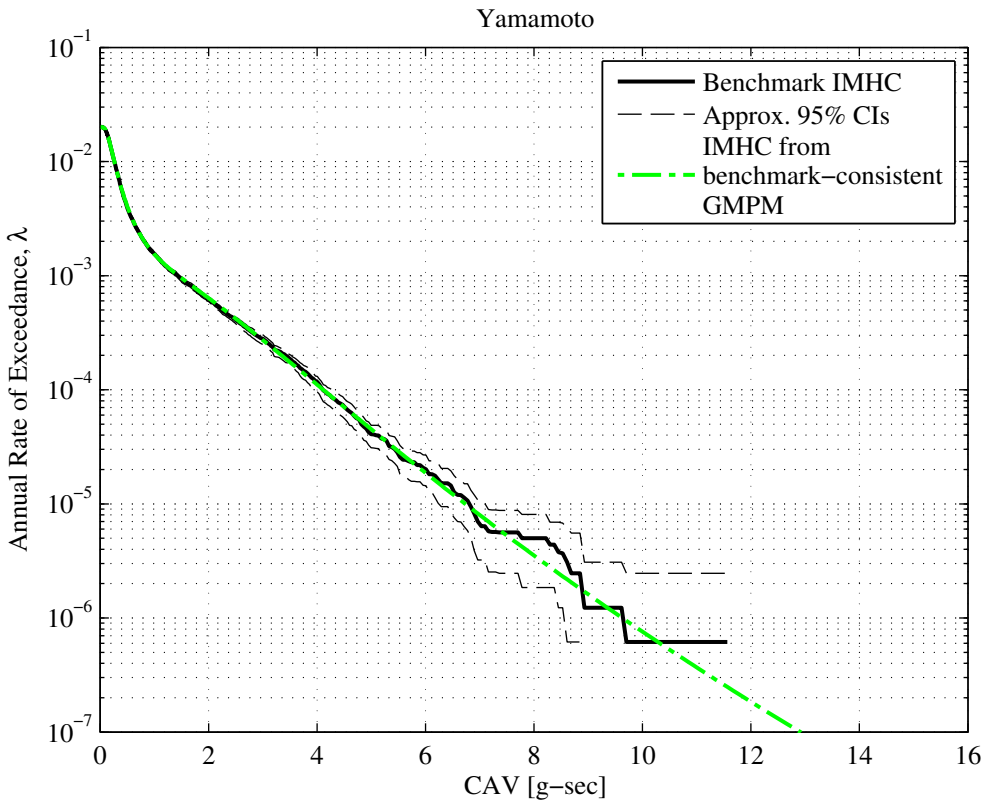

Figure B.17: Benchmark-consistency of GMPM for CAV under Yamamoto's stochastic model.

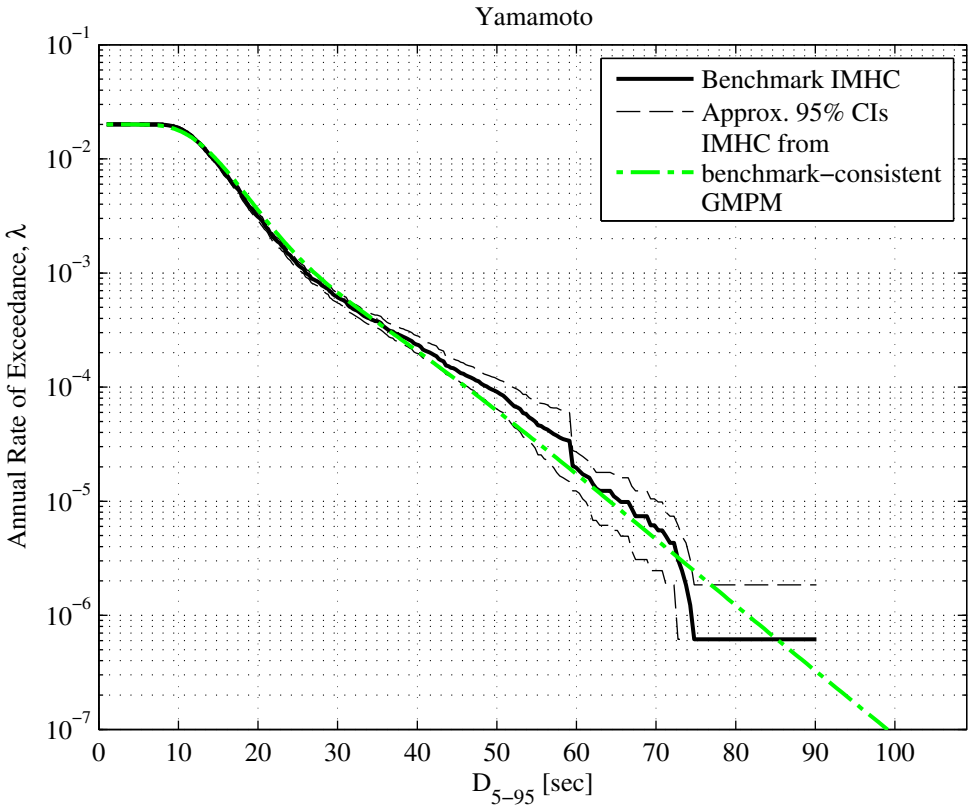

Figure B.18: Benchmark-consistency of GMPM for D_{5-95} under Yamamoto's stochastic model.

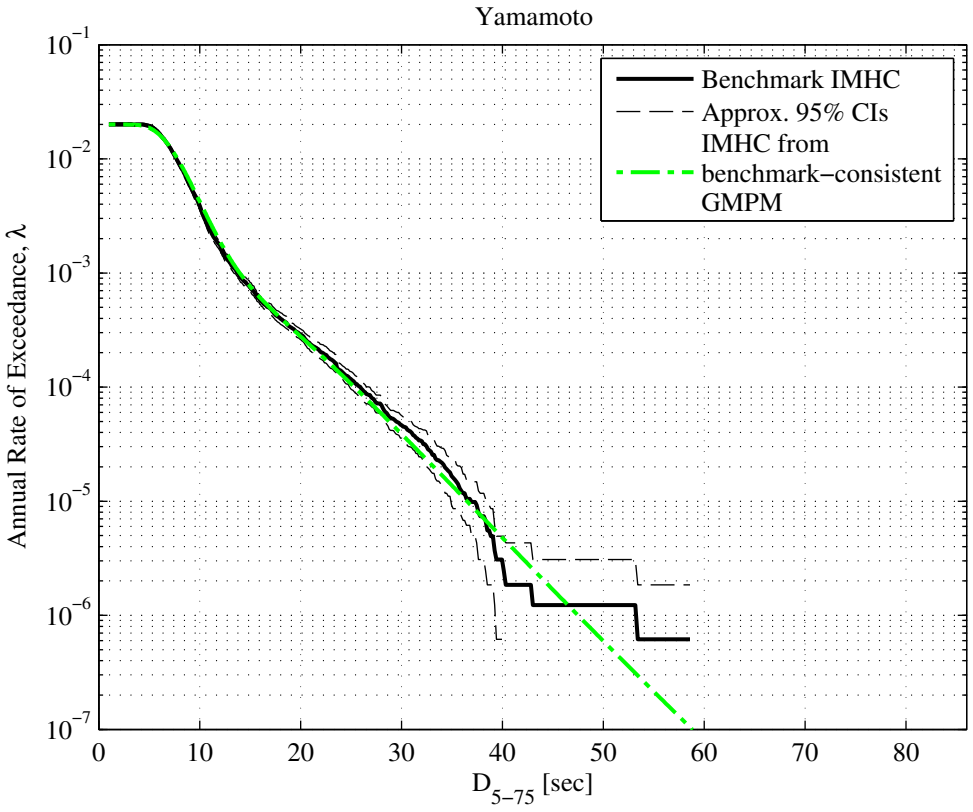

Figure B.19: Benchmark-consistency of GMPM for D_{5-75} under Yamamoto's stochastic model.

Appendix C

Additional Results for Chapter 5

In Chapter 5, results for the 20-story building frame were omitted for the GCIM method because they are similar to those presented for the CS-exact method. For completeness, these results for GCIM are provided in this appendix for both stochastic models: (i) Rezaeian's and (ii) Yamamoto's.

Figures C.1 and C.2 present the SDHCs of the 20-story frame that were determined by ground motions (GMs) selected from GCIM, for Rezaeian's and Yamamoto's GM models, respectiely. The four EDPs presented are the same as those discussed in Section 5.6: (i) peak (over time) roof displacement, PFD_{20}, (ii) peak first-story drift ratio, $PSDR_1$, (iii) peak roof acceleration, PFA_{20}, and (iv) maximum (over all floors) floor acceleration, MFA, which were chosen to illustrate responses that are often of interest in loss assessments in performance-based earthquake engineering. Practically speaking, the SDHC estimates from GCIM are unbiased for all EDPs and exceedance rates of the 20-story frame considered. This is to be expected since: (i) the SDHC estimates for the same frame from CS-exact were also essentially unbiased (Figures 5.5 and 5.6), and (ii) GCIM includes more features of the GM in the selection process than CS-exact.

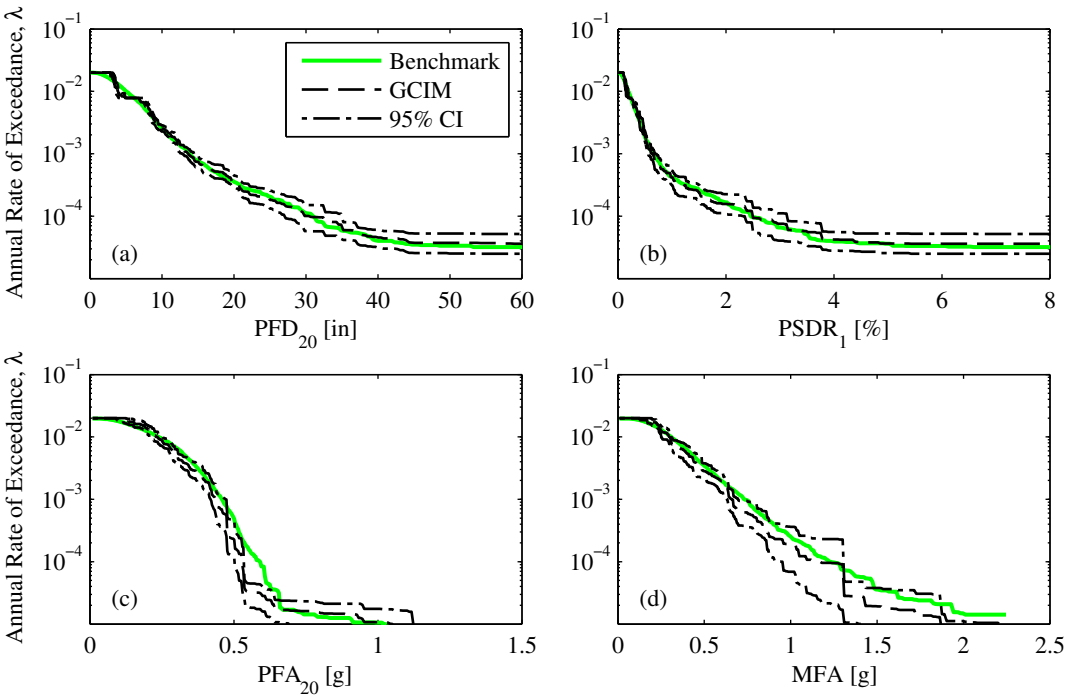

Figure C.1: Comparison of SDHC estimates for several EDPs of the 20-story frame from GCIM against benchmark (Rezaeian's GM model).

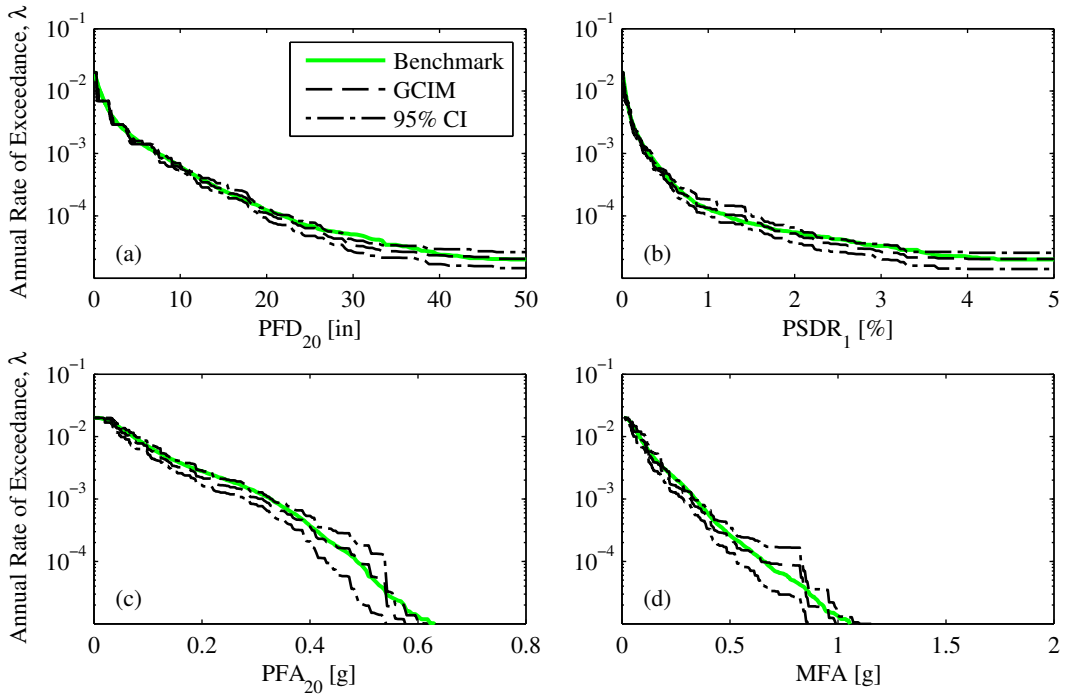

Figure C.2: Comparison of SDHC estimates for several EDPs of the 20-story frame from GCIM against benchmark (Yamamoto's GM model).

Appendix D

Additional Results for Chapter 6

In Chapter 6, the Importance Sampling (IS) approach for selecting ground motions (GMs) was evaluated and results were presented almost exclusively for GMs generated by Rezaeian's stochastic model. In this appendix, the salient results for Yamamoto's stochastic model are provided for completeness.

D.1 Importance Sampling with g_1 as the Importance Function

The subsequent figures complement those presented in Section 6.7 where unscaled GMs were selected with g_1 as the Importance Function (IF). For both frames, the vector of intensity measures (IMs) utilized to select GMs, denoted by **IM**, consists of: $A(T_1)$, $A(2T_1)$, $A(T_4)$, and D_{5-75}.

Figure D.1 examines hazard consistency of the GMs selected for the 4-story frame under Yamamoto's model. As expected from the design of the IS-based method, the selected GMs are hazard-consistent with respect to the four IMs that were chosen to select GMs, which are highlighted in red. More importantly, the selected GMs are *also* hazard-consistent with respect to other IMs that were excluded from the selection process (e.g., $A(4T_1)$, CAV, etc.); this is consistent with the observations obtained from studying Rezaeian's model. Consequently, the resulting SDHCs are expected to be unbiased.

This expectation is confirmed in Figure D.2, where the SDHCs of the 4-story frame, resulting from the GMs examined in Figure D.1, are presented. Specficially, SDHCs are shown for four EDPs: (i) peak (over time) roof displacement, PFD_4, (ii) peak first story drift ratio, $PSDR_1$, (iii) peak roof acceleration, PFA_4, and (iv) maximum (over height) story drift ratio (MSDR). As in the case of Rezaeian's model, the SDHCs resulting from the unscaled GMs selected by g_1 are unbiased for all of these EDPs because the 95% bootstrapped confidence intervals (CIs) cover the respective benchmarks, over a wide range of exceedance rates.

The preceding analysis with g_1 was also repeated for the 20-story frame. After selecting GMs to be hazard-consistent with respect to **IM** as in Figure D.1, RHAs of the 20-story frame were performed. Applying Equation 4.5b to the computed values of EDPs leads to the SDHCs depicted in Figure D.3 for four EDPs: (i) peak roof displacement, PFD_{20}, (ii) peak first story drift ratio, $PSDR_1$, (iii) peak roof acceleration, PFA_{20}, and (iv) MSDR. As in the case of Rezaeian's model, Figure D.3 demonstrates that the SDHCs resulting from the unscaled GMs selected by g_1 are unbiased for all EDPs considered.

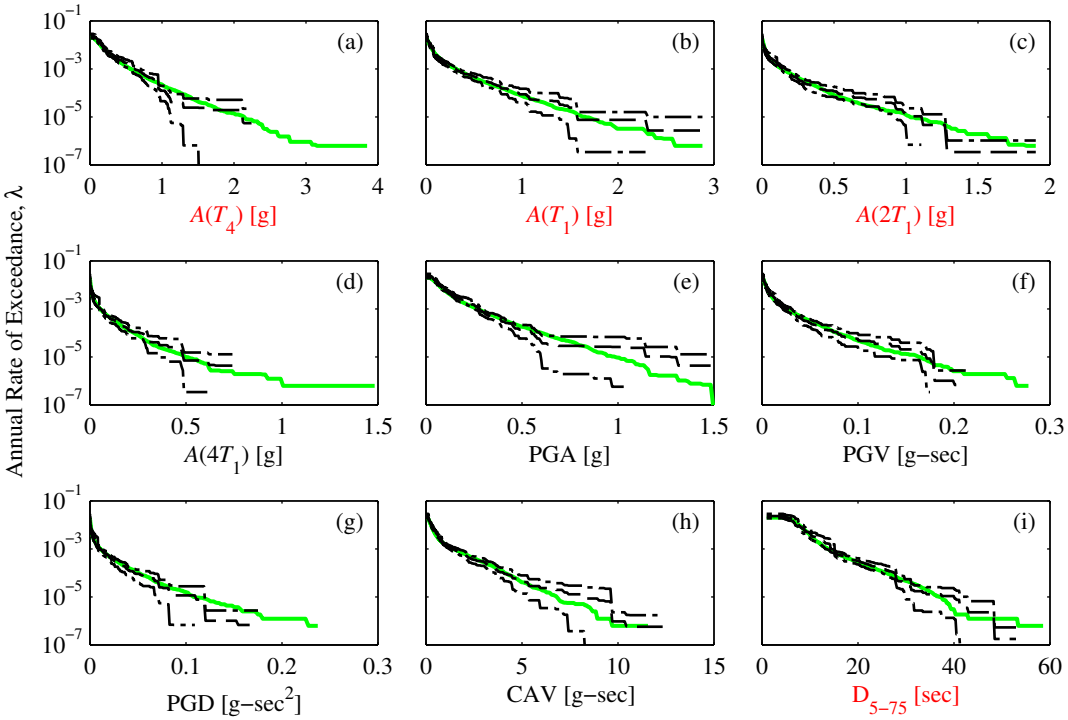

Figure D.1: Hazard consistency of the motions selected with g_1 for the 4-story frame, with respect to: (a) $A(T_4)$; (b) $A(T_1)$; (c) $A(2T_1)$; (d) $A(4T_1)$; (e) PGA; (f) PGV; (g) PGD; (h) CAV; and (i) D_{5-75}. Benchmark in solid green, estimate from IS in dashed black, and 95% CI of estimate from IS in chained black (Yamamoto's GM model).

D.2 Importance Sampling with g_3 as the Importance Function

The subsequent figures complement those presented in Section 6.7 where unscaled GMs were selected with g_3 as the IF, and the vector of IMs employed to select GMs for each frame consists of: $A(T_1)$, $A(2T_1)$, $A(T_4)$, and D_{5-75}. As discussed in Sections 6.4 and 6.7, the IF g_3 is developed from Equation 6.6 by choosing η and g_2 such that the epistemic uncertainty of the hazard curves for $A(T_1)$ and $A(2T_1)$ are minimized at low annual rates of exceedance (see Figure 6.2). This new IF is studied to illustrate the effects of the IF on the epistemic uncertainty of all hazard curve estimates.

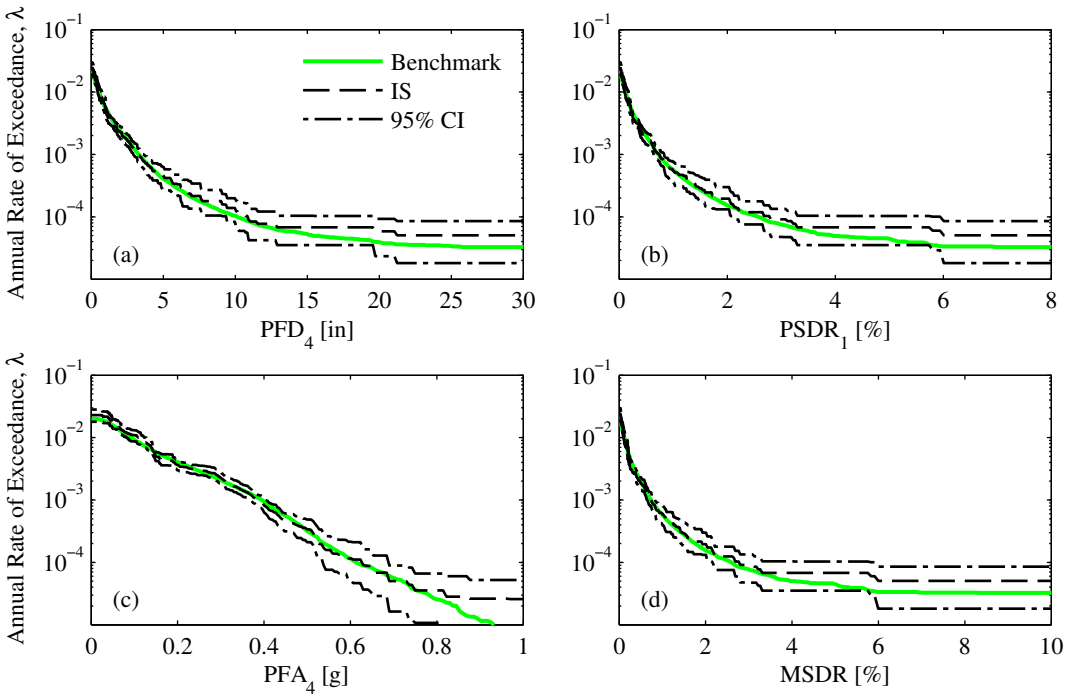

Figure D.2: Comparison of SDHC estimates for several EDPs of the 4-story frame from IS, with g_1 as the IF, against benchmark (Yamamoto's GM model).

Figure D.4 summarizes the GMs selected for the 4-story frame from g_3 as the IF. Because the IF g_3 places more probability density at large values of $A(T_1)$ and $A(2T_1)$ than the IF g_1 (Figure 6.1), the epistemic uncertainty of the hazard curve estimates for these two IMs is reduced at exceedance rates less than about 10^{-4} (compare Figure D.4b-c against Figure D.1b-c). Furthermore, the epistemic uncertainty of the hazard curve estimates for other IMs (e.g., PGA, CAV, etc.) is also reduced at low exceedance rates. When the EDPs of the 4-story frame are highly sensitive to large values of $A(T_1)$ and $A(2T_1)$, we expect the epistemic uncertainty of the resulting SDHC estimates to also be reduced.

Figure D.5 presents the SDHCs of the 4-story frame, resulting from GMs selected by g_3. Comparing this figure against Figure D.2, we observe that the SDHCs in both cases are unbiased but the epistemic uncertainty in the estimates differ. At low annual rates of exceedance, the epistemic uncertainty in the SDHCs from g_3 is smaller than that for SDHCs determined from g_1.

Ground motions were also selected by g_3 for the 20-story frame. After confirming hazard consistency of the selected GMs, as illustrated by Figure D.4 for the 4-story frame, RHAs of the frame were performed and the computed values of EDPs were in turn used to estimate the SDHCs. These SDHCs are shown in Figure D.6. As in the case of the 4-story frame for both stochastic models, the choice of g_3 changes the epistemic uncertainty but not the accuracy of the resulting SDHCs. Comparing Figure D.6 for g_3 against Figure D.3 for g_1, we observe

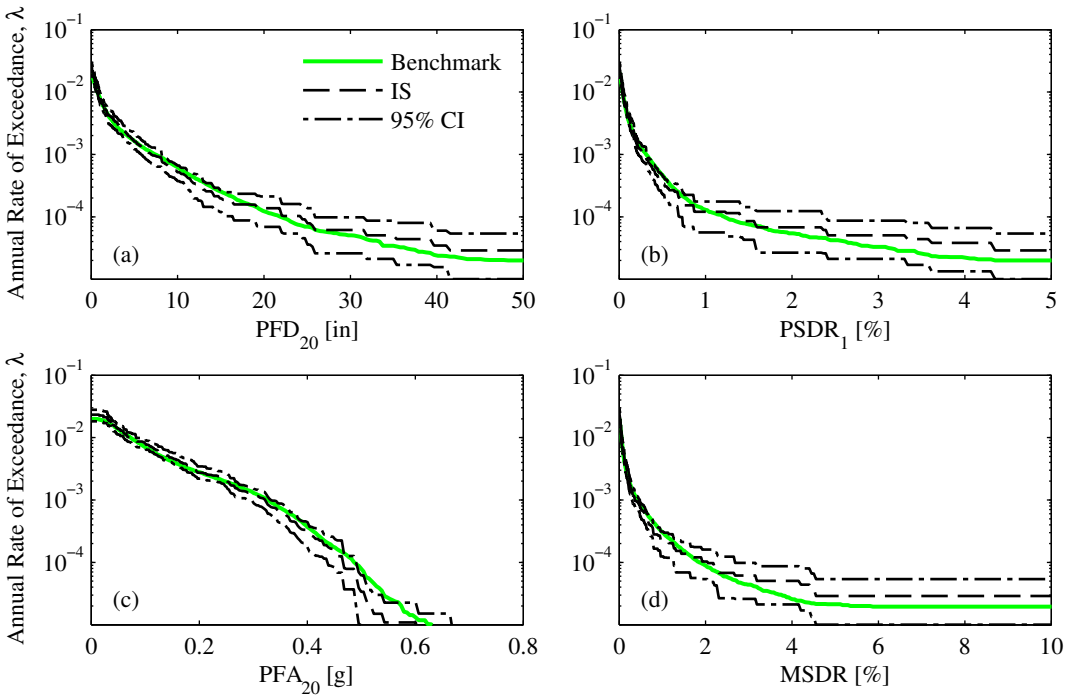

Figure D.3: Comparison of SDHC estimates for several EDPs of the 20-story frame from IS, with g_1 as the IF, against benchmark (Yamamoto's GM model).

that the SDHC estimates are unbiased in both cases but the epistemic uncertainty differs; for displacements and drifts, g_3 reduces the epistemic uncertainty whereas for accelerations, g_3 slightly increases the epistemic uncertainty. This indicates that large levels of $A(T_1)$ and $A(2T_1)$ do not have a dominant influence on large accelerations of this building.

D.3 Importance Sampling with a Non-Structure-Specific Vector of Intensity Measures

The subsequent figures complement those presented in Section 6.9 where unscaled GMs were selected with a non-structure-specific vector of IMs and g_3 as the IF. Motivated by the desire to estimate SDHCs for multiple structures from a single ensemble of GMs, the vector of IMs for selecting GMs was chosen to consist of non-structure-specific IMs: PGA, PGV, PGD, and D_{5-75}.

Figure D.7 examines hazard consistency of the GMs selected from the non-structure-specific vector of IMs. As expected from the design of the IS-based procedure, the selected motions are hazard-consistent with respect to the four IMs, which are highlighted in red. Because these IMs are strongly correlated with many other IMs and because GMs have not been scaled, the selected GMs are also hazard-consistent with respect to other IMs (e.g.,

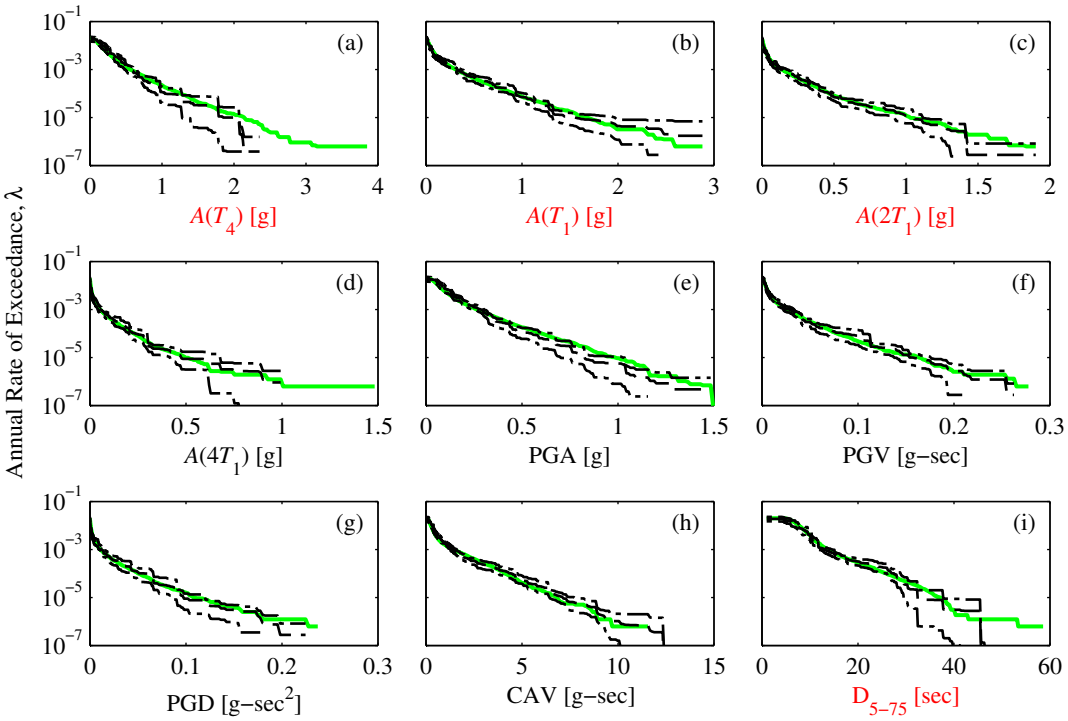

Figure D.4: Hazard consistency of the motions selected with g_3 for the 4-story frame, with respect to: (a) $A(T_4)$; (b) $A(T_1)$; (c) $A(2T_1)$; (d) $A(4T_1)$; (e) PGA; (f) PGV; (g) PGD; (h) CAV; and (i) D_{5-75}. Benchmark in solid green, estimate from IS in dashed black, and 95% CI of estimate from IS in chained black (Yamamoto's GM model).

CAV and spectral accelerations at various periods of vibration). Such hazard consistency suggests that the single ensemble of GMs may lead to accurate SDHC estimates for several systems.

This expectation is confirmed in Figures D.8-D.9, where the SDHCs that were estimated from the *same* ensemble of GMs, are shown for the 4-story and 20-story frames, respectively. Even though the same set of GMs was utilized for each frame, these figures demonstrate that the resulting SDHCs are unbiased for all EDPs and exceedance rates of interest. However, the epistemic uncertainty of the displacement and drift hazard curves for the 4-story frame is smaller than those for the 20-story frame. This suggests that if small epistemic uncertainty in the SDHCs is desired for many systems when utilizing a single ensemble of GMs, then the total number of GMs in the ensemble should be more than what has been documented in this study (which is $n = 300$ GMs).

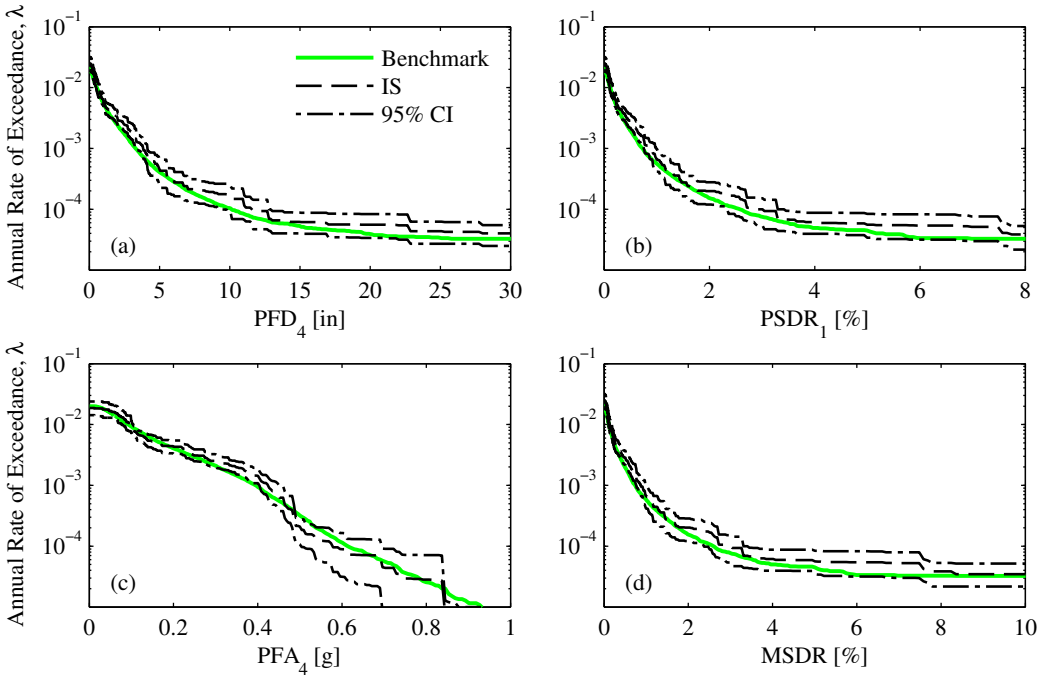

Figure D.5: Comparison of SDHC estimates for several EDPs of the 4-story frame from IS, with g_3 as the IF, against benchmark (Yamamoto's GM model).

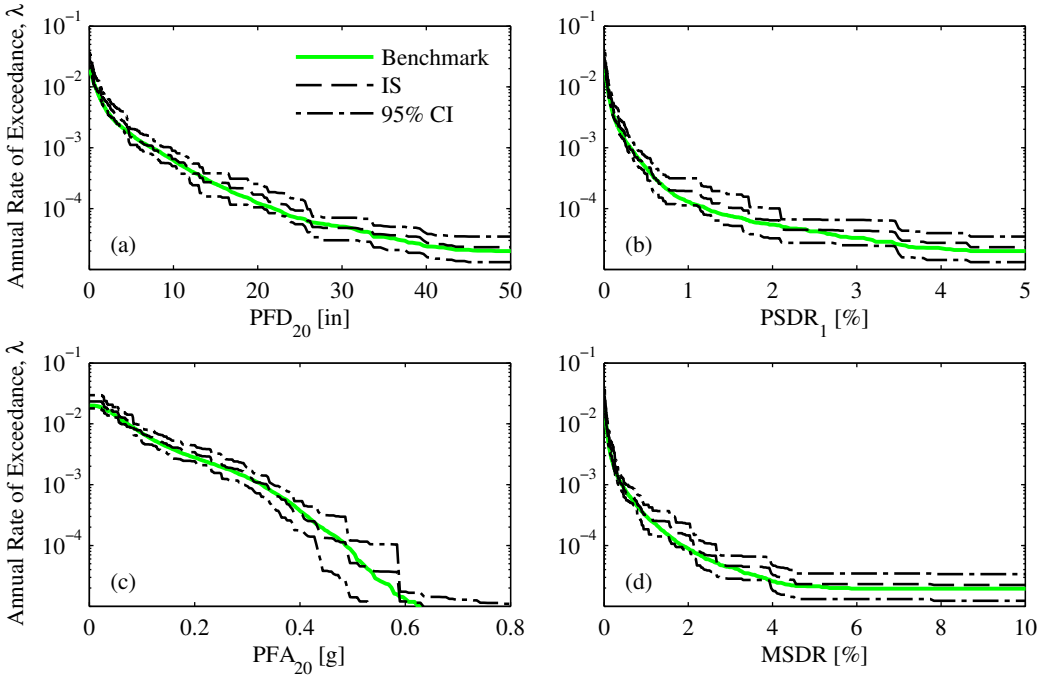

Figure D.6: Comparison of SDHC estimates for several EDPs of the 20-story frame from IS, with g_3 as the IF, against benchmark (Yamamoto's GM model).

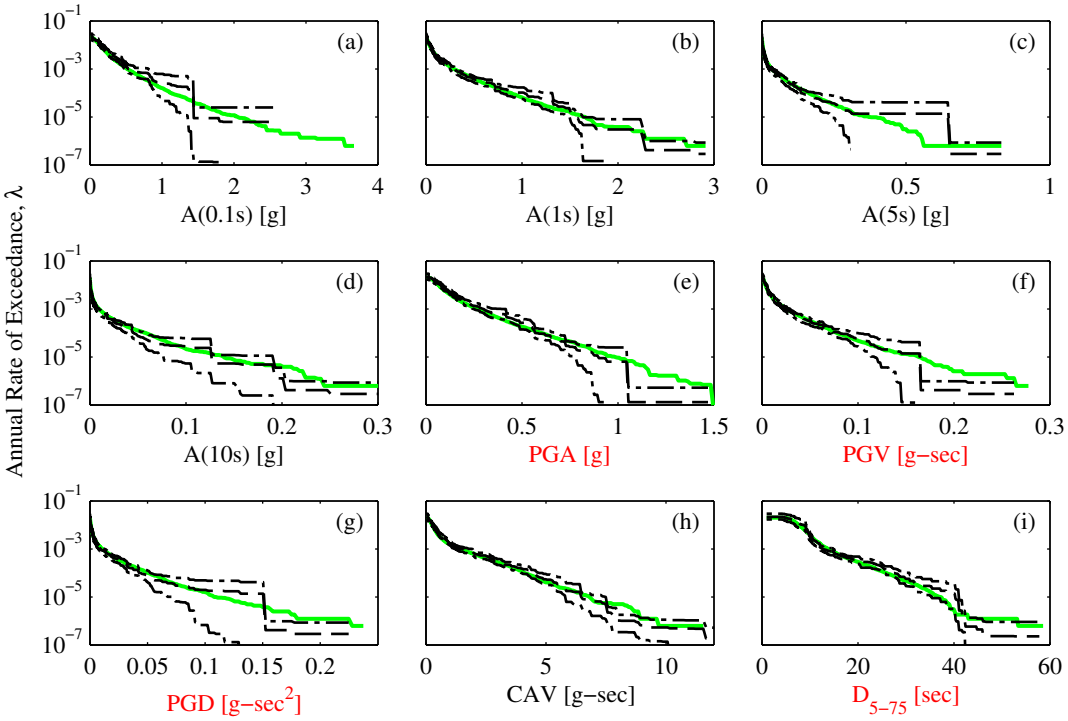

Figure D.7: Hazard consistency of the motions selected from a non-structure-specific **IM**, with respect to: (a) $A(0.1s)$; (b) $A(1s)$; (c) $A(5s)$; (d) $A(10s)$; (e) PGA; (f) PGV; (g) PGD; (h) CAV; and (i) D_{5-75}. Benchmark in solid green, estimate from IS in dashed black, and 95% CI of estimate from IS in chained black (Yamamoto's GM model).

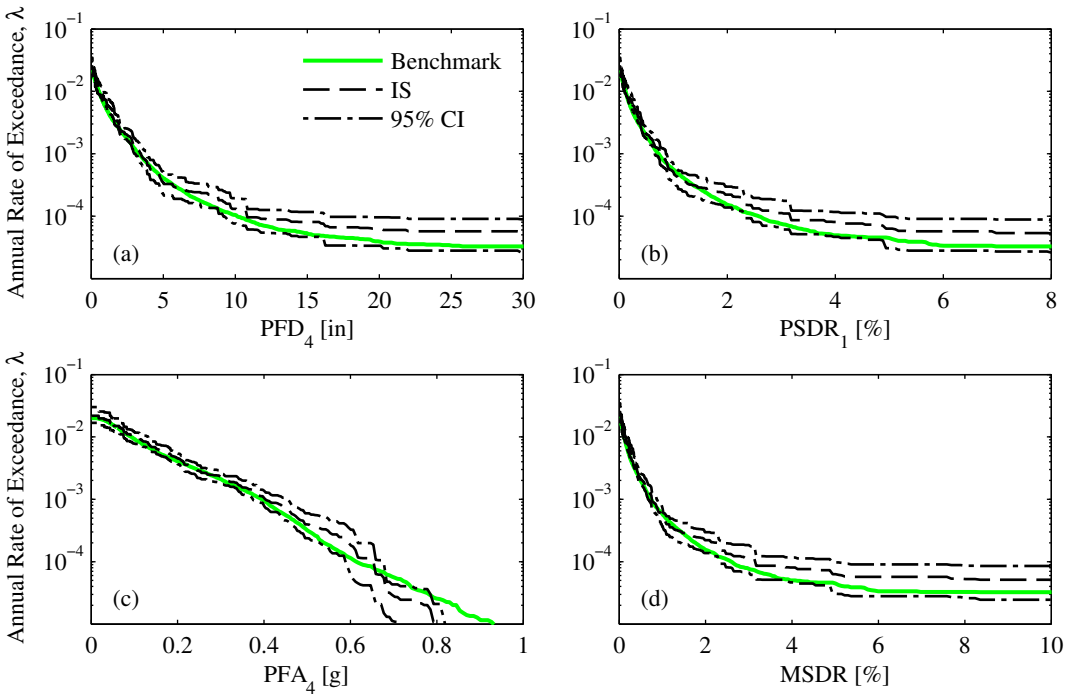

Figure D.8: Comparison of SDHC estimates for several EDPs of the 4-story frame from a single non-structure-specific set of GMs, against benchmark (Yamamoto's GM model).

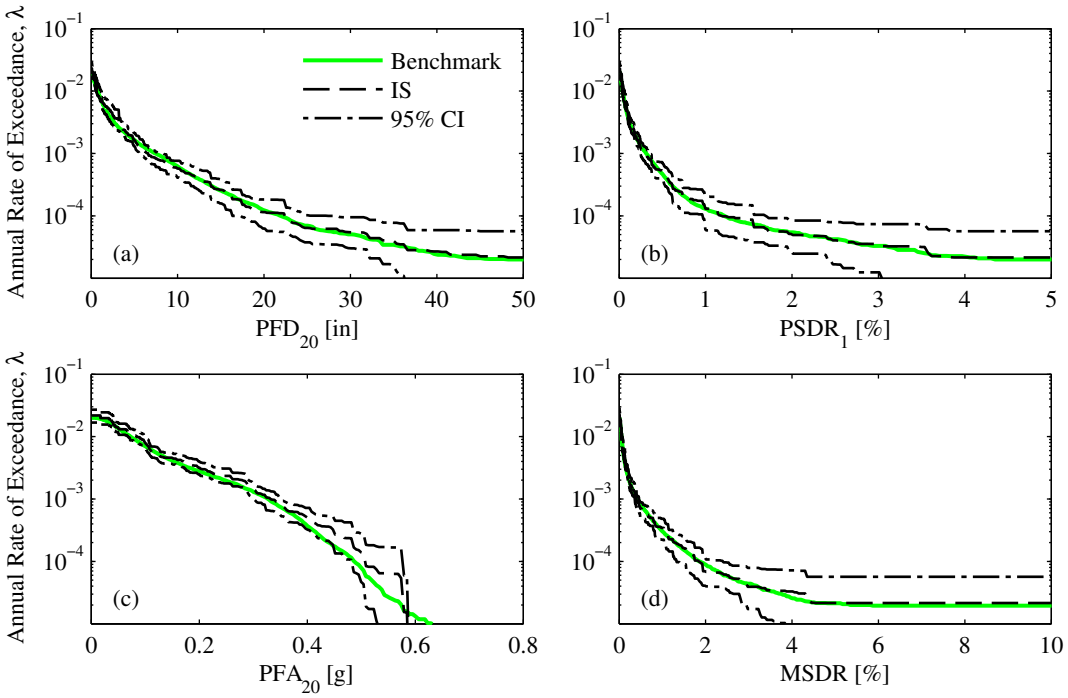

Figure D.9: Comparison of SDHC estimates for several EDPs of the 20-story frame from the same set of GMs utilized in Figures D.7-D.8, against benchmark (Yamamoto's GM model).

PEER REPORTS

PEER reports are available as a free PDF download from http://peer.berkeley.edu/publications/peer_reports_complete.html. Printed hard copies of PEER reports can be ordered directly from our printer by following the instructions at http://peer.berkeley.edu/publications/peer_reports.html. For other related questions about the PEER Report Series, contact the Pacific Earthquake Engineering Research Center, 325 Davis Hall mail code 1792, Berkeley, CA 94720. Tel.: (510) 642-3437; Fax: (510) 665-1655; Email: peer_editor@berkeley.edu

PEER 2015/11 *Selection and Scaling of Ground Motions for Nonlinear Response History Analysis of Buildings in Performance-Based Earthquake Engineering.* N. Simon Kwong and Anil K. Chopra. December 2015.

PEER 2015/10 *Structural Behavior of Column-Bent Cap Beam-Box Girder Systems in Reinforced Concrete Bridges Subjected to Gravity and Seismic Loads. Part II: Hybrid Simulation and Post-Test Analysis.* Mohamed A. Moustafa and Khalid M. Mosalam. November 2015.

PEER 2015/09 *Structural Behavior of Column-Bent Cap Beam-Box Girder Systems in Reinforced Concrete Bridges Subjected to Gravity and Seismic Loads. Part I: Pre-Test Analysis and Quasi-Static Experiments.* Mohamed A. Moustafa and Khalid M. Mosalam. September 2015.

PEER 2015/08 *NGA-East: Adjustments to Median Ground-Motion Models for Center and Eastern North America.* August 2015.

PEER 2015/07 *NGA-East: Ground-Motion Standard-Deviation Models for Central and Eastern North America.* Linda Al Atik. June 2015.

PEER 2015/06 *Adjusting Ground-Motion Intensity Measures to a Reference Site for which V_{S30} = 3000 m/sec.* David M. Boore. May 2015.

PEER 2015/05 *Hybrid Simulation of Seismic Isolation Systems Applied to an APR-1400 Nuclear Power Plant.* Andreas H. Schellenberg, Alireza Sarebanha, Matthew J. Schoettler, Gilberto Mosqueda, Gianmario Benzoni, and Stephen A. Mahin. April 2015.

PEER 2015/04 *NGA-East: Median Ground-Motion Models for the Central and Eastern North America Region.* April 2015.

PEER 2015/03 *Single Series Solution for the Rectangular Fiber-Reinforced Elastomeric Isolator Compression Modulus.* James M. Kelly and Niel C. Van Engelen. March 2015.

PEER 2015/02 *A Full-Scale, Single-Column Bridge Bent Tested by Shake-Table Excitation.* Matthew J. Schoettler, José I. Restrepo, Gabriele Guerrini, David E. Duck, and Francesco Carrea. March 2015.

PEER 2015/01 *Concrete Column Blind Prediction Contest 2010: Outcomes and Observations.* Vesna Terzic, Matthew J. Schoettler, José I. Restrepo, and Stephen A Mahin. March 2015.

PEER 2014/20 *Stochastic Modeling and Simulation of Near-Fault Ground Motions for Performance-Based Earthquake Engineering.* Mayssa Dabaghi and Armen Der Kiureghian. December 2014.

PEER 2014/19 *Seismic Response of a Hybrid Fiber-Reinforced Concrete Bridge Column Detailed for Accelerated Bridge Construction.* Wilson Nguyen, William Trono, Marios Panagiotou, and Claudia P. Ostertag. December 2014.

PEER 2014/18 *Three-Dimensional Beam-Truss Model for Reinforced Concrete Walls and Slabs Subjected to Cyclic Static or Dynamic Loading.* Yuan Lu, Marios Panagiotou, and Ioannis Koutromanos. December 2014.

PEER 2014/17 *PEER NGA-East Database.* Christine A. Goulet, Tadahiro Kishida, Timothy D. Ancheta, Chris H. Cramer, Robert B. Darragh, Walter J. Silva, Youssef M.A. Hashash, Joseph Harmon, Jonathan P. Stewart, Katie E. Wooddell, and Robert R. Youngs. October 2014.

PEER 2014/16 *Guidelines for Performing Hazard-Consistent One-Dimensional Ground Response Analysis for Ground Motion Prediction.* Jonathan P. Stewart, Kioumars Afshari, and Youssef M.A. Hashash. October 2014.

PEER 2014/15 *NGA-East Regionalization Report: Comparison of Four Crustal Regions within Central and Eastern North America using Waveform Modeling and 5%-Damped Pseudo-Spectral Acceleration Response.* Jennifer Dreiling, Marius P. Isken, Walter D. Mooney, Martin C. Chapman, and Richard W. Godbee. October 2014.

PEER 2014/14 *Scaling Relations between Seismic Moment and Rupture Area of Earthquakes in Stable Continental Regions*. Paul Somerville. August 2014.

PEER 2014/13 *PEER Preliminary Notes and Observations on the August 24, 2014, South Napa Earthquake*. Grace S. Kang (Editor), Stephen A. Mahin (Editors). September 2014.

PEER 2014/12 *Reference-Rock Site Conditions for Central and Eastern North America: Part II – Attenuation (Kappa) Definition*. Kenneth W. Campbell, Youssef M.A. Hashash, Byungmin Kim, Albert R. Kottke, Ellen M. Rathje, Walter J. Silva, and Jonathan P. Stewart. August 2014.

PEER 2014/11 *Reference-Rock Site Conditions for Central and Eastern North America: Part I - Velocity Definition*. Youssef M.A. Hashash, Albert R. Kottke, Jonathan P. Stewart, Kenneth W. Campbell, Byungmin Kim, Ellen M. Rathje, Walter J. Silva, Sissy Nikolaou, and Cheryl Moss. August 2014.

PEER 2014/10 *Evaluation of Collapse and Non-Collapse of Parallel Bridges Affected by Liquefaction and Lateral Spreading*. Benjamin Turner, Scott J. Brandenberg, and Jonathan P. Stewart. August 2014.

PEER 2014/09 *PEER Arizona Strong-Motion Database and GMPEs Evaluation*. Tadahiro Kishida, Robert E. Kayen, Olga-Joan Ktenidou, Walter J. Silva, Robert B. Darragh, and Jennie Watson-Lamprey. June 2014.

PEER 2014/08 *Unbonded Pretensioned Bridge Columns with Rocking Detail*. Jeffrey A. Schaefer, Bryan Kennedy, Marc O. Eberhard, John F. Stanton. June 2014.

PEER 2014/07 *Northridge 20 Symposium Summary Report: Impacts, Outcomes, and Next Steps*. May 2014.

PEER 2014/06 *Report of the Tenth Planning Meeting of NEES/E-Defense Collaborative Research on Earthquake Engineering*. December 2013.

PEER 2014/05 *Seismic Velocity Site Characterization of Thirty-One Chilean Seismometer Stations by Spectral Analysis of Surface Wave Dispersion.* Robert Kayen, Brad D. Carkin, Skye Corbet, Camilo Pinilla, Allan Ng, Edward Gorbis, and Christine Truong. April 2014.

PEER 2014/04 *Effect of Vertical Acceleration on Shear Strength of Reinforced Concrete Columns.* Hyerin Lee and Khalid M. Mosalam. April 2014.

PEER 2014/03 *Retest of Thirty-Year-Old Neoprene Isolation Bearings.* James M. Kelly and Niel C. Van Engelen. March 2014.

PEER 2014/02 *Theoretical Development of Hybrid Simulation Applied to Plate Structures.* Ahmed A. Bakhaty, Khalid M. Mosalam, and Sanjay Govindjee. January 2014.

PEER 2014/01 *Performance-Based Seismic Assessment of Skewed Bridges.* Peyman Kaviani, Farzin Zareian, and Ertugrul Taciroglu. January 2014.

PEER 2013/26 *Urban Earthquake Engineering. Proceedings of the U.S.-Iran Seismic Workshop.* December 2013.

PEER 2013/25 *Earthquake Engineering for Resilient Communities: 2013 PEER Internship Program Research Report Collection.* Heidi Tremayne (Editor), Stephen A. Mahin (Editor), Jorge Archbold Monterossa, Matt Brosman, Shelly Dean, Katherine deLaveaga, Curtis Fong, Donovan Holder, Rakeeb Khan, Elizabeth Jachens, David Lam, Daniela Martinez Lopez, Mara Minner, Geffen Oren, Julia Pavicic, Melissa Quinonez, Lorena Rodriguez, Sean Salazar, Kelli Slaven, Vivian Steyert, Jenny Taing, and Salvador Tena. December 2013.

PEER 2013/24 *NGA-West2 Ground Motion Prediction Equations for Vertical Ground Motions.* September 2013.

PEER 2013/23 *Coordinated Planning and Preparedness for Fire Following Major Earthquakes.* Charles Scawthorn. November 2013.

PEER 2013/22 *GEM-PEER Task 3 Project: Selection of a Global Set of Ground Motion Prediction Equations.* Jonathan P. Stewart, John Douglas, Mohammad B. Javanbarg, Carola Di Alessandro, Yousef Bozorgnia, Norman A. Abrahamson, David M. Boore, Kenneth W. Campbell, Elise Delavaud, Mustafa Erdik and Peter J. Stafford. December 2013.

PEER 2013/21 *Seismic Design and Performance of Bridges with Columns on Rocking Foundations.* Grigorios Antonellis and Marios Panagiotou. September 2013.

PEER 2013/20 *Experimental and Analytical Studies on the Seismic Behavior of Conventional and Hybrid Braced Frames.* Jiun-Wei Lai and Stephen A. Mahin. September 2013.

PEER 2013/19 *Toward Resilient Communities: A Performance-Based Engineering Framework for Design and Evaluation of the Built Environment.* Michael William Mieler, Bozidar Stojadinovic, Robert J. Budnitz, Stephen A. Mahin and Mary C. Comerio. September 2013.

PEER 2013/18 *Identification of Site Parameters that Improve Predictions of Site Amplification.* Ellen M. Rathje and Sara Navidi. July 2013.

PEER 2013/17 *Response Spectrum Analysis of Concrete Gravity Dams Including Dam-Water-Foundation Interaction.* Arnkjell Løkke and Anil K. Chopra. July 2013.

PEER 2013/16 *Effect of hoop reinforcement spacing on the cyclic response of large reinforced concrete special moment frame beams.* Marios Panagiotou, Tea Visnjic, Grigorios Antonellis, Panagiotis Galanis, and Jack P. Moehle. June 2013.

PEER 2013/15 *A Probabilistic Framework to Include the Effects of Near-Fault Directivity in Seismic Hazard Assessment.* Shrey Kumar Shahi, Jack W. Baker. October 2013.

PEER 2013/14 *Hanging-Wall Scaling using Finite-Fault Simulations.* Jennifer L. Donahue and Norman A. Abrahamson. September 2013.

PEER 2013/13 *Semi-Empirical Nonlinear Site Amplification and its Application in NEHRP Site Factors.* Jonathan P. Stewart and Emel Seyhan. November 2013.

PEER 2013/12 *Nonlinear Horizontal Site Response for the NGA-West2 Project.* Ronnie Kamai, Norman A. Abramson, Walter J. Silva. May 2013.

PEER 2013/11 *Epistemic Uncertainty for NGA-West2 Models.* Linda Al Atik and Robert R. Youngs. May 2013.

PEER 2013/10 *NGA-West 2 Models for Ground-Motion Directionality.* Shrey K. Shahi and Jack W. Baker. May 2013.

PEER 2013/09 *Final Report of the NGA-West2 Directivity Working Group.* Paul Spudich, Jeffrey R. Bayless, Jack W. Baker, Brian S.J. Chiou, Badie Rowshandel, Shrey Shahi, and Paul Somerville. May 2013.

PEER 2013/08 *NGA-West2 Model for Estimating Average Horizontal Values of Pseudo-Absolute Spectral Accelerations Generated by Crustal Earthquakes.* I. M. Idriss. May 2013.

PEER 2013/07 *Update of the Chiou and Youngs NGA Ground Motion Model for Average Horizontal Component of Peak Ground Motion and Response Spectra.* Brian Chiou and Robert Youngs. May 2013.

PEER 2013/06 *NGA-West2 Campbell-Bozorgnia Ground Motion Model for the Horizontal Components of PGA, PGV, and 5%-Damped Elastic Pseudo-Acceleration Response Spectra for Periods Ranging from 0.01 to 10 sec.* Kenneth W. Campbell and Yousef Bozorgnia. May 2013.

PEER 2013/05 *NGA-West 2 Equations for Predicting Response Spectral Accelerations for Shallow Crustal Earthquakes.* David M. Boore, Jonathan P. Stewart, Emel Seyhan, Gail M. Atkinson. May 2013.

PEER 2013/04 *Update of the AS08 Ground-Motion Prediction Equations Based on the NGA-West2 Data Set.* Norman Abrahamson, Walter Silva, and Ronnie Kamai. May 2013.

PEER 2013/03 *PEER NGA-West2 Database.* Timothy D. Ancheta, Robert B. Darragh, Jonathan P. Stewart, Emel Seyhan, Walter J. Silva, Brian S.J. Chiou, Katie E. Wooddell, Robert W. Graves, Albert R. Kottke, David M. Boore, Tadahiro Kishida, and Jennifer L. Donahue. May 2013.

PEER 2013/02 *Hybrid Simulation of the Seismic Response of Squat Reinforced Concrete Shear Walls.* Catherine A. Whyte and Bozidar Stojadinovic. May 2013.

PEER 2013/01 *Housing Recovery in Chile: A Qualitative Mid-program Review.* Mary C. Comerio. February 2013.

PEER 2012/08 *Guidelines for Estimation of Shear Wave Velocity.* Bernard R. Wair, Jason T. DeJong, and Thomas Shantz. December 2012.

PEER 2012/07 *Earthquake Engineering for Resilient Communities: 2012 PEER Internship Program Research Report Collection.* Heidi Tremayne (Editor), Stephen A. Mahin (Editor), Collin Anderson, Dustin Cook, Michael Erceg, Carlos Esparza, Jose Jimenez, Dorian Krausz, Andrew Lo, Stephanie Lopez, Nicole McCurdy, Paul Shipman, Alexander Strum, Eduardo Vega. December 2012.

PEER 2012/06 *Fragilities for Precarious Rocks at Yucca Mountain.* Matthew D. Purvance, Rasool Anooshehpoor, and James N. Brune. December 2012.

PEER 2012/05 *Development of Simplified Analysis Procedure for Piles in Laterally Spreading Layered Soils.* Christopher R. McGann, Pedro Arduino, and Peter Mackenzie–Helnwein. December 2012.

PEER 2012/04 *Unbonded Pre-Tensioned Columns for Bridges in Seismic Regions.* Phillip M. Davis, Todd M. Janes, Marc O. Eberhard, and John F. Stanton. December 2012.

PEER 2012/03 *Experimental and Analytical Studies on Reinforced Concrete Buildings with Seismically Vulnerable Beam-Column Joints.* Sangjoon Park and Khalid M. Mosalam. October 2012.

PEER 2012/02 *Seismic Performance of Reinforced Concrete Bridges Allowed to Uplift during Multi-Directional Excitation.* Andres Oscar Espinoza and Stephen A. Mahin. July 2012.

PEER 2012/01 *Spectral Damping Scaling Factors for Shallow Crustal Earthquakes in Active Tectonic Regions.* Sanaz Rezaeian, Yousef Bozorgnia, I. M. Idriss, Kenneth Campbell, Norman Abrahamson, and Walter Silva. July 2012.

PEER 2011/10 *Earthquake Engineering for Resilient Communities: 2011 PEER Internship Program Research Report Collection.* Eds. Heidi Faison and Stephen A. Mahin. December 2011.

PEER 2011/09 *Calibration of Semi-Stochastic Procedure for Simulating High-Frequency Ground Motions.* Jonathan P. Stewart, Emel Seyhan, and Robert W. Graves. December 2011.

PEER 2011/08 *Water Supply in regard to Fire Following Earthquake.* Charles Scawthorn. November 2011.

PEER 2011/07 *Seismic Risk Management in Urban Areas. Proceedings of a U.S.-Iran-Turkey Seismic Workshop.* September 2011.

PEER 2011/06 *The Use of Base Isolation Systems to Achieve Complex Seismic Performance Objectives.* Troy A. Morgan and Stephen A. Mahin. July 2011.

PEER 2011/05 *Case Studies of the Seismic Performance of Tall Buildings Designed by Alternative Means.* Task 12 Report for the Tall Buildings Initiative. Jack Moehle, Yousef Bozorgnia, Nirmal Jayaram, Pierson Jones, Mohsen Rahnama, Nilesh Shome, Zeynep Tuna, John Wallace, Tony Yang, and Farzin Zareian. July 2011.

PEER 2011/04 *Recommended Design Practice for Pile Foundations in Laterally Spreading Ground.* Scott A. Ashford, Ross W. Boulanger, and Scott J. Brandenberg. June 2011.

PEER 2011/03 *New Ground Motion Selection Procedures and Selected Motions for the PEER Transportation Research Program.* Jack W. Baker, Ting Lin, Shrey K. Shahi, and Nirmal Jayaram. March 2011.

PEER 2011/02 *A Bayesian Network Methodology for Infrastructure Seismic Risk Assessment and Decision Support.* Michelle T. Bensi, Armen Der Kiureghian, and Daniel Straub. March 2011.

PEER 2011/01 *Demand Fragility Surfaces for Bridges in Liquefied and Laterally Spreading Ground.* Scott J. Brandenberg, Jian Zhang, Pirooz Kashighandi, Yili Huo, and Minxing Zhao. March 2011.

PEER 2010/05 *Guidelines for Performance-Based Seismic Design of Tall Buildings.* Developed by the Tall Buildings Initiative. November 2010.

PEER 2010/04 *Application Guide for the Design of Flexible and Rigid Bus Connections between Substation Equipment Subjected to Earthquakes.* Jean-Bernard Dastous and Armen Der Kiureghian. September 2010.

PEER 2010/03 *Shear Wave Velocity as a Statistical Function of Standard Penetration Test Resistance and Vertical Effective Stress at Caltrans Bridge Sites.* Scott J. Brandenberg, Naresh Bellana, and Thomas Shantz. June 2010.

PEER 2010/02 *Stochastic Modeling and Simulation of Ground Motions for Performance-Based Earthquake Engineering.* Sanaz Rezaeian and Armen Der Kiureghian. June 2010.

PEER 2010/01 *Structural Response and Cost Characterization of Bridge Construction Using Seismic Performance Enhancement Strategies.* Ady Aviram, Božidar Stojadinović, Gustavo J. Parra-Montesinos, and Kevin R. Mackie. March 2010.

PEER 2009/03 *The Integration of Experimental and Simulation Data in the Study of Reinforced Concrete Bridge Systems Including Soil-Foundation-Structure Interaction.* Matthew Dryden and Gregory L. Fenves. November 2009.

PEER 2009/02 *Improving Earthquake Mitigation through Innovations and Applications in Seismic Science, Engineering, Communication, and Response. Proceedings of a U.S.-Iran Seismic Workshop.* October 2009.

PEER 2009/01 *Evaluation of Ground Motion Selection and Modification Methods: Predicting Median Interstory Drift Response of Buildings.* Curt B. Haselton, Ed. June 2009.

PEER 2008/10 *Technical Manual for Strata.* Albert R. Kottke and Ellen M. Rathje. February 2009.

PEER 2008/09 *NGA Model for Average Horizontal Component of Peak Ground Motion and Response Spectra.* Brian S.-J. Chiou and Robert R. Youngs. November 2008.

PEER 2008/08 *Toward Earthquake-Resistant Design of Concentrically Braced Steel Structures.* Patxi Uriz and Stephen A. Mahin. November 2008.

PEER 2008/07 *Using OpenSees for Performance-Based Evaluation of Bridges on Liquefiable Soils.* Stephen L. Kramer, Pedro Arduino, and HyungSuk Shin. November 2008.

PEER 2008/06 *Shaking Table Tests and Numerical Investigation of Self-Centering Reinforced Concrete Bridge Columns.* Hyung IL Jeong, Junichi Sakai, and Stephen A. Mahin. September 2008.

PEER 2008/05 *Performance-Based Earthquake Engineering Design Evaluation Procedure for Bridge Foundations Undergoing Liquefaction-Induced Lateral Ground Displacement.* Christian A. Ledezma and Jonathan D. Bray. August 2008.

PEER 2008/04 *Benchmarking of Nonlinear Geotechnical Ground Response Analysis Procedures.* Jonathan P. Stewart, Annie On-Lei Kwok, Yousseff M. A. Hashash, Neven Matasovic, Robert Pyke, Zhiliang Wang, and Zhaohui Yang. August 2008.

PEER 2008/03 *Guidelines for Nonlinear Analysis of Bridge Structures in California.* Ady Aviram, Kevin R. Mackie, and Božidar Stojadinović. August 2008.

PEER 2008/02 *Treatment of Uncertainties in Seismic-Risk Analysis of Transportation Systems.* Evangelos Stergiou and Anne S. Kiremidjian. July 2008.

PEER 2008/01 *Seismic Performance Objectives for Tall Buildings.* William T. Holmes, Charles Kircher, William Petak, and Nabih Youssef. August 2008.

PEER 2007/12 *An Assessment to Benchmark the Seismic Performance of a Code-Conforming Reinforced Concrete Moment-Frame Building.* Curt Haselton, Christine A. Goulet, Judith Mitrani-Reiser, James L. Beck, Gregory G. Deierlein, Keith A. Porter, Jonathan P. Stewart, and Ertugrul Taciroglu. August 2008.

PEER 2007/11 *Bar Buckling in Reinforced Concrete Bridge Columns.* Wayne A. Brown, Dawn E. Lehman, and John F. Stanton. February 2008.

PEER 2007/10 *Computational Modeling of Progressive Collapse in Reinforced Concrete Frame Structures.* Mohamed M. Talaat and Khalid M. Mosalam. May 2008.

PEER 2007/09 *Integrated Probabilistic Performance-Based Evaluation of Benchmark Reinforced Concrete Bridges.* Kevin R. Mackie, John-Michael Wong, and Božidar Stojadinović. January 2008.

PEER 2007/08 *Assessing Seismic Collapse Safety of Modern Reinforced Concrete Moment-Frame Buildings.* Curt B. Haselton and Gregory G. Deierlein. February 2008.

PEER 2007/07 *Performance Modeling Strategies for Modern Reinforced Concrete Bridge Columns.* Michael P. Berry and Marc O. Eberhard. April 2008.

PEER 2007/06 *Development of Improved Procedures for Seismic Design of Buried and Partially Buried Structures.* Linda Al Atik and Nicholas Sitar. June 2007.

PEER 2007/05 *Uncertainty and Correlation in Seismic Risk Assessment of Transportation Systems.* Renee G. Lee and Anne S. Kiremidjian. July 2007.

PEER 2007/04 *Numerical Models for Analysis and Performance-Based Design of Shallow Foundations Subjected to Seismic Loading.* Sivapalan Gajan, Tara C. Hutchinson, Bruce L. Kutter, Prishati Raychowdhury, José A. Ugalde, and Jonathan P. Stewart. May 2008.

PEER 2007/03 *Beam-Column Element Model Calibrated for Predicting Flexural Response Leading to Global Collapse of RC Frame Buildings.* Curt B. Haselton, Abbie B. Liel, Sarah Taylor Lange, and Gregory G. Deierlein. May 2008.

PEER 2007/02 *Campbell-Bozorgnia NGA Ground Motion Relations for the Geometric Mean Horizontal Component of Peak and Spectral Ground Motion Parameters.* Kenneth W. Campbell and Yousef Bozorgnia. May 2007.

PEER 2007/01 *Boore-Atkinson NGA Ground Motion Relations for the Geometric Mean Horizontal Component of Peak and Spectral Ground Motion Parameters.* David M. Boore and Gail M. Atkinson. May. May 2007.

PEER 2006/12 *Societal Implications of Performance-Based Earthquake Engineering.* Peter J. May. May 2007.

PEER 2006/11 *Probabilistic Seismic Demand Analysis Using Advanced Ground Motion Intensity Measures, Attenuation Relationships, and Near-Fault Effects.* Polsak Tothong and C. Allin Cornell. March 2007.

PEER 2006/10 *Application of the PEER PBEE Methodology to the I-880 Viaduct.* Sashi Kunnath. February 2007.

PEER 2006/09 *Quantifying Economic Losses from Travel Forgone Following a Large Metropolitan Earthquake.* James Moore, Sungbin Cho, Yue Yue Fan, and Stuart Werner. November 2006.

PEER 2006/08 *Vector-Valued Ground Motion Intensity Measures for Probabilistic Seismic Demand Analysis*. Jack W. Baker and C. Allin Cornell. October 2006.

PEER 2006/07 *Analytical Modeling of Reinforced Concrete Walls for Predicting Flexural and Coupled–Shear-Flexural Responses*. Kutay Orakcal, Leonardo M. Massone, and John W. Wallace. October 2006.

PEER 2006/06 *Nonlinear Analysis of a Soil-Drilled Pier System under Static and Dynamic Axial Loading.* Gang Wang and Nicholas Sitar. November 2006.

PEER 2006/05 *Advanced Seismic Assessment Guidelines.* Paolo Bazzurro, C. Allin Cornell, Charles Menun, Maziar Motahari, and Nicolas Luco. September 2006.

PEER 2006/04 *Probabilistic Seismic Evaluation of Reinforced Concrete Structural Components and Systems.* Tae Hyung Lee and Khalid M. Mosalam. August 2006.

PEER 2006/03 *Performance of Lifelines Subjected to Lateral Spreading.* Scott A. Ashford and Teerawut Juirnarongrit. July 2006.

PEER 2006/02 *Pacific Earthquake Engineering Research Center Highway Demonstration Project.* Anne Kiremidjian, James Moore, Yue Yue Fan, Nesrin Basoz, Ozgur Yazali, and Meredith Williams. April 2006.

PEER 2006/01 *Bracing Berkeley. A Guide to Seismic Safety on the UC Berkeley Campus.* Mary C. Comerio, Stephen Tobriner, and Ariane Fehrenkamp. January 2006.

PEER 2005/16 *Seismic Response and Reliability of Electrical Substation Equipment and Systems.* Junho Song, Armen Der Kiureghian, and Jerome L. Sackman. April 2006.

PEER 2005/15 *CPT-Based Probabilistic Assessment of Seismic Soil Liquefaction Initiation.* R. E. S. Moss, R. B. Seed, R. E. Kayen, J. P. Stewart, and A. Der Kiureghian. April 2006.

PEER 2005/14 *Workshop on Modeling of Nonlinear Cyclic Load-Deformation Behavior of Shallow Foundations.* Bruce L. Kutter, Geoffrey Martin, Tara Hutchinson, Chad Harden, Sivapalan Gajan, and Justin Phalen. March 2006.

PEER 2005/13 *Stochastic Characterization and Decision Bases under Time-Dependent Aftershock Risk in Performance-Based Earthquake Engineering.* Gee Liek Yeo and C. Allin Cornell. July 2005.

PEER 2005/12 *PEER Testbed Study on a Laboratory Building: Exercising Seismic Performance Assessment.* Mary C. Comerio, editor. November 2005.

PEER 2005/11 *Van Nuys Hotel Building Testbed Report: Exercising Seismic Performance Assessment.* Helmut Krawinkler, editor. October 2005.

PEER 2005/10 *First NEES/E-Defense Workshop on Collapse Simulation of Reinforced Concrete Building Structures.* September 2005.

PEER 2005/09 *Test Applications of Advanced Seismic Assessment Guidelines.* Joe Maffei, Karl Telleen, Danya Mohr, William Holmes, and Yuki Nakayama. August 2006.

PEER 2005/08 *Damage Accumulation in Lightly Confined Reinforced Concrete Bridge Columns.* R. Tyler Ranf, Jared M. Nelson, Zach Price, Marc O. Eberhard, and John F. Stanton. April 2006.

PEER 2005/07 *Experimental and Analytical Studies on the Seismic Response of Freestanding and Anchored Laboratory Equipment.* Dimitrios Konstantinidis and Nicos Makris. January 2005.

PEER 2005/06 *Global Collapse of Frame Structures under Seismic Excitations*. Luis F. Ibarra and Helmut Krawinkler. September 2005.

PEER 2005//05 *Performance Characterization of Bench- and Shelf-Mounted Equipment.* Samit Ray Chaudhuri and Tara C. Hutchinson. May 2006.

PEER 2005/04 *Numerical Modeling of the Nonlinear Cyclic Response of Shallow Foundations.* Chad Harden, Tara Hutchinson, Geoffrey R. Martin, and Bruce L. Kutter. August 2005.

PEER 2005/03 *A Taxonomy of Building Components for Performance-Based Earthquake Engineering.* Keith A. Porter. September 2005.

PEER 2005/02 *Fragility Basis for California Highway Overpass Bridge Seismic Decision Making*. Kevin R. Mackie and Božidar Stojadinović. June 2005.

PEER 2005/01 *Empirical Characterization of Site Conditions on Strong Ground Motion.* Jonathan P. Stewart, Yoojoong Choi, and Robert W. Graves. June 2005.

PEER 2004/09 *Electrical Substation Equipment Interaction: Experimental Rigid Conductor Studies.* Christopher Stearns and André Filiatrault. February 2005.

PEER 2004/08 *Seismic Qualification and Fragility Testing of Line Break 550-kV Disconnect Switches.* Shakhzod M. Takhirov, Gregory L. Fenves, and Eric Fujisaki. January 2005.

PEER 2004/07 *Ground Motions for Earthquake Simulator Qualification of Electrical Substation Equipment.* Shakhzod M. Takhirov, Gregory L. Fenves, Eric Fujisaki, and Don Clyde. January 2005.

PEER 2004/06 *Performance-Based Regulation and Regulatory Regimes.* Peter J. May and Chris Koski. September 2004.

PEER 2004/05 *Performance-Based Seismic Design Concepts and Implementation: Proceedings of an International Workshop.* Peter Fajfar and Helmut Krawinkler, editors. September 2004.

PEER 2004/04 *Seismic Performance of an Instrumented Tilt-up Wall Building*. James C. Anderson and Vitelmo V. Bertero. July 2004.

PEER 2004/03 *Evaluation and Application of Concrete Tilt-up Assessment Methodologies.* Timothy Graf and James O. Malley. October 2004.

PEER 2004/02 *Analytical Investigations of New Methods for Reducing Residual Displacements of Reinforced Concrete Bridge Columns.* Junichi Sakai and Stephen A. Mahin. August 2004.

PEER 2004/01 *Seismic Performance of Masonry Buildings and Design Implications.* Kerri Anne Taeko Tokoro, James C. Anderson, and Vitelmo V. Bertero. February 2004.

PEER 2003/18 *Performance Models for Flexural Damage in Reinforced Concrete Columns.* Michael Berry and Marc Eberhard. August 2003.

PEER 2003/17 *Predicting Earthquake Damage in Older Reinforced Concrete Beam-Column Joints.* Catherine Pagni and Laura Lowes. October 2004.

PEER 2003/16 *Seismic Demands for Performance-Based Design of Bridges.* Kevin Mackie and Božidar Stojadinović. August 2003.

PEER 2003/15 *Seismic Demands for Nondeteriorating Frame Structures and Their Dependence on Ground Motions.* Ricardo Antonio Medina and Helmut Krawinkler. May 2004.

PEER 2003/14 *Finite Element Reliability and Sensitivity Methods for Performance-Based Earthquake Engineering.* Terje Haukaas and Armen Der Kiureghian. April 2004.

PEER 2003/13 *Effects of Connection Hysteretic Degradation on the Seismic Behavior of Steel Moment-Resisting Frames.* Janise E. Rodgers and Stephen A. Mahin. March 2004.

PEER 2003/12 *Implementation Manual for the Seismic Protection of Laboratory Contents: Format and Case Studies.* William T. Holmes and Mary C. Comerio. October 2003.

PEER 2003/11 *Fifth U.S.-Japan Workshop on Performance-Based Earthquake Engineering Methodology for Reinforced Concrete Building Structures.* February 2004.

PEER 2003/10 *A Beam-Column Joint Model for Simulating the Earthquake Response of Reinforced Concrete Frames.* Laura N. Lowes, Nilanjan Mitra, and Arash Altoontash. February 2004.

PEER 2003/09 *Sequencing Repairs after an Earthquake: An Economic Approach.* Marco Casari and Simon J. Wilkie. April 2004.

PEER 2003/08 *A Technical Framework for Probability-Based Demand and Capacity Factor Design (DCFD) Seismic Formats*. Fatemeh Jalayer and C. Allin Cornell. November 2003.

PEER 2003/07 *Uncertainty Specification and Propagation for Loss Estimation Using FOSM Methods.* Jack W. Baker and C. Allin Cornell. September 2003.

PEER 2003/06 *Performance of Circular Reinforced Concrete Bridge Columns under Bidirectional Earthquake Loading*. Mahmoud M. Hachem, Stephen A. Mahin, and Jack P. Moehle. February 2003.

PEER 2003/05 *Response Assessment for Building-Specific Loss Estimation.* Eduardo Miranda and Shahram Taghavi. September 2003.

PEER 2003/04 *Experimental Assessment of Columns with Short Lap Splices Subjected to Cyclic Loads*. Murat Melek, John W. Wallace, and Joel Conte. April 2003.

PEER 2003/03 *Probabilistic Response Assessment for Building-Specific Loss Estimation.* Eduardo Miranda and Hesameddin Aslani. September 2003.

PEER 2003/02 *Software Framework for Collaborative Development of Nonlinear Dynamic Analysis Program.* Jun Peng and Kincho H. Law. September 2003.

PEER 2003/01 *Shake Table Tests and Analytical Studies on the Gravity Load Collapse of Reinforced Concrete Frames.* Kenneth John Elwood and Jack P. Moehle. November 2003.

PEER 2002/24 *Performance of Beam to Column Bridge Joints Subjected to a Large Velocity Pulse.* Natalie Gibson, André Filiatrault, and Scott A. Ashford. April 2002.

PEER 2002/23 *Effects of Large Velocity Pulses on Reinforced Concrete Bridge Columns.* Greg L. Orozco and Scott A. Ashford. April 2002.

PEER 2002/22 *Characterization of Large Velocity Pulses for Laboratory Testing.* Kenneth E. Cox and Scott A. Ashford. April 2002.

PEER 2002/21 *Fourth U.S.-Japan Workshop on Performance-Based Earthquake Engineering Methodology for Reinforced Concrete Building Structures*. December 2002.

PEER 2002/20 *Barriers to Adoption and Implementation of PBEE Innovations.* Peter J. May. August 2002.

PEER 2002/19 *Economic-Engineered Integrated Models for Earthquakes: Socioeconomic Impacts.* Peter Gordon, James E. Moore II, and Harry W. Richardson. July 2002.

PEER 2002/18 *Assessment of Reinforced Concrete Building Exterior Joints with Substandard Details.* Chris P. Pantelides, Jon Hansen, Justin Nadauld, and Lawrence D. Reaveley. May 2002.

PEER 2002/17 *Structural Characterization and Seismic Response Analysis of a Highway Overcrossing Equipped with Elastomeric Bearings and Fluid Dampers: A Case Study.* Nicos Makris and Jian Zhang. November 2002.

PEER 2002/16 *Estimation of Uncertainty in Geotechnical Properties for Performance-Based Earthquake Engineering.* Allen L. Jones, Steven L. Kramer, and Pedro Arduino. December 2002.

PEER 2002/15 *Seismic Behavior of Bridge Columns Subjected to Various Loading Patterns.* Asadollah Esmaeily-Gh. and Yan Xiao. December 2002.

PEER 2002/14 *Inelastic Seismic Response of Extended Pile Shaft Supported Bridge Structures.* T.C. Hutchinson, R.W. Boulanger, Y.H. Chai, and I.M. Idriss. December 2002.

PEER 2002/13 *Probabilistic Models and Fragility Estimates for Bridge Components and Systems.* Paolo Gardoni, Armen Der Kiureghian, and Khalid M. Mosalam. June 2002.

PEER 2002/12 *Effects of Fault Dip and Slip Rake on Near-Source Ground Motions: Why Chi-Chi Was a Relatively Mild M7.6 Earthquake.* Brad T. Aagaard, John F. Hall, and Thomas H. Heaton. December 2002.

PEER 2002/11 *Analytical and Experimental Study of Fiber-Reinforced Strip Isolators*. James M. Kelly and Shakhzod M. Takhirov. September 2002.

PEER 2002/10 *Centrifuge Modeling of Settlement and Lateral Spreading with Comparisons to Numerical Analyses***.** Sivapalan Gajan and Bruce L. Kutter. January 2003.

PEER 2002/09 *Documentation and Analysis of Field Case Histories of Seismic Compression during the 1994 Northridge, California, Earthquake.* Jonathan P. Stewart, Patrick M. Smith, Daniel H. Whang, and Jonathan D. Bray. October 2002.

PEER 2002/08 *Component Testing, Stability Analysis and Characterization of Buckling-Restrained Unbonded Braces™.* Cameron Black, Nicos Makris, and Ian Aiken. September 2002.

PEER 2002/07 *Seismic Performance of Pile-Wharf Connections.* Charles W. Roeder, Robert Graff, Jennifer Soderstrom, and Jun Han Yoo. December 2001.

PEER 2002/06 *The Use of Benefit-Cost Analysis for Evaluation of Performance-Based Earthquake Engineering Decisions*. Richard O. Zerbe and Anthony Falit-Baiamonte. September 2001.

PEER 2002/05 *Guidelines, Specifications, and Seismic Performance Characterization of Nonstructural Building Components and Equipment*. André Filiatrault, Constantin Christopoulos, and Christopher Stearns. September 2001.

PEER 2002/04 *Consortium of Organizations for Strong-Motion Observation Systems and the Pacific Earthquake Engineering Research Center Lifelines Program: Invited Workshop on Archiving and Web Dissemination of Geotechnical Data, 4–5 October 2001*. September 2002.

PEER 2002/03 *Investigation of Sensitivity of Building Loss Estimates to Major Uncertain Variables for the Van Nuys Testbed.* Keith A. Porter, James L. Beck, and Rustem V. Shaikhutdinov. August 2002.

PEER 2002/02 *The Third U.S.-Japan Workshop on Performance-Based Earthquake Engineering Methodology for Reinforced Concrete Building Structures*. July 2002.

PEER 2002/01 *Nonstructural Loss Estimation: The UC Berkeley Case Study.* Mary C. Comerio and John C. Stallmeyer. December 2001.

PEER 2001/16 *Statistics of SDF-System Estimate of Roof Displacement for Pushover Analysis of Buildings.* Anil K. Chopra, Rakesh K. Goel, and Chatpan Chintanapakdee. December 2001.

PEER 2001/15 *Damage to Bridges during the 2001 Nisqually Earthquake.* R. Tyler Ranf, Marc O. Eberhard, and Michael P. Berry. November 2001.

PEER 2001/14 *Rocking Response of Equipment Anchored to a Base Foundation.* Nicos Makris and Cameron J. Black. September 2001.

PEER 2001/13 *Modeling Soil Liquefaction Hazards for Performance-Based Earthquake Engineering.* Steven L. Kramer and Ahmed-W. Elgamal. February 2001.

PEER 2001/12 *Development of Geotechnical Capabilities in OpenSees.* Boris Jeremić. September 2001.

PEER 2001/11 *Analytical and Experimental Study of Fiber-Reinforced Elastomeric Isolators*. James M. Kelly and Shakhzod M. Takhirov. September 2001.

PEER 2001/10 *Amplification Factors for Spectral Acceleration in Active Regions.* Jonathan P. Stewart, Andrew H. Liu, Yoojoong Choi, and Mehmet B. Baturay. December 2001.

PEER 2001/09 *Ground Motion Evaluation Procedures for Performance-Based Design.* Jonathan P. Stewart, Shyh-Jeng Chiou, Jonathan D. Bray, Robert W. Graves, Paul G. Somerville, and Norman A. Abrahamson. September 2001.

PEER 2001/08 *Experimental and Computational Evaluation of Reinforced Concrete Bridge Beam-Column Connections for Seismic Performance*. Clay J. Naito, Jack P. Moehle, and Khalid M. Mosalam. November 2001.

PEER 2001/07 *The Rocking Spectrum and the Shortcomings of Design Guidelines.* Nicos Makris and Dimitrios Konstantinidis. August 2001.

PEER 2001/06 *Development of an Electrical Substation Equipment Performance Database for Evaluation of Equipment Fragilities*. Thalia Agnanos. April 1999.

PEER 2001/05 *Stiffness Analysis of Fiber-Reinforced Elastomeric Isolators.* Hsiang-Chuan Tsai and James M. Kelly. May 2001.

PEER 2001/04 *Organizational and Societal Considerations for Performance-Based Earthquake Engineering.* Peter J. May. April 2001.

PEER 2001/03 *A Modal Pushover Analysis Procedure to Estimate Seismic Demands for Buildings: Theory and Preliminary Evaluation.* Anil K. Chopra and Rakesh K. Goel. January 2001.

PEER 2001/02 *Seismic Response Analysis of Highway Overcrossings Including Soil-Structure Interaction.* Jian Zhang and Nicos Makris. March 2001.

PEER 2001/01 *Experimental Study of Large Seismic Steel Beam-to-Column Connections.* Egor P. Popov and Shakhzod M. Takhirov. November 2000.

PEER 2000/10 *The Second U.S.-Japan Workshop on Performance-Based Earthquake Engineering Methodology for Reinforced Concrete Building Structures.* March 2000.

PEER 2000/09 *Structural Engineering Reconnaissance of the August 17, 1999 Earthquake: Kocaeli (Izmit), Turkey.* Halil Sezen, Kenneth J. Elwood, Andrew S. Whittaker, Khalid Mosalam, John J. Wallace, and John F. Stanton. December 2000.

PEER 2000/08 *Behavior of Reinforced Concrete Bridge Columns Having Varying Aspect Ratios and Varying Lengths of Confinement.* Anthony J. Calderone, Dawn E. Lehman, and Jack P. Moehle. January 2001.

PEER 2000/07 *Cover-Plate and Flange-Plate Reinforced Steel Moment-Resisting Connections.* Taejin Kim, Andrew S. Whittaker, Amir S. Gilani, Vitelmo V. Bertero, and Shakhzod M. Takhirov. September 2000.

PEER 2000/06 *Seismic Evaluation and Analysis of 230-kV Disconnect Switches.* Amir S. J. Gilani, Andrew S. Whittaker, Gregory L. Fenves, Chun-Hao Chen, Henry Ho, and Eric Fujisaki. July 2000.

PEER 2000/05 *Performance-Based Evaluation of Exterior Reinforced Concrete Building Joints for Seismic Excitation.* Chandra Clyde, Chris P. Pantelides, and Lawrence D. Reaveley. July 2000.

PEER 2000/04 *An Evaluation of Seismic Energy Demand: An Attenuation Approach.* Chung-Che Chou and Chia-Ming Uang. July 1999.

PEER 2000/03 *Framing Earthquake Retrofitting Decisions: The Case of Hillside Homes in Los Angeles.* Detlof von Winterfeldt, Nels Roselund, and Alicia Kitsuse. March 2000.

PEER 2000/02 *U.S.-Japan Workshop on the Effects of Near-Field Earthquake Shaking.* Andrew Whittaker, ed. July 2000.

PEER 2000/01 *Further Studies on Seismic Interaction in Interconnected Electrical Substation Equipment.* Armen Der Kiureghian, Kee-Jeung Hong, and Jerome L. Sackman. November 1999.

PEER 1999/14 *Seismic Evaluation and Retrofit of 230-kV Porcelain Transformer Bushings*. Amir S. Gilani, Andrew S. Whittaker, Gregory L. Fenves, and Eric Fujisaki. December 1999.

PEER 1999/13 *Building Vulnerability Studies: Modeling and Evaluation of Tilt-up and Steel Reinforced Concrete Buildings.* John W. Wallace, Jonathan P. Stewart, and Andrew S. Whittaker, editors. December 1999.

PEER 1999/12 *Rehabilitation of Nonductile RC Frame Building Using Encasement Plates and Energy-Dissipating Devices.* Mehrdad Sasani, Vitelmo V. Bertero, James C. Anderson. December 1999.

PEER 1999/11 *Performance Evaluation Database for Concrete Bridge Components and Systems under Simulated Seismic Loads.* Yael D. Hose and Frieder Seible. November 1999.

PEER 1999/10 *U.S.-Japan Workshop on Performance-Based Earthquake Engineering Methodology for Reinforced Concrete Building Structures.* December 1999.

PEER 1999/09 *Performance Improvement of Long Period Building Structures Subjected to Severe Pulse-Type Ground Motions*. James C. Anderson, Vitelmo V. Bertero, and Raul Bertero. October 1999.

PEER 1999/08 *Envelopes for Seismic Response Vectors.* Charles Menun and Armen Der Kiureghian. July 1999.

PEER 1999/07 *Documentation of Strengths and Weaknesses of Current Computer Analysis Methods for Seismic Performance of Reinforced Concrete Members.* William F. Cofer. November 1999.

PEER 1999/06 *Rocking Response and Overturning of Anchored Equipment under Seismic Excitations.* Nicos Makris and Jian Zhang. November 1999.

PEER 1999/05 *Seismic Evaluation of 550 kV Porcelain Transformer Bushings.* Amir S. Gilani, Andrew S. Whittaker, Gregory L. Fenves, and Eric Fujisaki. October 1999.

PEER 1999/04 *Adoption and Enforcement of Earthquake Risk-Reduction Measures.* Peter J. May, Raymond J. Burby, T. Jens Feeley, and Robert Wood.

PEER 1999/03 *Task 3 Characterization of Site Response General Site Categories.* Adrian Rodriguez-Marek, Jonathan D. Bray, and Norman Abrahamson. February 1999.

PEER 1999/02 *Capacity-Demand-Diagram Methods for Estimating Seismic Deformation of Inelastic Structures: SDF Systems*. Anil K. Chopra and Rakesh Goel. April 1999.

PEER 1999/01 *Interaction in Interconnected Electrical Substation Equipment Subjected to Earthquake Ground Motions.* Armen Der Kiureghian, Jerome L. Sackman, and Kee-Jeung Hong. February 1999.

PEER 1998/08 *Behavior and Failure Analysis of a Multiple-Frame Highway Bridge in the 1994 Northridge Earthquake.* Gregory L. Fenves and Michael Ellery. December 1998.

PEER 1998/07 *Empirical Evaluation of Inertial Soil-Structure Interaction Effects.* Jonathan P. Stewart, Raymond B. Seed, and Gregory L. Fenves. November 1998.

PEER 1998/06 *Effect of Damping Mechanisms on the Response of Seismic Isolated Structures.* Nicos Makris and Shih-Po Chang. November 1998.

PEER 1998/05 *Rocking Response and Overturning of Equipment under Horizontal Pulse-Type Motions.* Nicos Makris and Yiannis Roussos. October 1998.

PEER 1998/04 *Pacific Earthquake Engineering Research Invitational Workshop Proceedings, May 14–15, 1998: Defining the Links between Planning, Policy Analysis, Economics and Earthquake Engineering.* Mary Comerio and Peter Gordon. September 1998.

PEER 1998/03 *Repair/Upgrade Procedures for Welded Beam to Column Connections.* James C. Anderson and Xiaojing Duan. May 1998.

PEER 1998/02 *Seismic Evaluation of 196 kV Porcelain Transformer Bushings.* Amir S. Gilani, Juan W. Chavez, Gregory L. Fenves, and Andrew S. Whittaker. May 1998.

PEER 1998/01 *Seismic Performance of Well-Confined Concrete Bridge Columns.* Dawn E. Lehman and Jack P. Moehle. December 2000.

ONLINE PEER REPORTS

The following PEER reports are available by Internet only at http://peer.berkeley.edu/publications/peer_reports_complete.html.

PEER 2012/103 *Performance-Based Seismic Demand Assessment of Concentrically Braced Steel Frame Buildings.* Chui-Hsin Chen and Stephen A. Mahin. December 2012.

PEER 2012/102 *Procedure to Restart an Interrupted Hybrid Simulation: Addendum to PEER Report 2010/103.* Vesna Terzic and Bozidar Stojadinovic. October 2012.

PEER 2012/101 *Mechanics of Fiber Reinforced Bearings.* James M. Kelly and Andrea Calabrese. February 2012.

PEER 2011/107 *Nonlinear Site Response and Seismic Compression at Vertical Array Strongly Shaken by 2007 Niigata-ken Chuetsu-oki Earthquake.* Eric Yee, Jonathan P. Stewart, and Kohji Tokimatsu. December 2011.

PEER 2011/106 *Self Compacting Hybrid Fiber Reinforced Concrete Composites for Bridge Columns.* Pardeep Kumar, Gabriel Jen, William Trono, Marios Panagiotou, and Claudia Ostertag. September 2011.

PEER 2011/105 *Stochastic Dynamic Analysis of Bridges Subjected to Spacially Varying Ground Motions.* Katerina Konakli and Armen Der Kiureghian. August 2011.

PEER 2011/104 *Design and Instrumentation of the 2010 E-Defense Four-Story Reinforced Concrete and Post-Tensioned Concrete Buildings.* Takuya Nagae, Kenichi Tahara, Taizo Matsumori, Hitoshi Shiohara, Toshimi Kabeyasawa, Susumu Kono, Minehiro Nishiyama (Japanese Research Team) and John Wallace, Wassim Ghannoum, Jack Moehle, Richard Sause, Wesley Keller, Zeynep Tuna (U.S. Research Team). June 2011.

PEER 2011/103 *In-Situ Monitoring of the Force Output of Fluid Dampers: Experimental Investigation.* Dimitrios Konstantinidis, James M. Kelly, and Nicos Makris. April 2011.

PEER 2011/102 *Ground-motion prediction equations 1964 - 2010.* John Douglas. April 2011.

PEER 2011/101 *Report of the Eighth Planning Meeting of NEES/E-Defense Collaborative Research on Earthquake Engineering.* Convened by the Hyogo Earthquake Engineering Research Center (NIED), NEES Consortium, Inc. February 2011.

PEER 2010/111 *Modeling and Acceptance Criteria for Seismic Design and Analysis of Tall Buildings.* Task 7 Report for the Tall Buildings Initiative - Published jointly by the Applied Technology Council. October 2010.

PEER 2010/110 *Seismic Performance Assessment and Probabilistic Repair Cost Analysis of Precast Concrete Cladding Systems for Multistory Buildlings.* Jeffrey P. Hunt and Božidar Stojadinovic. November 2010.

PEER 2010/109 *Report of the Seventh Joint Planning Meeting of NEES/E-Defense Collaboration on Earthquake Engineering. Held at the E-Defense, Miki, and Shin-Kobe, Japan, September 18–19, 2009.* August 2010.

PEER 2010/108 *Probabilistic Tsunami Hazard in California.* Hong Kie Thio, Paul Somerville, and Jascha Polet, preparers. October 2010.

PEER 2010/107 *Performance and Reliability of Exposed Column Base Plate Connections for Steel Moment-Resisting Frames.* Ady Aviram, Božidar Stojadinovic, and Armen Der Kiureghian. August 2010.

PEER 2010/106 *Verification of Probabilistic Seismic Hazard Analysis Computer Programs.* Patricia Thomas, Ivan Wong, and Norman Abrahamson. May 2010.

PEER 2010/105 *Structural Engineering Reconnaissance of the April 6, 2009, Abruzzo, Italy, Earthquake, and Lessons Learned.* M. Selim Günay and Khalid M. Mosalam. April 2010.

PEER 2010/104 *Simulating the Inelastic Seismic Behavior of Steel Braced Frames, Including the Effects of Low-Cycle Fatigue.* Yuli Huang and Stephen A. Mahin. April 2010.

PEER 2010/103 *Post-Earthquake Traffic Capacity of Modern Bridges in California.* Vesna Terzic and Božidar Stojadinović. March 2010.

PEER 2010/102 *Analysis of Cumulative Absolute Velocity (CAV) and JMA Instrumental Seismic Intensity (I_{JMA}) Using the PEER–NGA Strong Motion Database.* Kenneth W. Campbell and Yousef Bozorgnia. February 2010.

PEER 2010/101 *Rocking Response of Bridges on Shallow Foundations.* Jose A. Ugalde, Bruce L. Kutter, and Boris Jeremic. April 2010.

PEER 2009/109 *Simulation and Performance-Based Earthquake Engineering Assessment of Self-Centering Post-Tensioned Concrete Bridge Systems.* Won K. Lee and Sarah L. Billington. December 2009.

PEER 2009/108 *PEER Lifelines Geotechnical Virtual Data Center.* J. Carl Stepp, Daniel J. Ponti, Loren L. Turner, Jennifer N. Swift, Sean Devlin, Yang Zhu, Jean Benoit, and John Bobbitt. September 2009.

PEER 2009/107 *Experimental and Computational Evaluation of Current and Innovative In-Span Hinge Details in Reinforced Concrete Box-Girder Bridges: Part 2: Post-Test Analysis and Design Recommendations.* Matias A. Hube and Khalid M. Mosalam. December 2009.

PEER 2009/106 *Shear Strength Models of Exterior Beam-Column Joints without Transverse Reinforcement.* Sangjoon Park and Khalid M. Mosalam. November 2009.

PEER 2009/105 *Reduced Uncertainty of Ground Motion Prediction Equations through Bayesian Variance Analysis.* Robb Eric S. Moss. November 2009.

PEER 2009/104 *Advanced Implementation of Hybrid Simulation.* Andreas H. Schellenberg, Stephen A. Mahin, Gregory L. Fenves. November 2009.

PEER 2009/103 *Performance Evaluation of Innovative Steel Braced Frames.* T. Y. Yang, Jack P. Moehle, and Božidar Stojadinovic. August 2009.

PEER 2009/102 *Reinvestigation of Liquefaction and Nonliquefaction Case Histories from the 1976 Tangshan Earthquake.* Robb Eric Moss, Robert E. Kayen, Liyuan Tong, Songyu Liu, Guojun Cai, and Jiaer Wu. August 2009.

PEER 2009/101 *Report of the First Joint Planning Meeting for the Second Phase of NEES/E-Defense Collaborative Research on Earthquake Engineering.* Stephen A. Mahin et al. July 2009.

PEER 2008/104 *Experimental and Analytical Study of the Seismic Performance of Retaining Structures.* Linda Al Atik and Nicholas Sitar. January 2009.

PEER 2008/103 *Experimental and Computational Evaluation of Current and Innovative In-Span Hinge Details in Reinforced Concrete Box-Girder Bridges. Part 1: Experimental Findings and Pre-Test Analysis.* Matias A. Hube and Khalid M. Mosalam. January 2009.

PEER 2008/102 *Modeling of Unreinforced Masonry Infill Walls Considering In-Plane and Out-of-Plane Interaction.* Stephen Kadysiewski and Khalid M. Mosalam. January 2009.

PEER 2008/101 *Seismic Performance Objectives for Tall Buildings.* William T. Holmes, Charles Kircher, William Petak, and Nabih Youssef. August 2008.

PEER 2007/101 *Generalized Hybrid Simulation Framework for Structural Systems Subjected to Seismic Loading.* Tarek Elkhoraibi and Khalid M. Mosalam. July 2007.

PEER 2007/100 *Seismic Evaluation of Reinforced Concrete Buildings Including Effects of Masonry Infill Walls.* Alidad Hashemi and Khalid M. Mosalam. July 2007.

The Pacific Earthquake Engineering Research Center (PEER) is a multi-institutional research and education center with headquarters at the University of California, Berkeley. Investigators from over 20 universities, several consulting companies, and researchers at various state and federal government agencies contribute to research programs focused on performance-based earthquake engineering.

These research programs aim to identify and reduce the risks from major earthquakes to life safety and to the economy by including research in a wide variety of disciplines including structural and geotechnical engineering, geology/seismology, lifelines, transportation, architecture, economics, risk management, and public policy.

PEER is supported by federal, state, local, and regional agencies, together with industry partners.

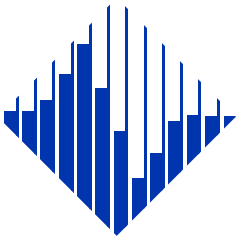

PEER Core Institutions:
University of California, Berkeley (Lead Institution)
California Institute of Technology
Oregon State University
Stanford University
University of California, Davis
University of California, Irvine
University of California, Los Angeles
University of California, San Diego
University of Southern California
University of Washington

PEER reports can be ordered at http://peer.berkeley.edu/publications/peer_reports.html or by contacting

Pacific Earthquake Engineering Research Center
University of California, Berkeley
325 Davis Hall, mail code 1792
Berkeley, CA 94720-1792
Tel: 510-642-3437
Fax: 510-642-1655
Email: peer_editor@berkeley.edu

ISSN 1547-0587X